Stability of Embankments Founded on Soft Soil
Improved with Deep-Mixing-Method Columns

Michael P. Navin

Dissertation submitted to the faculty of the Virginia Polytechnic Institute and State University in
partial fulfillment of the requirements for the degree of

Doctor of Philosophy
In
Civil and Environmental Engineering

Dr. G.M. Filz (Chair)
Dr. J.M. Duncan
Dr. M.S. Gutierrez
Dr. R.D. Kriz
Dr. M.P. Singh

August 1, 2005
Blacksburg, VA

Keywords: Numerical analysis, deep mixing, slope stability, ground improvement

Stability of Embankments Founded on Soft Soil
Improved with Deep-Mixing-Method Columns

Michael P. Navin

ABSTRACT

Foundations constructed by the deep mixing method have been used to successfully support embankments, structures, and excavations in Japan, Scandinavia, the U.S., and other countries. The current state of practice is that design is based on deterministic analyses of settlement and stability, even though deep mixed materials are highly variable. Conservative deterministic design procedures have evolved to limit failures. Disadvantages of this approach include (1) designs with an unknown degree of conservatism and (2) contract administration problems resulting from unrealistic specifications for deep mixed materials.

This dissertation describes research conducted to develop reliability-based design procedures for foundations constructed using the deep mixing method. The emphasis of the research and the included examples are for embankment support applications, but the principles are applicable to foundations constructed for other purposes.

Reliability analyses for foundations created by the deep mixing method are described and illustrated using an example embankment. The deterministic stability analyses for the example embankment were performed using two methods: limit equilibrium analyses and numerical stress-strain analyses. An important finding from the research is that both numerical analyses and reliability analyses are needed to properly design embankments supported on deep mixed columns. Numerical analyses are necessary to address failure modes, such as column bending and tilting, that are not addressed by limit equilibrium analyses, which only cover composite shearing. Reliability analyses are necessary to address the impacts of variability of the deep mixed materials and other system components.

Reliability analyses also provide a rational basis for establishing statistical specifications for deep mixed materials. Such specifications will simplify administration of construction contracts and reduce claims while still providing assurance that the design intent is satisfied.

It is recommended that reliability-based design and statistically-based specifications be implemented in practice now.

Table of Contents

LIST OF FIGURES

vii

LIST OF TABLES

LIST OF SYMBOLS

a_s	area replacement ratio
a_t	total area of columns under footing
B	length of prism
B	the center-to-center spacing between rows
c	cohesion
$c_{average}$	average cohesion value
c_{clay}	clay cohesion value
c_{column}	column cohesion value
c'_{soil}	drained effective stress cohesion intercept for soil
c_u	mean undrained shear strength of the untreated soil
c_v	coefficient of consolidation
d	depth
D	deflection
D_i	height of prism
D_{max}	maximum distance
D_{max}	maximum deflection
D_r	relative density
E	Young's Modulus
e	void ratio
E_{50}	secant modulus of elasticity
E_{col}	modulus of elasticity of the column
E_{max}	maximum Young's Modulus
f	density function
FS	factor of safety
FS_{LE}	factor of safety from limit equilibrium
FS_{NM}	factor of safety from numerical methods
G	shear modulus
$G_{average}$	average shear modulus value used for panels and soil between panels
G_{clay}	clay shear modulus value

G_{column}	column shear modulus value
H	horizontal force
H	height of the embankment
h_w	differential ground water level
I	moment of inertia
K	bulk modulus
k	permeability
K_0	effective stress lateral earth pressure coefficient
$K_{average}$	average bulk modulus value used for panels and soil between panels
K_{clay}	clay bulk modulus value
K_{column}	column bulk modulus value
K_u	undrained bulk modulus value
K_w	bulk modulus value of water
k_h	design seismic coefficient
L_s	width of prism
l	length
M	slope of the critical state line
M_{col}	constrained compression modulus of the column
mpc	preconsolidation pressure parameter (FLAC)
$mp1$	reference pressure parameter (FLAC)
M_{soil}	constrained modulus of the soil
m_v	compressibility parameter
mv_1	reference volume parameter (FLAC)
n	number of samples
n	stress concentration ratio
n	centrifugal acceleration factor
N_c	number of calculations
N_v	number of random variables
OCR	over consolidation ratio
P	load
p	mean stress

$p(f)$	probability of failure
$p(s)$	probability of satisfactory performance
$p(u)$	probability of unsatisfactory performance
p_0	initial pressure
P_a	active earth force
PI	plasticity index
P_p	passive earth force
p_P	preconsolidation pressure
q	shear stress
q	embankment pressure
q_{max}	maximum unconfined compression strength
q_u	unconfined compression strength
r	stiffness ratio
s	separation distance
s	center-to-center spacing of columns
S_{2D}	section modulus of the two-dimensional strip
S_{3D}	section modulus of the round column
SR	settlement ratio
S_r	stress ratio appropriate to orientation of failure surface
s_u	undrained shear strength
V	coefficient of variation
V	vertical force
V_{FS}	coefficient of variation of factor of safety
V_s	variation for settlement
w	applied pressure
$w{:}c$	water-to-cement ratio
wc	water content
x_i	measurement values
z	distance from ground surface to failure surface
ΔFS	change in factor of safety,
Δp	change in pressure in the soil

ΔS	change in settlement,
α	inclination of the failure surface
β	reliability index
β	drained cohesion intercept factor
β_F	reliability index for factor of safety
δ	autocorrelation distance
ε	settlement of the soil
ε_s	shear strain
ε_v	volumetric strain
ϕ	friction angle
ϕ'_{col}	drained friction angle of the column
$\phi_{u,col}$	undrained total stress friction angle for column
ϕ_{emb}	embankment friction angle
ϕ_{soil}	undrained friction angle of the soil
ϕ'_{soil}	drained effective stress friction angle for soil
$\phi_{u,soil}$	undrained total stress friction angle for soil
γ	unit weight of treated soil
γ_l	unit weight of the embankment
γ'_{col}	effective unit weight of the column
γ_f^{col}	unit weight of the fictitious layer above the stone column
γ_f^{soil}	unit weight of the fictitious layer above the soil
γ_{soil}	unit weight of the soil
γ_w	unit weight of water
γ_b	buoyant unit weight
η	porosity
η	reduction in clay strength
η_f	slope of the critical state line
κ	slope of the recompression line
λ	slope of the virgin compression line

λ	ratio of field to lab strength
μ	mean
μ_{col}	ratio of stress change in the stone column from the embankment to the average applied vertical stress from the embankment
μ_{soil}	ratio of stress change in the soil from the embankment load to the average applied vertical stress from the embankment
ν	Poisson's ratio
ν_{col}	Poisson's ratio of the column
ρ	correlation coefficient
σ	stress
σ	standard deviation
σ_a	sum of the axial stresses
σ_{b2D}	the extreme fiber bending stress in the strip
σ_{b3D}	equivalent extreme fiber bending stress in a round column
σ_{FS}	standard deviation of factor of safety
σ_n	total normal stress on the failure plane
σ'_n	effective normal stress on the failure plane
τ	composite shear strength along the sliding surface
τ_d	drained shear strength along the sliding surface
$\tau_{d,col}$	drained shear strength of the column
$\tau_{d,soil}$	drained shear strength of the unimproved soil
τ_u	composite undrained shear strength along the sliding surface
$\tau_{u,col}$	undrained shear strength of the column
$\tau_{u,soil}$	undrained shear strength of the soil
υ	specific volume
Λ	critical state parameter

1. INTRODUCTION

When roadways traverse low-lying areas, embankments may be necessary to bring the roadways up to functional elevations. Such embankments, if placed on highly compressible soft clays or problematic organic soils, may experience long term settlements and edge stability problems. An economical means to improve existing soils in these cases is use of prefabricated vertical drains combined with gradual placement of the embankment fill. This well-established technique can permit construction of embankments on soft ground at a lower construction cost than by using the column-supported embankment technology. However, use of vertical drains and gradual embankment placement requires considerable time for consolidation and strengthening of the soft ground, and this approach can also induce settlement in adjacent facilities, such as would occur when an existing road embankment is being widened.

Column-supported embankments are constructed over soft ground to accelerate construction, improve embankment stability, control total and differential settlements, and protect adjacent facilities. The columns that extend into and through the soft ground can be of several different types: driven piles, vibro-concrete columns, deep-mixing-method columns, stone columns, etc. The columns are selected to be stiffer and stronger than the existing site soil, and if properly designed, they can prevent excessive movement of the embankment. If accelerated construction is necessary, or if adjacent existing facilities need to be protected, then column-supported embankments may be an appropriate technical solution. Column-supported embankments are in widespread use in Japan, Scandinavia, and the United Kingdom, and they are becoming more common in the U.S. and other countries. The column-supported embankment technology has potential application at many soft-ground sites, including coastal areas where existing embankments are being widened and new embankments are being constructed.

The cost of column-supported embankments depends on several design features, including the type, length, diameter, spacing, and arrangement of columns. Geotechnical design engineers establish these details based on considerations of load transfer, settlement, and stability. A report by Filz and Stewart (2005) addresses the load transfer and settlement issues. Established procedures are available for analyzing the stability of embankments supported on driven piles

and on stone columns. Stability analysis methods for embankments supported on piles and stone columns are presented in appendices to this report. In Japan and Scandinavia, transportation embankments on soft ground are often supported on columns installed by deep mixing methods (DMM). This technology is also finding more frequent application in other countries, including the United States. Limit equilibrium methods are used for analyzing the stability of embankments supported on deep-mixing-method columns, but these methods only reflect composite shearing through the columns and soil, and they do not reflect the more critical failure modes of column bending and tilting that can occur when the columns are strong.

The primary emphasis of this research dissertation is on stability of embankments supported on columns installed by the deep mixing method because (1) new embankments at the I-95/U.S. Route 1 interchange, in Alexandria, Virginia, were being designed using columns installed by the deep mixing method at the time this research was initiated and (2) more uncertainty exists in the literature about this case than for embankments supported on driven piles or stone columns.

In the deep mixing method, stabilizers are mixed into the ground using rotary mixing tools to increase the strength and decrease the compressibility of the ground. The various techniques that constitute the deep mixing method originated independently in Sweden and Japan in the 1960's (Porbaha 1998). Bruce (2001) defines the deep mixing method as "the methods by which materials of various types, but usually of cementatious nature, are introduced and blended into the soil through hollow, rotated shafts equipped with cutting tools, and mixing paddles or augers, that extend for various distances above the tip." In the dry method of deep mixing, dry lime, cement, fly ash, and/or other stabilizers are delivered pneumatically to the mixing tool at depth. In the wet method of deep mixing, cement-water slurry is introduced through the hollow stem of the mixing tools. Since its inception, deep mixing has been widely used to improve the strength and reduce the compressibility of soft soils.

There is a range of behavior covered by driven piles, stone columns, and deep-mixed columns used to support embankments over soft soils. Stone columns and piles can be seen as the two ends of the spectrum, with the behavior of lime, lime-cement, and soil-cement columns somewhere in between. The differences in behavior between these foundation types are due to

column strength, stiffness, and ability to transmit a bending moment. Driven piles are essentially designed to carry the full weight of the embankment and transmit all loads to deeper soils. Stability analyses of embankments founded on stone columns are performed by using a composite shear strength based on the shear strength of the soil, the shear strength of the columns, and the area replacement ratio. This approach reasonably approximates composite behavior when the column type is granular. Stone columns are only somewhat stronger than in-situ material, and they are unable to transmit a bending moment along their length.

Currently, standard practice is to analyze the stability of embankments founded on ground treated with deep-mixed columns by using a composite shear strength based on the shear strength of the soil, the shear strength of the columns, and the area replacement ratio (CDIT 2002, EuroSoilStab 2002, Broms 1999, Kivelo 1998, Wei et al. 1990). In concept, this is the same approach as used for stone columns, however, there are several constraints placed on the analysis of deep-mixed foundations. The details of existing methods to perform stability analyses of embankments founded on deep-mixed columns are included as Appendix C.

Although shear failure is the assumed failure mode for existing methods of analysis, recent research by Kitazume et al. (1996) reveals that deep-mixed columns can fail in several different modes, including bending and tilting failure (CDIT 2002). Kivelo (1998) investigated the ultimate shear strength of lime-cement columns considering bending, but his approach is not currently incorporated into stability analysis procedures, mainly owing to lack of complete understanding of this phenomenon (Porbaha 2000). When slope stability is a concern for embankments founded on soil reinforced with columns, CDIT (2002) recommends that numerical analyses be performed concurrent with slope stability analyses to investigate displacements. Displacements from numerical analyses may provide designers an indication of whether failure mechanisms other than shear failure may occur.

A principle outcome of this research is to recommend that engineers use numerical stress-strain analyses to calculate the stability of embankments supported on columns installed by the deep mixing method. Such analyses do reflect the multiple realistic failure mechanisms that can occur

when strong columns are installed in weak ground. Detailed recommendations for performing numerical analyses in this application are presented.

Another important recommendation is that engineers should use reliability analyses in conjunction with numerical analyses of the stability of embankments supported on deep-mixing-method columns. Reliability analyses are necessary because deep-mixed materials are highly variable and because typical variations in clay strength can induce abrupt tensile failure in the columns, unless properly accounted for in design.

An additional benefit of reliability-based design is that it permits rational development of statistically based specifications for constructing deep-mixed materials. Such specifications can reduce construction contract administration problems because they allow for some low strength values while still provide assurance that the design intent is being met.

The primary purpose of this research is to develop reliable procedures that geotechnical engineers can use to analyze the stability of column-supported embankments. Although this research focused on columns installed by the deep mixing method, the stability analysis methods presented here are also expected to apply to vibro-concrete piles.

This dissertation begins with a literature review of stability of column-supported embankments, as presented in Chapter 2. Several preliminary investigations were performed to establish the methodology to analyze geotechnical problems with the software FLAC (Fast Lagrangian Analysis of Continua) (ITASCA 2002) in Chapter 3. Verification analyses were performed for the centrifuge experiments by Kitazume et al. (2000) in Chapter 4. Verification analyses were performed in both two and three dimensions for the centrifuge experiments by Inagaki et al. (2002) in Chapter 5. Chapter 6 describes numerical analyses of the instrumented test embankment at the intersection of US I-95 and Virginia State Route 1 in Alexandria, near Washington D.C. (Shiells et al. 2003, Stewart et al. 2004). The analysis results are in reasonably good agreement with the data from the experiments and the test embankment. A summary of key findings from these verification studies and the development of recommendations for stability analysis of column-supported embankments are included in Chapter 7. Compilation

and statistical analyses of data sets of strength and stiffness of deep-mixed materials reveal the random nature of deep-mixed materials and are included in Chapter 8. Reliability analyses incorporate the large variation of strength measured in deep-mixed columns in slope stability analyses, as presented in Chapter 9. The analysis of an example embankment in Chapter 9 illustrates how the combination of numerical analysis with reliability analysis is needed to completely understand the complex behavior of these systems. Design recommendations for practicing engineers are included in Chapter 10. A summary of the research, conclusions, and recommendations for further work are included in Chapter 11.

Relevant background information from the published literature is in the appendices. A procedure to analyze the stability of embankments founded on soft soil that has been improved with driven piles is included as Appendix A. Procedures for stability analysis of embankments founded on soft soil improved with stone columns are presented in Appendix B. A summary of previously published methods used in Japan and Scandinavia to analyze the stability of embankments founded on soft soil that has been improved with deep-mixed columns is included as Appendix C. Appendix D is a summary of published engineering properties of deep-mixed materials.

2. LITERATURE REVIEW

2.1. Introduction

This literature review was based on searches using Compendex®, Web of Science®, and other search engines, including those supported by the American Society of Civil Engineers, the Federal Highway Administration, and the Swedish Geotechnical Institute. The contents of relevant journals and conference proceedings were also surveyed. Much information has been published on the use of deep-mixing-method columns to support roadway embankments and similar structures. Five hundred literature sources have been collected for this study that include case histories, research, current state of the art reports, and design methodologies. However, many of these sources deal primarily with settlement control rather than issues related to the edge stability of these systems. Because this research is concerned with the edge stability of embankments founded on deep-mixing-method columns, articles related to issues of stability rather than settlement receive the most attention in this literature review. This chapter presents information published on this topic grouped into the following five categories; (1) installation and overview of deep-mixing columns, (2) property values and variability of deep-mixing-method materials, (3) analysis methods for stability of embankments supported on deep-mixed columns, (4) case histories and previous research, and (5) related columnar technologies. Obviously, some sources cover more than one of these categories.

2.2. Installation and overview of deep-mixed columns

Deep mixing includes a broad range of installation methods and technologies, most of which are proprietary. Several sources published in the last few years are devoted to construction equipment, installation, application, and cost of these technologies. The focus of this research is on the effectiveness of columns created by the deep mixing method for the edge stability of embankments, but readers interested in general aspects of deep mixing can refer to the sources listed in Table 2-1.

Table 2-1. References describing construction of deep-mixed columns

Reference	Title
Aoi (2002)	Execution procedure of Japanese dry method (DJM).
Bruce and Bruce (2003)	The practitioner's guide to deep mixing.
Burke (2002)	North American single-axis wet method of deep mixing.
Federal Highway Administration, FHWA-SA-98-086R	Demonstration project 116 Ground improvement technical summaries, Vols. I & II.
Hansbo and Massarsch (2005)	Standardization of deep mixing methods
Holm (2002)	Nordic dry deep mixing method execution procedure.
Nakanishi (2002)	Execution and equipment of cement deep mixing (CDM) method.
Porbaha (2001)	State of the art in construction aspects of deep mixing technology.
Porbaha (1998a)	State of the art in deep mixing technology; Part I. Basic concepts and overview.
Porbaha (1998b)	State of the art in deep mixing technology; Part II. Applications.
Stocker and Seidel (2005)	Twenty-seven years of soil mixing in Germany: The Bauer mixed-in-place-technique
Terashi (2002)	Development of deep mixing machine in Japan.
Yasui et al. (2005)	Recent technical trends in dry mixing (DJM) in Japan

2.3. Property values and variability of deep-mixing-method materials

An extensive review of literature containing property information resulting from deep mixing is presented in Appendix D. Some of the principal findings from Appendix D are summarized here.

The engineering properties of soils stabilized by the deep mixing method are influenced by many factors including the water, clay, and organic contents of the soil; the type, proportions, and amount of binder materials; installation mixing process; installation sequence and geometry; effective in-situ curing stress; curing temperature; curing time; and loading conditions. Given all

the factors that affect the strength of treated soils, the Japanese Coastal Development Institute of Technology (CDIT 2002) states that it is not possible to predict within a reasonable level of accuracy the strength that will result from adding a particular amount of reagent to a given soil, based on the in-situ characteristics of the soil. Consequently, mix design studies must be performed using soils obtained from a project site. Laboratory preparation and testing of specimens is discussed by Jacobson et al. (2005) for the dry method and by Filz et al (2005) for the wet method. Even relatively modest variations in binder materials may result in greatly different properties of the mixture. Also, field mixed and cured materials will differ from laboratory mixed and cured material. Construction contractors have experience relating the strength of laboratory mixed and cured specimens to the strength of field mixed and cured materials. Furthermore, engineering properties of mixtures are time dependent, due to long-term pozzolanic processes that occur when mixing cement or lime with soil. Design is generally based on the 28-day strength of the mixture.

Most strength and stiffness information about deep-mixed materials comes from unconfined compression tests. Numerous studies (Miura et al. 2002, CDIT 2002, Shiells et al. 2003, Dong et al. 1996, Matsuo 2002, Bruce 2001, Jacobson et al. 2005, EuroSoilStab 2002, Takenaka and Takenaka 1995, Hayashi et al. 2003) show that the unconfined compressive strength, q_u, of deep-mixed materials increases with increasing stabilizer content, increasing mixing efficiency, increasing curing time, increasing curing temperature, decreasing water content of the mixture, and decreasing organic content of the base soil. One interesting interaction of these factors is that increasing the water content of the mixture can increase mixing efficiency, so that in the case of low-water-content clays, adding water to the mixture can increase the mixture strength (McGinn and O'Rourke 2003). Nevertheless, it remains true that, for thoroughly mixed materials, a decrease in the water-to-cement ratio of the mixture produces an increase in the unconfined compressive strength.

For soils treated by the dry method of deep mixing, values of unconfined compressive strength may range from about 2 to 400 psi, and for soils treated by the wet method of deep mixing, values of the unconfined compressive strength may range from about 20 to 4,000 psi (Japanese Geotechnical Society 2000, Baker 2000, Jacobson et al. 2003). For a wet deep-mixing project at

the Oakland Airport in California, the minimum and average values of unconfined compressive strength were specified to be 100 and 150 psi, respectively (Yang et al. 2001). For the I-95/Route 1 interchange project, which also employed the wet method of deep mixing, the minimum and average values of unconfined compressive strength were specified to be 100 and 160 psi, respectively (Shiells et al. 2003, Lambrechts et al. 2003).

Variability of the unconfined compressive strength can be expressed in terms of the coefficient of variation, which is the standard deviation divided by the mean. Values of the coefficient of variation in the published literature for deep-mixed materials range from about 0.15 to 0.75 (Kawasaki et al. 1981, Honjo 1982, Takenaka and Takenaka 1995, Unami and Shima 1996, Matsuo 2002, Larsson 2005).

Secant values of Young's modulus of elasticity determined at 50% of the unconfined compressive strength, E_{50}, have been related to the unconfined compressive strength, q_u. For the dry method of deep mixing, values of the ratio of E_{50} to q_u have been reported in the range from 50 to 250 (Baker 2000, Broms 2003, Jacobson et al. 2005). For the wet method of deep-mixing, values of the ratio of E_{50} to q_u have been reported in the range from 75 to 1000 (Ou et al. 1996).

Reported values of Poisson's ratio for deep-mixed material ranges from 0.25 to 0.50 (CDIT 2002, McGinn and O'Rourke 2003, Terashi 2003, Porbaha et al. 2005).

The unit weight of soils treated by deep mixing is not greatly affected by the treatment process. For the dry method of deep mixing, Broms (2003) reports that the unit weight of stabilized organic soil with high initial water content can be greater than the unit weight of untreated soil and that the unit weights of inorganic soils are often reduced by dry mix stabilization. The Japanese CDIT (2002) reports that the total unit weight of the dry-mixed soil increases by about 3% to 15% above the unit weight of the untreated soil. CDM (1985) indicates that, for soils treated by the wet method of deep mixing, the change in unit weight is negligible. However, at the Boston Central Artery/Tunnel Project, McGinn and O'Rourke (2003) report that a significant decrease in unit weight occurred because the initial unit weight of the clay was relatively high and water was added to pre-condition the clay before mixing.

2.4. Analysis methods for stability of embankments supported on deep-mixed columns

Two reports published recently summarize most of what is currently known about embankments founded on DMM columns, and how these systems are implemented in practice: EuroSoilStab (2002), and CDIT (2002). A third report by Broms (2003) covers much of this material, and includes many ideas about the behavior of DMM columns that have been published over the past twenty-five years. All three of these references describe slope stability analysis methods that are based on limit equilibrium.

The stability of ground improved with deep-mixing-method columns is often analyzed using a short term, undrained analysis because the shear strengths of the columns and the soil between columns generally increase over time. A composite, or weighted average, undrained shear strength is used to evaluate slope stability for ground improved with columns, assuming complete interaction between stiff columns and the softer surrounding soil (Broms and Boman 1979). Embankment stability is typically analyzed assuming a circular shear surface as shown in Figure 2-1.
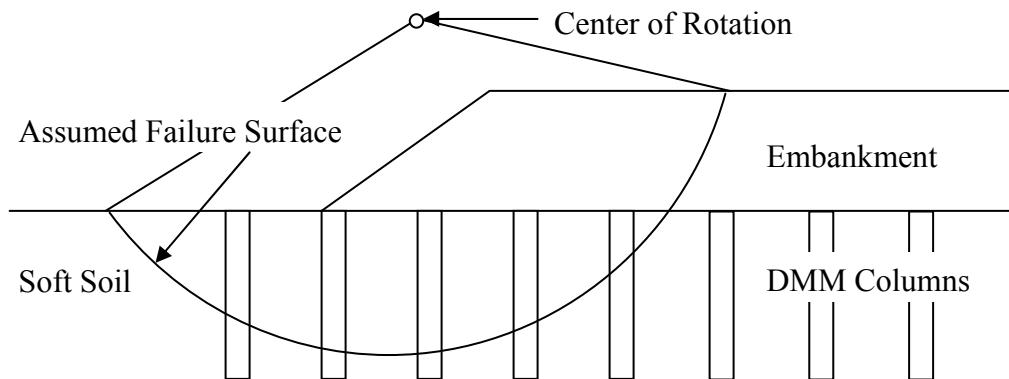
Figure 2-1. Circular sliding surface (after Broms and Boman 1979)

Broms and Boman (1979) recommended the composite shear strength analysis for lime piles, which are softer than the lime-cement and soil-cement columns in use today. The interaction of these stiffer and more brittle columns with the surrounding unstabilized soil may be different from the interaction in ground stabilized with lime columns, so the applicability of a composite

10

shear strength analysis to ground stabilized with lime-cement and soil-cement columns is uncertain (Broms 1999). High shear forces and bending moments can be transferred to the stiffer columns, causing the columns to fail in bending or by tilting (Kivelo and Broms 1999). Back calculations of a failed embankment in Scandinavia indicated that column strengths would need to be only 10% of the actual measured column strengths for shearing to account for the failure (Broms 2003). This indicates that other column failure modes were involved in the embankment failure.

Kivelo (1998) investigated the ultimate shear strength of lime-cement columns considering bending, but his approach is not currently incorporated into stability analysis procedures, mainly owing to lack of complete understanding of this phenomenon (Porbaha 2000). Rather, limitations are placed on the shear strengths used in the stability analysis. Furthermore, the use of isolated vertical deep-mixed columns is avoided under certain circumstances. Table 2-2 includes a list of adjustments and procedures that have been applied to permit safe design and construction of these composite foundations without analyzing all of the known failure mechanisms. These recommendations are described in detail in Appendix C.

Table 2-2. Design recommendations and procedures for deep-mixing-method columns

Item Number	Description
1	Account for Strain Incompatibility (CDIT 2002)
2	Impose Shear Strength Limits (EuroSoilStab 2002)
3	Use Residual Strengths (Kitazume et al. 2000)
4	Reduce Strength for Low Confining Pressures (Broms 1999)
5	Use Drained Strengths (EuroSoilStab 2002)
6	Use Combined Strength Envelopes (Drained and Undrained) (EuroSoilStab 2002)
7	Limit Isolated Columns to the Active Zone (EuroSoilStab 2002)
8	No Isolated Columns when Native Ground Steeper than 1v on 7h (EuroSoilStab 2002)
9	No Isolated Columns when Unimproved Foundation FS less than 1.0 (EuroSoilStab 2002)
10	Non-circular Failure Surface through Remolded Soil below Columns (Broms 2003)
11	Design Columns to Carry Full Embankment Load (Broms 2003)
12	Use Geosynthetic Layers to Prevent Lateral Deflection (Broms 2003)
13	Preload the Site (Broms 2003)
14	Check Block Sliding Stability (CDIT 2002)
15	Check Extrusion between Panels (CDIT 2002)
16	Perform a Finite Element Analysis (CDIT 2002)

In order to stabilize embankments, columns are often overlapped in rows constructed perpendicular to the centerline of the embankment. These rows of columns, also referred to as panels, are shown in Figure 2-2. Panels are often connected with longitudinal walls, sometimes referred to as shear walls. Such column arrangements are analyzed with the same stability analysis as isolated columns. Additional stability checks performed to insure global stability are also included in Appendix C.
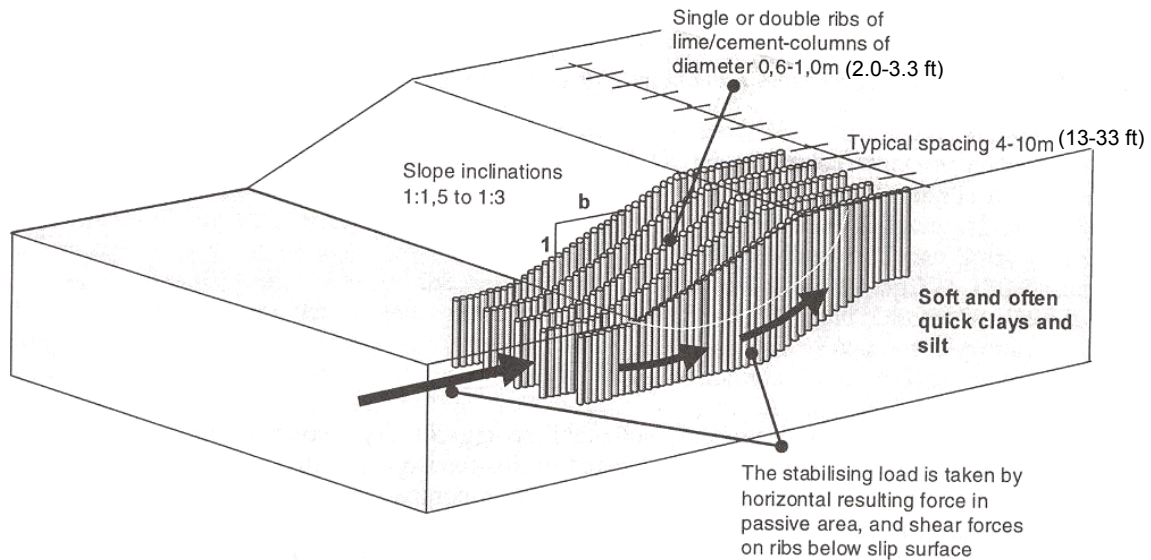
Figure 2-2. Slope stabilization with lime-cement columns (Watn et al. 1999)

2.5. Case histories and previous research performed

Although the design methods summarized above and described in detail in Appendix C only account for shear failure, work has been performed to investigate other failure modes of embankments founded on soft soil improved with DMM columns. Published work in this area consists of case histories of field performance, centrifuge test results, numerical analyses, state-of-practice reports, and other types of scholarly discussions on column behavior.

Although many case histories have been published illustrating the settlement reduction achieved with the use of DMM columns, few case histories document instances where these foundation systems exhibit slope stability problems. Terashi (2003) mentions that bending failure of DMM columns has happened in a couple of unreported cases. Broms (2003) evaluates two case histories in Scandanavia where he believes progressive stability failure has occurred. Kivelo (1998) also documents these two failures, and the original case histories were published in Swedish by Jacklin et al. (1994) and Arner et al. (1996).

An embankment constructed at the Island of Orust, Sweden failed during the final stage of construction. The six-meter-high embankment was placed on a one-meter crust overlying seven to twenty meters of soft marine clays. The embankment was constructed on 2.0-ft-diameter

13

lime/cement columns extended to a depth of 49-ft and arranged in a square pattern with 3.3 and 5.9-ft spacing. These arrangements result in area replacement ratios of 27 and 12 percent, respectively. The embankment experienced up to a meter of settlement, which was attributed to an edge stability failure.

A test embankment at Norral, Sweden experienced large vertical and horizontal displacements. These deflections were also attributed to an edge stability failure. The 26-foot-high embankment was placed on a three-foot crust overlying 25 to 30 feet of soft clay and organic silt. The embankment was constructed on 2.0-ft and 2.6-ft diameter lime/cement columns arranged in a square pattern beneath the center of the embankment, with panels used for the side slopes of the embankment. The 2.0-ft columns had a center-to-center spacing of 3.6-ft and the 2.6-ft columns had a center to center spacing of 4.6-ft. These arrangements result in area replacement ratios of 23 and 26 percent, respectively.

A list of field tests, centrifuge tests, and numerical analysis of embankments founded on columns is included as Table 2-3. Unfortunately, only a few of these investigations considered the slope stability of embankments founded on deep-mixed columns. Field tests included in this table use means other than columns to prevent slope failure, and they concentrate on settlement reduction. However, three series of centrifuge tests have been performed to evaluate the performance of DMM columns used to improve soft clay subject to embankment type loading: (1) Miyake et al. (1991), (2) Kitazume et al. (1996), and (3) Inagaki et al. (2002).

Table 2-3. Research into the behavior of column-supported embankments

Reference	Improvement Method	Test/Analysis	Loading
Alamgir et al. (1996)	Columnar inclusion	FEM	Embankment settlement
Almeida et al. (1985)	Staged construction	Centrifuge	Embankment
Asaoka et al. (1994)	SCP	Field case/FEM	Tank settlement
Aubeny et al. (2002)	Piles with geotextile	FEM	Embankment
Bai et al. (2001)	Soil -cement columns	FEM	Embankment settlement
Baker (1999)	Lime-cement columns	FEM	Embankment settlement
Balaam and Booker (1985)	Stone columns	FEM	Vertical
Ekstrom et al. (1994)	Soil -cement columns	Test fill	Settlement
Enoki et al. (1991)	SCP	Lab triaxial test	Composite shear
Han and Gabr (2002)	Piles	FDM	Settlement
Greenwood (1991)	Stone columns	Load tests	Vertical
Ilander et al. (1999)	Lime-cement columns	Test embankment/FEM	Settlement
Inagaki et al. (2002)	Cement columns	Centrifuge/FEM	Embankment
Jagannatha et al. (1991)	Stone columns	Load tests	Vertical
Jones et al. (1990)	Piles with geotextile	FEM	Embankment
Kaiqui (2000)	Cement columns	FEM	Embankment
Karastanev et al. (1997)	(Kitazume tests)		
Kempfert et al. (1997)	Piles with geotextile	FEM	Embankment settlement
Kempton et al. (1998)	Piles with geotextile	FDM	Embankment settlement
Kimura et al. (1983)	SCP	Centrifuge	Vertical
Kitazume et al. (2000)	Cement columns	Centrifuge/FEM	Vertical and lateral
Kitazume et al. (1996)	SCP	Centrifuge	Vertical and backfill
Long and Bredenberg (1999)	Lime-cement columns	FEM	Deep excavations
Miyake et al. (1991)	Cement columns	Centrifuge/FEM	Embankment
Rogbeck et al. (1998)	Piles with geotextile	FDM	Embankment settlement
Russel and Pierpoint (1997)	Piles with geotextile	FDM	Embankment settlement
Takemura et al. (1991)	SCP	Centrifuge	Embankment
Terashi et al. (1991)	SCP	Centrifuge/Full scale	Tank settlement
Terashi and Tanaka (1983)	Soil-cement columns	FEM	Settlement
Watabe et al. (1996)	SCP & pile	Centrifuge	Retaining structure

notes: SCP is sand compacted pile, FEM is finite element method, FDM is finite difference method

Miyake et al. (1991) performed centrifuge tests to model edge stability of an embankment supported by columns. Clay slurry was poured into the model box and consolidated with self-weight under a centrifugal acceleration of 80g. Cylindrical holes were excavated with a thin walled sampler and replaced with polyvinyl chloride bars intended to represent cement-treated soil columns. These tests were performed to investigate the effect that location of the treated zone has on embankment stability. The three patterns of improvement are listed in Table 2-4, and a schematic diagram is shown in Figure 2-3.

Centrifuge tests performed on the three improvement configurations illustrate the advantage of improving soil beneath the full height of the embankment rather than beneath the side slopes. Improvement pattern (a) located beneath the slope experienced large lateral deformations while cases (b) and (c) experienced no significant movement in the tests.

Table 2-4. Miyaki et al. (1991) test cases

Case No.	Diameter of Columns (in)	Number of Columns	Replacement Ratio (%)	Pattern
1	0.59	64	49.6	a
2	0.59	64	49.6	b
3	0.59	15+49	23.2, 38.0	c
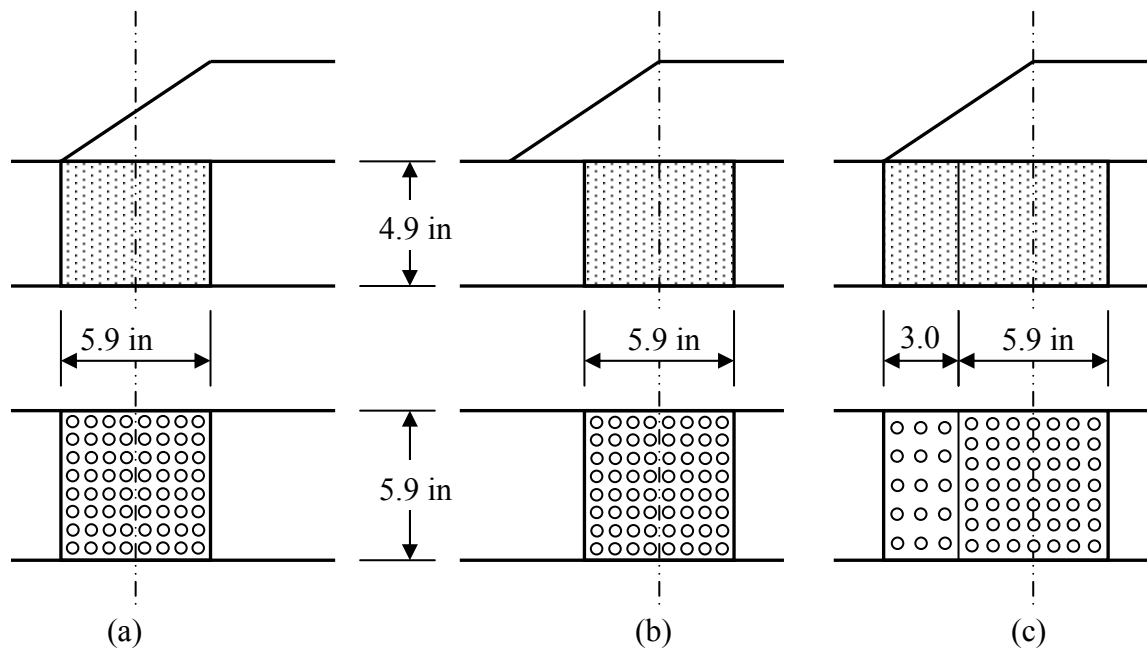
Figure 2-3. Miyaki et al. (1991) centrifuge test schematics

Kitazume et al. (1996) performed centrifuge tests using an inclined load on soft clay improved with soil-cement dowels that illustrate the effect failure modes other than slip surfaces have on stability. A drainage layer of sand was placed at the bottom of the model test box. Clay slurry was poured into forms at both ends of the model test box and consolidated under load on the laboratory floor. The columns were cast outside the model test box using soil-cement slurry and, after curing, they were arranged in a rectangular pattern in the middle of the box. Clay slurry

with higher water content was then pumped between columns. The schematic is included as
Figure 2-4.
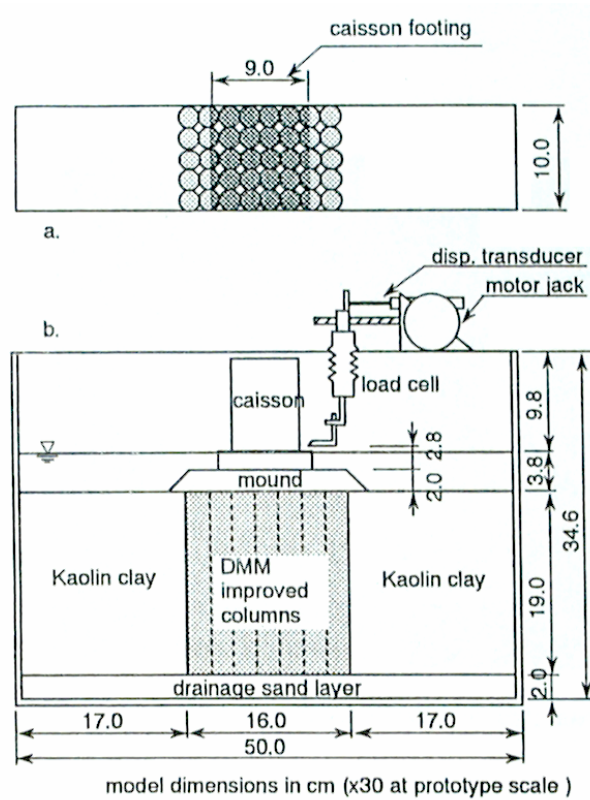
Figure 2-4. Model schematic (Kitazume et al. 1996)

Racking, or tilting of columns and bending failure in the columns can be seen in the photographs
of the centrifuge test results shown in Figure 2-5.   The horizontal and vertical loads causing
failure in the experiments were compared to the loads causing failure from a slope stability
analysis. The experimental loads were much smaller than the failure loads from the slope
stability analyses. When bending failure was included in the slope stability analyses, the results
matched experiments much more closely, as shown in Figure 2-6.
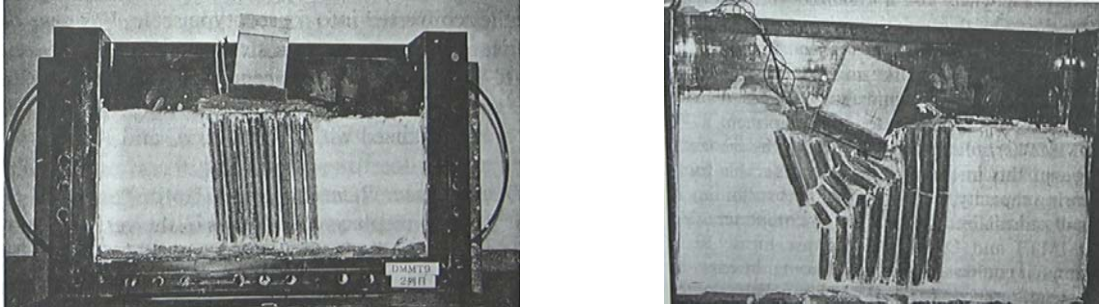
Figure 2-5. Column tilting and column bending (Kitazume et al. 2000)
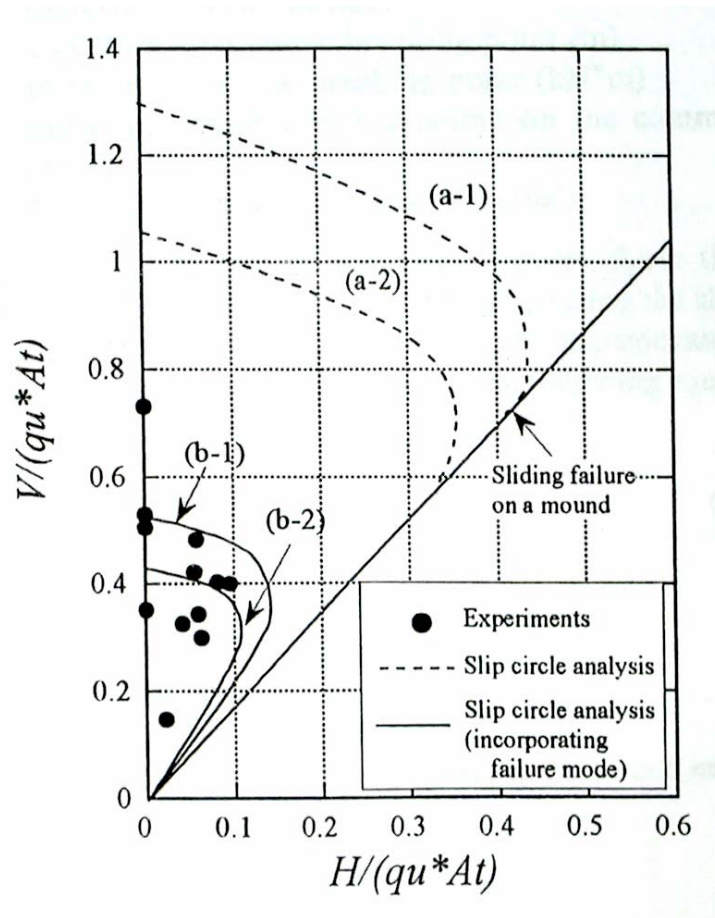
Figure 2-6. Slip circle analysis with and without bending failure mode

(after Kitazume et al 2000)

The dashed line (a-1) in Figure 2-6 corresponds to an undrained slope stability analysis assuming a circular shear surface with the shear strength of the columns equal to one-half the unconfined compressive strength. Due to the potential for progressive failure of these foundations, Terashi et al. (1983) recommend using residual shear strengths for stability analyses. Kitazume et al.

18

(2000) used a residual strength that is 80 percent of the design strength based on the work of Tatsuoka et al. (1983). The dashed line (a-2) incorporates this residual strength. Still, measured failure loads were much smaller than indicated by this analysis. The solid lines (b-1) and (b-2) represent the results of stability analyses incorporating bending failure for the design and residual strengths, respectively. It can be seen that line b-2 is in reasonable agreement with the experimental results. Kitazume et al. (2000) include a rough approximation of bending failure in the stability analyses. The method of stability analysis used to develop lines (b-1) and (b-2) in Figure 2-6 is not intended as a predictive measure of failure.

Finite element analyses were also used to model the experiments. Kitazume et al. (2000) used Mohr-Coulomb properties for the clay and elastic properties for the columns. This approach could not model bending failure in the columns, but it did effectively model column tilting. The researchers determined that tilting failure depended on clay strength outside the zone improved by columns.

Inagaki et al. (2002) performed centrifuge tests to show the effect that deep-mixing columns had on soft clay foundations for embankments. A schematic diagram of their tests is included as Figure 2-7. The centrifuge model was created by pouring clay slurry over a compacted sand base and allowing the clay to consolidate under normal gravity. Columns were installed in the model by coring holes in the clay and filling them with soil-cement slurry. Three experiments were performed with different column geometries used to support the slope. Two cases were run with columns extending down to the base sand layer. These tests showed bending failure of the interior columns and tilting failure of columns at the toe. One case was configured with columns stopping short of the base sand layer. These "floating" columns did not show bending or tilting failure; however, they did experience larger lateral deflections.

Inagaki et al. (2002) performed numerical analyses of the centrifuge tests using a finite element model. The soft clay was modeled using a water-soil coupled, elasto-plastic model known as the Sekiguchi/Ohta Model. This is a modified cam-clay model that incorporates soil anisotropy. The embankment and columns were modeled as elastic materials. The two-dimensional plane-strain model was able to match column deflections very closely.
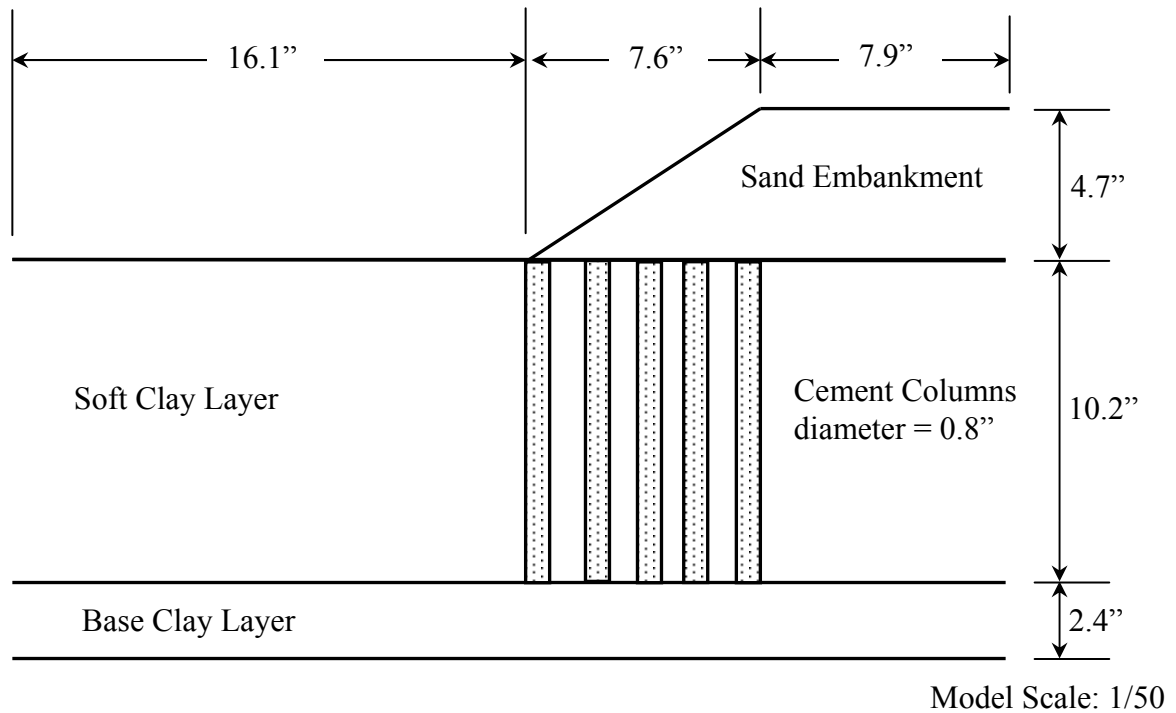
Figure 2-7. Inagaki et al. (2002) centrifuge test schematic

A research dissertation (Kivelo 1998) addressed the edge stability of embankments founded on lime-cement columns, and incorporated moment capacity into a limit equilibrium analysis with a non-circular shear surface. He resolved the limiting horizontal force acting along the shear surface that could be carried by columns based on several possible failure mechanisms shown in Figure 2-8. These failure mechanisms were originally developed by Broms (1972) when he addressed the use of piles to stabilize slopes. Failure mode d in Figure 2-8 represents flow of the soil around intact columns.

Kivelo (1998) provides equations for these failure modes; however, there are some obstacles to implementing them in a slope stability analysis. The presence of columns changes the location of the critical failure surface, so the equations need to be incorporated into a computer program to search for the critical failure surface. The equations determine a horizontal force applied at the location of the failure surface. It is very conservative to only include the horizontal component of the resisting force acting along the shear surface for steep inclinations of the failure surface. The failure modes based on bending failure require values of the allowable bending capacity for columns, and there is substantial uncertainty in the bending capacity of

deep-mixed columns. Kivelo (1998) presents a method to determine the bending capacity of columns based on the plasticized area of the column, but does not explain how to find that area. The bending capacity is determined using an assumption that the columns have no tension capacity.
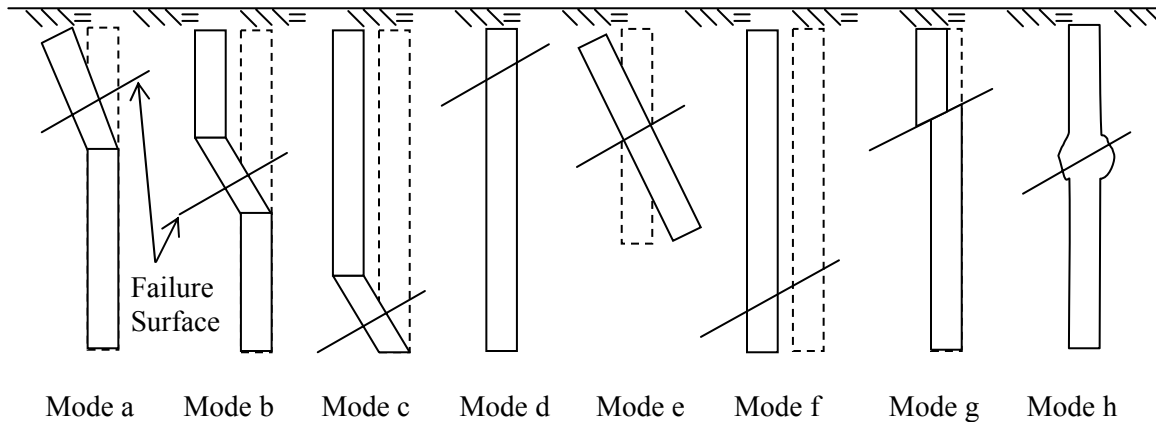
Figure 2-8. Failure mechanisms for deep-mixing-method columns (Kivelo 1998)

Kivelo and Broms (1999) state that embankments founded on soft soils and improved with brittle, stiff columns will fail in a progressive manner. This behavior was noted in the centrifuge tests performed by Kitazume et al. (1996). As the failing soil mass begins to strain, stresses concentrate in the first row of columns. If the first row of columns fails to arrest the sliding mass, load is then concentrated on the second row of columns. Broms (2003) applies a method to evaluate progressive failure to the two documented failures in Scandinavia mentioned above. Although this method is interesting, it has not been validated by testing or investigated by other authors.

2.6. Related columnar technologies

There is much information in the literature that can be applied to the edge stability of columns used to support embankments that is written about technologies other than deep mixing. These technologies include stone columns used to support embankments, pile-supported embankments, and piles used to stabilize slopes.

2.6.1. Stone columns

Stone columns and sand columns, which are similar ground improvement technologies, result in a vertical column of material that is stronger than the surrounding native soil. These methods of ground improvement have been used successfully to enable embankment construction over deposits of soft soil. An FHWA manual (Barksdale and Bachus 1983) clearly summarizes design methodology for stone columns used for embankment construction, including edge stability analyses. Sand columns, which have been used in Japan, follow the same design methodologies as are used for stone columns. The analysis methods for embankments founded on soft soil improved with stone columns are included as Appendix B.

It is useful to understand the work that has been done with stone columns because the design methods are very similar to those used for deep-mixed columns. Concepts such as area replacement ratio, composite strength, and stress concentration apply to both technologies. Appendix B describes how to perform the slope stability analysis of an embankment founded on stone columns using limit equilibrium slope stability analysis programs. Some of the concepts related to analysis of embankments on stone columns have been applied in this research to limit equilibrium or numerical analyses of the stability of embankments founded on deep-mixed columns.

2.6.2. Pile-supported embankments

Piles are designed to carry the full weight of the embankment. Appendix A describes how to perform the slope stability analysis of an embankment founded on piles. Filz and Stewart (2005) covers the design aspects required to transfer embankment loads to the pile foundation with a bridging layer. Many case histories are in the literature for geotextile reinforced, pile supported (GRPS) embankments. These case histories have been summarized by Aubeny and Briaud (2003) and included here as Table 2-5.

Piled raft foundations are somewhat similar to pile supported embankments. Numerous articles have been published on piled raft foundations, which are not covered here, other than to include the modulus values recommended by Poulos (2002) for soil beneath the raft, based on the work of Decourt (1989,1995). The soil Young's modulus below the raft is twice the value N from a

standard penetration test in MPa (20.9 times N in tsf). The soil Young's modulus along the piles and below the piles is three times the value N in MPa (31.3 times N in tsf).

Table 2-5. Case histories for GRPS embankments (from Aubeny and Briaud 2003)

Case No.	Reference	Application	Soil condition	Pile type	Geosynthetic type	Design parameters
1	Reid et al. (1983)	Near bridge abutment	Soft clay	Concrete dis-placement pile	Membrane (paraweb)	H=10m, s=3.5-4.5m, a=1.1-1.5m, P_c=5-14%, N=1
2	Barksdale et al. (1983)	Railway	Very soft peat	Rigid stone columns	Fabric	H=7.6m,s=1.6-2.2m,d=0.51-0.56m,T=0, P_c=6-8%, N=1
3	Jones et al. (1990)	Railway	Very soft allu-vium and peat.	Semi-precast concrete pile.	Geotextile "Paralink"	H=3-5m, s=2.75m,a=1.4m, T=0.5m, P_c=20%, N=1
4	Tsukada et al. (1993)	Street pavement	Peat	Concrete pile	Geogrid "Tensar SS2"	H=1.5m, s=2.1m, d=0.8m, P_c=11%, N=1,T=0
5	Holtz et al. (1993)	Pavement	Uniform grey clay	Timber pile	Geotextile "multifilament	H=5-6m,s=1.5m,a=1m, P_c=44%, N=3
6	Bell et al. (1994)	Toll Plaza	Highly com-pressible peat and es-tuarine clay	VCC The columns.	Tensar SS2 geo-grid	H=2.5-6.0m,s=2.2-2.7m, d=0.4m, N=2
7	Card et al. (1995)	Docklands Light Railway (DLR)	Silty organic clay, Peat and Clay/sand	Driven or con-tinuous flight au-gured piles	Biaxial Tensar SS2 geogrid	H=2.5-3m,s=3m, a=1m, N=3, d=0.45m.
8	Topolnicki (1996)	Highway and tramway	Loose fill, peat Organic clay	VCC	Geogrid "Tensar SS1" and 'Tensar SS2"	H<1.5m,s=1.8-2.5m, d=0.55m, P_c =9-17%, N=2-3, T=0
9	Brandl et al. (1997)	Railway	Peat and organic silt	Driven pile	Geogrid	H>2m, s=1.90m,d=0.118m, a=1.0m, P_c =35%, N=3.
10	Geo-Institute (1997)	Highway em-bankment bridge abutment	A mixture of soft clays, silts and sands with bands of peat	VCC/Stone columns	Geotextile	H<7m, s=1.6m for VCC and s=2.2m for stone column. N=1.
11	Jenner et al (1998)	Bypass	Peat and soft silty alluvial strata	VCC	Tensar SS1 and Tensar SS2 geogrid	H=4-7m,s=2.05-2.35, d=0.45m,a=0.75m,N=2-3.
12	Rogbeck et al. (1998)	Full scale testing.	Loose silt and fine sand	Precast concrete pile	Geogrid	H=1.7m, s=2.4m, a=1.2m, P_c=25%,N=1
13	Kuo, et al. (1998)	MSE Walls	Very soft waste clay	Timber pile.	Geotextile	H=6m,s=1.5m,d=0.3m, P_c=3%, N=2.
14	Alzamora et al. (2000)	Segmental re-taining walls	0 to 1 blow count organic silt and clay	Jet grout column	Uniaxial Geogrid	H=2-8.2m, s=3m, d=1.2m, P_c =13%, N=3

Note: H- embankment fill height; s-pile spacing at centers; d-pile diameter; a- cap width; T- cap thickness; c-cushion thickness; e-efficacy (%); P_c-percent coverage of pile caps; N- number of geosynthetic layers; VCC- vibro concrete column; Efficacy- defined percentage of the embankment load carried by pile cap.

2.6.3. Piles used to stabilize slopes

Viggiani (1981) provides a summary of the use of piles to stabilize landslides. Piles have been used in slopes for over 100 years, even though a well established and widely used design

procedure is still to be developed. Although Vigianni notes that some failures have occurred (Root 1958, Baker and Marshall 1958), there have also been successes (DeBeer and Wallays 1970, Ito and Matsui 1975, Sommer 1977, Fukuoka 1977). Essentially, the design of these piles is a three step process; (1) determine the shear force required to increase the factor of safety by the desired amount, (2) evaluate the maximum shear force that each pile can receive from the sliding soil and transmit to the stable underlying soil, (3) select the type and number of piles and their most appropriate locations on the slope.

Step (1) generally uses limit equilibrium to determine the resisting force required. Generally, piles are used when only a small increase in stability is required. If the factor of safety is one, it is possible to evaluate the shear force needed to increase the factor of safety by the desired amount. If the factor of safety is anything other than one, Hutchinson (1977) describes the difficulty of assessing existing stability and improvement.

There are several different approaches used to determine the resisting force in step (2):

- Consider the piles as cantilevers provided they penetrate into stable soil 1/3 their length (Baker and Yoder , 1958).
- Calculate the force based on rupture conditions, and estimate a range of yield values for the pile-soil interaction (DeBeers and Wallays 1970, DeBeer 1949, Brinch Hansen 1961)
- Apply a theory of plastic deformations or viscous flow. This determines the force acting on piles in a row when soil is forced to squeeze between piles. Ito and Matsui (1977) determined the soil force acting on piles above the critical surface as a function of soil strength, pile diameter, spacing, and position.
- Introduce a coefficient of horizontal subgrade reaction, which determines pile-soil interaction (Fukuoka 1977).
- Evaluate the ultimate load of a vertical pile acted upon by a horizontal load for cohesive soil (Broms 1964).

Hassiotis and Chameau (1984) present a procedure to analyze piles used to stabilize slopes that determines forces acting on piles above the critical surface based on plastic equilibrium and

determines forces acting on piles below the critical surface based on subgrade reaction. The authors also provide a computer program to perform these calculations.

Reese et al. (1992) present a four step method to analyze drilled shafts used to stabilize slopes;

1) Estimate loads due to earth pressures.

2) Assess the resistance of soil below the sliding surface.

3) Estimate the response of the drilled shaft – above and below the sliding surface.

4) Estimate factor of safety for the slope reinforced with drilled shafts.

Vigianni expands on the approach taken by Broms (1964) to investigate the pile resistance in a soft layer of known thickness, overlying a firm underlying soil. The shear surface is assumed to be between the two layers, and both the force acting on the upper part of the pile and the force acting on the lower part of the pile can be determined using Equation 2-1.

$$p_y = k \, c \, d \, L \tag{2-1}$$

where p_y is the horizontal load in the pile, d is the pile diameter, L is the length of pile either above or below the failure surface, c is the cohesion either above or below the failure surface, and k is a bearing capacity factor. It is interesting to note that Reese (1958) found k to be about 2 at the soil surface and to increase with depth until reaching a constant value at $3d$. Broms (1964) uses a simplified pattern with p_y equal to zero at the ground surface and increasing with depth until reaching a constant value at $1.5d$. When this type of failure mode is applied to deep-mixing-method columns, Kivelo (1998) recommends using a k value of 9.

Broms (1972) presented multiple failure mechanisms for piles, for which equations were later applied to deep-mixed columns used to support embankments (Kivelo 1998) and summarized in Section 2.5.

3. FINITE DIFFERENCE ANALYSIS

3.1. Introduction

Finite difference is a method of numerical analysis that can be used to solve differential equations, including the equations of motion for deformable bodies. Fast Lagrangian Analysis of Continua (FLAC) is a proprietary program that solves these equations and is commonly used to perform numerical analyses of geotechnical problems. The Lagrangian approach to continuum mechanics incorporates stress, strain, and the relationship between stress and strain. In engineering, where problems are of a large spatial extent relative to particle size, it is advantageous to model these problems with properties that are representative of continua rather than attempt to model the behavior of isolated particles that constitute that continuum.

Itasca Consulting Group, Inc. produces both a two-dimensional finite difference program called FLAC^{2D} (Itasca 2002a), and a three-dimensional finite difference program called FLAC^{3D} (Itasca 2002b). There are some differences between these two programs, but analyses performed with the two-dimensional program can be duplicated with the three-dimensional program, and this chapter uses the term FLAC in reference to both programs.

Because numerical analyses are sensitive to material modeling and numerical modeling issues, it is important that verification analyses be performed. It is also important that principles of mechanics be followed to avoid getting the right answers for the wrong reasons. In this research, numerical analyses of the I-95/Route 1 test embankment and published centrifugal model studies were performed to verify suitability of the analysis methods employed, as described in Chapters 4 through 6.

This chapter describes the methodology used by FLAC and presents the results of preliminary investigations used to establish the methodology to analyze the geotechnical problems that are the subject of this research. Where possible, numerical analysis results are compared to results from other methods of analysis to verify analysis procedures.

3.2. Basic mechanics of FLAC

In FLAC, loads are applied and deflections are determined through a stepping process based on the equations of motion. A schematic of the incremental process used in every step is shown in Figure 3-1. This incremental approach allows for modeling large deflections, which is not a capability of many finite element codes. FLAC is also capable of capturing progressive failure, where soil loads are redistributed as columns fail.
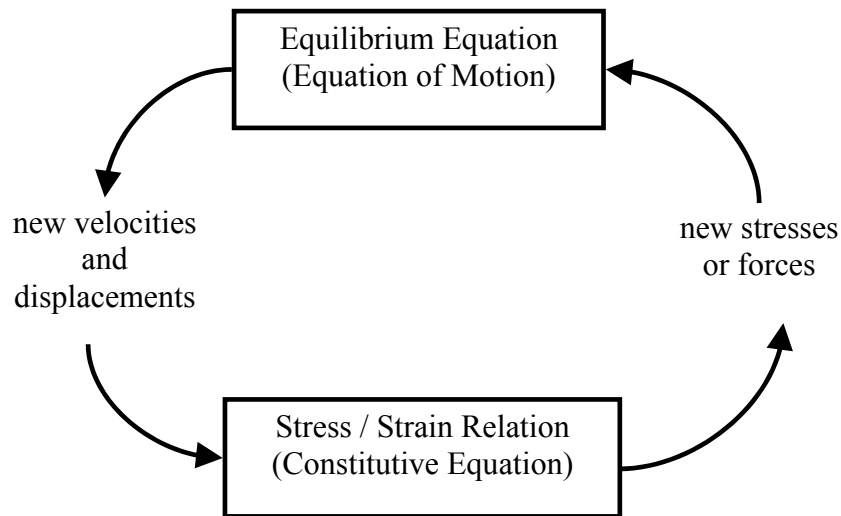
Figure 3-1. Incremental formulation used in FLAC (Itasca 2002a)

Strains and stresses are determined at nodes in the finite difference method of analysis. Conceptually, the nodes are connected by a series of springs, where constitutive models dictate spring response. These constitutive models are defined by the user to represent soil, and any other materials, in the zones between nodes. The FLAC constitutive models used in this research include: Elastic, Modified Cam Clay, Mohr-Coulomb, and the Ubiquitous Joint Model. All four of these models have a region where material response is defined by elastic behavior. The Modified Cam Clay model has an elastic region up to a cap, beyond which soil experiences strain-hardening behavior. The Mohr-Coulomb model has an elastic region up to a failure surface defined by the Mohr-Coulomb criteria (c, ϕ). Shear stresses at failure result in perfectly plastic behavior. The Ubiquitous Joint Model is the Mohr-Coulomb Model with planes of weakness acting in a specified direction.

3.3. Stress and strain invariants

Constitutive models in FLAC are formulated using stress invariants p and q, which represents normal and shear stresses, respectively, and the strain invariants ε_v and ε_s, which represent volumetric and shear strains, respectively. These stress and strain invariants relate to principal stresses and principal strains shown in Equations 3-1 through 3-4.

$$p = \frac{\sigma_1 + \sigma_2 + \sigma_3}{3} \tag{3-1}$$

$$q = \frac{1}{\sqrt{2}} \sqrt{(\sigma_1 - \sigma_2)^2 + (\sigma_2 - \sigma_3)^2 + (\sigma_1 - \sigma_3)^2} \tag{3-2}$$

$$\varepsilon_V = \varepsilon_1 + \varepsilon_2 + \varepsilon_3 \tag{3-3}$$

$$\varepsilon_S = \frac{\sqrt{2}}{3} \sqrt{(\varepsilon_1 - \varepsilon_2)^2 + (\varepsilon_2 - \varepsilon_3)^2 + (\varepsilon_1 - \varepsilon_3)^2} \tag{3-4}$$

3.3.1 Axi-symmetric conditions

For axi-symmetric conditions, where $\sigma_2 = \sigma_3$ and $\varepsilon_2 = \varepsilon_3$, the expressions in Equations 3-1 through 3-4 reduce to Equations 3-5 through 3-8.

$$p = \frac{\sigma_1 + 2\sigma_3}{3} \tag{3-5}$$

$$q = \sigma_1 - \sigma_3 \tag{3-6}$$

$$\varepsilon_V = \varepsilon_1 + 2\varepsilon_3 \tag{3-7}$$

$$\varepsilon_S = \frac{2}{3}(\varepsilon_1 - \varepsilon_3) \tag{3-8}$$

3.3.2. Plane-strain conditions

The invariants commonly used in geotechnical engineering when considering plane-strain problems are shown in Equations 3-9 through 3-12. These are known as MIT invariants, and they are not the same as the invariants defined in Equations 3-1 through 3-4.

$$p = \frac{\sigma_1 + \sigma_3}{2} \tag{3-9}$$

$$q = \frac{\sigma_1 - \sigma_3}{2} \tag{3-10}$$

$$\varepsilon_V = \varepsilon_1 + \varepsilon_3 \tag{3-11}$$

$$\varepsilon_S = \varepsilon_1 - \varepsilon_3 \tag{3-12}$$

Most soils laboratories in the United States present test results using MIT invariants. However, MIT invariants do not account for out of plane stress, σ_2, and are not used in the FLAC programs. FLAC uses the invariants listed in Equations 3-1 through 3-4 for plane-strain analyses.

Hooke's law, which is presented in Equation 3-13, can be used to account for the out of plane stress for incremental loading in the plane-strain condition.

$$\begin{Bmatrix} d\sigma_1 \\ d\sigma_2 \\ d\sigma_3 \end{Bmatrix} = \begin{bmatrix} K + \frac{4}{3}G & K - \frac{2}{3}G & K - \frac{2}{3}G \\ K - \frac{2}{3}G & K + \frac{4}{3}G & K - \frac{2}{3}G \\ K - \frac{2}{3}G & K - \frac{2}{3}G & K + \frac{4}{3}G \end{bmatrix} \begin{Bmatrix} d\varepsilon_1 \\ d\varepsilon_2 \\ d\varepsilon_3 \end{Bmatrix} \tag{3-13}$$

where K = Bulk Modulus and G = Shear Modulus

By setting $d\varepsilon_2 = 0$ for the case of plane-strain, and using the stress invariants p and q and the strain invariants ε_v and ε_s, this matrix simplifies to Equation 3-14 and Equation 3-15. This derivation is presented as Figure 3-2.

$$dp = Kd\varepsilon_v \tag{3-14}$$

$$dq = 3Gd\varepsilon_s \tag{3-15}$$

$$\text{i.} \quad d\sigma_1 = \left(K + \frac{4}{3}G\right)d\varepsilon_1 + \left(K - \frac{2}{3}G\right)d\varepsilon_3$$

$$d\sigma_2 = \left(K - \frac{2}{3}G\right)d\varepsilon_1 + \left(K - \frac{2}{3}G\right)d\varepsilon_3$$

$$d\sigma_3 = \left(K - \frac{2}{3}G\right)d\varepsilon_1 + \left(K + \frac{4}{3}G\right)d\varepsilon_3$$

$$\text{ii.} \quad dp = \frac{d\sigma_1 + d\sigma_2 + d\sigma_3}{3}$$

$$\text{iii.} \quad 3dp = 3Kd\varepsilon_1 + 3Kd\varepsilon_3$$

$$\text{iv.} \quad d\varepsilon_V = d\varepsilon_1 + d\varepsilon_3 \qquad d\varepsilon_2 = 0$$

$$\text{v.} \quad dp = Kd\varepsilon_v$$

$$\text{vi.} \quad dq = \frac{1}{\sqrt{2}}\sqrt{(d\sigma_1 - d\sigma_2)^2 + (d\sigma_2 - d\sigma_3)^2 + (d\sigma_1 - d\sigma_3)^2}$$

$$\text{vii.} \quad 2dq^2 = (2G)^2 d\varepsilon_1^2 + (-2G)^2 d\varepsilon_3^2 + (2Gd\varepsilon_1 - 2Gd\varepsilon_3)^2$$

$$\text{viii.} \quad dq^2 = 4G^2 d\varepsilon_1^2 - 4G^2 d\varepsilon_1 d\varepsilon_3 + 4G^2 d\varepsilon_3^2$$

$$\text{ix.} \quad dq = \sqrt{2}\sqrt{2G^2 d\varepsilon_1^2 - 2G^2 d\varepsilon_1 d\varepsilon_3 + 2G^2 d\varepsilon_3^2}$$

$$\text{x.} \quad dq = G\sqrt{2}\sqrt{(d\varepsilon_1 - d\varepsilon_3)^2 + d\varepsilon_1^2 + d\varepsilon_3^2}$$

$$\text{xi.} \quad d\varepsilon_S = \frac{\sqrt{2}}{3}\sqrt{(d\varepsilon_1 - d\varepsilon_3)^2 + (d\varepsilon_1)^2 + (d\varepsilon_3)^2} \qquad d\varepsilon_2 = 0$$

$$\text{xii.} \quad dq = 3Gd\varepsilon_s$$

Figure 3-2. Application of Hooke's law to plane-strain analyses

3.4. Hand check with FLAC models

Some hand checks of FLAC can be performed using straightforward expressions that relate principal stresses and principal strains.

3.4.1. Elastic Model

A 1 ft x 1 ft element supported as shown in Figure 3-3 is subjected to a distributed vertical load of $\Delta\sigma_v = 2070$ psf. The values of $E = 5$ x 10^6 psf, and $\nu = 0.3$ were used. The initial stress

30

conditions are irrelevant if the material is in equilibrium prior to loading, and deflections are only a consequence of additional loading for a linear elastic material.

Distributed load, σ_y = 2070 psf
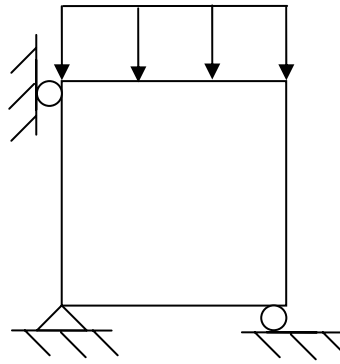
Figure 3-3. Unconfined compression of elastic element

The specimen is 2-foot diameter, and one foot high. The radial strain, ε_2, is obtained from Equation 3-16 using $\sigma_1 = 2070$ psf.

$$\varepsilon_2 = \frac{1}{E}\left[\sigma_2 - v(\sigma_1 + \sigma_3)\right] \qquad (3\text{-}16)$$

From Equation 3-16, $\varepsilon_2 = 0.0001242$.

The vertical strain, ε_1, is obtained from Equation 3-17.

$$\varepsilon_1 = \frac{1}{E}\left[\sigma_1 - v(\sigma_2 + \sigma_3)\right] \qquad (3\text{-}17)$$

From Equation 3-17, $\varepsilon_1 = -0.000414$.

The horizontal and vertical strains calculated with FLAC are identical to the values obtained from hand calculations:

$\varepsilon_y = -4.14 \times 10^{-4}$

$\varepsilon_x = 1.242 \times 10^{-4}$

Horizontal constraints are implied on the left side of the model for axi-symmetric conditions, and the same results are obtained with or without specifying these constraints in FLAC.

3.4.1.2. *Plane-strain analysis*

In this case, the lateral strain, ε_3, is obtained from Equation 3-18.

$$\varepsilon_3 = \frac{1+v}{E}\left[\sigma_3(1-v)-v(\sigma_1)\right] \tag{3-18}$$

From Equation 3-2a, $\varepsilon_3 = 0.00016146$.

The vertical strain, ε_1, is obtained from Equation 3-19.

$$\varepsilon_1 = \frac{1+v}{E}\left[\sigma_1(1-v)-v(\sigma_3)\right] \tag{3-19}$$

From Equation 3-19, $\varepsilon_1 = -0.0003767$.

The horizontal and vertical strains calculated with FLAC are identical to the values obtained using hand calculations:

$\varepsilon_y = -3.765 \times 10^{-4}$

$\varepsilon_x = 1.615 \times 10^{-4}$

The plane-strain problem was also run without using the horizontal constraints. This resulted in a vertical displacement of -3.765×10^{-4} ft, and a lateral displacement of 8.075×10^{-5} ft in both directions (half the value determined for the properly constrained problem in each direction). Generally, it is important to properly constrain the problems for analysis, but it is interesting to note that a horizontal constraint was not required for this FLAC analysis.

3.4.2. Modified Cam Clay model

A single element was analyzed with the Modified Cam Clay model in FLAC and compared to hand calculations, which were performed with a spreadsheet. This investigation includes both drained and undrained loading under both axi-symetric and plane-strain conditions. Initially, the

element is subjected to a vertical stress of 1050 psf and a horizontal stresses of 450 psf, as shown in Figure 3-4. Properties for the clay are as shown in Table 3-1.

Distributed load, σ_y = 1050 psf

Distributed load,
$\sigma_x = \sigma_z$ = 450 psf
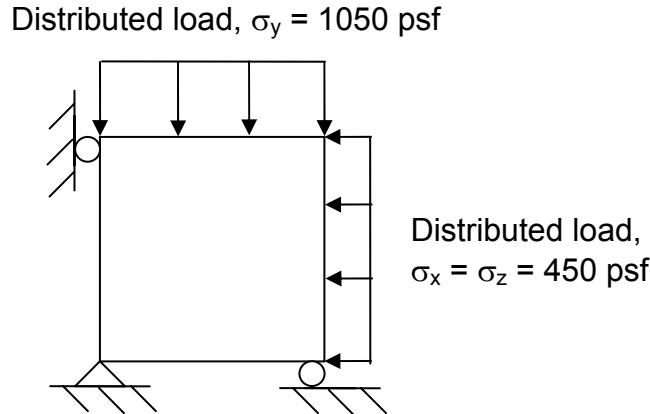
Figure 3-4. Compression of Modified Cam Clay element

Table 3-1. Clay material properties

γ (pcf)	M	ν	λ	κ	e	k (cm/s)	mpc (psf)	mp1 (psf)	mv_1
119	1.8	0.3	0.116	0.019	2.17	1.8×10^{-3}	1000	644	3.16

For the axi-symmetric analysis in undrained loading, a constant downward velocity was applied until the element reached the critical state line, which occurred with an additional vertical load of 344 psf. At this point, the element was subjected to a total vertical pressure of 1394 psf, and a total horizontal pressure of 450 psf. From that point on the critical state line, the sample was allowed to drain under constant total stress. The effective stress path for this sequence of loading is shown in Figure 3-5.

Figure 3-5 also includes the stress path for the drained, axi-symmetric analysis in which the element was subjected to a vertical stress increment of 344 psf.

Figures 3-5 through 3-7 show how FLAC and the spreadsheet calculations match for axi-symmetric analyses in both drained and undrained loading by comparing the path of the invariants p, q, ε_v, and ε_s.
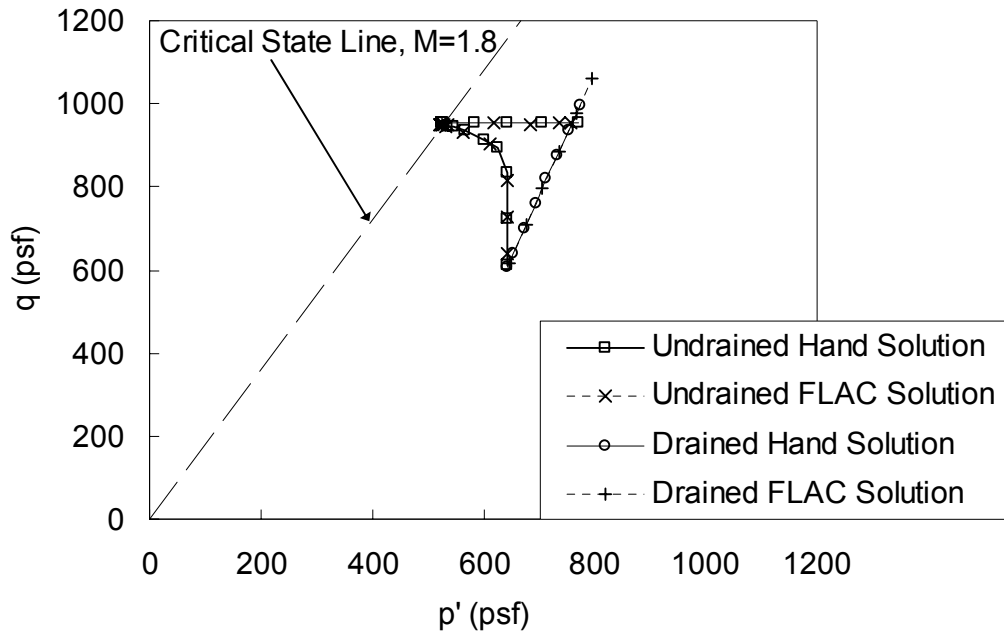
Figure 3-5. Modified Cam Clay model – axi-symmetric conditions p'-q plot
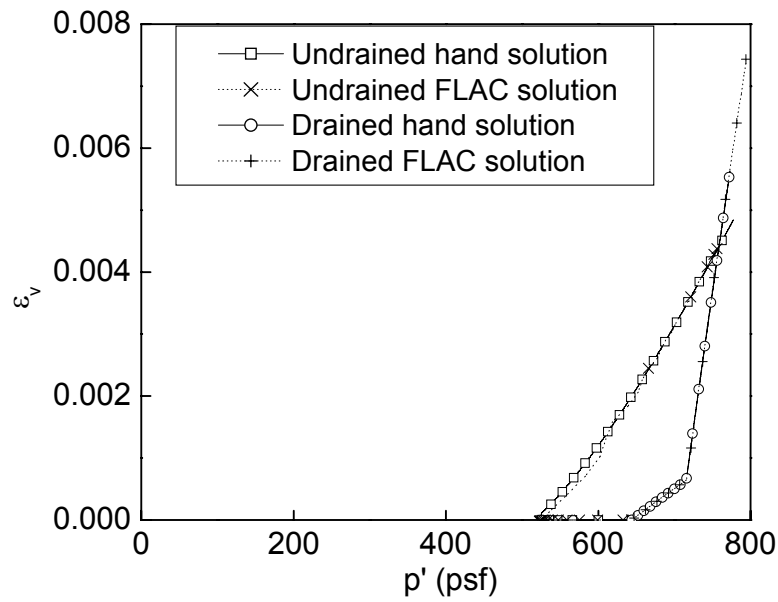
Figure 3-6. Modified Cam Clay model – axi-symmetric conditions p'-ε_v plot
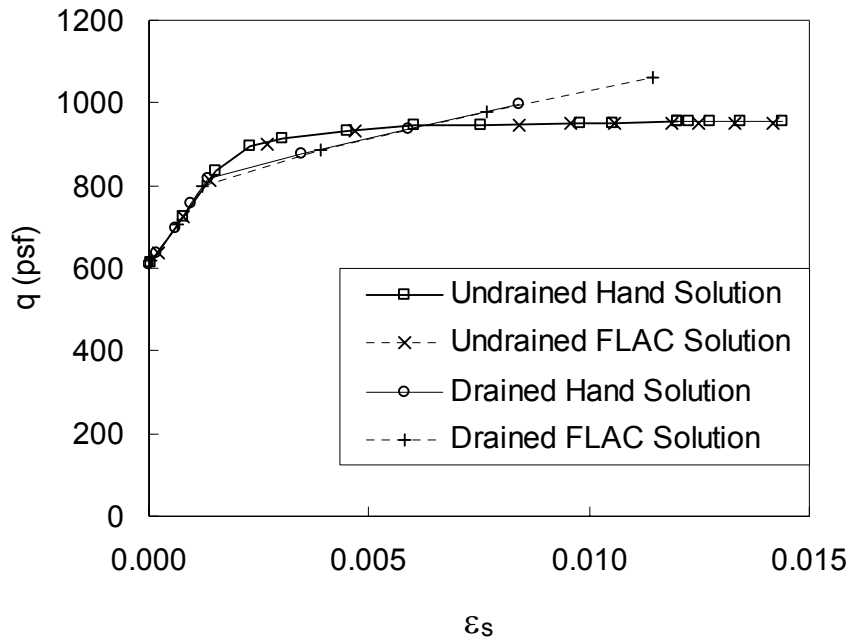
Figure 3-7. Modified Cam Clay model – axi-symmetric conditions q-ε_s plot

In order to compare FLAC results with hand calculations for the plane-strain condition, the hand calculations used the Poisson's ratio value in Table 3-1 to calculate the out of plane stress, σ_2, in the elastic region. In the elasto-plastic region, the hand solution was formulated to calculate σ_2 in addition to the stress invariants, p and q, based on the cap in the Modified Cam Clay model. Knowing σ_2, the invariants p, q, ε_v, and ε_s were then related to principle stresses and strains using Equations 3-1 through 3-4. A spreadsheet was created to implement this hand calculation procedure. Figures 3-8 through 3-10 show how FLAC and the spreadsheet match for both drained and undrained analyses for plane-strain conditions.
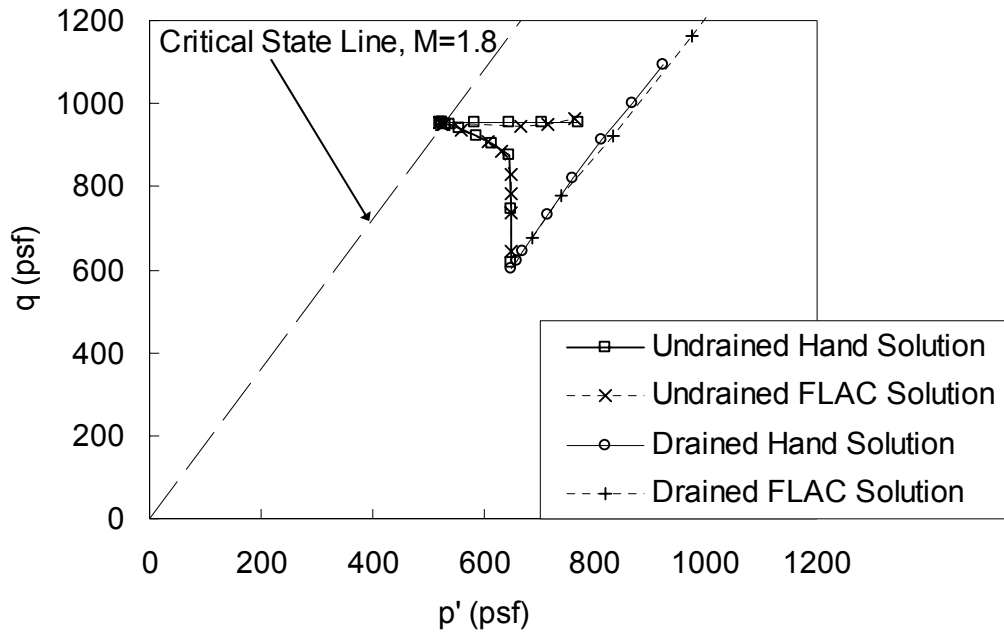
Figure 3-8. Modified Cam Clay model – plane-strain conditions *p'*-*q* plot
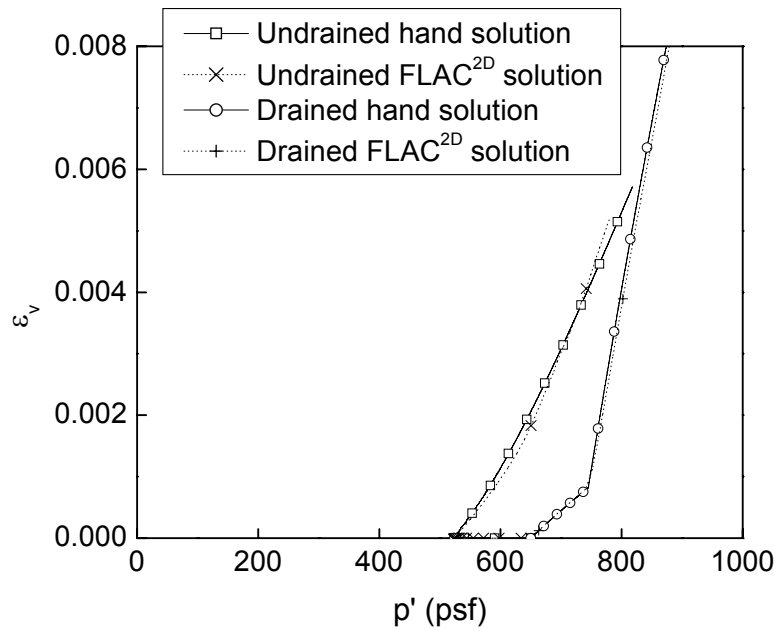
Figure 3-9. Modified Cam Clay model – plane-strain conditions *p'*-ε_v plot
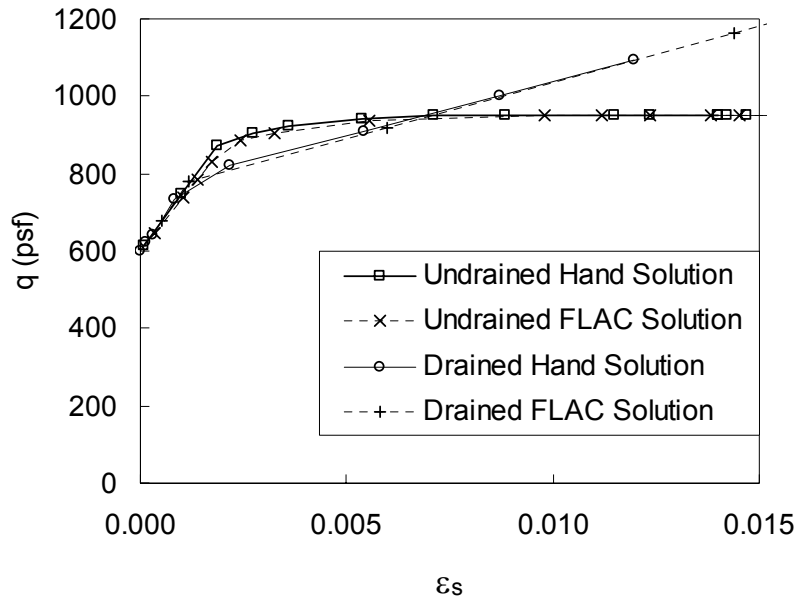
Figure 3-10. Modified Cam Clay model – plane-strain conditions q-ε_s plot

As mentioned above, soil lab test results are often presented in terms of MIT invariants, but parameters used in FLAC must agree with the set of invariants defined in Equations 3-1 through 3-4. One example is the Modified Cam Clay parameter η_f, which is the slope of the critical state line. FLAC uses the symbol M to designate the slope of this line. With MIT invariants, the slope of the critical-state line is designated by Equation 3-20.

$$M = \frac{q}{p} = \sin \varphi \qquad (3\text{-}20)$$

For the Modified Cam Clay Model used in FLAC, the slope of the critical-state line is designated by Equation 3-21 in triaxial compression, and Equation 3-22 in triaxial extension.

$$M = \frac{q}{p} = \frac{6 \sin \varphi}{3 - \sin \varphi} \text{ (triaxial compression)} \qquad (3\text{-}21)$$

$$M = \frac{q}{p} = \frac{6 \sin \varphi}{3 + \sin \varphi} \text{ (triaxial extension)} \qquad (3\text{-}22)$$

37

For plane-strain analyses, the actual value of M will be somewhere between the value for triaxial compression and the value for triaxial extension. For plane-strain analyses of column-supported embankment, where loads applied to the foundation are compressive, the out of plane stress due to loading will also be compressive, and the value of M at critical state should be closer to Equation 3-21 than Equation 3-22.

3.5. Pore fluid

The response of soils to loading depends on the behavior of both the solid particles and the fluid that occupies the space between solid particles. FLAC can perform a two-phase analysis that incorporates soil-fluid interaction to predict the soil response to loading.

The undrained bulk modulus for a material containing both soil and water is higher than the bulk modulus of water or the bulk modulus of the soil skeleton alone. The undrained bulk modulus, K_u, of a saturated soil should equal the value determined by Equation 3-23.

$$K_u = K + \frac{K_w}{\eta} \tag{3-23}$$

where η is the soil porosity.

Water is assumed to have no shear strength in FLAC, so the shear modulus both with and without pore water is the same.

When pore fluid is involved, FLAC will be unstable if the bulk modulus of water, K_w, is much higher than the stiffness of the soil. This problem is more pronounced for low values of porosity, η. This is the nature of the explicit (forward) formulation used in the program FLAC. The instability problem can be reduced in this incremental type of analysis by slowing the rate of loading (i.e. smaller incremental loads, lower permeability when drainage is allowed, smaller time steps). The FLAC manual provides some guidance for the selection of a suitable value of K_w. It is "not computationally necessary to use a value of K_w larger than roughly 20 times $\eta(K +$

4G/3), and should not be made higher than the physical value of water (2 x 10^9 Pa)" (Itasca 2002a).

To investigate these issues, an elastic soil with a bulk modulus of 1x10^6 psf was subjected to a isotropic compressive load as shown in Figure 3-11.
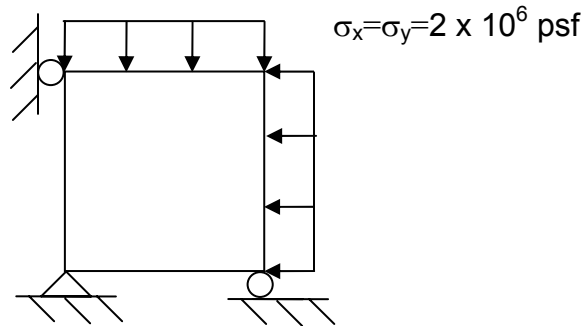
Figure 3-11. Isotropic consolidation of a single element

The intent of this example is to assess Equation 3-23. Isotropic compression is very stable in FLAC, even for extremely large stiffness contrasts, as evident in the plot of volumetric strain versus volumetric stress shown in Figure 3-12. The bulk modulus of water is four orders of magnitude higher than the bulk modulus of soil in these analyses. The stress-strain curves in this figure are smooth straight lines. One line represents a porosity of $\eta = 0.5$ and the other represents $\eta = 0.2$. It can be seen that Equation 3-23 is in good agreement with the FLAC results.
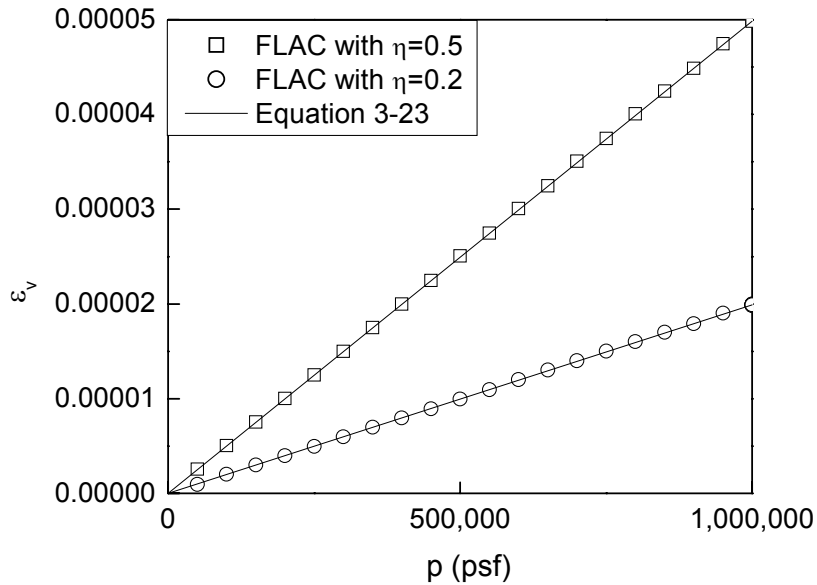
Figure 3-12. p-ε_v plot for isostropic compression

When the sample is subjected to anisotropic compression as shown in Figure 3-13, FLAC can become somewhat unstable at relatively low stiffness contrasts. The plot in Figure 3-14 shows volumetric stress vs. volumetric strain using bulk modulus of water values one order of magnitude higher and two orders of magnitude higher than the value for the bulk modulus of soil. The stress-strain curves in this figure are not smooth straight lines, and comparison of Figures 3-12 and 3-14 suggest that instability is associated with shear stresses. Although the FLAC results in Figure 3-14 do exhibit some numerical instability, it can also be seen that the FLAC results are in reasonably good agreement with Equation 3-23. The four cases shown in Figures 3-12 and 3-14 are summarized in Table 3-2.
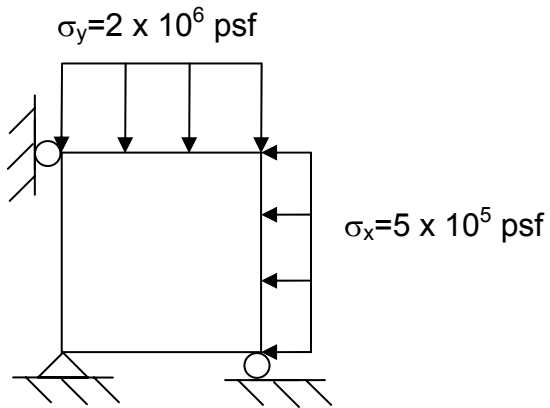
Figure 3-13. Anisotropic consolidation of 1 x 1 element
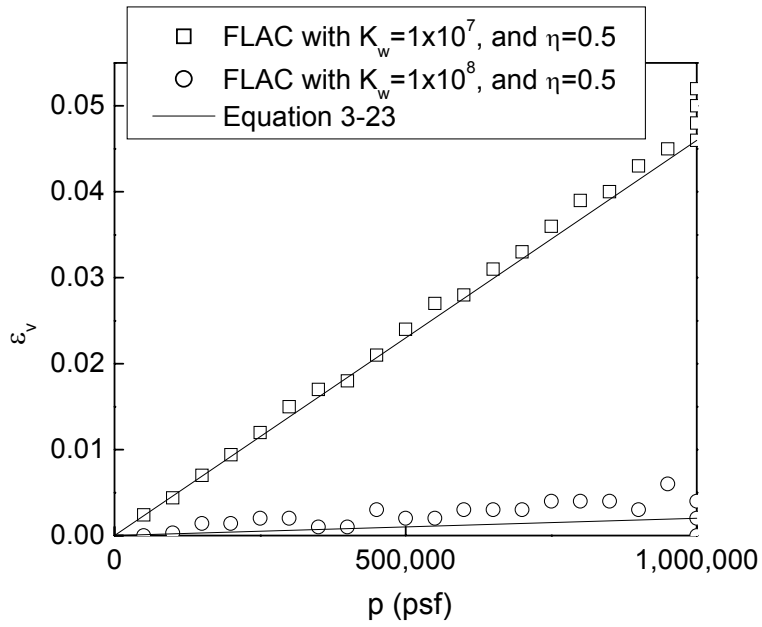
Figure 3-14. p-ε_v plot for anisostropic compression

Table 3-2. Summary of FLAC runs for pore pressure study

Soil K (psf)	Water K (psf)	η	K_u (psf)	Compression
1×10^6	1×10^{10}	0.5	2×10^{10}	Isotropic
1×10^6	1×10^{10}	0.2	5×10^{10}	Isotropic
1×10^6	1×10^7	0.5	2.1×10^7	Anisotropic
1×10^6	1×10^8	0.5	2.01×10^8	Anisotropic

For the one-zone example problem with $\eta = 0.5$ and $K_w = 1 \times 10^8$ psf, the lateral displacement was 2.67×10^{-4} ft and the vertical displacement was -2.71×10^{-4} ft. The small amount of volume change is due to the finite compressibility of water.

In the analysis of the test embankment for the I-95/Rt. 1 Interchange, which is included in Chapter 6, the effect that an artificially low bulk modulus of water has on calculated deflections was investigated. These investigations revealed that a bulk modulus of water that was too low resulted in behavior similar to drained behavior. An artificially low bulk modulus of water also causes problems for soft soil between stiff columns. This was discovered during analyses of the Inagaki et al. (2002) experiments described in Chapter 5.

3.6. An alternative to a two-phase analysis

Rather than perform a two-phase analysis, under some conditions it is appropriate to model soil behavior without pore pressures. Two cases where this simplification is common are the short term, undrained case, and the long term, drained case. The undrained parameters used in the short term analysis represent soil behavior before pore pressures have dissipated. The drained parameters used in the long term analysis represent soil behavior without build-up of pore pressures due to loading. In this research, where embankments are rapidly constructed on soft, low permeability clays, pore pressures increase in the clay, and they have a detrimental effect on embankment stability compared to the case of a slowly applied load without development of excess pore pressures. The critical case for slope stability of embankments constructed on soft, low permeability clay is the undrained case. A comparison between a two-phase analysis, using

the Modified Cam Clay model to represent soft clay and an undrained analysis, using the Mohr-Coulomb model to represent soft clay is included in Chapter 5.

3.7. FISH

FISH is a programming language embedded within FLAC that enables the user to define new variables and functions (Itasca 2002a). FISH functions are used to collect calculated node deflections, as well as zone stresses and pore pressures in many of the numerical analyses performed in this research. These functions are defined in the data file, generally in the beginning of the file. The name given to the FISH function can then be used just as other FLAC commands. A user comfortable with any programming language will be comfortable defining FISH functions.

3.8. Ramp loading

Instability may occur in FLAC when loads are applied rapidly. The 'history ramp' function may be used to apply loads in a gradual manner and alleviate this source of instability. As an example, the 1 ft by 1ft Modified Cam Clay specimen was subjected to a drained loading in plane-strain, similar to Section 3.4.2. When multiple zones comprise the specimen, the results shown in Figures 3-7 through 3-9 can be obtained with a gradually applied load, but this example becomes unstable if the distributed load is applied too rapidly. FLAC results are shown in Figure 3-15 for one zone and 90 zones representing the problem domain. It can be seen that about 10,000 loading steps are needed to achieve convergence when 90 zones are used.
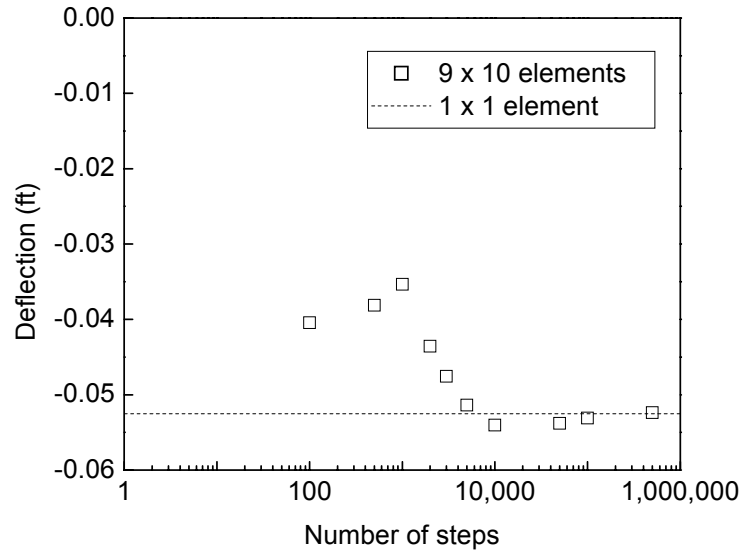
Figure 3-15. Number of steps for ramp loading vs. displacement

Similar instability problems will occur in two-phase analyses if the time step used for FLAC computations is too large. A stable time step is calculated by FLAC based on model mesh size and material properties, but in many situations instability will still occur using this value for the time step during groundwater flow. These problems can be corrected by using a smaller groundwater time step (with the FLAC command 'set gwdt').

In other situations, it is necessary to take special measures to prevent erratic behavior in these simple verification studies. For example, in the verification studies described above that involved pore pressure dissipation, the flow is toward a fixed boundary at the top of the problem domain where the pore pressure was set to zero. This type of analysis works fine in FLAC for a single zone, but problems occur when the 1 ft by 1ft region is divided into many zones. In this situation, zones along the boundary behave poorly when the specimen has high pore pressure and has a fixed value of zero pore pressure along the boundary. These problems can be eliminated with a FISH function that sets pore pressure at the boundary to a value slightly less than the pore pressure in the zones along the boundary. The FISH function then slowly ramps down the pore pressure to zero.

Many instability problems encountered with the simple verification problems described in this chapter do not seem to occur when analyzing full models of real world problems.

3.9. Comparison of lateral deflections due to vertical loads in drained, undrained, and consolidation analyses

A series of analyses were performed to investigate the lateral deflections produced by a vertical load in drained, undrained, and consolidation analyses using FLAC. For this study, a 40' deep clay layer in plane-strain was subjected to a vertical surface pressure of 1000 psf using the mesh shown in Figure 3-16, with a 32' clay layer overlying an 8' sand layer. Lateral deflections were recorded in the model to represent a vertical inclinometer located at the edge of the surface pressure. Both drained and consolidation analyses were performed. The consolidation analyses were divided into two parts: (1) undrained loading followed by (2) dissipation of excess pore pressures.
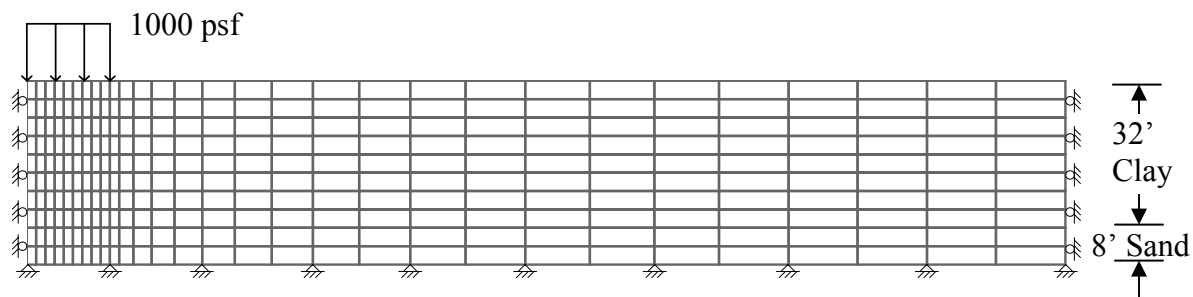
Figure 3-16. Normal stress on a Cam Clay foundation with vertical columns

The analyses were performed with and without stiff columns extending to the bottom of the clay layer. The Mohr-Coulomb model was used for the columns and the base sand layer. Property values of the clay, the base sand layer, and the columns, when used, are shown in Tables 3-3 and 3-4.

Table 3-3. Material properties

Material	γ (pcf)	c (psf)	ϕ (degrees)	E (psf)	ν
Clay layer	100	Modified Cam Clay			0.3
Base sand layer	125	0	45	1.58×10^6	0.25
Columns	100	3130	0	7.50×10^6	0.25

Table 3-4. Modified Cam Clay properties for clay layer

M	ν	λ	κ	e	k (cm/s)	mpc (psf)	mp1 (psf)	mv_1
1.8	0.3	0.5	0.05	2.165	1×10^{-6}	2000	200	3.2

Deflections from the drained analysis and both parts of the consolidation analysis for the initial case with no columns were calculated using FLAC and they are shown in Figure 3-17. The undrained lateral deflections are much larger than the drained deflections. Also, lateral movements were small during dissipation of excess pore pressures were allowed to dissipate, and they tended to be in the direction toward the load rather than away from it.
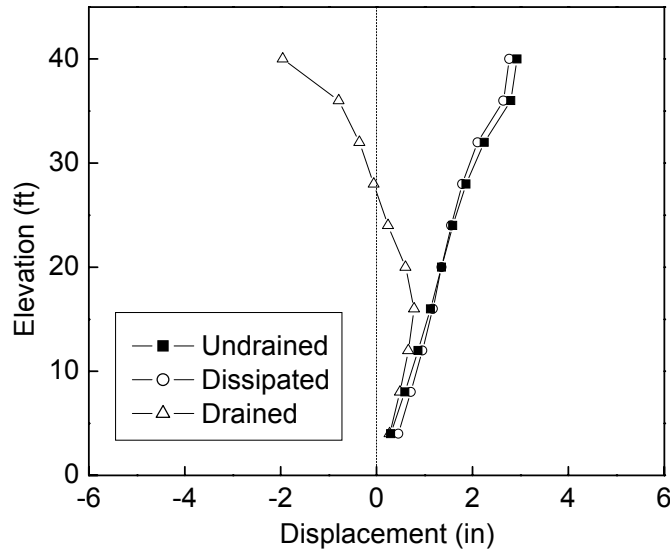
Figure 3-17. Deflections with no vertical columns

Figure 3-18 shows undrained lateral deflections when vertical columns are used. For analyses where columns were used, the applied load was doubled to 2000 psf, yet lateral deflections were significantly reduced compared to the case without columns. When pore pressures were allowed to dissipate, a small increment of movement back towards the load occurred, similar to what took place for the analyses without columns.
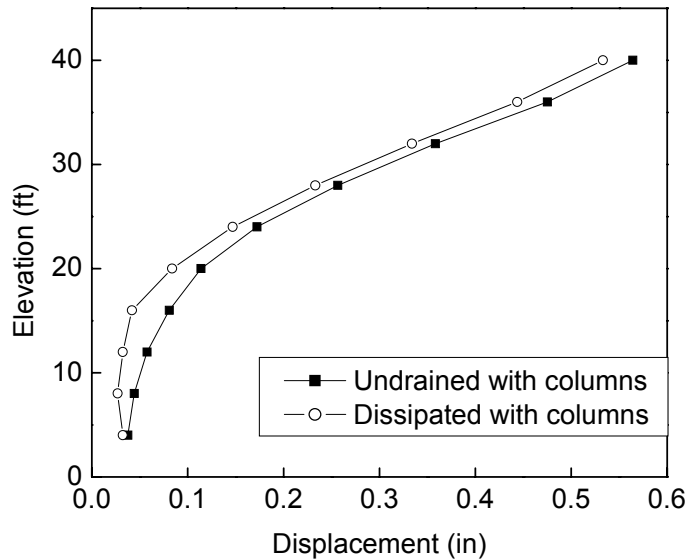
Figure 3-18. Deflections with Mohr-Coulomb columns

3.10. Beam study

A mesh refinement study was performed to determine the number of zones that would be needed to accurately represent a column under lateral loading. This study included both a cantilever beam subject to a concentrated force and a beam with pin and roller connections subject to a distributed load. The investigation into the behavior of the cantilever beam indicate that a minimum of three zones across the width of the column with an aspect ratio around one provide an accurate assessment of displacement. Fewer than three zones do not represent beam behavior well at all. These results prompted an investigation into the mesh refinement for the test embankment analysis included in Chapter 6.

3.10.1. Cantilever beam

In order to determine the number of elements required across the width of a column, the beam shown in Figure 3-19 was analyzed with FLAC to determine the effect of mesh refinement.
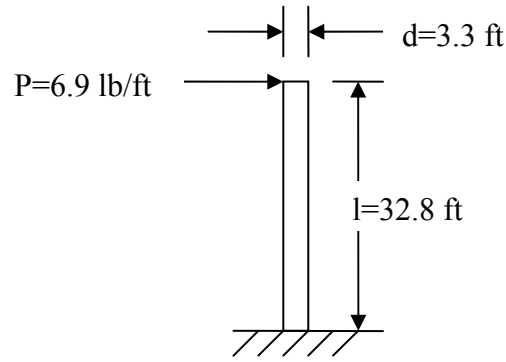
Figure 3-19. Elastic beam deflection problem

The beam has a Young's Modulus, E, of 4177 psf, with a Poisson's ratio, v, of 0.45. The maximum deflection, Δ_{max}, was also determined with Equation 3-24.

$$\Delta_{max} = \frac{Pl^3}{3EI} \tag{3-24}$$

where P is the concentrated force, l is the beam length, and I is the moment of inertia of the beam in the direction of loading.

The deflection at any point along the length, Δ_x, can be determined with Equation (3-25).

$$\Delta_x = \frac{P}{6EI}\left(2l^3 - 3l^2x + x^3\right) \tag{3-25}$$

where x is the location along the beam.

Because FLAC solutions were determined for a plane-strain analysis, Equation 3-25 had to be adjusted to approximate a wide beam. This is done by increasing the Young's modulus with Equation 3-26 (Roark and Young 1975).

$$E_{wide} = \frac{E}{1-v^2} \tag{3-26}$$

As can be expected, the accuracy of the FLAC2D results improves with finer meshes. Keeping a 1:1 aspect ratio, the improvement with mesh refinement for the Poisson's ratio of 0.45 is shown in Figure 3-20.
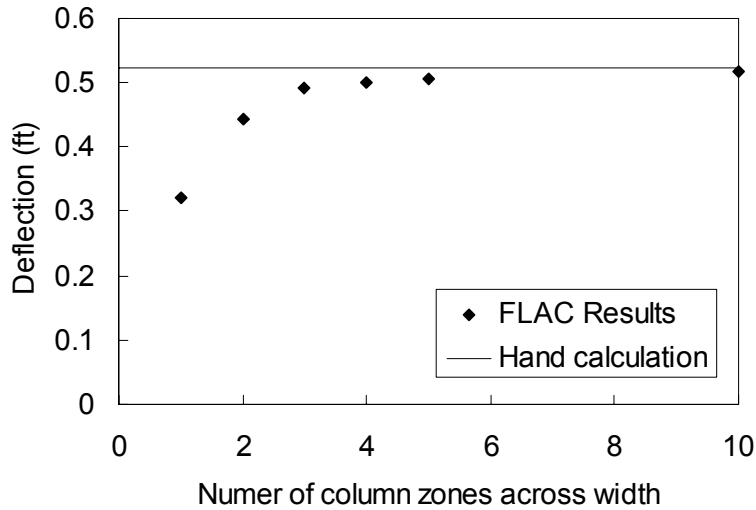
Figure 3-20. Improvement in accuracy for 1:1 aspect ratio

Figure 3-21 illustrates how lower values of Poisson's ratio require more elements to achieve an accurate solution.
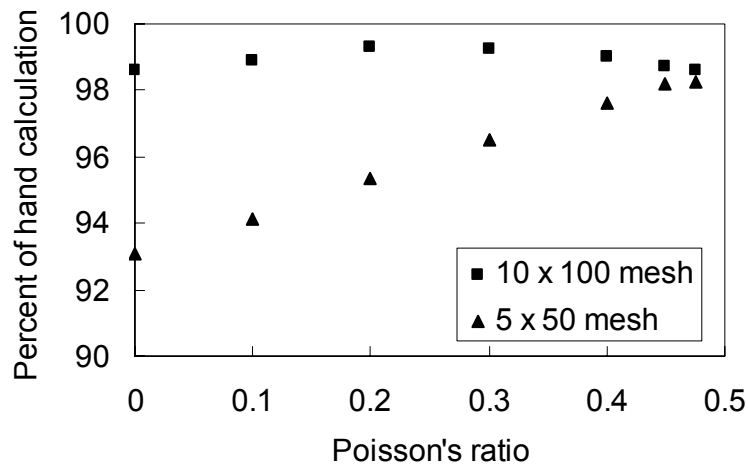
Figure 3-21. Effect of Poisson's ratio and mesh refinement on accuracy

Further investigation into the beam behavior revealed that the aspect ratio has as large an effect on FLAC accuracy as mesh refinement. Figure 3-22 shows how aspect ratio affects computed displacements. Figure 3-23 shows how aspect ratio affects computed stresses. Stresses are computed in the outer zones closest to the base.
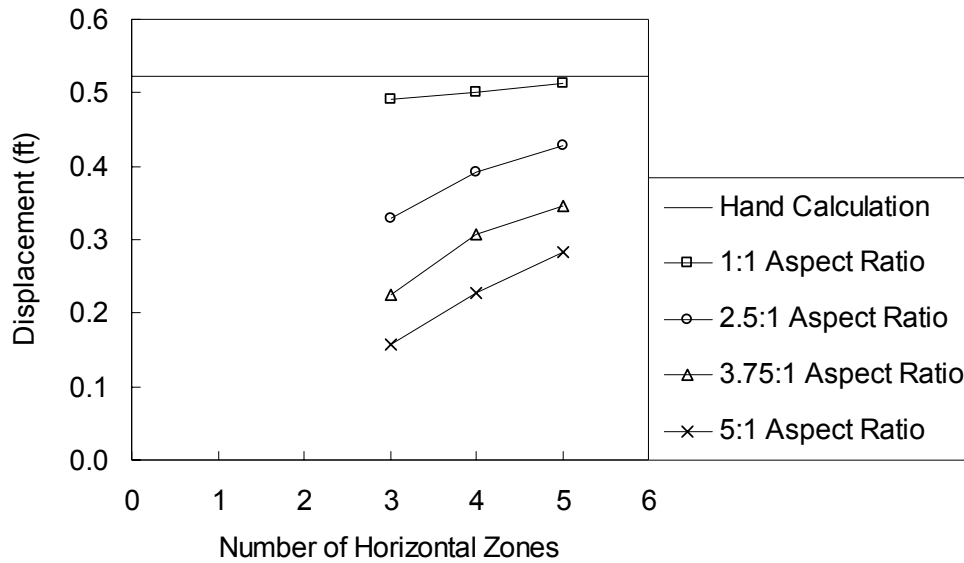
Figure 3-22. Effect of aspect ratio on computed displacements
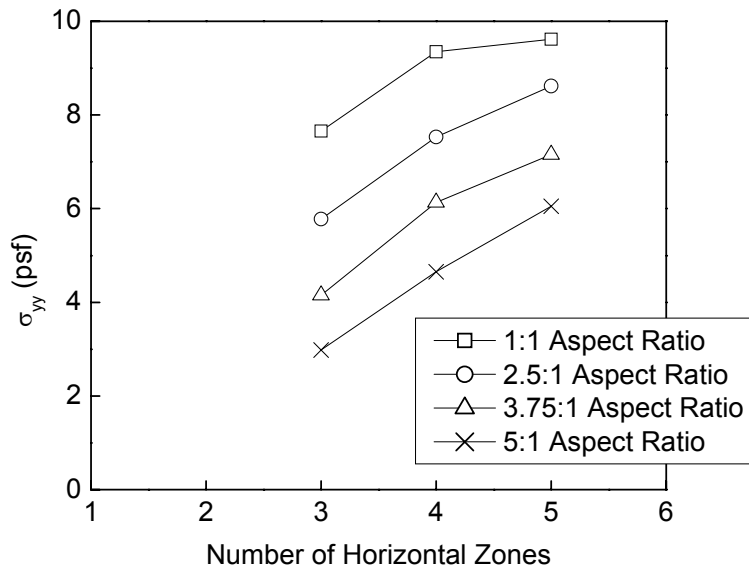
Figure 3-23. Effect of aspect ratio on computed stress

For this type of concentrated loading, the aspect ratio and the number of zones in the mesh both have an effect on computed deflections and stresses. This could be a critical issue because the models for column-supported embankments require long, slender elements for the columns, with aspect ratios between 3:1 and 4:1 in some instances. Also, only three zones were used for each strip representing columns. Looking at Figures 3-22 and 3-23 where three zones are used, it appears that using an aspect close to unity may be more important than increasing the number of zones without improving the aspect ratio.

3.10.2. Column extraction

The preceeding investigation into the bending of an isolated beam raised concerns about mesh refinement for the columns in the analysis of column-supported embankments. In order to check the accuracy of stresses computed in the columns, one column with 41 x 3 zones was removed from the mesh from the analysis of the test embankment described in Chapter 6. A mesh of 246 x 6 zones was attached to the mesh in place of zones removed from the test embankment mesh. The 3.75:1 aspect ratio for the 41 x 3 mesh improved to 1.25:1 for the 246 x 6 mesh. The replaced column was the one closest to the edge of the vertical face of the embankment, subjected to the highest column loads. As shown in Figures 3-24 thru 3-27, vertical stresses, horizontal stresses, pore pressures, and shear stresses in the relatively coarse column with a poor aspect ratio are very similar to those in the much finer column with a much better aspect ratio. From this investigation, the number of zones used to model columns in the test embankment should be sufficient.
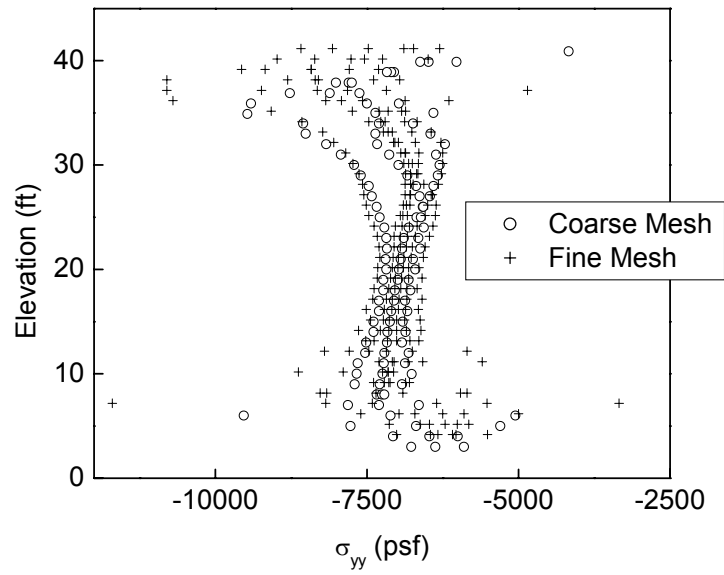
Figure 3-24. Vertical stress in column
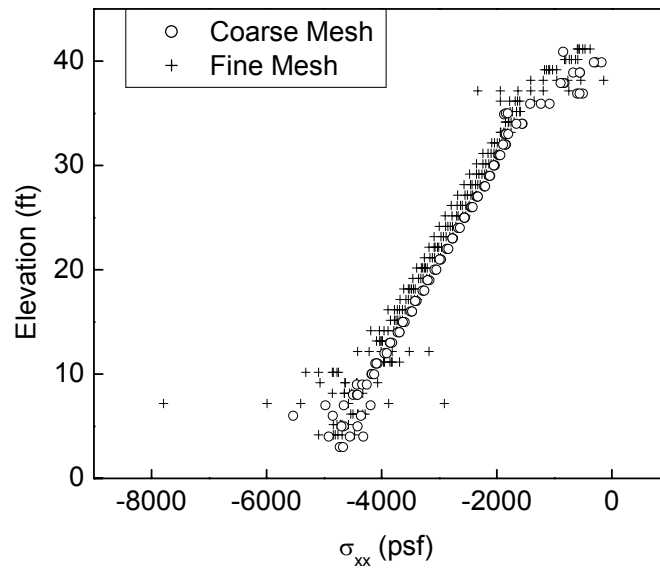
Figure 3-25. Horizontal stress in column
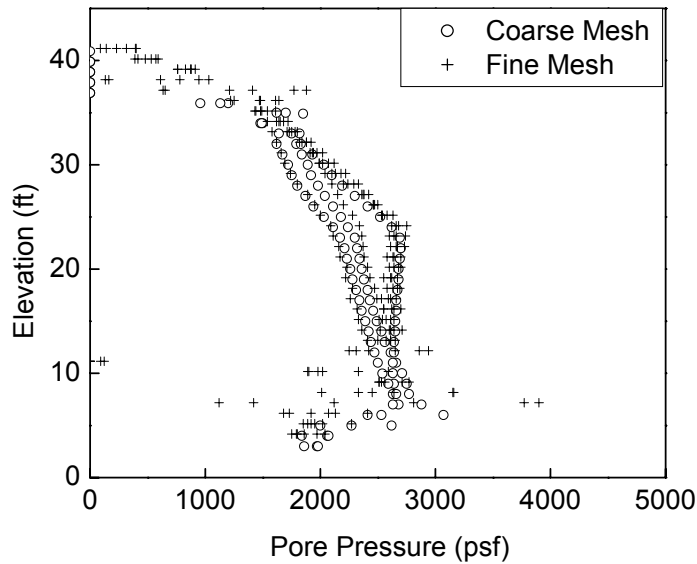
Figure 3-26. Pore pressure in column
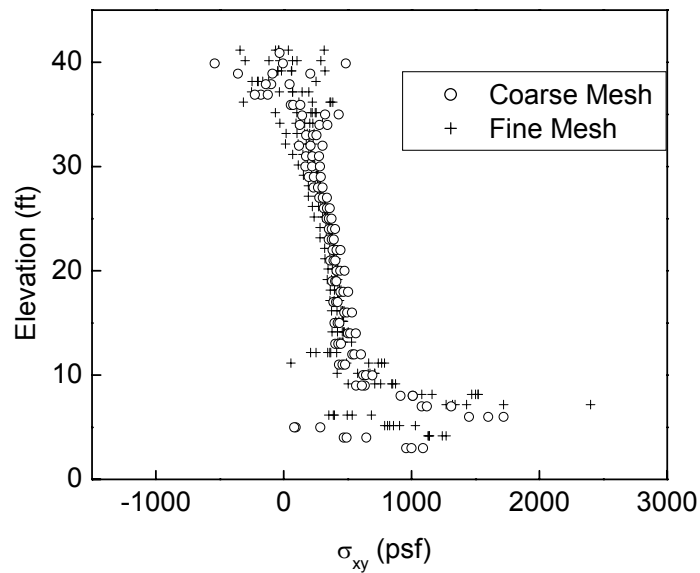
Figure 3-27. Shear stress in column

3.11. Three-dimensional analysis

Itasca produces a three-dimensional finite difference program called FLAC^{3D} (2002b). Some aspects of the three-dimensional program are different from the two-dimensional program, FLAC^{2D}. There are large differences between the two programs regarding mesh generation.

53

Obviously, defining geometry in three dimensions is much more difficult than defining geometry in two dimensions. Every node and zone in FLAC^{2D} is specified by i and j values defined by the user, whereas nodes and zones in FLAC^{3D} are specified by node and zone numbers generated by the program.

Pre-defined shapes available in FLAC^{3D} such as the "brick" shown in Figure 3-28 make it simple to define problem geometry; however, some of the shapes should be used with caution. Some of these pre-defined shapes appear to lend themselves readily to the three-dimensional analysis of columns, as shown in Figure 3-29. Unfortunately, the arrangement of cylindrical shapes is not the most efficient arrangement for these shapes. The circular cross section of the column is divided in a radial fashion, and the "pie" shaped zones that result from this geometry have poor aspect ratios, especially toward the center of the circle. This difficulty is compounded when the out-of-plane dimension is taken into consideration. The FLAC manuals state that aspect ratios should not exceed 1:5. Such aspect ratios are difficult to achieve in all three dimensions with pre-shaped cylindrical zones.
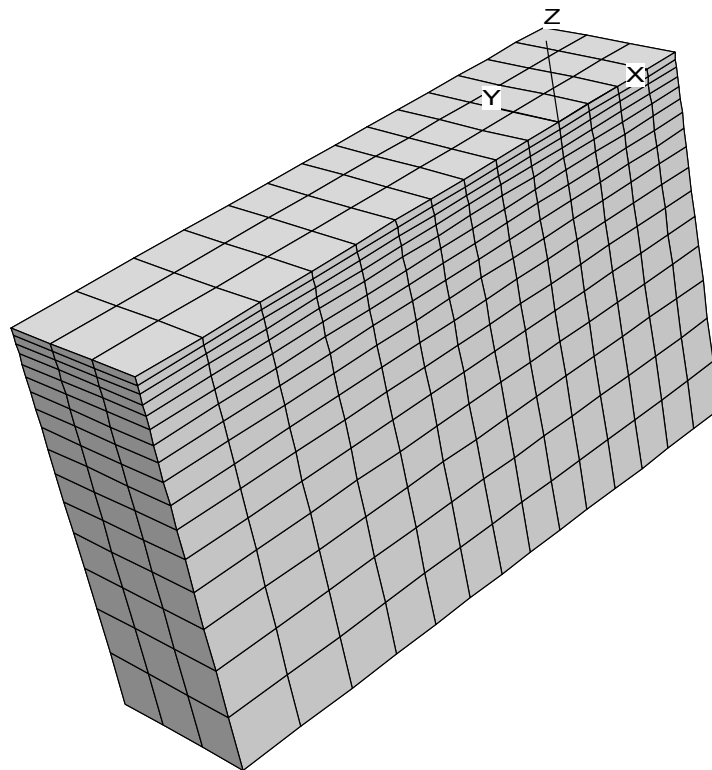
Figure 3-28. Pre-defined "brick" shape in FLAC^{3D}
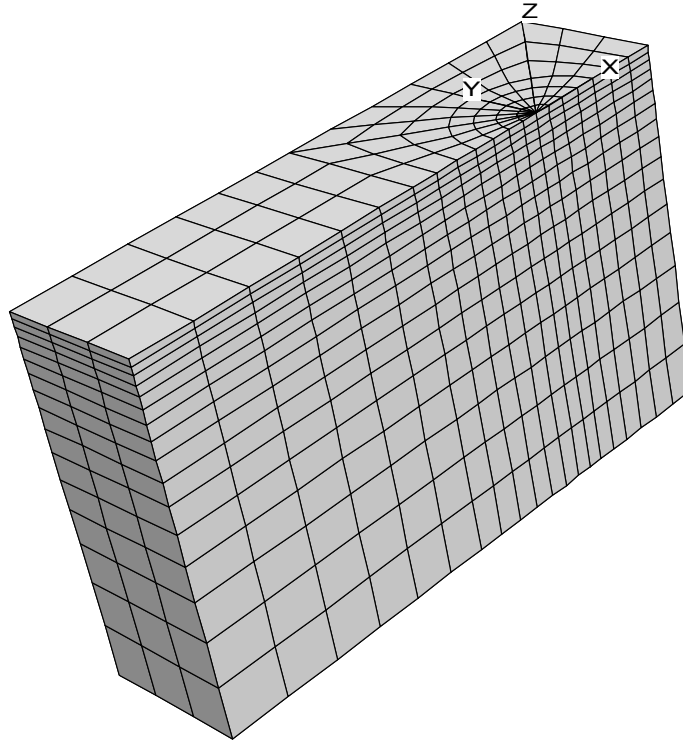
Figure 3-29. Pre-defined cylindrical shapes in FLAC^{3D}

To illustrate this point, columns dimensions from the Inagaki et al. (2002) centrifuge tests, presented in Chapter 5, were analyzed as a beam with a pin connection at one end and a roller connection on the other. These columns are 42.7 ft long and 3.3 ft in diameter. A column with this geometry, and a Young's Modulus of $1.25\text{x}10^6$ psf, is subjected to a distributed load acting along the center-line of the column as shown in Figure 3-30.
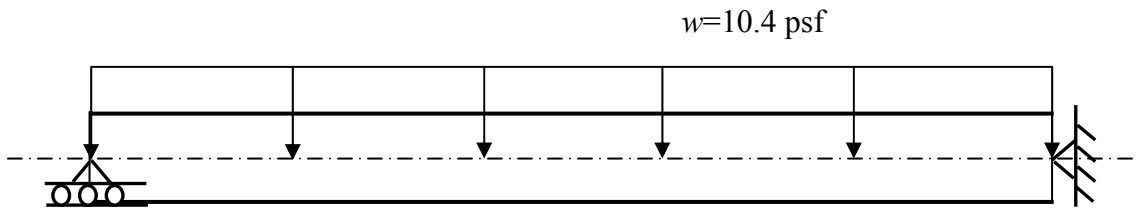
Figure 3-30. Column fixed at two ends

Displacement at the mid-point of the column was also calculated with Equation 3-27.

$$\Delta = \frac{5wl^4}{384EI}$$
(3-27)

FLAC^{3D} was used to calculate the midpoint deflection of the column using the three meshes shown in Figure 3-31. The mesh with 36 zones in cross-section and the mesh with 64 zones in cross-section can be easily created in FLAC^{3D} using the "generate cylinder" command. The mesh with 32 zones can be created manually by defining the location of every point in three dimensions. Although it requires more work to generate the 32 zone mesh, it is more efficient than either the 64 zone mesh or the 36 zone mesh. This is shown in Figure 3-32, where deflection calculated with each mesh is expressed as a percentage of the deflection calculated using Equation 3-27.
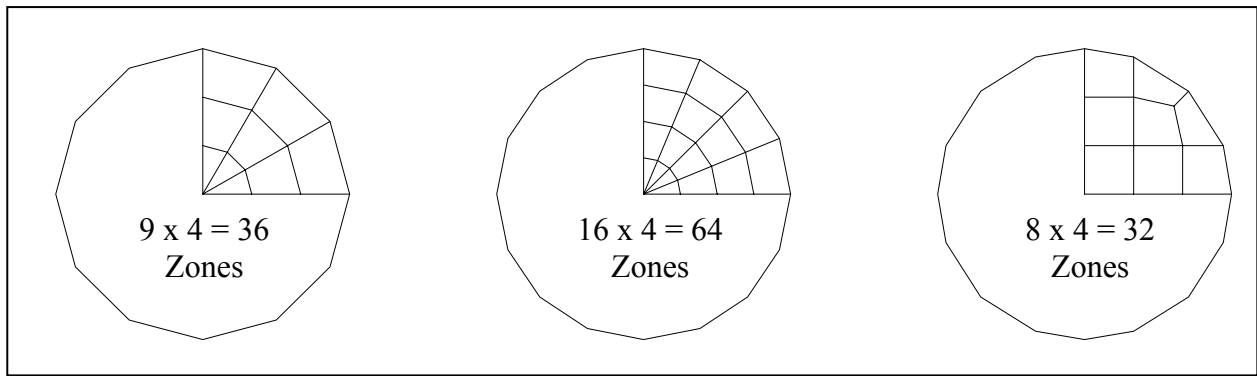
Figure 3-31. Cross section of three-dimensional meshes used to model column behavior in FLAC^{3D}
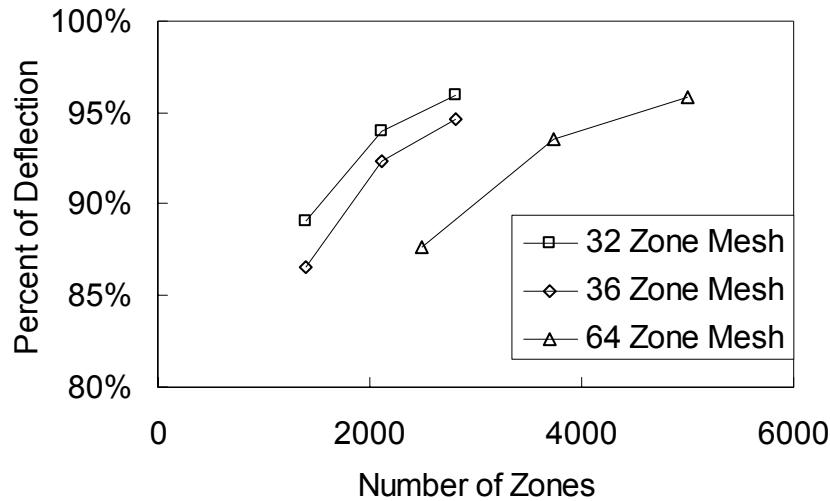
Figure 3-32. Normalized deflection of column calculated using three different meshes

There are other, more subtle differences between FLAC^{2D} and FLAC^{3D}. One example of the differences occurs when defining the initial stresses s_{xx}, s_{yy}, and s_{zz} for a problem. FLAC^{2D} defines initial stresses with the commands "initial" and "variance," where "initial" defines stress at the first coordinate given, and "variance" defines the total change in stress across the region between the first and second coordinates. FLAC^{3D} defines initial stresses with the commands "initial" and "gradiant," where "initial" defines the difference in stress from a value FLAC^{3D} computes based on unit weight, gravity, and the z-coordinate for the material, and "gradiant" defines the incremental change in stress with depth between the first and second coordinates. The initialization procedure used by FLAC^{3D} assumes uniform material between this coordinate and the origin regardless of problem geometry and material types. In order to avoid mistakes due to this procedure it may be helpful to specify stresses in every zone rather than use the "gradient" command.

3.12. Factor of Safety

Generally, numerical analyses are used to determine stresses and deflections in geotechnical engineering problems. FLAC also has an automated procedure to evaluate the factor of safety by reducing strength values to determine the point of impending failure, at which the model is no longer in equilibrium. This factor of safety procedure, fos, in FLAC can only be used when all zones in the mesh are represented by the Mohr-Coulomb model. While this function exists in FLAC^{3D}, it is not feasible to run a fos analysis in three dimensions in this research because the large number of zones needed for column-supported embankments make the fos run time in FLAC^{3D} much too long.

For the analysis of column supported embankments, it is prudent to first compare the factor of safety for the same embankment without columns determined with the fos procedure with the factor of safety without columns computed using a limit equilibrium, slope stability analysis. Use of the factor of safety calculation is illustrated in Chapter 9.

3.13. Case history information

An important method to verify numerical analysis procedures is to match centrifugal model studies and case history data, as described in the next three chapters. Two centrifuge tests that

represent the state-of-the-art in understanding the behavior of deep-mixed columns subject to inclined loading are described and analyzed in Chapters 4 and 5. The authors of these centrifuge studies performed numerical analyses that calculated the same response as measured in their centrifuge tests.   FLAC is used in this report to repeat those numerical analyses, and the same methodology was used to perform numerical analyses of the I-95/Rt. 1 interchange, as described in Chapter 6.

3.14. Summary

This chapter describes some of the verification studies that were performed to calibrate numerical analyses procedures for use with the program FLAC. Simple analyses were performed with elastic and modified cam clay material models, and compared to hand calculations. These analyses illustrate that both drained and undrained analyses accurately calculate soil response to loading.

An investigation was performed to determine the number of zones that are required for strips in plane strain to accurately represent column behavior. In two dimensions, three zones across the width of each strip representing columns in the mesh, and aspect ratios less than 5:1, as recommended in the FLAC manual, do closely approximate column behavior. In three dimensions, the meshed automatically generated by FLAC^{3D} to represent cylinder shapes do not efficiently model column behavior.

4. ANALYSES OF CENTRIFUGE MODEL TESTS
OF A COLUMN-SUPPORTED CAISSON

4.1. Introduction

This section describes FLAC analyses of the centrifuge model tests performed by Kitazume et al. (1996), who also performed finite element analyses of their model tests. The prototype model is a caisson, subject to both a vertical load and a horizontal force, founded on soft clay improved with soil-cement columns. The centrifuge test and subsequent FEM analyses were performed at 1:30 prototype scale, at 30g. The FLAC analyses were performed at full scale.

4.2. Centrifuge tests

Kitazume et al. (1996) performed centrifuge tests using an inclined load on soft clay improved with soil-cement dowels. A drainage layer of sand was placed at the bottom of the model test box. Clay slurry was poured into forms at both ends of the model test box and consolidated under load on the laboratory floor. The columns were cast outside the model test box using soil-cement slurry and, after curing, they were arranged in a rectangular pattern in the middle of the box. Clay slurry with higher water content was then pumped between columns. A schematic digram is included as Figure 4-1.

The results illustrate the effect that failure modes other than slip surfaces can have on stability. Racking, or tilting, of columns and bending failure in the columns can be seen in the photographs of the centrifuge tests shown in Figure 4-2.

The horizontal and vertical loads causing failure in the experiments were compared to the loads causing failure from limit equilibrium slope stability analyses. The experimental loads were much smaller than the failure loads from the limit equilibrium analyses (Kitazume et al. 2000).

The series of centrifuge tests are listed in Table 4-1, which includes each combination of vertical and horizontal loads causing failure (full scale, and in terms of kip/ft). Kitazume et al. (2000) present horizontal load vs. displacement curves for tests DMMT3, DMMT11, and DMMT12. Kitazume et al. (2000) performed finite element analyses based on the test results from DMMT11.

3.9"

1.1"

1.5"

0.8"

13.6"

7.5"

0.8"

caisson

Applied
Force

mound

DMM
improved
columns

clay

clay

drainage sand layer

6.7"

6.3"

6.7"

19.7"

a. Profile View

3.5" over caisson footing

3.9"
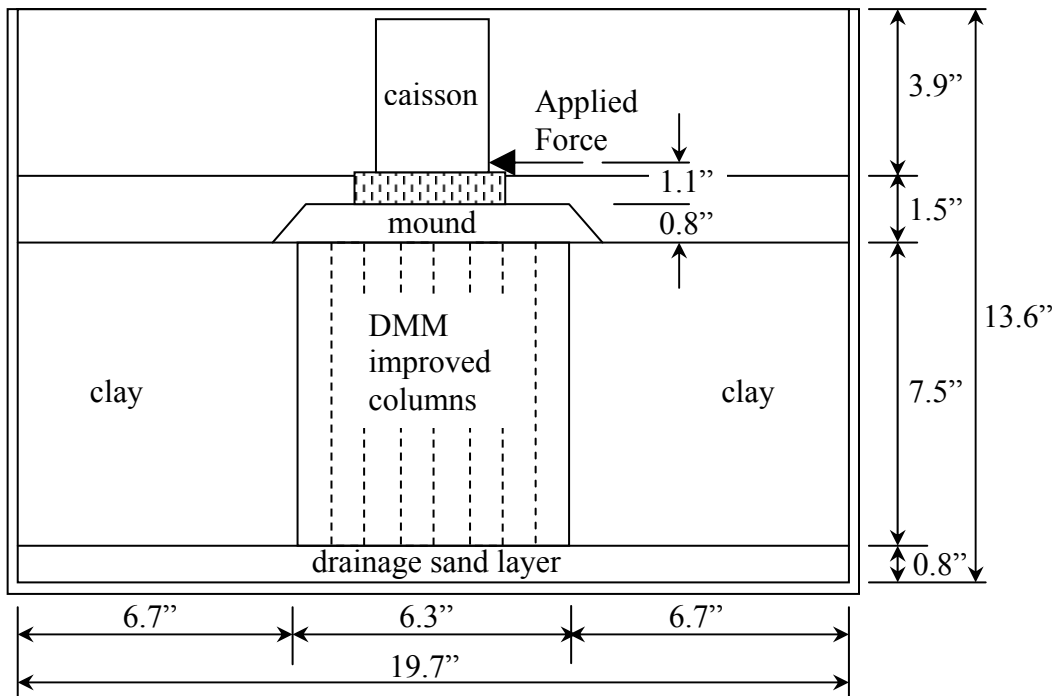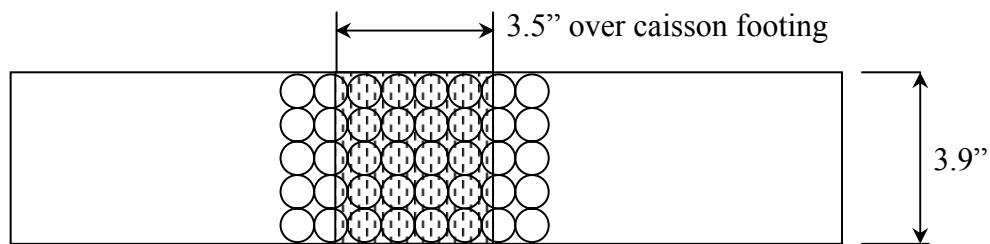
b. Plan View

Figure 4-1. Kitazume et al. (1996) model schematic (x30 at prototype scale)
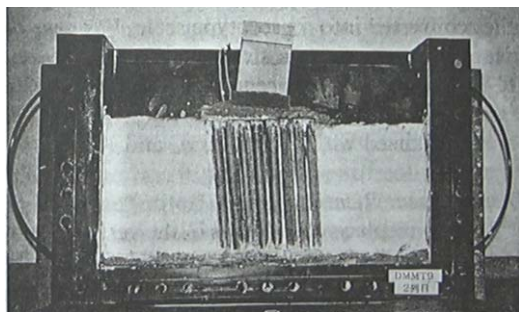
(a) DMMT 9-2
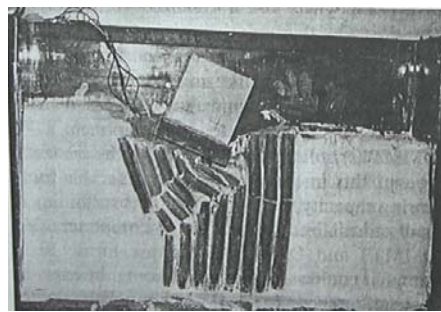
(b) DMMT 3

Figure 4-2. Column Tilting and Column Bending (Kitazume et al. 2000)

Table 4-1. Test conditions for centrifuge tests performed by Kitazume et al. (2000)

Test Case	Column strength, q_u (psi)	Replacement area ratio, a_s (%)	Vertical load at failure		Horizontal load at failure	
			V (kip/ft)	$V/(q_u a_t)$	H (kip/ft)	$H/(q_u a_t)$
DMMT1	75	56	25.9	0.481	3.1	0.0579
DMMT2	110	79	58.6	0.529	0	0
DMMT3	83	79	25.0	0.299	5.2	0.0615
DMMT4	45	79	18.2	0.403	3.6	0.0805
DMMT5	31	79	12.5	0.4	2.9	0.0945
DMMT6	82	79	41.7	0.505	0	0
DMMT7	53	79	38.9	0.731	0	0
DMMT9-1	3945	79	25.8	0.007	8.2	0.0021
DMMT9-2	3945	79	53.6	0.004	10.1	0.0026
DMMT10	126	79	53.6	0.421	6.9	0.0545
DMMT11	297	79	44.3	0.148	5.8	0.0195
DMMT12	128	79	44.3	0.343	7.6	0.0589
DMMT13	135.5	79	44.3	0.325	5.7	0.0414
DMMT14	223	79	32.7	0.146	4.7	0.0211
DMMT15	798	79	32.7	0.408	9.0	0.0112
DMMT16	189	79	66.7	0.351	0	0

Kitazume et al. (2000) normalized vertical and horizontal loading in Table 4-1 based on the column unconfined compression strength, q_u, and the total area of columns beneath the caisson, a_t. The authors observed that centrifuge tests performed with a high vertical load relative to column strength exhibit a pronounced bending failure pattern under lateral loading. The difference in failure pattern between tests DMMT-9 and DMMT-3 illustrate the effect of normalized vertical load, as shown in Figure 4-2.

4.3. Numerical analysis performed by Kitazume et al. (2000)

Kitazume et al. (2000) performed finite element analysis for test case DMMT-11. Based on their results from all tests performed, the authors deemed test DMMT-11 to be representative of system behavior when the caisson is subjected to both vertical and lateral loading. This section describes a new numerical analysis, performed with FLAC, using parameters from the FEM analysis presented in Kitazume et al. (2000). Although the FEM analyses were presented in model scale, the FLAC analyses were performed at prototype scale.

Rows of columns were represented with eight strips in the foundation that result in the same area replacement ratio used in the centrifuge tests. The relatively high replacement ratio of 79% resulted in strips 1.6-ft wide representing columns, and strips 0.4-ft wide between columns. Five zones are used in the mesh across the width of the strips representing columns, and three zones across the strips representing soil between columns. Columns extend from the ground surface to the drainage sand layer.

In their analyses, Kitazume et al. (2000) use an elastic model for the caisson and columns. The base sand, clay, and mound sand each use the Mohr-Coulomb failure criterion to separate elastic from perfectly plastic behavior. The authors listed material properties they used to perform numerical analyses, which are included in Table 4-2. The undrained cohesive strength of the clay increases with depth as indicated by the six layers shown in Table 4-2. The cohesion of the clay pumped between the columns is assumed to be one tenth the cohesion of the consolidated clay outside the columns. Kitazume et al. (2000) provide a cohesion value for the columns, but they do not use this value in their finite element analysis.

No unit weight information is included in the article. However, an average buoyant unit weight for the clay can be determined from the applied pressure of 767 psf used to consolidate the clay on the lab floor. This pressure was chosen to correspond to an over-consolidation ratio of one at the bottom of the clay layer under the 30g load. The buoyant unit weight of the clay is then determined from the following calculations:

$$(d)(1\text{-}1/30)(\gamma_b) = 767 \text{ psf} \qquad \text{or}$$

$$\gamma_b = (^{30}/_{29})(767 \text{ psf} / 18.7 \text{ ft}) = 42.4 \text{ pcf}$$

Standing water is present in the schematic for the prototype, but it is not mentioned in the article. In the FLAC analyses, it was assumed the mound and base sand both have a saturated unit weight of 132 psf. The unit weight of the caisson corresponds to the vertical load applied by the caisson, as indicated in Table 4-1.

Table 4-2. Model properties (after Kitazume et al. 2000)

Material		γ (pcf)	c (psf)	ϕ	E (psf)	ν
Sand layer		131.6	0	35	208847	0.33
Clay Ground	1	104.8	88	0	25187	0.3
	2	104.8	86	0	22180	0.3
	3	104.8	83	0	19465	0.3
	4	104.8	80	0	17418	0.3
	5	104.8	76	0	15747	0.3
	6	104.8	71	0	14035	0.3
Clay between DMM columns	1	104.8	8.8	0	2519	0.3
	2	104.8	8.6	0	2218	0.3
	3	104.8	8.3	0	1946	0.3
	4	104.8	8.0	0	1742	0.3
	5	104.8	7.6	0	1575	0.3
	6	104.8	7.1	0	1403	0.3
DMM columns		104.8	10442	0	4176940	0.45
Mound		131.6	0	35	104423	0.33
Caisson		*	Elastic		2088470	0.33

* note: Caisson weight is determined from vertical force as explained in text.

The Kitazume et al. (2000) analyses employ joint elements along the base of the columns. These elements use a reduced modulus value in tension to allow for column tilting. An interface in this location can be applied in FLAC by removing one row from the mesh, and attaching nodes above and below the removed row, then defining an interface to connect these pairs of nodes. However, this interface was not included in the FLAC analyses because the sand layer has no tension capacity.

The centrifuge test used a load applied at a constant horizontal velocity. Likewise, a constant velocity was used in FLAC to model the horizontal applied force. Numerical analysis of a load causing failure is more convenient to apply as a constant velocity rather than an increasing force. However, a much lower velocity is required for the finite difference procedure to be numerically stable than is used in the centrifuge test. The model velocity was .004 inch/second. At the prototype scale, that equals 0.12 inch/second = .01 feet/second. The velocity applied in the

FLAC model was 1.03x10^6 feet/second. The applied force to maintain this velocity was determined by summing all forces around the boundary of the model.

Consolidation stresses in the clay were determined based on the buoyant unit weight of clay and the applied pressure at the surface used to consolidate the clay prior to testing as described previously. Initial stresses in the horizontal directions were determined based on a drained Poisson's ratio of 0.35, which is lower than the undrained Poisson's ratio of 0.45 that is listed in Table 4-2 and applicable to undrained loading after consolidation. The at rest earth pressure coefficient, K_0, can be determined from the Poisson's ratio, v, using Equation 4-1.

$$K_0 = \frac{v}{1-v} = \frac{0.35}{0.65} = 0.54 \qquad\qquad (4\text{-}1)$$

Initial horizontal stresses are higher than would be indicated by Equation 4-1 because the clay is overconsolidated. The effect of the overconsolidation ratio, OCR, on initial lateral stresses was included by calculating the at-rest earth pressure coefficient, K_0^{OCR}, using Equation 4-2.

$$K_0^{OCR} = (1 - \sin\varphi)*OCR^{\sin\varphi} \qquad\qquad (4\text{-}2)$$

Preliminary calculations with FLAC revealed that failure occurred in the mound at relatively low horizontal loads. Failure in the mound is interesting because Broms (2001) wrote a discussion to the Kitazume et al. (2000) article including bearing capacity computations, considering lateral spreading of columns, that result in lateral spreading in the sand layer. This discussion gave the original authors the opportunity to mention that the only type of failure seen in the mound was a deep-seated failure surface the cut through the sand layer, as well as the columns and unimproved clay. For these reasons the ubiquitous joint model was used in FLAC to model the sand mound. The shear strength in the mound was set artificially high; however, vertical failure planes through the mound have the properties of no cohesion and ϕ equal 35-degrees shown in Table 4-2.

Results of the FLAC^{2D} analysis were plotted with the results from DMMT11 and the finite element results presented in Kitazume et al. (2000), and they match reasonably well, as shown in Figure 4-3. The normalized horizontal displacement, δ, in Figure 4-3, is the horizontal deflection divided by the width of the caisson. It should be noted that the cohesion value used to determine Young's modulus of the column, as listed in Table 4-2 from Kitazume et al. (2000) is only 25% of the unconfined compression strength for test DMMT11, as listed in Table 4-1.
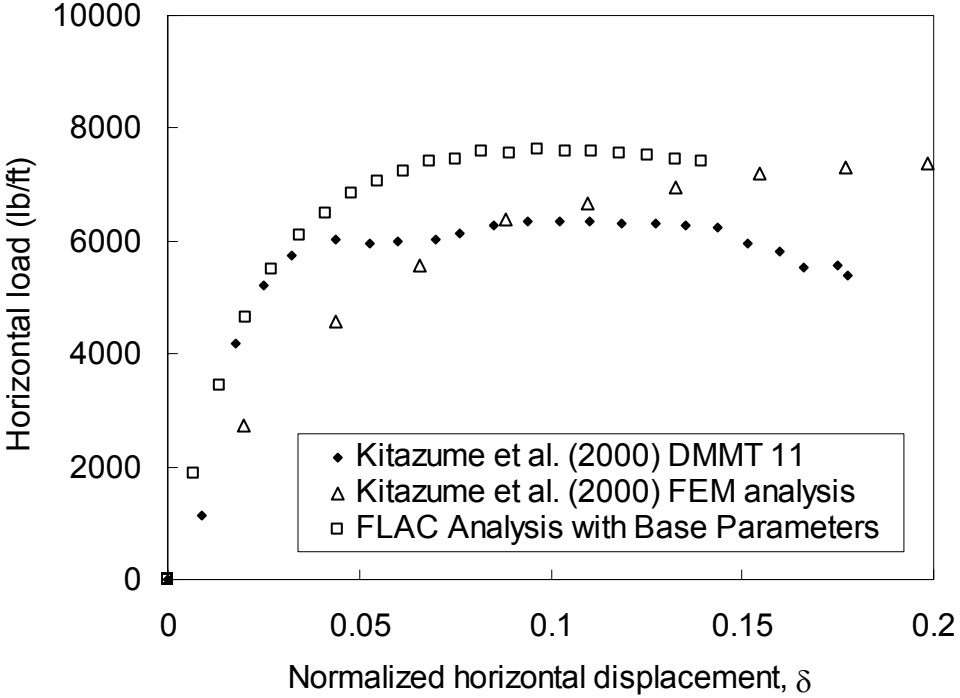
Figure 4-3. Centrifuge results and numerical model calculation of caisson deflection using an elastic model for columns

4.4. Further numerical analyses performed with FLAC

The finite element analysis performed by Kitazume et al. (2000) used elastic columns. Although the results in Figure 4-3 match the centrifuge data reasonably well, the analysis does not allow bending failure in the columns.

This problem was reanalyzed, incorporating Mohr-Coulomb failure criteria for the columns. A series of analyses were performed, using each combination of column strength, vertical load, and lateral load shown in Table 4-1. In each analysis, the column cohesion value is assumed to be

half the value of q_u shown in Table 4-1. Young's Modulus in the columns is assumed to be 200 * q_u, which is the same ratio used for the analysis in Section 4.4. The load-displacement curve corresponding with centrifuge test DMMT11 is shown in Figure 4-4. For this analysis, column strength, and the corresponding Young's Modulus, is roughly twice the value used in the Kitazume et al. (2000) analyses shown in Figure 4-3. The results shown in Figure 4-4 suggest that allowing for column failure criterion eliminates the need to artificially lower parameter values for the columns, which is required when no failure criterion is used for the column.
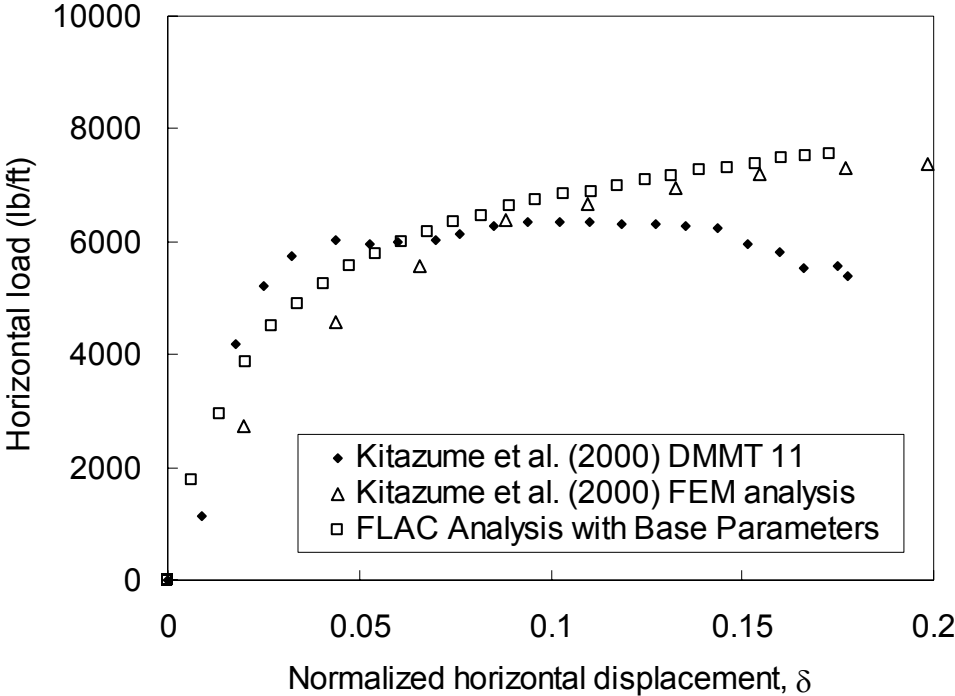
Figure 4-4. FEM results using an elastic model for columns, FLAC results using a Mohr-Coulomb model for columns, and centrifuge results of caisson deflection

The deformed mesh for the analysis corresponding with test DMMT 9-2b is included as Figure 4-5, while the deformed mesh for the analysis corresponding with test DMMT 3 is included as Figure 4-6. These deformed meshes show how FLAC is able to replicate tilting and bending failure, and match the behavior shown in Figure 4-2.
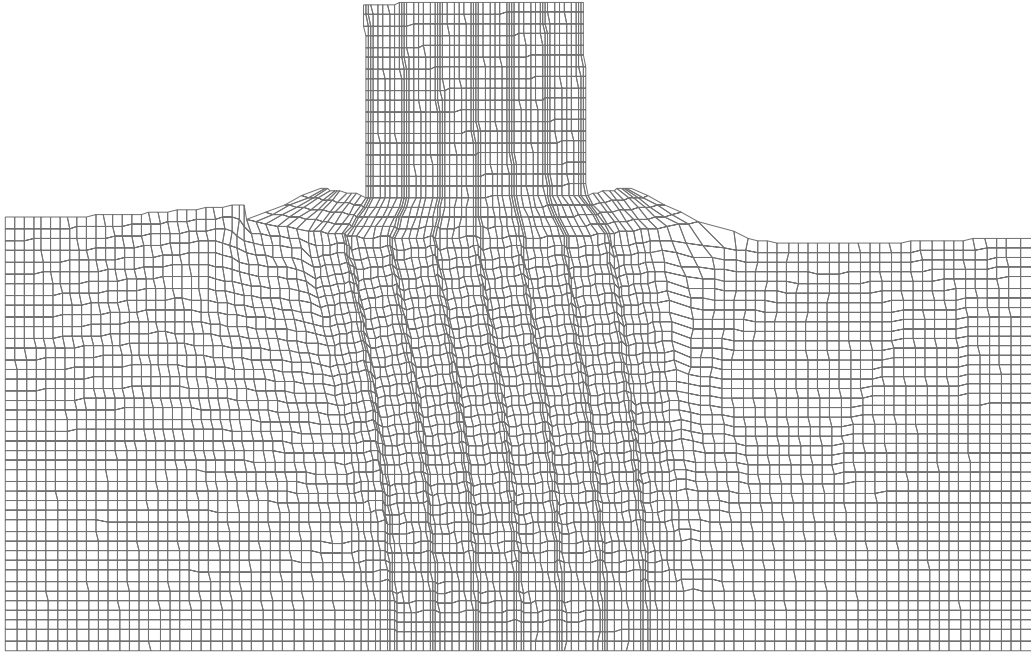
Figure 4-5. Deformed mesh corresponding with test DMMT 9-2
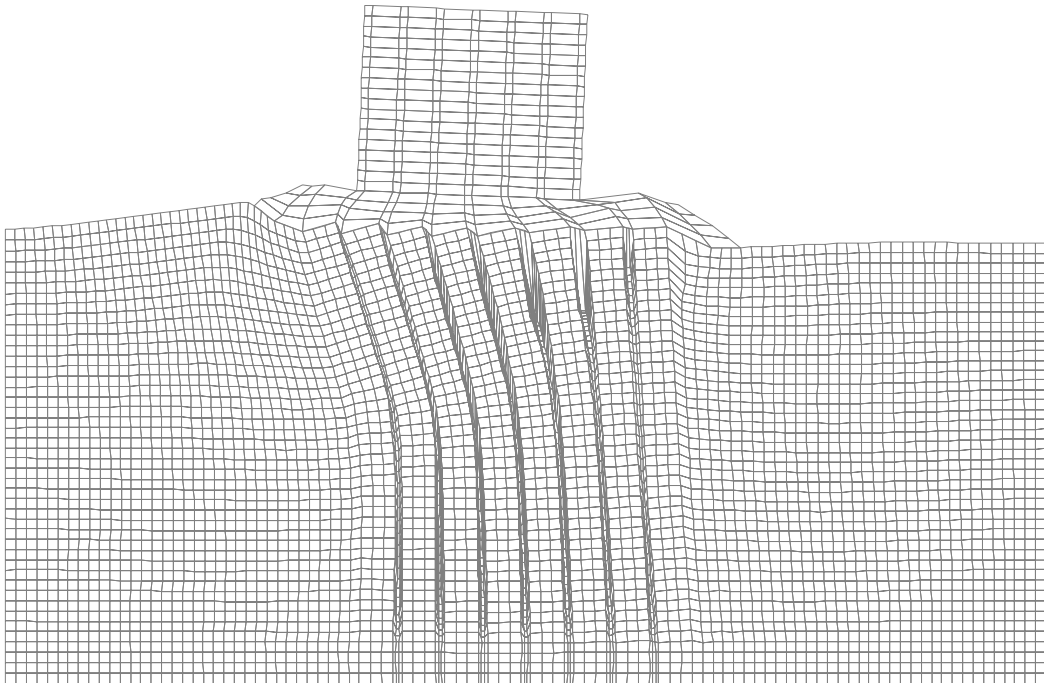
Figure 4-6. Deformed mesh corresponding with test DMMT 3

Kitazume et. al (2000) present the results of their centrifuge tests in terms of normalized vertical and horizontal loads, which are shown in Figure 2-3, and also presented here as Figure 4-7 for convenience. In this figure, the authors denote with two failure lines the limiting loads that can occur in the model based on circular shear failure. One failure line uses peak shear strength that is assumed to be one-half of q_u, and the other failure line uses residual strength, which is assumed to be 80% of peak strength. The authors also include two failure lines that incorporate bending failure of the columns in the analysis. Again, one failure line uses peak shear strength that is assumed to be one-half of q_u, the other failure line uses residual strength, which is assumed to be 80% of peak strength.

The results from the FLAC analyses are plotted along with the results from the centrifuge tests in Figure 4-8. Failure is assumed to occur in the FLAC analyses when the normalized horizontal displacement, shown as δ in Figures 4-3 and 4-4, is 10 percent. For each centrifuge test result shown in Figure 4-8, there is a corresponding numerical analysis result that uses the same vertical force and column strength as in the centrifuge test. Considering the amount of scatter in the results from the centrifuge tests listed in Table 4-1, the FLAC analyses match the results of these tests quite well.

4.5. Summary

The centrifuge tests and subsequent numerical analyses performed by Kitazume et al. (2000) are an excellent example of the behavior of deep-mixed columns in soft clay that are subjected to vertical and horizontal loading. FLAC was used to match model behavior using parameter values provided by the original authors. An interesting outcome of these analyses is that FLAC was able to capture bending failure in columns for centrifuge tests performed with low column strength.
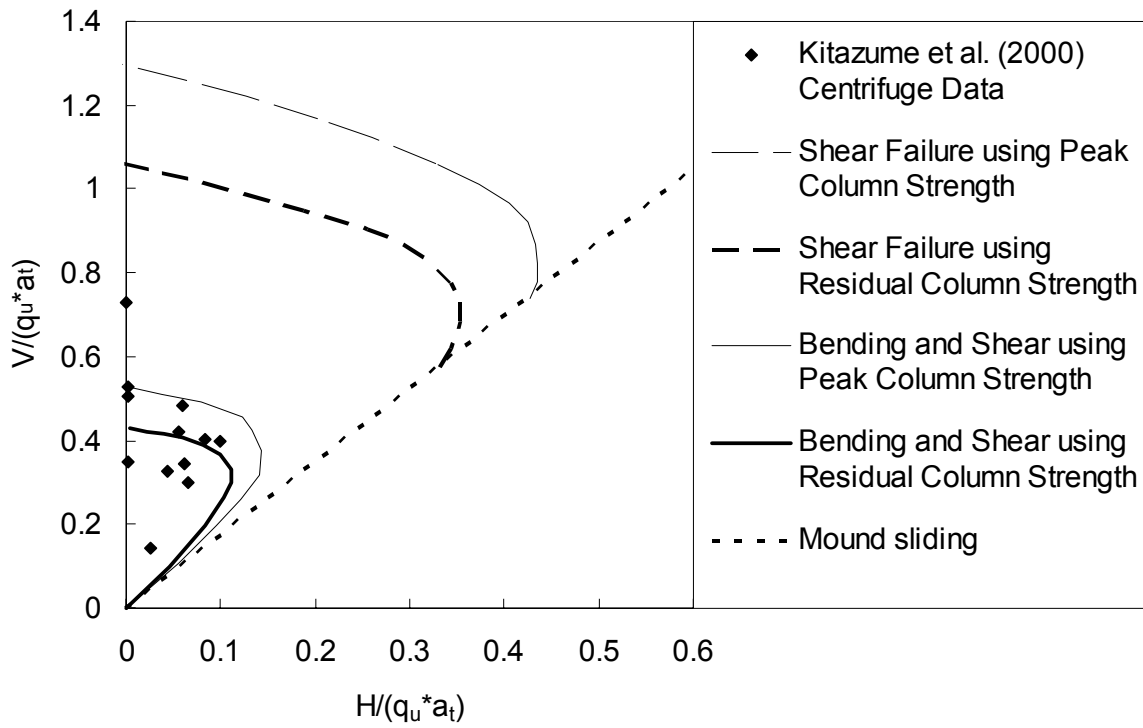
Figure 4-7. Results of centrifuge tests performed by Kitazume et al. (2000)
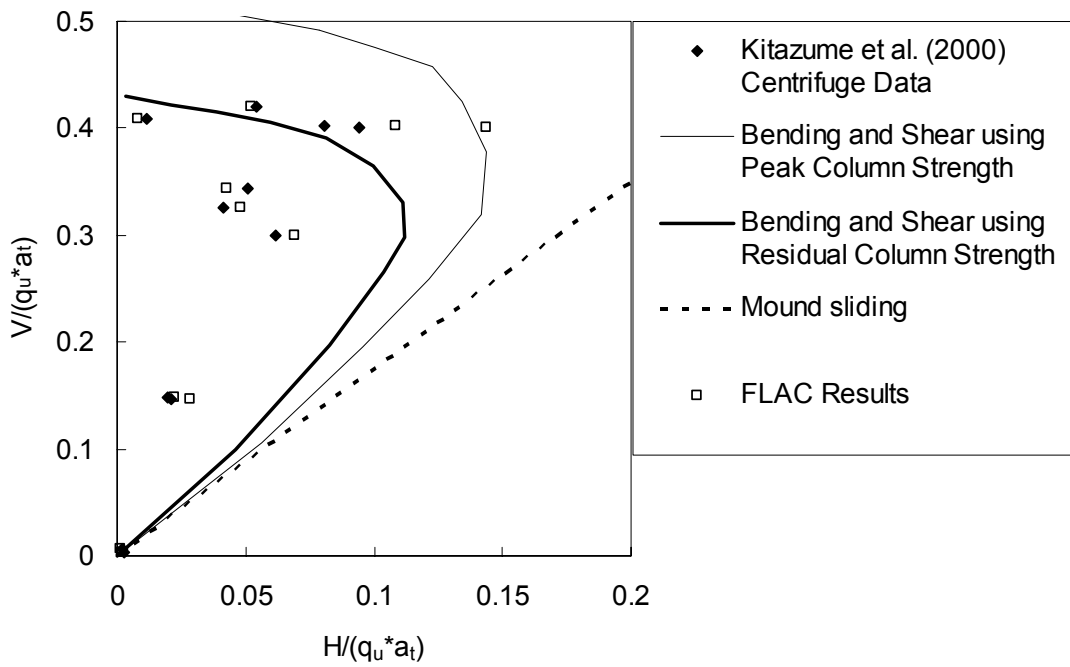
Figure 4-8. Results from numerical analyses and centrifuge tests

69

5. ANALYSIS OF CENTRIFUGE MODEL TESTS
OF A COLUMN-SUPPORTED EMBANKMENT

5.1. Introduction

This section describes FLAC analyses of the centrifuge model tests by Inagaki et al. (2002), who also performed finite element analyses (FEM) of their model tests. The Inagaki et al. (2002) centrifuge tests provide a baseline for evaluating the two-dimensional and three-dimensional numerical analyses presented in this chapter. After verifying numerical analysis results with the work performed by Inagaki et al. (2002), additional investigations were performed with FLAC to study the behavior of other column arrangements used to support embankments and to investigate stresses in the columns.

5.2. Centrifuge tests

The centrifuge tests were performed with an acceleration of 50g. Sand was placed at the bottom of the model test box. Clay slurry was poured over the sand and consolidated with a pressure of 2047 psf under an acceleration of one gravity to create the soft clay layer. This procedure resulted in a soil that was overconsolidated near the surface and normally consolidated at the bottom of the clay layer when subsequently accelerated to 50g. Columns were installed with a 20% replacement ratio by coring 0.8-inch-diameter holes in a square pattern in plan view with 1.6-inch center-to-center spacings, and replacing the clay with a soil-cement mix. The embankment was placed at 50g in three equal lifts with a final 1 vertical on 1.6 horizontal side slope. This construction resulted in an embankment 4.7 inches high overlying 10.2 inches of clay and 2.4 inches of sand in model scale. The profile schematic is included as Figure 5-1. With an acceleration of 50 g, the model dimensions are multiplied by 50 to obtain prototype scale. Thus, the prototype sand layer is 9.8-feet thick, the clay layer is 42.7-feet thick, the embankment is 19.7 feet high, the column diameter is 3.3 feet, and the column center-to-center spacing is 6.6 feet.
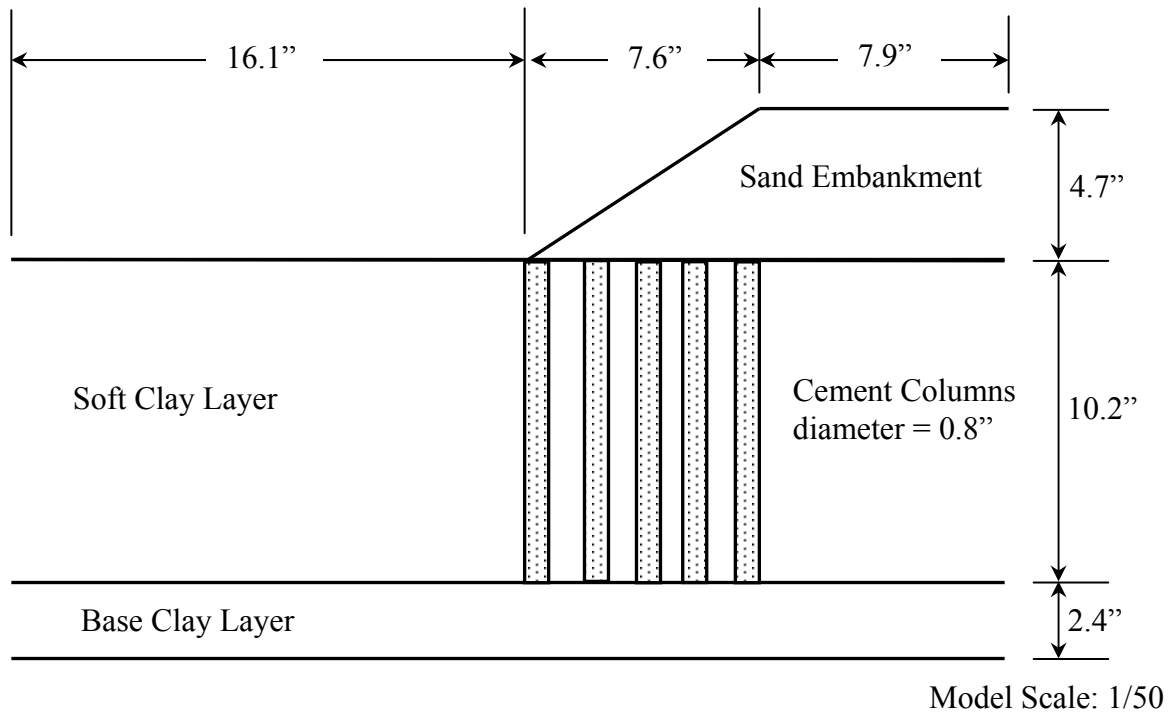
Figure 5-1. Inagaki et al. (2002) centrifuge test schematic

5.3. Numerical analysis performed by Inagaki et al. (2002)

Inagaki et al. (2002) performed a two-dimensional plane-strain finite element analyses of the centrifuge tests. A Sekiguchi/Ohta Model (Sekiguchi et al. 1977) was used for the clay. This is a water-soil coupled, elasto-plastic, Modified Cam-Clay model that incorporates soil anisotropy.

The embankment, columns, and sand layer were modeled as elastic materials. The parameters used in the FEM analysis performed by Inagaki et al. (2000) are listed in Table 5-1. The authors did not provide unit weight information for the cement columns. Inagaki et al. (2002) also note the Young's modulus of the embankment was set to a low value so the tension stress of the embankment would not influence deflections. Results from the finite element analyses closely matched measured column deflections in the centrifuge tests.

Table 5-1. Properties provided by Inagaki et al. (2002)

Material	Wet density (pcf)	Parameter Values
Soft clay layer	107	c_u = 376 psf, Cc = 0.35, c_v = 45 to 250cm^2/day, PI = 24.6, ϕ' = 28.8°, K_0 = 0.543, k = 10^{-6} cm/sec, λ = 0.152, Λ = 0.658, M = 1.151
Base sand layer	100	D_r = 90.6%, E = 438,600 psf, v = 0.3
Embankment	117	ϕ_d = 34°, E = 20,900 psf, v = 0.3
Cement Column	107	E = 200q_u, q_u = 6,270 psf, v = 0.4

5.4. FLAC two-phase analysis

In this research, FLAC was used to analyze the centrifuge model tests of Inagaki et al. (2002), and the results are compared with their calculations. The centrifuge test was performed at 1:50 scale, but the FLAC analyses were performed at full prototype scale. The material property values used in the FLAC analyses are listed in Table 5-2.

Table 5-2. Properties used in the FLAC water-soil coupled analyses

Material	Wet density (pcf)	Parameters
Soft clay layer	107	K_{max} = 1.33x10^5 psf, v = 0.352, M = 1.151, λ = 0.152, κ = 0.052, k = 10^{-6} cm/sec, υ = 2.38
Base sand layer	100	E = 4.39x10^5 psf, v = 0.3
Embankment	117	E = 2.09x10^4 kN/m^2, v = 0.3
Cement Column	107	E = 1.25x10^6 psf, v = 0.4

The Sekiguchi/Ohta model used by Inagaki et al. (2002) for the clay layer was replaced with the Modified Cam-Clay model which is programmed into FLAC, and consequently results in much less computation time than a user programmed version of the Sekiguchi/Ohta model. Even so, the water-soil coupled analyses of this model took several days using FLAC^{2D}, and a three-dimensional analysis would take many times longer.

The Poisson's ratio, ν, listed in Table 5-2 for the soft clay layer was determined from Equation 5-1 using the value of K_0 provided in Table 5-1.

$$\nu = \frac{K_0}{1 + K_0} \tag{5-1}$$

The critical state parameters M and λ for the clay were provided in Table 5-1. The value of κ was determined from Equation 5-2.

$$\kappa = \lambda(1 + \Lambda) \tag{5-2}$$

The specific volume, υ, is simply $1 + e$. The void ratio for the clay layer was determined assuming the material was saturated, using the density shown in Table 5-1, and assuming $G_s = 2.7$. This produces values of e equal to 1.38 and υ equal to 2.38.

In every iteration, FLAC calculates the value for the soil bulk modulus, K, based on the Modified Cam Clay parameter values of specific volume, υ, mean pressure, p, and κ by Equation 5-3.

$$K = \frac{\upsilon p}{\kappa} \tag{5-3}$$

For the Modified Cam-Clay model, FLAC requires the input parameter, K_{max}, which is an upper bound for the soil bulk modulus. Choosing a value of K_{max} that is too high may cause the model to be slow to converge. Choosing a value of K_{max} that is too low will cause the model to stop. In a FLAC example problem (Itasca 2002) for an embankment on a Modified Cam-Clay foundation, K_{max} was set to twice the value of K at the bottom of the clay layer. This approach was also used in the analyses of the Inagaki et al. (2000) centrifuge tests. The effective vertical stress, σ_v', at the bottom of the clay layer is the surcharge pressure, 2047 psf, plus the buoyant unit weight of the clay under an acceleration of 1g. The effective vertical stress at the bottom of the layer is 2085 psf. The horizontal stress at the bottom of the clay layer is $\sigma_h' = K_0\sigma_v' = 1132$

psf. Therefore, the mean stress, $p = (2085 + 2 \times 1132) / 3 = 1450$ psf. K_{max} was set to correspond to twice the mean stress, so that $K_{max} = 2 \times 2.38 \times 1450$ psf $/ 0.052 = 1.33 \times 10^5$ psf, as shown in Table 5-2.

Results from numerical analyses are greatly influenced by initial stresses. Initial total stresses are used in FLAC to define initial stresses. Initial pore water pressures were specified assuming a static ground water table at the gound surface. The initial total vertical stresses applied in the FLAC analyses were determined from the unit weights used in Table 5-2. The initial horizontal stresses were determined considering the model was consolidated under an applied vertical stress of 2047 psf, prior to being placed in the centrifuge. This resulted in the upper portions of the clay layer being overconsolidated. The base sand layer was normally consolidated, and horizontal effective stresses were calculated using the at-rest lateral earth pressure coefficient shown in Equation 5-4.

$$K_0 = 1 - \sin \varphi \tag{5-4}$$

Initial effective horizontal stresses for the clay layer were determined using an at-rest lateral earth pressure coefficient that incorporated the overconsolidation ratio, OCR, according to Equation 5-5.

$$K_0{}^{OCR} = (1 - \sin \varphi) * OCR^{\sin \varphi} \tag{5-5}$$

The friction angle was determined from the slope of the critical state line, M, using Equation 3-21 for triaxial compression. The friction angle, ϕ, of the clay was also checked using the Poisson's ratio, v, from Equations 5-1 and 5-4 (Duncan and Wong 1999). Based on these two methods, the value of 28 degrees was selected. Using the resulting value of K0 from Equation 5-5, the horizontal effective stresses were calculated. Then, initial pore pressures and effective horizontal stresses were then summed to find the initial total horizontal stresses required for FLAC.

When groundwater is used in FLAC, the program includes the weight of water occupying pore space for submerged soils. The weight of water in the soil is based on the porosity and unit weight of water. Unit weights for the clay layer and the base sand layer were adjusted from the values listed in Table 5-2 to account for this weight of water within the soil matrix.

The geometry shown in Figure 5-1 was discretized into 5913 zones for the two-dimensional plane-strain analyses. Five rows of deep-mixed columns in the improvement zone were represented by vertical strips, with the center-to-center spacing equal to the spacing of the rows of deep-mixed columns installed in the centrifuge model at prototype scale. The mesh used for these analyses was created with three zones in the horizontal direction representing each column, and three zones between columns representing soil. Two separate analyses were performed, one with narrow strip widths and one with wide strip widths. The width of narrow strips was chosen to result in the same area replacement ratio of 20% that corresponds to the column diameter and spacing used in the centrifuge model. The width of wide strips was chosen to result in the same moment of inertia as the circular columns. The column diameter and strip widths are summarized in Table 5-3.

Table 5-3. Deep-mixed element widths

Element	Width (ft)	
	Model Scale	Prototype Scale
3D Column	0.066	3.28
2D Narrow Strip	0.026	1.30
2D Wide Strip	0.044	2.20

Columns were added in the numerical model by changing zones representing columns from clay properties to the column properties shown in Table 5-2. Three different column configurations were analyzed to correspond to three different models that were tested in the centrifuge. Case 1 had five rows of columns that extend from the top of the clay layer to the top of the base sand layer. Case 2 had five rows of "floating" columns that only extend from the top of the clay layer down nine meters into the thirteen-meter-thick clay layer. Case 3 had three rows of columns that extend from the top of the clay layer to the top of the base sand layer. A FLAC analysis was

75

performed for each of the three cases using the two-dimensional narrow strip width shown in Table 5-3. Further analyses, which are described later in this chapter, were performed for all three cases using three-dimensional columns and the two-dimensional wide strip width shown in Table 5-3.

For the FLAC analyses of each of the three cases, the embankment was placed in three lifts. After each lift of the embankment was placed, the model was run to equilibrium with no drainage allowed. Then, pore pressures were allowed to dissipate while drainage was allowed to occur for five hours.

The centrifuge test allowed six days for pore pressure dissipation during fill construction. Inagaki et al. (2000) also continued to allow pore pressures to dissipate for a period of 240 days. Inagaki et al. (2002) do not specify whether this is real time or model time, but it is assumed the time reported for pore pressure dissipation in the centrifuge is some type of model time. Model time in a centrifuge for dynamic analyses is equal to real time multiplied by the factor n, where n is the centrifugal acceleration. At an acceleration of 50g, this would still require nearly five days in the centrifuge. The Institute of Geotechnical Engineering in Zurich (2004) indicates that the scaling factor for model time in terms of diffusion may be n^2, rather than n. Regardless, the FLAC model was only allowed to dissipate pore pressures for fifteen hours during embankment placement, and two additional days after fill construction, which is much less time than the model time allowed for in the centrifuge. However, it was found in the FLAC analyses that lateral deflections reached a maximum at the end of undrained loading and did not increase as pore pressures dissipated. From this response, it was determined that a short consolidation time would be sufficient to determine lateral deflections.

Inagaki et al. (2002) present lateral deflection along the length of columns for all three cases investigated. The deflections measured in the centrifuge and calculated with their model are essentially identical. After the third lift was completed in the FLAC analyses, displacements were calculated at several depths in each column and plotted against the centrifuge test results as shown in Figures 5-2, 5-3, and 5-4. It can be seen in these figures that the FLAC analyses generally match deflections measured in the centrifuge very well.
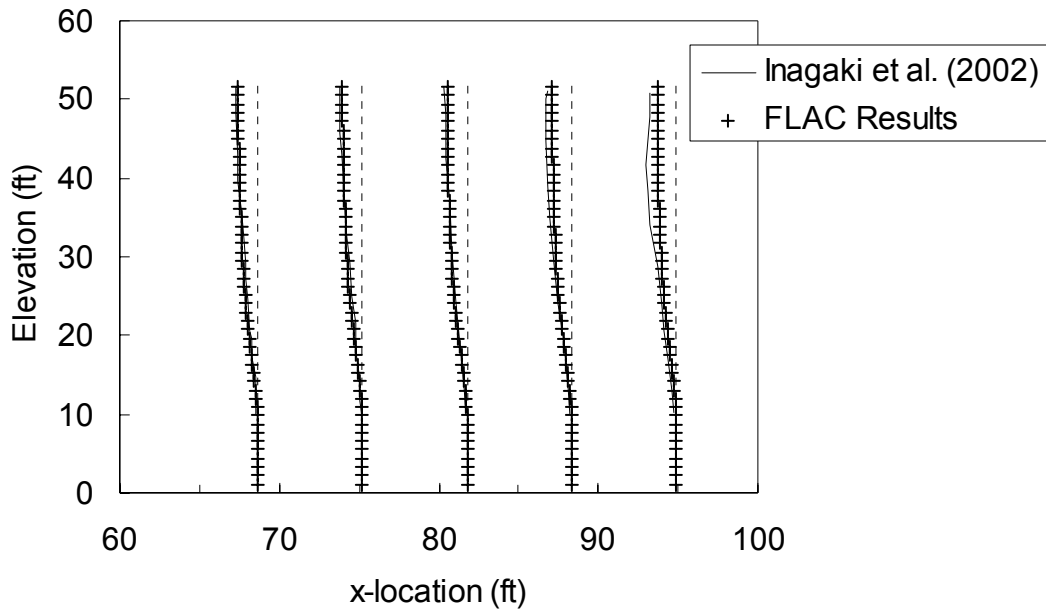
Figure 5-2. Horizontal deformations for Case 1
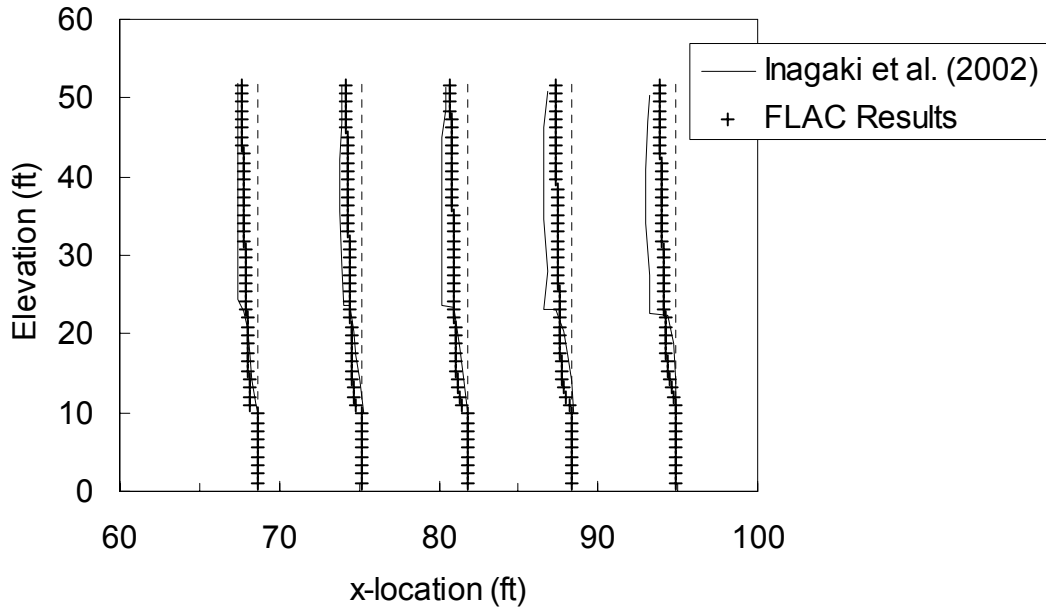
Figure 5-3. Horizontal deformations for Case 2
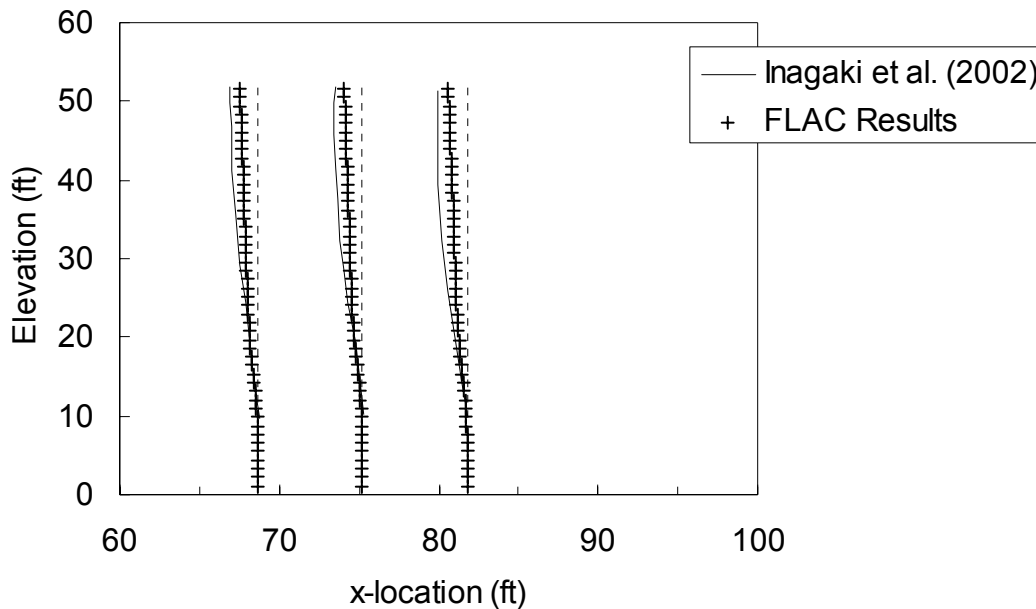
Figure 5-4. Horizontal deformations for Case 3

5.5. Mohr-Coulomb approximation of clay behavior

Another set of analyses were performed using the Mohr-Coulomb model for the soft clay layer rather than the Modified Cam Clay model used in the previous analyses. This set of analyses did not include pore water, which was included in the previous analyses. The property values used for the undrained analyses with a Mohr-Coulomb model for the clay are listed in Table 5-3. The undrained strength of the clay was set equal to the value of s_u = 376 psf reported by Inagaki et al. (2000). The Young's Modulus for the clay layer was set equal to the value of 2.63 x 10^5 psf, which is an undrained, E_{50} modulus value estimated based on the plastic index of 24.6, s_u = 376 psf, and the range of overconsolidation ratios for the clay layer, from a chart published by Duncan and Buchagnani (1976). Initial total stresses for these undrained analyses without pore water were the same as in the previous analyses.

The soil property values include the total unit weights and undrained strengths listed in Table 5-4. An undrained Poisson's ratio of 0.49 was used for the clay and the columns. Using a higher Poisson's ratio would result in a better match for undrained behavior of the clay and columns, but may also lead to numerical instabilities. For FEM analyses, Duncan et al. (1980) recommend

that the value of Poisson's ratio be limited to values less than or equal to 0.49. Elastic properties for the base sand and embankment were identical to those used in Table 5-2. Good agreement between measured and calculated displacements was obtained for Case 1 and Case 3 which have end bearing columns, but the calculated deflections were substantially larger than the measured deflections for Case 2 with "floating columns."

Table 5-4. Parameters used in undrained analyses

Material	γ (pcf)	c (psf)	ϕ (degrees)	E (psf)	ν
Clay layer	107	376	0	2.63×10^5	0.49
Base sand layer	100	elastic		4.39×10^5	0.3
Embankment	117	elastic		2.09×10^4	0.3
Columns	107	elastic		1.23×10^6	0.49

Because the calculated deflections for Case 2 were much larger than measured, and because only the clay characteristics were changed between the analyses based on the material property values listed in Tables 5-2 and 5-3, two series of FLAC analyses were performed to compare the behavior of a Modified Cam Clay material with the clay properties in Table 5-2 to the behavior of a Mohr-Coulomb material with the clay properties in Table 5-4.

The first series of analyses is isotropic compression of a single element with loading conditions chosen to represent soil in the middle of the clay layer. The results of these analyses are shown in Figure 5-5. The Modified Cam Clay properties of the clay layer in Table 5-2 were used with both a drained and an undrained analysis. The Mohr-Coulomb properties of the clay layer in Table 5-4 were used to represent an undrained analysis. As can be seen in Figure 5-5, using Mohr-Coulomb properties with a Poisson's ratio of 0.49 result in small volumetric strains, similar to results using Modified Cam Clay properties in an undrained anlaysis.

The second series of analyses were simple shear analyses of a single element with loading conditions chosen to represent soil at different depths in the clay layer. The results of this type of analysis for an element of soil at a depth below the bottom of the columns in Case 2 are shown

in Figure 5-6. Two items can be seen in Figure 5-6 that show the difference between the shear behavior of the Modified Cam Clay material with the clay properties listed in Table 5-2 and the shear behavior of the Mohr-Coulomb material with the clay properties listed in Table 5-4. The Mohr-Coulomb properties produced a stiffer response than the Modified Cam Clay properties up to a limiting shear stress around 350 psf. When the sample reached this limiting shear stress, it experienced perfectly plastic shear deformation in contrast to the Modified Cam Clay model which continued to offer additional resistance to shear throughout the range of loading.
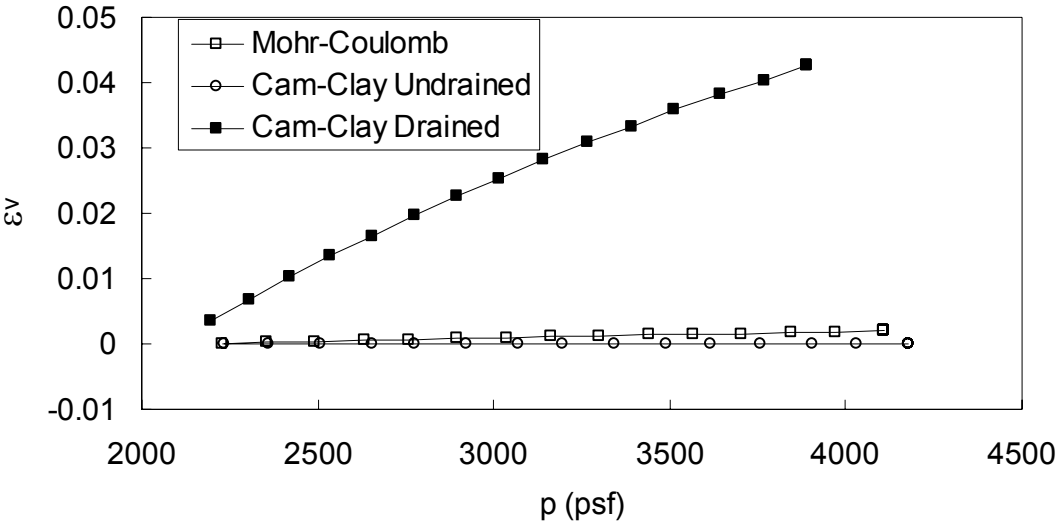
Figure 5-5. Isotropic compression of single element with FLAC

Based on the pressure of 98 kPa used to consolidate the sample, the ratio of undrained strength (s_u =18 kPa) to preconsolidation pressure (s_u/p) would only be 0.18, which is a low estimate for the region in the clay layer loaded in simlpe shear. Terzaghi et al. (1996) show the value of s_u/p to be around 0.23 when clay with a plasticity index of 24.6 is loaded in simple shear. The undrained strength corresponding to $s_u/p = 0.23$ is 23 kPa. This value of shear strength was used to represent the clay in another set of FLAC analyses of the Inagaki et al. (2002) centrifuge tests using the Mohr-Coulomb model for the clay.

In this additional set of FLAC analyses, undrained soil modulus values for the clay layer were obtained using the Modified Cam-Clay model, with the parameter values provided by Inagaki et

al. (2002). The shear modulus for the clay was determined from the results of a series of simple shear analyses corresponding to different depths throughout the clay layer. Each analysis resulted in behavior similar to the results shown in Figure 5-6. It was found that the shear modulus increased approximately linearly with depth and ranged from 850 psf at the ground surface to 27,000 psf at the bottom of the clay layer, as shown in Figure 5-7. These values of shear modulus were used in conjunction with the assumed value of Poisson's ratio of 0.49 to calculate the Young's Modulus.
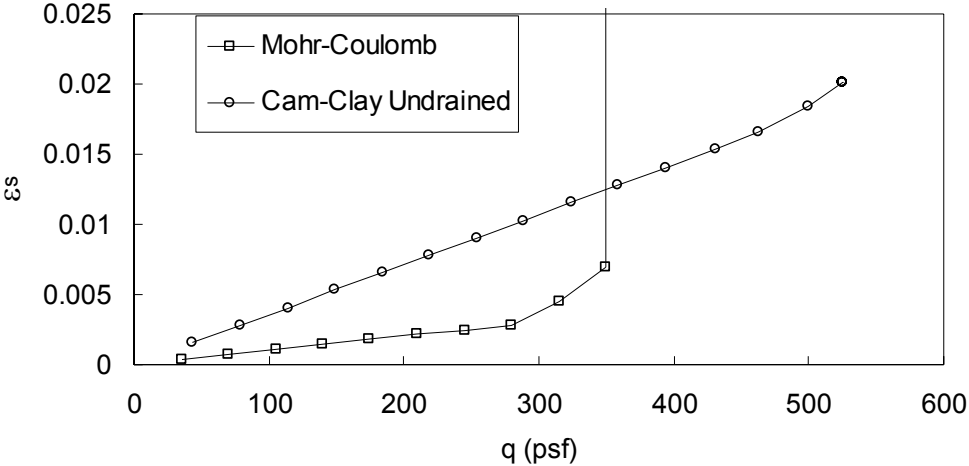
Figure 5-6. Simple shear of single element with FLAC
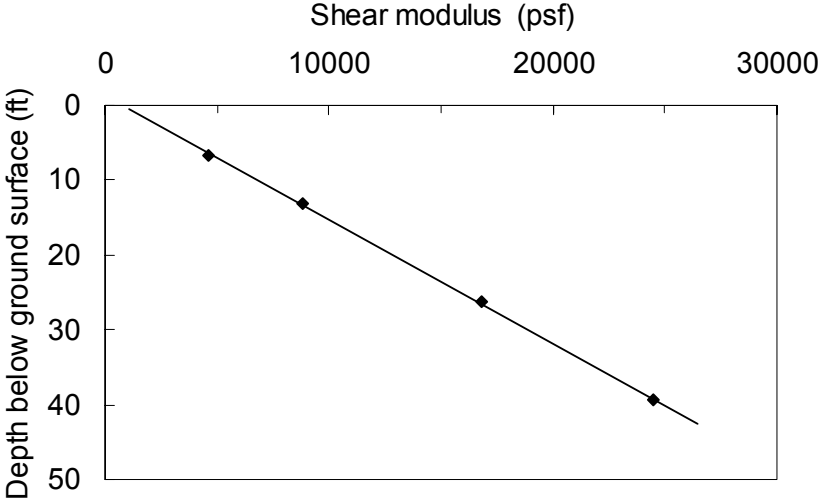
Figure 5-7. Shear modulus value in the clay

The revised material property values used in the FLAC analyses are summarized in Table 5-5. The results of the FLAC analyses of the Inagaki et al. (2002) centrifuge tests using the revised

81

Mohr-Coulomb properties for the clay layer are presented in Figures 5-8, 5-9 and 5-10. It can be seen that the analyses using the revised Mohr-Coulomb properties are in good agreement with the analyses that used the Modified Cam Clay representation of the clay, and that both sets of analyses are in reasonably good agreement with the results of Inagaki et al. (2002). This investigation revealed that rather than using water-soil coupled analyses, an undrained analysis with carefully selected modulus and strength values for the clay layer produced accurate calculations of lateral deflections for the cases investigated.

Table 5-5. Revised clay parameters for undrained analyses

Material	γ (kg/m^3)	c (kPa)	ϕ (degrees)	E (kPa)	ν
Embankment	1878	elastic		1000	0.3
Clay layer	1714	0.23p	0	*	0.49
Base sand layer	1608	elastic		21000	0.3
Columns	1714	elastic		60000	0.49

* note: Modulus values increase with depth as described in text and shown in Figure 5-7
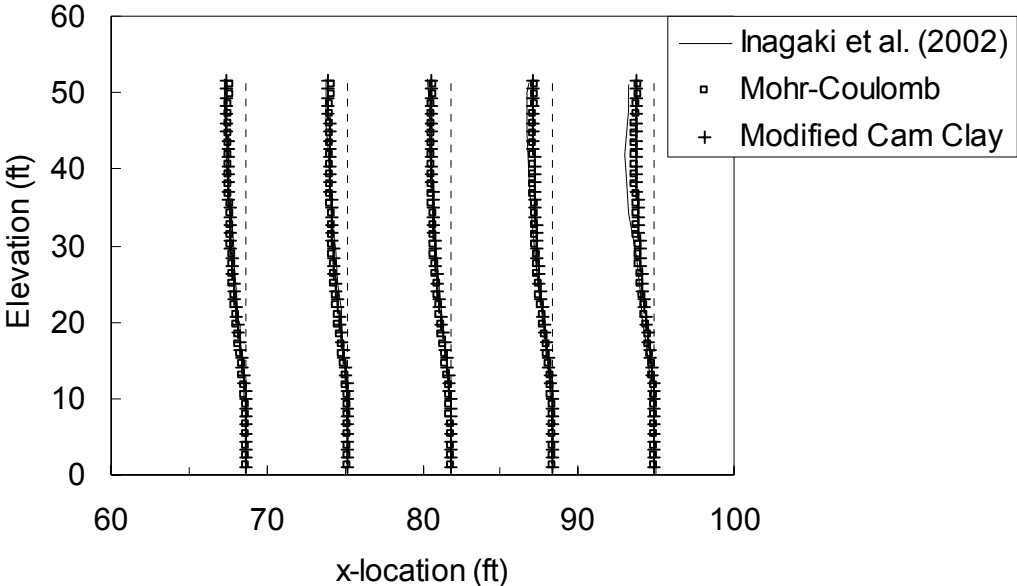
Figure 5-8. Horizontal deformations for Case 1 with Mohr-Coulomb properties for the clay layer
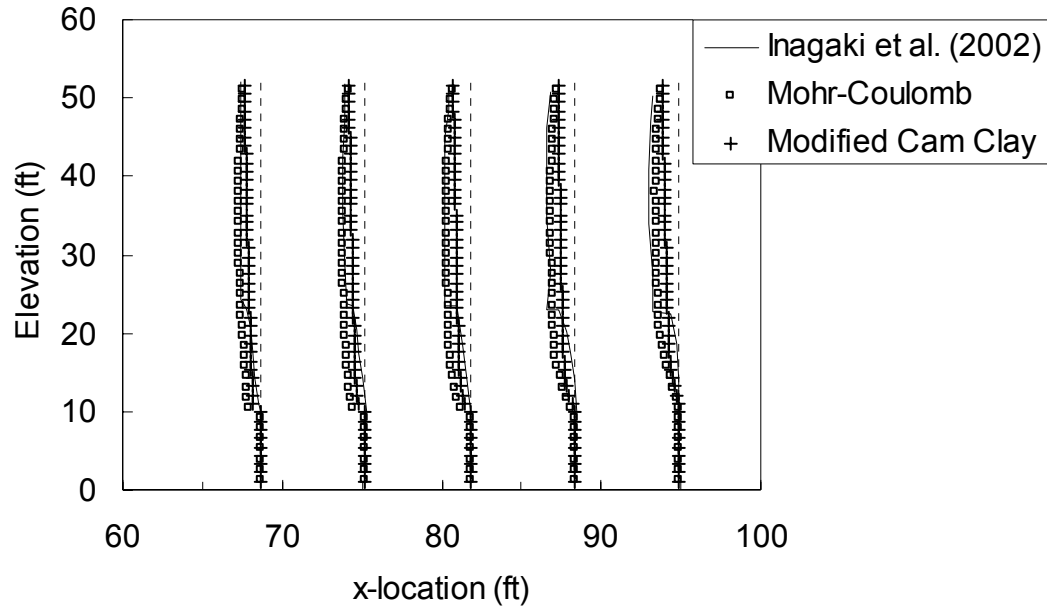
Figure 5-9. Horizontal deformations for Case 2 with Mohr-Coulomb properties for the clay layer
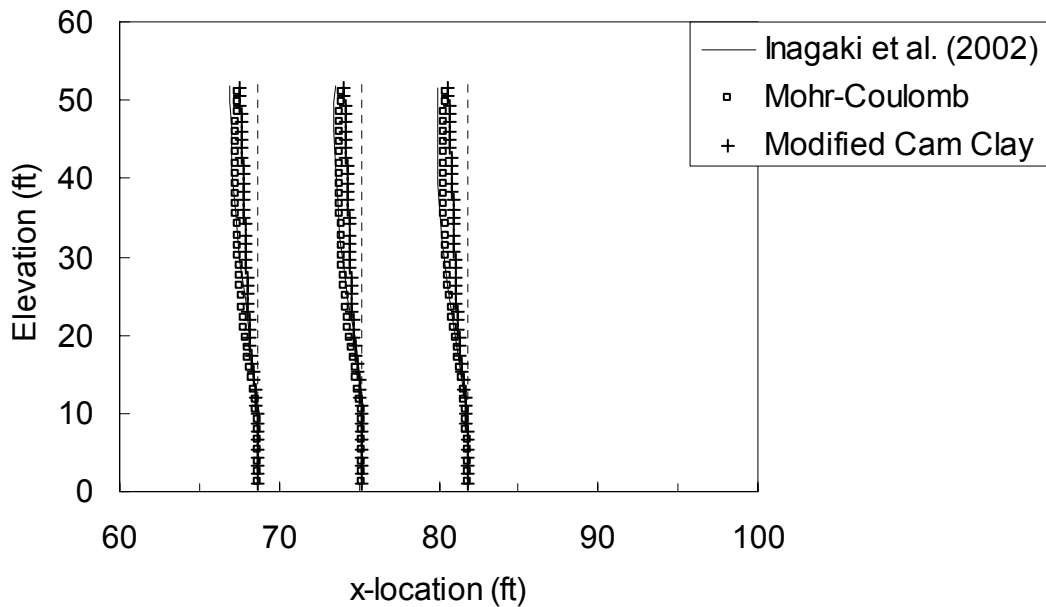
Figure 5-10. Horizontal deformations for Case 3 with Mohr-Coulomb properties for the clay layer

5.6. Three-dimensional analyses

Undrained, three-dimensional analyses of Cases 1 through 3 were performed using FLAC^{3D}. In

three dimensions, symmetry was used to analyze only the portion indicated in the plan view in

Figure 5-11. For the three-dimensional analysis, the geometry was divided into 52,560 zones.

The three-dimensional mesh used to model the column-supported embankment is shown in

Figure 5-12.
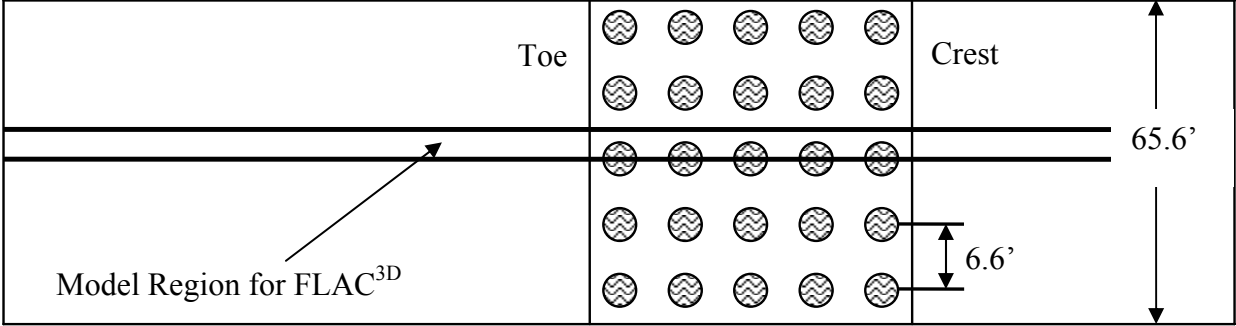
Figure 5-11. Plan view of Inagaki et al. (2002) centrifuge model for 3D analyses

a. Profile

b. Plan
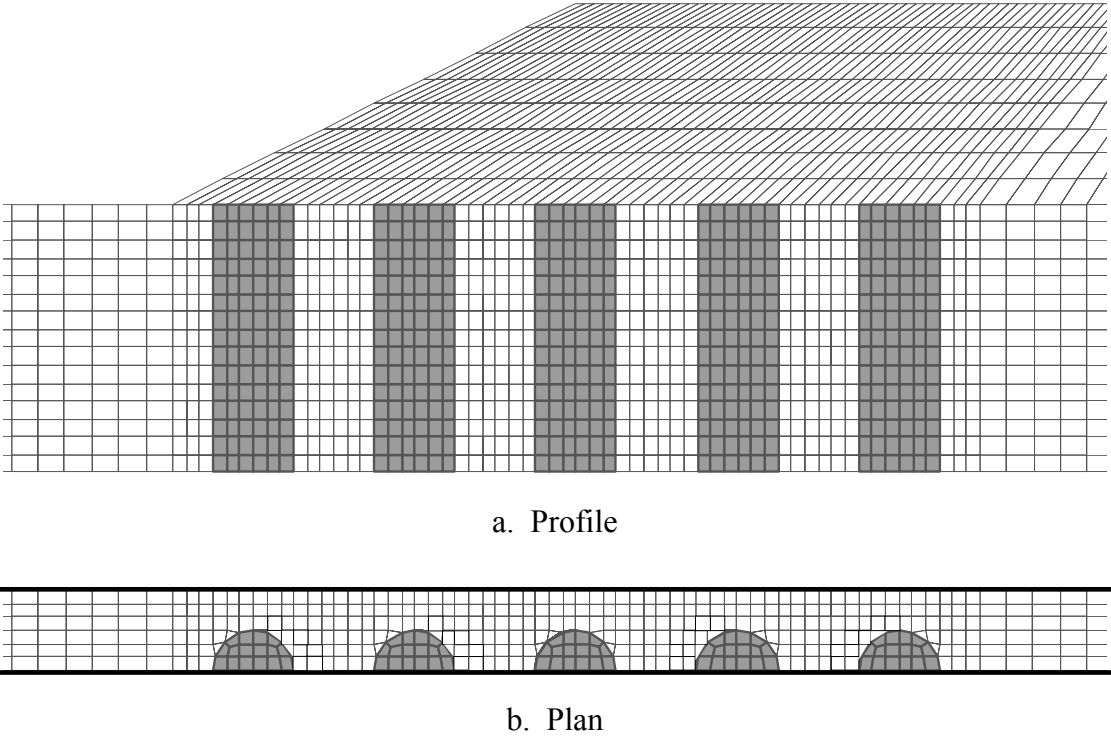
Figure 5-12. FLAC^{3D} mesh for the model region around columns

The three-dimensional analyses were performed using the properties listed in Table 5-5,

including Mohr-Coulomb properties for the Clay layer. Initial stresses for the three-dimensional

analyses were set in the same manner as for the two-dimensional analyses described above. The

shear modulus value that was determined as explained previously for the two-dimensional analyses was also used for the three-dimensional analyses. The results from these three-dimensional analyses are shown in Figures 5-13, 5-14 and 5-15. It can be seen that the 3D analyses produced slightly smaller lateral deflections than the 2D analyses. The same area replacement ratio was used in the 2D and 3D analyses, and this produces the same axial stiffness of the columns in both cases. However, using the same area replacement ratio produces a smaller bending stiffness in the 2D representation than in the 3D representation, and this could contribute to the slightly smaller lateral deformations calculated in 3D than in 2D.
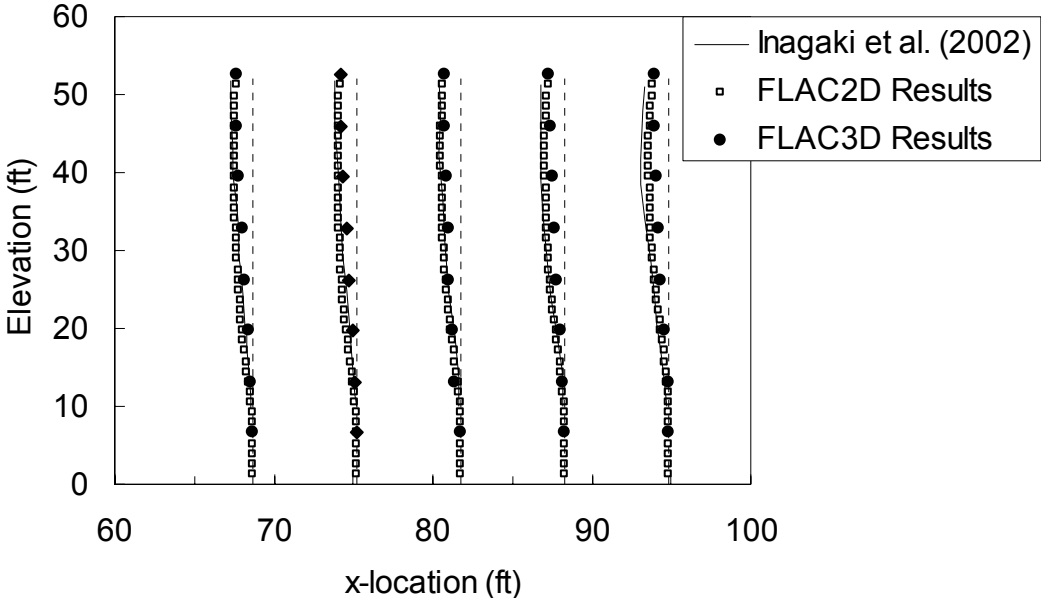
Figure 5-13. Horizontal deformations for Case 1 computed with FLAC^{2D} and FLAC^{3D}
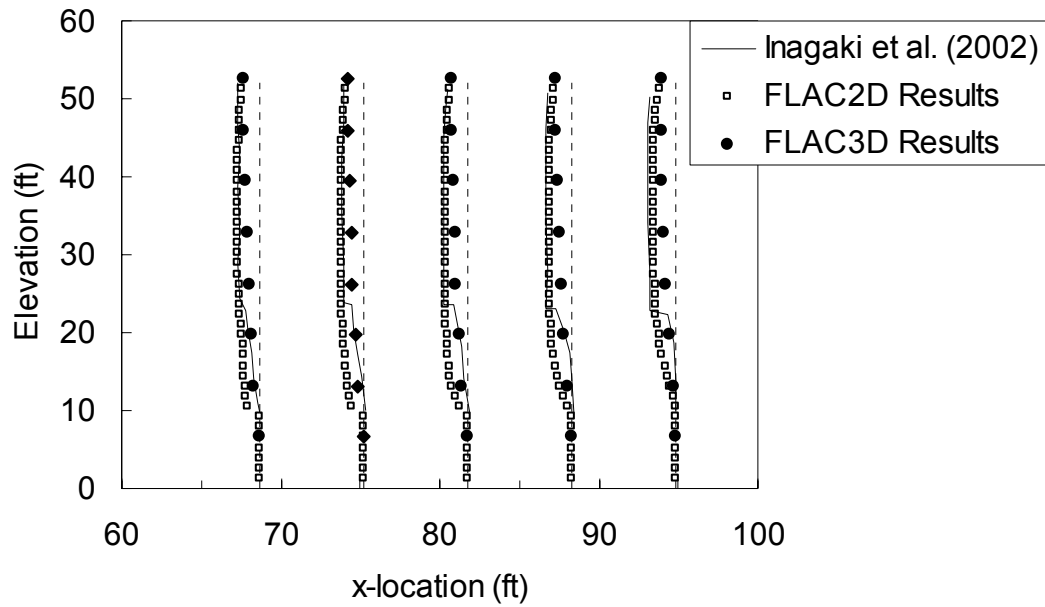
Figure 5-14. Horizontal deformations for Case 2 computed with FLAC^{2D} and FLAC^{3D}
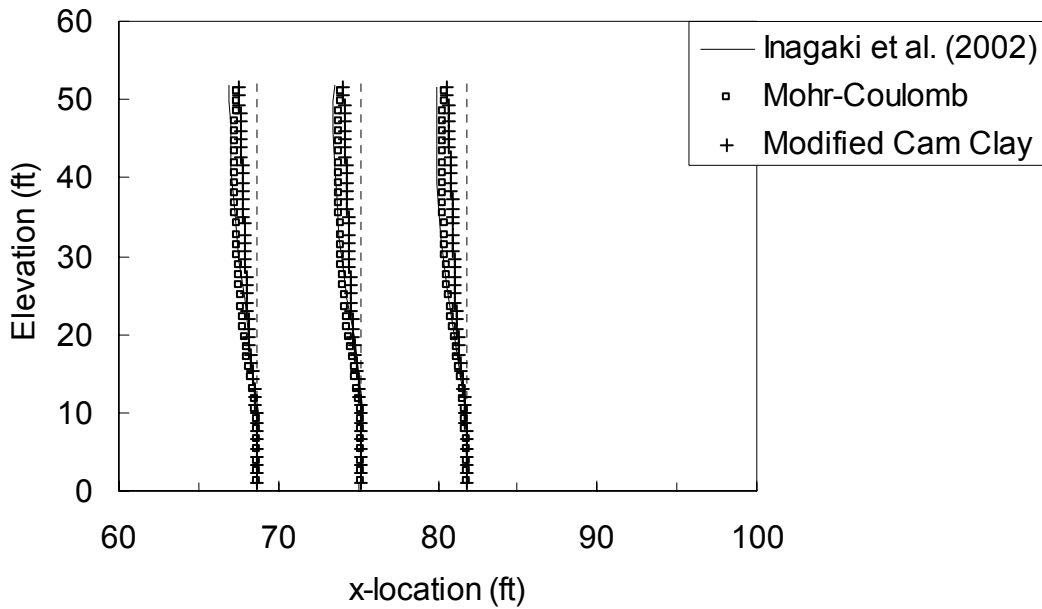
Figure 5-15. Horizontal deformations for Case 3 computed with FLAC^{2D} and FLAC^{3D}

For the five-end-bearing-column case, results for the two-dimensional analyses using both narrow strips and wide strips, as well as results from the three-dimensional analysis all closely match the measured column displacements from Inagaki et al. (2002). This can be seen in a plot

of displacement versus depth for the first column located under the toe, as shown in Figure 5-16. Because there is no columnar support under the center portion of the embankment in this analysis, the embankment load produces large lateral pressures in the clay and large lateral deflections of the columns. System behavior is largely influenced by the shear modulus of the clay, and there is little difference between deflections from narrow strips, wide strips, or the three-dimensional analysis.
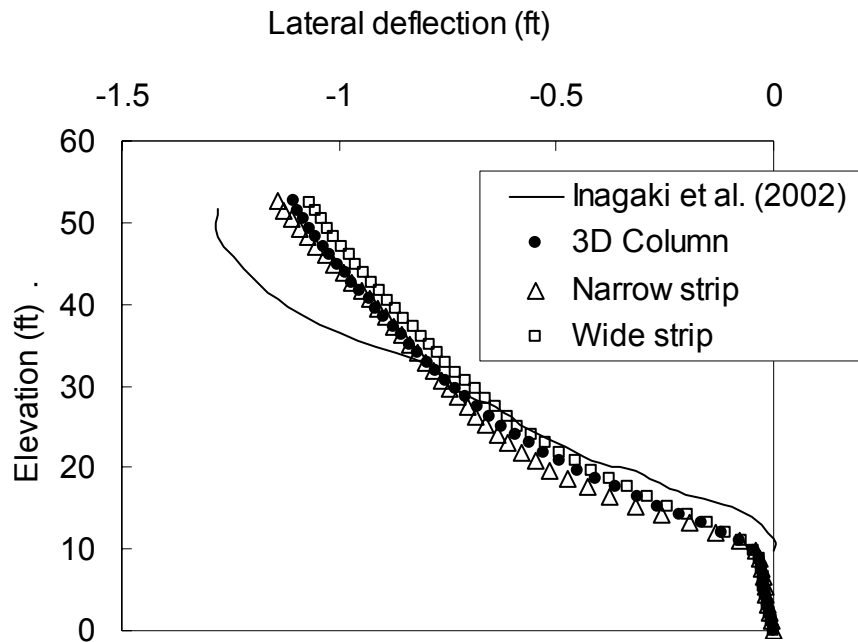
Figure 5-16. Deflections for 1st column in Case 1

5.7. Columns used to support full height of embankment

A second set of analyses was performed with five additional columns to extend the treatment zone from the toe of the embankment to the centerline boundary of the model on the right-hand side, in order to support the full embankment, as would be done in practice. The ten columns in this analysis were at the same geometry and spacing as the five columns in the first analysis, and extend from the ground surface to the top of the sand layer. This geometry was discretized into 6243 zones for the two-dimensional plane-strain analyses and 65,160 zones for the three-dimensional analyses. Centrifuge model test results from Inagaki et al. (2002) are available for the five-column case, but not for the ten-column case.

A plot of displacement versus depth for the first column located under the toe for the case with ten columns is shown in Figure 5-17. As can be seen in this figure, the plane-strain analysis using narrow strips matches the three-dimensional analysis, but plane-strain analysis using wide strips produces much smaller displacements. For the case with ten columns, the support provided by the columns is a larger part of the system stiffness than for the five-column case, and narrow strips more accurately represent overall system stiffness than wide strips in the two-dimensional analysis.
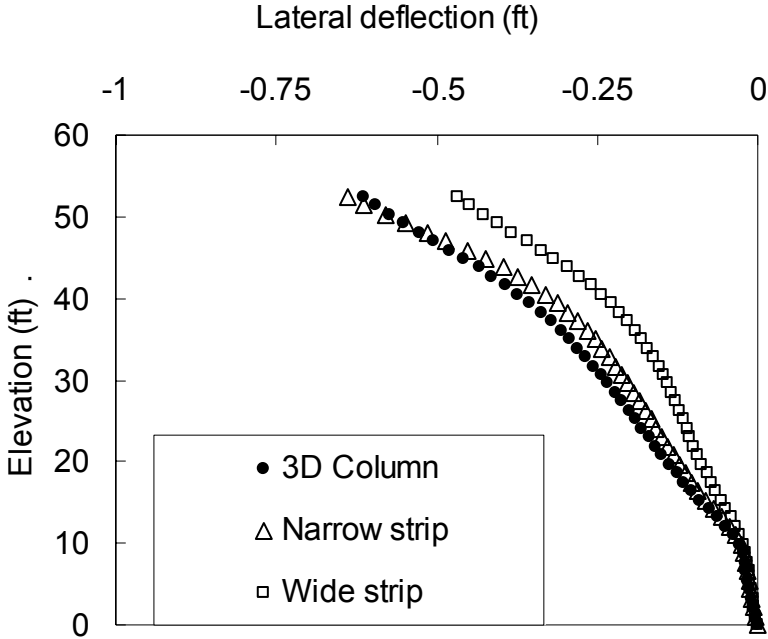
Figure 5-17. Deflections for 1st column in analysis with ten columns

5.8. Calculated column stresses

Given the brittle nature of DMM columns, especially in tension, it is important that stresses from numerical analysis are evaluated appropriately. Proper assessment of column stresses for the two-dimensional analyses is complicated by the fact that the geometry of the column is altered to a strip that has different sectional properties than a circular column. Therefore, the stresses resulting from numerical analysis cannot be interpreted from two-dimensional analyses in the same way as stresses from three-dimensional analyses.

The vertical stresses acting on the columns can be separated into two components: the axial stress, σ_a, which is the average of the vertical stresses across the column at a given elevation, and the bending stress, which is the difference between the vertical stress and the average stress. The symbol σ_b is used here to designate the extreme fiber bending stress at the greatest distance from the neutral axis.

To convert the vertical stresses in the columns from the two-dimensional analyses to values applicable to round columns, the bending stresses from the two-dimensional analyses are adjusted to produce an equal bending moment in the round, three-dimensional columns, as follows:

$$\sigma_{b3D} = \pm \frac{BS_{2D}}{S_{3D}} \sigma_{b2D} \qquad (5\text{-}6)$$

where σ_{b3D} = the equivalent extreme fiber bending stress in a round column, B = the center-to-center spacing between rows of round columns in the direction perpendicular to the plane of the two-dimensional analyses (see Figure 5-11), S_{2D} = the section modulus of the two-dimensional strip, i.e., the strip width squared divided by six, S_{3D} = the section modulus of the round column, σ_{b2D} = the extreme fiber bending stress in the strip from the two-dimensional numerical analyses. The vertical stresses from two-dimensional analyses equivalent to round columns, σ_{3D}, are the sum of the axial stresses, σ_a, and the converted bending stresses, σ_{b3D}, obtained from Equation 5-6. In the figures described below, values of σ_{3D} are compared with the corresponding values obtained directly from the three-dimensional analyses.

Figure 5-18 presents column stresses at depths of 7.3-ft and 21.3-ft. As with the study of lateral displacements in the previous section, the column presented in Figure 5-18 (a) is the first column in the five column case, located under the toe of the embankment. Figure 5-18 (b) shows the third column of the ten column case. The stresses from the two-dimensional analysis with narrow strips, the two-dimensional analysis with wide strips, and the three-dimensional analysis are included in this figure. The slopes of the lines show that, in comparison with the results of three-dimensional analyses, the two-dimensional model with narrow strips under-predicts bending stress, while the two-dimensional model with wide strips tends to be in reasonable

agreement with, or to over-predict, bending stresses. These trends are true for other columns, as well.

Figure 5-19 presents axial stress from the ten column case for both the first column under the toe and the last column under the full height of the embankment. The axial stresses are plotted along the entire length of the columns. As can be seen in this figure, the two-dimensional analysis with narrow strips produces results that are about the same or slightly greater than the results from the three-dimensional analysis. It is also evident in this figure that the two-dimensional analysis with wide strips can produce column axial stresses that are significantly smaller than the axial stresses from the three-dimensional analyses.
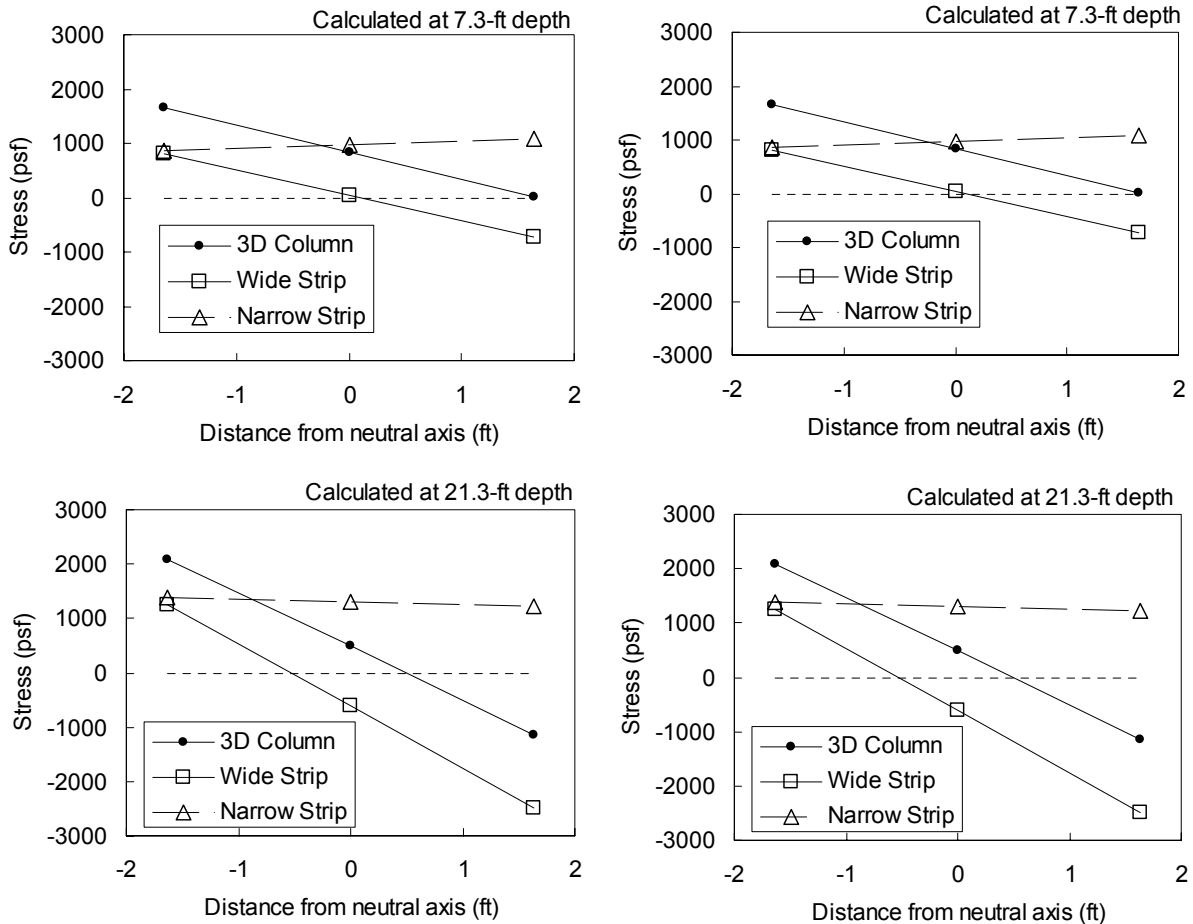
(a) First column of five columns case   (b) Third column of ten columns case

Figure 5-18. Vertical stresses in columns
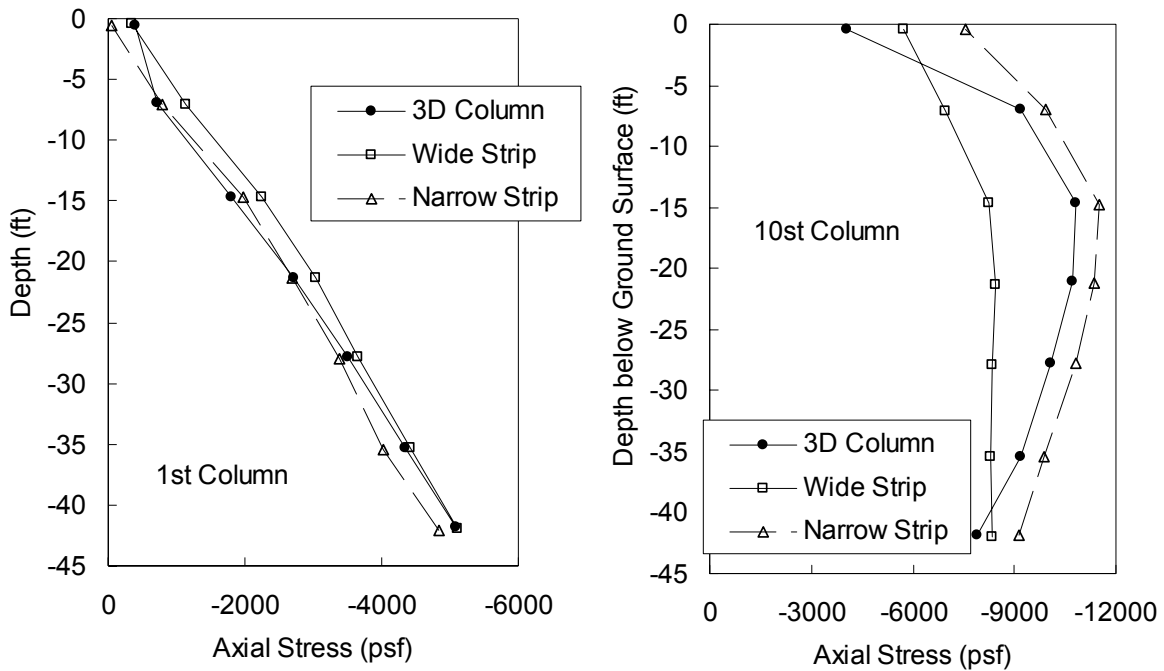
Figure 5-19. Axial stress of columns

5.9. Summary

The centrifuge tests performed by Inagaki et al. (2002) provide valuable insights into the behavior of isolated deep-mixed columns beneath the edge of embankments. These tests also provide a means to verify numerical analysis procedures used to analyze these complex systems. Undrained analyses can reasonably approximate the behavior of a more complex water-soil analysis of the clay response in these systems. Key findings for two- and three-dimensional analyses of embankments supported on isolated deep-mixing-method columns are that (1) lateral deflections from two-dimensional analyses are in relatively good agreement with lateral deflections from three-dimensional analyses at the same area replacement ratio, (2) two-dimensional analyses under-predict bending stresses seen in three-dimensional analyses at the same area replacement ratio, and (3) two-dimensional analyses using strip widths based on moment of inertia of the columns tend to over-predict the bending stresses and under-predict the axial stresses seen in three-dimensional analyses.

6. ANALYSIS OF THE TEST EMBANKMENT AT THE I-95 RT.1 INTERCHANGE

6.1. Introduction

A new 12-lane bridge will be constructed to replace an existing 6-lane bridge as part of the $2.4 billion Woodrow Wilson Bridge Reconstruction Project. This new bridge will require significant realignment and widening of the approach interchanges in Virginia and Maryland. On the Virginia side, the interchange between I-95 and US Route 1 is being reconstructed at an estimated cost of $350 million (VDOT 2001). To widen existing embankments, which are approximately 10 feet high, new embankments are being constructed. Alluvial deposits of very soft and highly compressible organic silts and clays underlie the I-95/Route 1 interchange. Significant primary and secondary consolidation settlements on the order of 2 to 5 feet were predicted beneath the new embankments (Shiells et al. 2003). In some areas, short-term embankment stability was a primary concern. Furthermore, project requirements included maintaining existing traffic flow and meeting a tight construction schedule.

To address these challenges, the "wet" and "dry" methods of deep mixing were considered for support of the new embankments (Lambrechts et al. 2003, Shiells et al. 2003). In the wet method, water-cement slurry is mixed with the soil, and in the dry method, dry lime and/or cement is mixed with the soil. Because this is the first large project of its type in the mid-Atlantic region and the first use of deep mixing by the Virginia Department of Transportation (VDOT), a program of laboratory mix design studies, field trials, and a test embankment was completed. Because there were more uncertainties about application of the dry method than the wet method at this site, the test embankment was supported on columns installed by the dry method. Ultimately, the wet method was selected for the production columns, but the test embankment provides an excellent case history of an instrumented embankment supported on columns installed by the dry method. This chapter presents numerical analyses of the test embankment.

6.2. Test embankment construction

A generalized cross-section and subsurface profile of the test embankment is shown in Figure 6-1. A total of 59 dry mixed columns were installed from September 11 through September 17,

2000. The columns were 32 inches in diameter, and were installed in a triangular pattern on 6-ft and 10-ft center-to-center spacings, corresponding to area replacement ratios of 17.9% and 6.4%, respectively. The closer spacings were used beneath the geosynthetic-reinforced retaining wall on the south end of the embankment. The tops of the columns were generally located about 4 feet below the existing ground surface, and the columns were specified to penetrate 3 feet into the medium dense to dense sands and gravels at a depth of approximately 38 feet below the original ground surface. As a result, the total length of the columns ranged from 33 to 40 feet, with an average installed length of 37 feet.

Based on the results of laboratory testing, an amendment dose rate of 150 kg/m^3 with 100% cement was specified for the columns beneath the test embankment. The contract required a minimum unconfined compressive strength of 51.5 psi at 14 days, and 80 psi at 28 days (VDOT 2001). In addition to the columns for the embankment, 23 other test columns with varying binder mixes and dose rates were installed outside of the test embankment footprint. Core sampling, pressuremeter tests, and reverse penetration (or pullout) tests were performed on the test columns.

The test embankment was constructed between October 4 and October 13, 2000. The embankment, which measured 50-foot square at the top, had a vertical geosynthetic-reinforced retaining wall on one side and 2H:1V slopes on the other three sides. The embankment had a height of approximately18 feet, and was constructed with crushed aggregate after an initial placement of approximately 3 feet of bank run sand and gravel. Instrumentation included settlement plates, settlement pins, an observation well, vertical inclinometers, a horizontal inclinometer, vibrating-wire piezometers, magnetic extensometers, pressure cells, and thermistors. The test embankment was removed in November 2001.
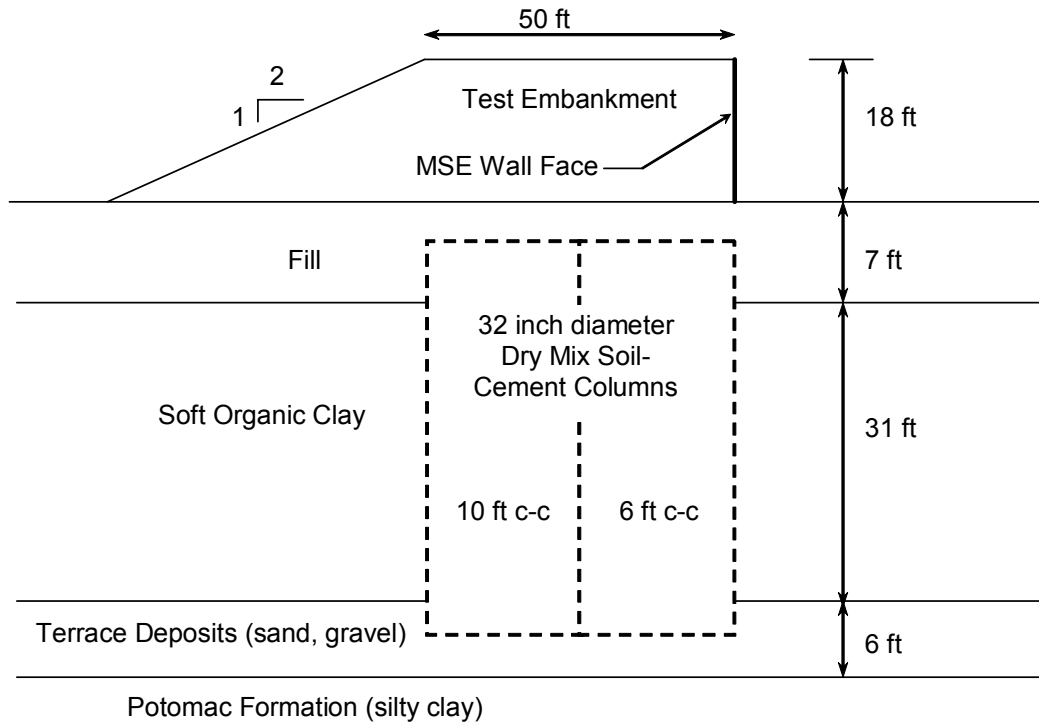
Figure 6-1. Typical section of test embankment and subsurface conditions

6.3. Subsurface conditions and material property values

Subsurface explorations performed in the area of the test embankment included two test borings, ten piezocone soundings, and six dilatometer soundings. Detailed results of the subsurface investigation and laboratory tests are presented in Haley & Aldrich, Inc. and Virginia Geotechnical Services, P.C. (2000). As shown in Figure 6-1, the uppermost material is man-made fill, which is underlain by soft organic clay. The clay is underlain by sand and gravel terrace deposits, which are underlain by very stiff to hard silty clay of the Potomac Formation. The ground water table is located approximately at the surface of the soft organic clay.

The material property values used in numerical analyses are listed in Table 6-1, and important characteristics of the materials are discussed below. Numerical parameter studies were performed by changing the values of the selected material properties as listed in Table 6-2. The properties in Table 6-2 were chosen for variation because it was anticipated that they could have significant influence on stress concentration on the columns and/or lateral deflections in the foundation. The values of these four properties were varied up and down by the same proportion, ±33%, which is within the range of published variations for these properties. Using

94

the same percent variation facilitates assessment of the relative significance of these factors on
system performance.

Table 6-1. Base case material property values used in the numerical analyses

	Fill	Soft Clay	Base Sand	Column	Embankment
Model type	Mohr-Coulomb	Cam Clay	Mohr-Coulomb	Mohr-Coulomb	see text
Dry or moist density, pcf	121	52	107	62	134
Sat. Density, pcf	-	92	127	104	-
Elastic Modulus, psf	see text	-	4×10^5	see text	1×10^6
Poisson's Ratio	0.3	0.3	0.31	0.33	0.23
Cohesion, psf	350 / 0	-	0	see text	0
Friction Angle, deg.	35	-	34	0	45
Dilation Angle, deg.	0	-	0	0	-
Critical Shear Stress Ratio, η_{crit}	-	1.3	-	-	-
Lambda, λ	-	0.375	-	-	-
Kappa, κ	-	0.038	-	-	-
Pressure at Specific Volume, psf	-	2000	-	-	-
Specific Volume	-	4.1	-	-	-
Preconsolidation Pressure, psf	-	see text	-	-	-
Hydraulic conductivity, cm/s	-	1.2×10^{-6}	1×10^{-1}	1×10^{-5}	-
Porosity	-	0.68	0.35	0.68	-

Table 6-2. Variable parameter values in the numerical studies

Parameter	33% Low Values	Base Case	33% High Values	Fitted Values
Fill E_{fill}, psf	3×10^5	4.5×10^5	6×10^5	4.5×10^5
Clay λ, κ	0.25, 0.025	0.375, 0.0375	0.5, 0.05	0.3, 0.03
Column c_{col}, psf	5000	7500	10000	8350
Column $E_{col}/q_{u,col}$	67	100	133	100

note: A c_{col} value of 2500 psf was also analyzed.

The man-made fill consists primarily of loose to medium dense fine sand, including some
medium stiff silty clay, with a representative Standard Penetration Test (SPT) N value of 14. A
linear-elastic, perfectly-plastic soil model with a Mohr-Coulomb failure criterion was used for
the fill, with a friction angle of 35 degrees, and a cohesion intercept of 350 psf extending to a

depth of 4-ft. The cohesion intercept was included to account for strength induced by negative pore water pressures above the water table and for the presence of silty clay in the fill. A range of values of modulus of elasticity, E_{fill}, from 300,000 to 600,000 psf was obtained using correlations by D'Appolonia et al. (1970), Mitchell and Gardner (1975), Bowles (1996), and Poulos (2002), and a base-case value of 450,000 psf was selected.

The soft organic clay was represented using the modified Cam Clay model. The model parameter values were obtained from an extensive laboratory test program that included triaxial compression, 1-D consolidation, and permeability tests (Haley & Aldrich, Inc. and Virginia Geotechnical Services, P.C. 2000). The consolidation tests disclosed that the clay is overconsolidated by about 625 psf, and this was incorporated in the analyses. The base-case values of the compressibility parameters lambda and kappa listed in Table 6-1 provide a good fit to the laboratory test data. The ±33% variations listed in Table 6-2 are within the range of values of coefficient of variation from 10 to 37% listed by Duncan (2001) for the compression index of soil.

The sand and gravel terrace deposits were represented using a linear-elastic, perfectly-plastic model with a Mohr-Coulomb failure criterion. Property values were obtained using correlations with a representative SPT N value of 19.

Deformations occurring in the very stiff to hard silty clay of the Potomac Formation were assumed to be relatively unimportant compared to the deformations of the other materials, and this unit was not included in the analyses.

Test results were not available to directly provide effective-stress based strength parameter values for the column material. Kivelo (1998) and Broms (2003) provide some recommendations for estimating effective-stress based strength parameter values from unconfined compression test results. McGinn and O'Rourke (2003) used an effective stress cohesion intercept of one-half the unconfined compression strength and an effective stress friction angle of zero in their numerical analyses of wet-mixing-method columns at the Central Artery project in Boston. In the analyses described below, we have followed the approach of

McGinn and O'Rourke (2003). It is recognized that, according to the recommendations of Kivelo (1998) and Broms (2003), this may overestimate the column strength at low effective normal stresses and underestimate the column strength at high effective normal stresses.

For dry-mix test columns with a dosage rate of 9.1 pcf and 100% cement located outside the test embankment, pressuremeter tests indicated an average shear strength of about 17.4 psi. Laboratory tests on core samples indicated an average unconfined compression strength, $q_{u,col}$, of about 36.3 psi, which is in reasonable agreement with the pressuremeter results. Reverse penetration tests indicated an average shear strength of approximately 70 psi, which is much higher than the strengths indicated by the pressuremeter tests or core samples. It was expected that the column strength and modulus values would be important in calculating the stress distribution and the displacements beneath the embankment. A parameter study was performed using column cohesion intercept, c_{col}, values of 17.4, 34.7, 52.1, and 69.4 psi.

The modulus of elasticity, E_{col}, of cement dry-mix columns ranges from 65 to 250 times the column unconfined compression strength, $q_{u,col}$, according to Baker (2000) and Broms (2003). Laboratory test results using soil from the I-95/Route 1 site indicated a factor of about 100 may apply, and this value was selected for the base case. In the numerical parameter study, the ratio of modulus of elasticity to unconfined compression strength was varied from 67 to 133. Poisson's ratio values reported in the literature for deep-mix materials range from about 0.1 to 0.5, and a value of 0.33 was used in these analyses.

The embankment property values correspond to those of a dense, well-graded sandy gravel. A linear elastic model was used for the plane-strain analyses because the MSE wall construction permitted a vertical fill face.

6.4. Numerical analyses

Numerical analyses of the test embankment were performed using the FLAC (Fast Lagrangian Analysis of Continua) computer program (ITASCA 2002). A two-dimensional, plane-strain, water-soil coupled analysis was performed using FLAC to calculate deflections that could be compared with those measured in the field. The field deflections were measured in a horizontal

inclinometer located along the base of the embankment and a vertical inclinometer located near the vertical face on one side of the embankment. A separate series of numerical analyses were performed using an axi-symmetric model to investigate stress concentration above the columns measured in pressure cells located beneath the test embankment (Stewart et al. 2003). The field measurements are included in Haley & Aldrich (2000).

The geometry shown in Figure 6-1 was discretized into 5952 zones. Eight rows of dry-mixed columns in the improvement zone were represented by idealized strips, with center-to-center spacings equivalent to those used in the field. The strip widths were chosen to result in the area replacement ratios of 18% and 6% used in the field. Three zones are used in the model for each column strip and each strip of clay between the columns in the profile. The profile of the mesh is shown in Figure 6-2. A separate, coarser mesh, which is included as Figure 6-3, was also created for the embankment geometry, and its use is described later in this chapter.
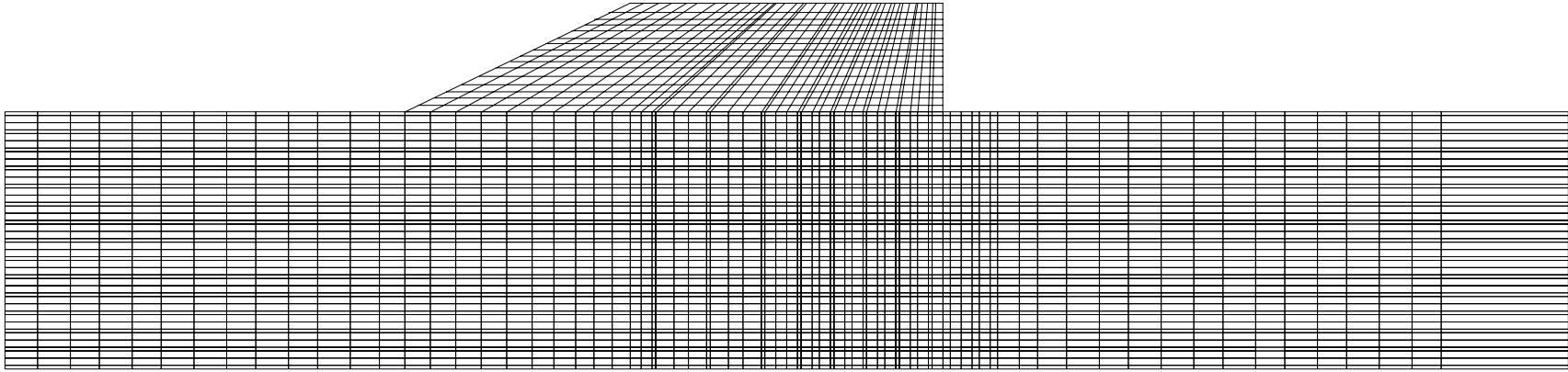
Figure 6-2. Test embankment mesh
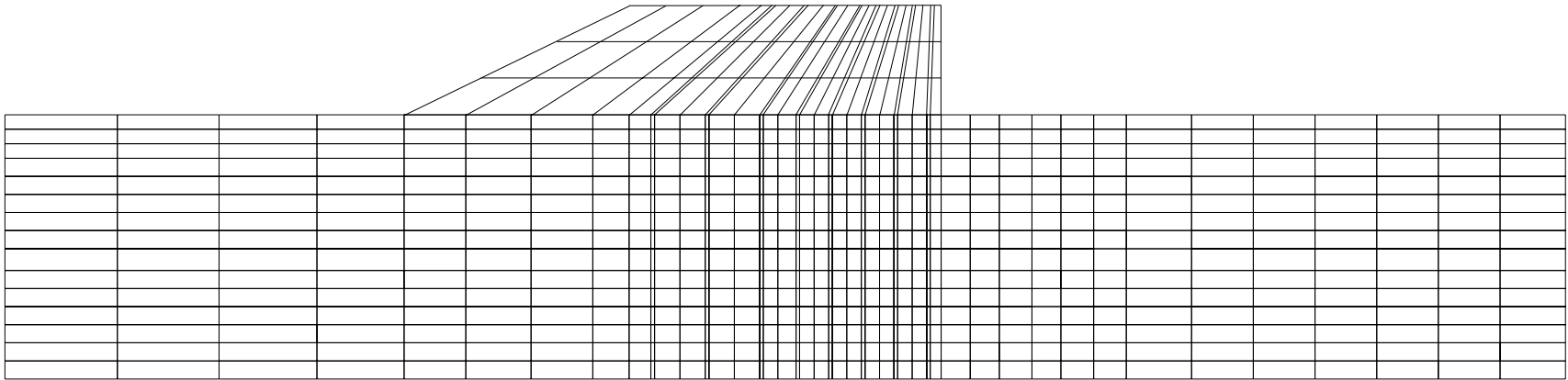
Figure 6-3. Test embankment coarse mesh

Varying the modulus of the existing fill had relatively little effect on the calculated deformations in the plane strain analysis. Results of the parameter study showed that lateral deformations are sensitive to variations in (1) column strength and the corresponding column modulus and (2) the clay stiffness.

Results for undrained analyses using a range of column strengths are shown in Figures 6-4 and 6-5, where it can be seen that the deflections increase as the column strength and modulus decrease, as expected. No columns failed in these analyses, so the influential parameter variation is column modulus, not strength. For these analyses, the modulus of the columns was set equal to 100 times the unconfined compressive strength and 200 times the shear strength. The analyses using the higher strength and higher modulus columns tend to be in good agreement with the measured lateral deformations, but the calculated settlements are less than the measured settlements in all cases.
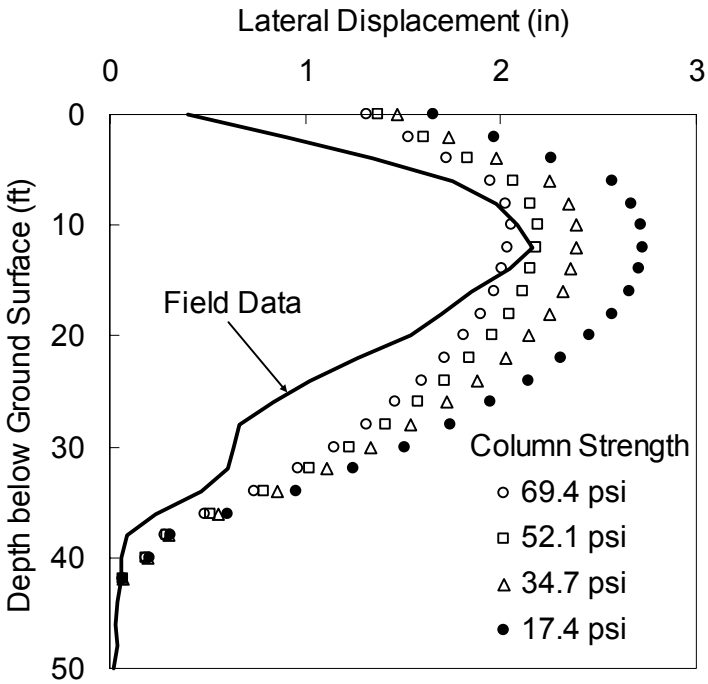
Figure 6-4. Lateral displacement in the undrained analysis
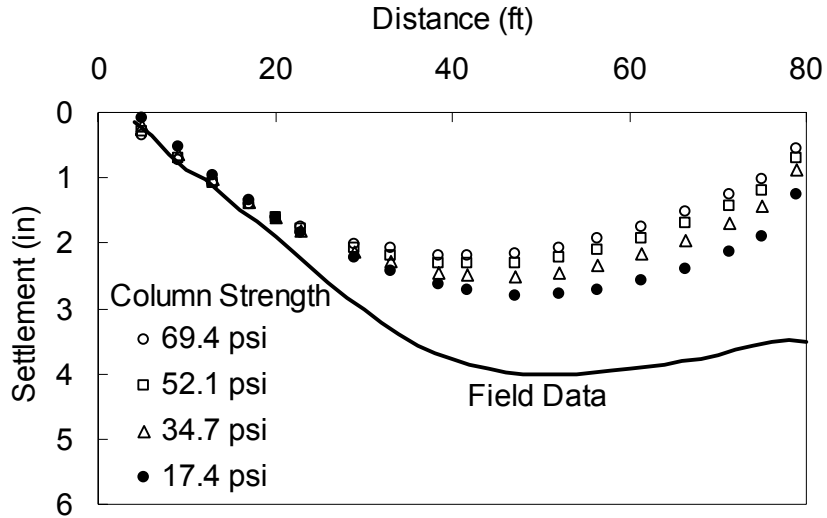
Figure 6-5. Settlement in the undrained analysis

Results for undrained analyses using a range of clay stiffness is shown in Figure 6-6, where it can be seen that the lateral deflections increase as the values of lambda and kappa of the clay increase. For undrained analyses, the saturated clay does not experience volume change, but increases in lambda and kappa correspond to decreases in shear modulus for undrained loading, which produce larger lateral deflections.

Lateral deflections increase with decreasing column strength, decreasing column modulus, decreasing shear modulus of the clay (increasing values of lambda and kappa), and decreasing modulus of the existing site fill. Of these properties, the values of lambda and kappa of the clay have the biggest influence on lateral deflections. This is due to (1) the relatively small values of replacement ratio in the treatment zones beneath the test embankment and (2) the influence of unimproved ground beyond the treatment zones.

Fitted parameter values were selected based on the results of the parameter study, taking into account both the response of the plane-strain investigation presented here, and the separate axi-symmetric investigation mentioned earlier in this chapter. A good overall fit of the calculations to the instrumentation data is achieved using a value of column strength equal to 58.0 psi and values of lambda and kappa equal to 0.3 and 0.03, together with the base case values of fill

modulus and column modulus-to-strength ratio. Using the calibrated numerical model, the calculated lateral deflections are shown in Figure 6-7.
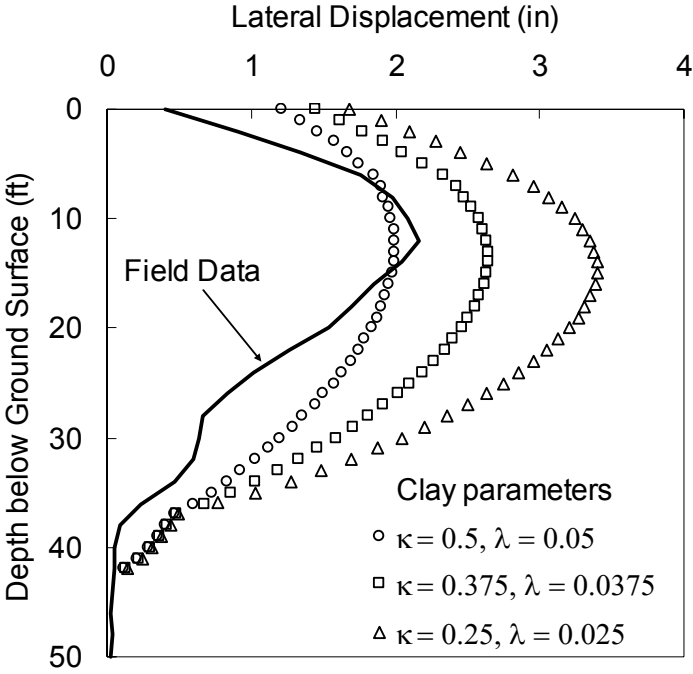
Figure 6-6. Undrained lateral displacements
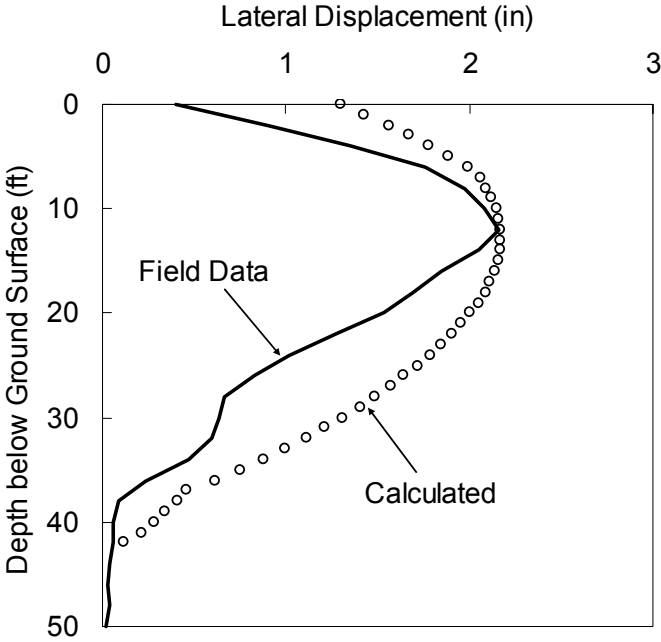
Figure 6-7. Undrained displacements for the calibrated model

The test embankment was placed over a nine day period, and it is expected that some consolidation would occur during this time. The second, coarser mesh shown in Figure 6-3 was created to evaluate the effect that consolidation during construction would have on displacements. The coarser mesh was used to analyze consolidation because the computation time required to perform consolidation analyses with the fine mesh is excessive. The coarser mesh only had 813 zones, but undrained analyses with the coarse mesh closely match the lateral and vertical deflections from undrained analyses with the finer mesh, as shown in Figures 6-8 and 6-9. In the consolidation analysis with the coarse mesh, the embankment was constructed in three lifts, with three days between each lift. Figure 6-8 shows that consolidation does not have a significant effect on lateral displacements, as expected. However, the increased settlements associated with consolidation during the construction period, as shown in Figure 6-9, match the field measurements reasonably well, especially near the center of the embankment.
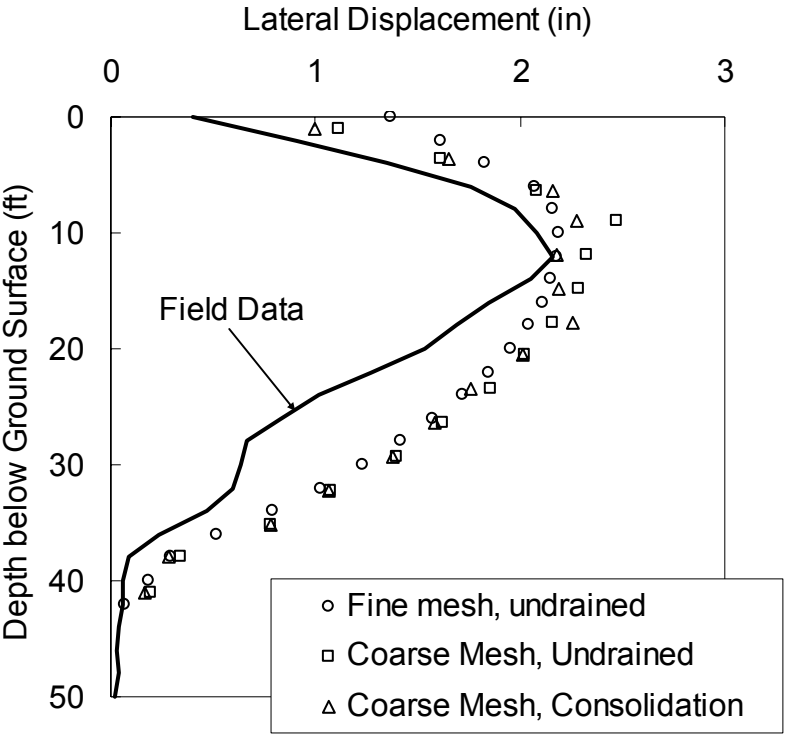
Figure 6-8. Lateral displacement with and without consolidation
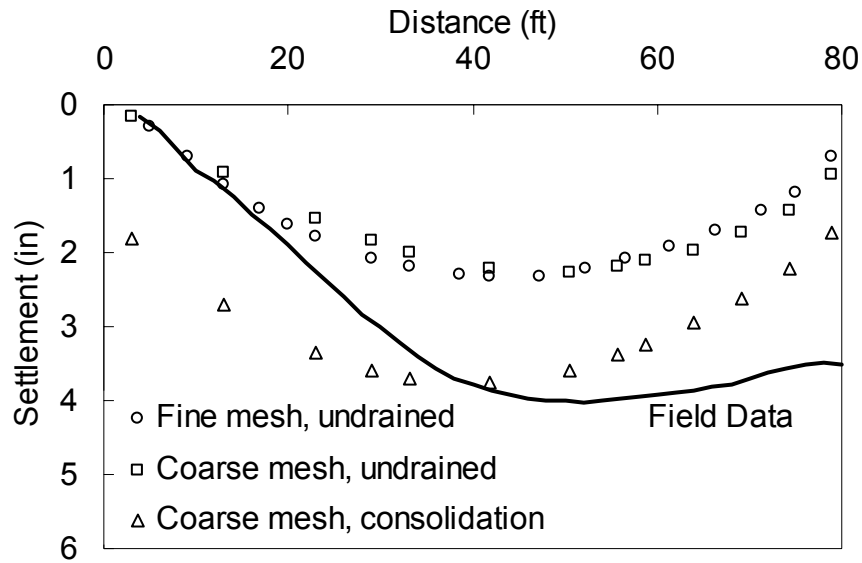
Figure 6-9. Settlement with and without consolidation

6.5. Summary

The numerical analyses of the test embankment at the I-95/Route 1 interchange illustrate how 2D, plane-strain analyses can be used to model the behavior of an embankment supported with deep-mixed columns. For this case history, the important parameters that affect the lateral displacement in the foundation measured at the edge of the test embankment are the column stiffness and the stiffness of the unimproved clay. The stiffness of the unimproved clay has the largest effect on calculated lateral displacement.

An important item that was learned with these analyses is that calculated displacements with a coarse mesh with only 813 zones provided a reasonably good match with displacements calculated using the finer mesh with 5952 zones. The finer mesh complies with the minimum density of zones recommended for column-supported embankments as a result of this research, as discussed further in Chapter 7.

7. GUIDELINES FOR NUMERICAL ANALYSIS OF COLUMN-SUPPORTED EMBANKMENTS

7.1. Introduction

The verification studies described in the previous chapters demonstrate that numerical analysis can effectively match the behavior of embankments and similar structures founded on soft clay improved with deep-mixed columns. This chapter summarizes key aspects of the numerical analysis procedures that were successfully applied using FLAC. These approaches are also thought to apply to embankments supported on vibro-concrete columns because, like deep-mixed columns, they are stiff columns with low tensile and bending strength.

7.2. Short-term "end of construction" case

Numerical analyses of centrifugal model experiments performed by Inagaki et al. (2002) and the numerical analysis of the VDOT test embankment for the I-95/Route 1 Interchange were performed using water-soil coupled analyses. These analyses employed the Modified Cam Clay Model for the soft clay in the foundation. Further investigations revealed that, for considerations of slope stability immediately after embankment construction, numerical analyses could be successfully performed using much simpler, short-term, "end of construction" analyses with undrained strength parameter values for low permeability materials, such as the clay and columns, and drained parameter values for high permeability materials and unsaturated materials, such as sand layers, fill, and embankments. The materials in the short-term analyses can be modeled using elastic properties in conjunction with the Mohr-Coulomb failure criterion.

Geotechnical engineers are accustomed to selecting unit weights, as well as the Mohr-Coulomb strength property values of cohesion, c, and friction angle, ϕ, for soils. In many cases, the elastic properties that are required for soils, i.e., the Young's modulus, E, and Poisson's ratio, v, can be selected based on published values in the literature (e.g., D'Appolonia et al. 1970, Mitchell and Gardner 1975, Duncan and Buchignani 1976, Bowles 1996, Duncan and McGregor 1998, Duncan and Wong 1999, and Poulos 2002). The Poisson's ratio for the clay and columns in short term analyses is nearly 0.5, however, to avoid numerical difficulties, a value lower than 0.5 must be used. For undrained materials in the fos analyses, $v = 0.45$ is suitable. Although it is convenient to select values of the elastic properties E and v, FLAC requires values of the bulk

modulus, K, and shear modulus, G. K and G can be determined from E and v using Equations 7-1 and 7-2.

$$K = \frac{E}{3(1-2v)}$$ (7-1)

$$G = \frac{E}{2(1+v)}$$ (7-2)

Kitazume et al. (1996) clearly observed bending failure in columns during centrifuge testing. Inagaki et al. (2002) noted that, after centrifuge testing, columns extracted from the model had cracked, and the authors felt this was indicative of bending failure. Both sets of authors performed numerical analysis of their centrifuge tests, but neither group allowed for failure of the columns, which were modeled as linear elastic materials. In order to understand the behavior of columns and overall stability of these systems against collapse, it is necessary to incorporate an appropriate failure criterion for the columns.

As part of this research, over 7,000 strength measurements were collected from nine deep-mixing projects around the United States. The data collected in this study, and summarized in Chapter 8, provide useful information about the strength and modulus values that have been achieved for columns installed by the deep mixing method. The approach described in Chapter 10 should be followed to establish an appropriate strength envelope for deep-mixed materials for use in analyses of embankment stability.

In FLAC, material densities rather than unit weights are the required input, so the user must convert unit weights to densities by dividing the unit weights by the acceleration of gravity.

7.3. Initial stresses

Initial stresses that exist in the soil prior to loading have an important impact on computed displacements, so these stresses should be established carefully if realistic displacements are the objective of the numerical analyses. Stresses throughout the foundation should be determined first without the presence of the deep-mixed columns. The recommended procedure is to

determine initial stresses in the soft soil based on drained Poisson's ratio values for the soil using buoyant unit weights below the water table. After calculating initial effective stresses, pore pressure should be added to obtain the initial total stresses. The sign convention in FLAC is that compressive stresses are negative, and tensile stresses are positive.

In geotechnical engineering, lateral earth pressures are frequently expressed in terms of the at-rest lateral earth pressure coefficient, K_0, which is the ratio of the effective lateral stress to the effective vertical stress. Values of Poisson's ratio, v, can be related to values of K_0 by using Equation 7-3.

$$v = \frac{K_0}{1 + K_0} \tag{7-3}$$

The value of K_0 can be estimated based on the soil's effective-stress friction angle using Equation 7-4 for normally consolidated soil. If the soil is overconsolidated, horizontal stresses in the soil are larger, and K_0 can be estimated using Equation 7-5.

$$K_0 = 1 - \sin \varphi \tag{7-4}$$

$$K_0 = (1 - \sin \varphi) * OCR^{\sin \varphi} \tag{7-5}$$

where ϕ = the effective stress friction angle and OCR = the overconsolidation ratio = the ratio of the preconsolidation pressure to the vertical effective stress. As an example, if $\phi' = 30$ degrees for a normally consolidated soil, the drained value of Poisson's ratio, v, will be 0.33 according to Equations 7-3 and 7-4.

The effective stress value of Poisson's ratio that is used for determining initial horizontal effective stresses need not be, and generally would not be, the same as the value used in Equations 7-1 and 7-2 to calculate values of K and G for undrained analyses. Values of Poisson's ratio in the neighborhood of 0.3 will generally be used with buoyant unit weights in a

"gravity turn-on" analysis to determine the initial effective stresses. In FLAC, this is done with either the command "set grav = 32.2" or "set grav = 9.81" depending on whether English or SI units are used. The pore water pressures are then added to the effective stresses to obtain total stresses. After the initial total stresses are established, the Poisson's ratio values for saturated materials are set equal to about 0.45 for subsequent undrained analyses of loading from the embankment.

The above procedure is recommended for analyses performed to obtain deformations. However, a simpler approach is possible for factor-of-safety calculations because the values of initial lateral stresses have no effect on the factor-of-safety values. In this case, the undrained values of Poisson's ratio can be used with total unit weights in a gravity turn-on analysis using the "set grav" command to establish lateral stresses. It is recommended that this procedure be used with all materials in the foundation either defined with the elastic model or with the Mohr-Coulomb model using artificially high cohesion values to ensure no failure occurs (e.g., a cohesion value of 1×10^{10}). After the initialization procedure is complete, the cohesion values can be set to the correct values. Experience demonstrates that this simpler procedure produces the same values of factor of safety as does the more elaborate procedure recommended above for deformation calculations.

7.4. Stepping

In FLAC, loads are applied and deflections are determined through a stepping process based on the equations of motion. Rather than specifying the number of steps that are required, it is more convenient to use the command "solve." The solve command analyzes the problem in steps until equilibrium is reached. A plot of displacement versus the number of steps will reveal whether or not the problem has reached equilibrium. If it is deemed the problem has not sufficiently reached equilibrium, the default stress imbalance criterion can be reduced. The default criterion is generally sufficient for factor of safety calculations.

7.5. Incremental loading

Embankment lifts should be used in the numerical analysis to mimic embankment construction in the field. When large loads are suddenly applied in FLAC, the equations of motion can result

in large oscillations until the problem reaches equilibrium. This is not a problem if all materials are linearly elastic, but when materials incorporate a failure criterion, these numerical oscillations can result in failure that does not realistically represent response to statically applied loads. In this research, it was found that lift thicknesses of up to three feet could be safely applied without causing difficulties.

7.6. Discretization

In numerical analysis, a mesh is used to discretize the problem geometry. This mesh, also referred to as a grid, is comprised of many individual elements. In FLAC, these elements are called zones to differentiate them from the elements used in finite element analyses. But to the user, elements and zones are similar. The FLAC (Itasca 2002) manual states the aspect ratio for zones should not exceed 1:5. Considering the large contrast in stiffness between columns and surrounding soil, it would be advantageous to use many zones to represent both of these materials when analyzing embankments founded on deep-mixed columns. However, when more than a few rows of columns are used, the number of zones needed to create the mesh geometry may become excessive. For small diameter columns, the vertical strips that represent the columns control the number of zones needed in the mesh. In this research, it was found that strips representing columns that have three zones across and aspect ratios less than 1:5 produced reasonably accurate results. Using this as a starting point, if more zones can be used to improve accuracy, it is more advantageous to lower the aspect ratio than it is to increase the number of zones across the width of the column strips. Often, it is prudent to use a finer concentration of zones in areas where stresses and displacements are critical, and a coarser concentration of zones in the portions of the grid that are not as critical, e.g., near the side boundaries.

7.7. Boundaries

The left and right boundaries of the model should be fixed in the x direction, and the boundary at the bottom of the model should be fixed in the x and y directions. Generally, either the left or right boundary represents a line of symmetry through the middle of the embankment. The boundary on the other side of the grid should be set far enough away that it does not influence lateral deflections. A rule of thumb is that the distance to the boundary from the embankment toe should be at least three times the height of the embankment. It was discovered that this

distance can be shorter, e.g., two times the embankment height, when only factor of safety calculations are performed.

7.8. Factor of safety "fos" calculations

FLAC has an automated procedure to evaluate the factor of safety by reducing strength values to determine the point of impending failure, at which the model is no longer in equilibrium. This factor of safety procedure, fos, in FLAC can only be used when all zones in the mesh are represented by the Mohr-Coulomb model. The fos calculation in FLAC should be performed after the full embankment and all other loads have been placed, and the geometry has reached equilibrium. It is suitable to reach equilibrium with all materials either defined with the elastic model or with the Mohr-Coulomb model using artificially high cohesion values, and then assigning the proper Mohr-Coulomb properties before performing fos calculations.

When no columns are present beneath the embankment, the factor of safety calculated with this procedure should closely match the factor of safety determined with a limit equilibrium slope stability analysis. It is recommended that such a comparison be performed prior to analyzing the problem with columns in place so that the implementation in FLAC can be verified.

7.8. Two-dimensional, plane-strain analysis of a three-dimensional problem

Much work was performed in this research to determine whether two-dimensional strips accurately represent column response in three dimensions. The problem is that one strip width and one Young's modulus cannot simultaneously represent axial stiffness and bending stiffness of the columns. Fortunately, for the cases investigated, strip widths calculated based on area replacement ratio in two-dimensional analyses matched three-dimensional analyses very closely. Investigations in Chapter 4 showed that two-dimensional, plane strain analyses match centrifuge test results of a column supported caisson subjected to inclined loading for a high replacement ratio of around eighty percent. Investigations in Chapter 5 showed that two-dimensional, plane strain analyses match both centrifuge test results and the three-dimensional numerical analysis of column a supported embankment for a low replacement ratio of around twenty percent.

7.9. Panels

Typically, columns under the side slopes of embankments are overlapped to form panels or grids. Columns are arranged in these patterns to avoid the bending and tilting failure associated with isolated columns. However, in addition to shear failure, panels can fail by "racking" or tilting, and soft soil may extrude between panels. CDIT (2002) and Broms (2003) recommend incorporating vertical planes of weakness in the panels to allow for racking. This can be done by incorporating vertical strips in the panels, and specifying lower strength values in those strips. Alternatively, deflection analyses can be performed using FLAC's "ubiquitous joint model" to incorporate vertical planes of weakness throughout the panels. However, the ubiquitous joint model cannot be used with fos calculations. Investigations showed that using a few narrow strips, e.g., 4 strips, of weakness had a significant effect on computed displacements and factor of safety, but there was little difference in displacement between the case with 4 strips and the ubiquitous joint model. This suggests that, for geometries similar to those analyzed in this research, 4 narrow strips of weak material is sufficient.

8. STATISTICAL ANALYSES OF DEEP-MIXING DATA

8.1. Introduction

The deep mixing method is widely used to support embankments in Europe, Asia, North America, and other parts of the world. Appendix D includes properties of deep-mixed material that have been published in the literature from construction projects and research that has been performed around the world. This literature shows the strength of deep-mixed material is highly variable, even at a single construction site, due to variability of the in-situ soil, variability of mixing effectiveness, and other factors. To assess the extent of this variability, data sets of measured strengths of deep-mixed material have been collected from several projects in the United States of America. Statistical analyses of these data sets have been performed. These analyses include basic statistics, data distributions, regressions, spatial correlations, and the relationship between deep-mixed material modulus and strength.

8.2. Basic statistics

As described in Appendix D.3, common measures of statistical variance include the standard deviation, σ, and the coefficient of variation, V, which is the standard deviation divided by the mean. The variability of strength data provided from six separate sources is shown in Table 8-1. All of the projects in Table 8-1 used the wet method of deep mixing, except for the dry-method columns that were used at a test location for the I-95 interchange project. The data sets from these sources have been separated where there is indication of change in site conditions, mixing method, or type of sample taken. In cases where data has been separated for these reasons, statistics are also presented for the total set of all samples. The statistical information from all samples from each source may help indicate differences in variability that arise due to other factors that can affect strength, such as regional geology and construction practices.

Table 8-1. Basic statistics for unconfined compression strength from deep-mixing projects

| Project | Sample Type | Strength | | | | Source |
		# Tests	Mean (psi)	σ (psi)	V	
Baker Library	Wet Grab	81	209	95.7	0.459	Weatherby (2004)
Capitol Visitor Center	Wet Grab	44	147	72.5	0.494	
Knafel Center	Wet Grab	106	226	118	0.522	
Total		231	204	107	0.520	
Port of Oakland	Core	118	433	225	0.521	Yang (2004)
Oakland Airport	Core	184	513	228	0.445	
Total		302	464	229	0.494	
Glen Road Interchange Ramps G&F	Core	184	473	162	0.343	Dasenbrock (2004)
Glen Road Interchange Ramps H&E	Core	634	412	175	0.425	
Total		818	426	180	0.421	
Blue Circle / Kinder Morgan Cement Silos	Wet Grab	487	682	506	0.742	Burke (2004)
Jackson Lake Dam - Owner Samples	Core	355	673	453	0.673	Farrar (2004)
Jackson Lake Dam - Contractor Samples	Wet Grab	1710	404	261	0.645	
Jackson Lake Dam - Owner Samples	Wet Grab	1018	333	263	0.789	
Total		2569	444	299	0.746	
I-95 Interchange - Dry method	Core	473	412	276	0.669	Shiells (2004)
I-95 Interchange - Wet method	Core	2199	496	329	0.663	
Total		2672	481	322	0.669	

Statistical information in the literature is summarized in Appendix D.3.3, and it indicates that there is a large variation of strength for improved soil created by deep mixing methods. Values of V reported in the literature typically range from 0.3 to 0.6, although values of V as low as 0.15 and as high as 1.35 have been reported. Values in Table 8-1 show that the variation in strength of improved soil from these projects ranges from 0.34 to 0.79, which is consistent with the values presented in the literature.

8.3. Distributions

The best known and most widely used distribution is the normal distribution (Ang and Tang 1975). The density function for the normal distribution is the familiar bell-shaped curve, which is symmetrical about the mean value of the distribution. For a particular value, x, the density function, f, according to the normal distribution is

$$f = \frac{1}{\sqrt{2\pi}\sigma} e^{-\frac{1}{2}\left(\frac{x-\mu}{\sigma}\right)^2} \qquad (8\text{-}1)$$

The lognormal distribution, which is a normal distribution of the natural logarithm of the data, is also commonly used. Many other distributions types, such as uniform, triangular, exponential, Poisson's, gamma, beta, Chi-squared, are described in Baecher and Christian (2003), Harr (1987), and Ang and Tang (1975).

Goodness of fit tests are used to quantify how closely a set of data matches a distribution type. The two most common types of these tests are the Chi-squared test and the Kolmogorov-Smirnov test. Both of these tests are described in Ang and Tang (1975).

McGinn and O'Rourke (2003) fit strength data from deep-mixing construction at the Boston Central Artery project to both normal and lognormal distributions. Results from the Kolmogorov-Smirnov goodness-of-fit tests showed that the lognormal distribution accurately described unconfined compression test results. This goodness-of-fit method is a measure of the maximum distance, D_{max}, from the cumulative distribution function (CDF) to the cumulative collection of empirical data. The assumed distribution type is valid if the value of D_{max} is less

than a critical value of D, which is based on the number of samples and the desired confidence level. The value of $D_{max} = 0.04$ shown in Figure 8-1 indicates that the data for the Central Artery project fits the lognormal distribution very well. In contrast, McGinn and O'Rourke (2003) compute the value of $D_{max} = 0.19$ for an arithmetic distribution, which is shown in Figure 8-2.
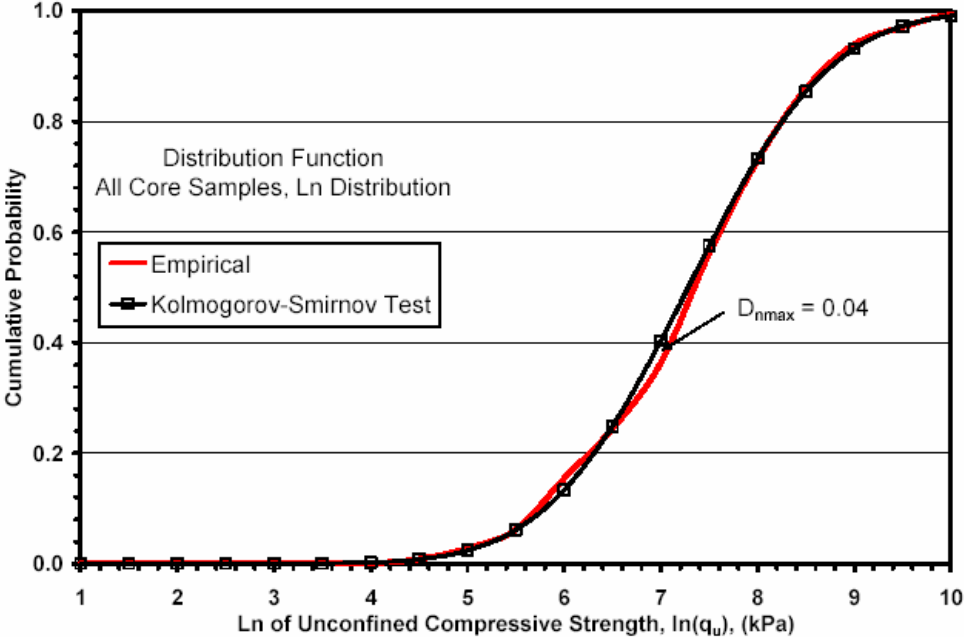
Figure 8-1. Kolmogorov-Smirnov goodness of fit test for a lognormal distribution of q_u
(McGinn and O'Rourke 2003)
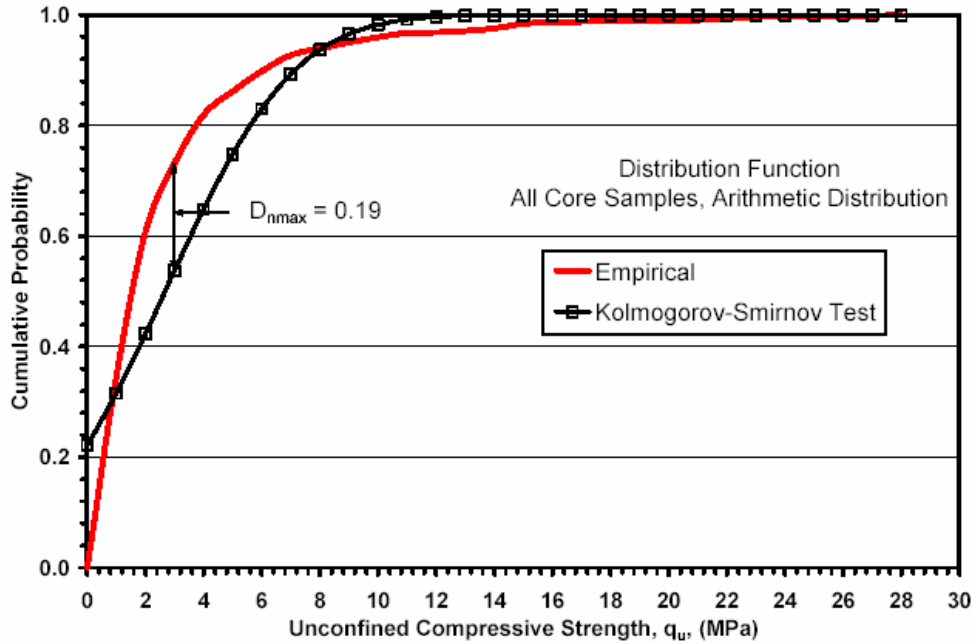
Figure 8-2. Kolmogorov-Smirnov goodness of fit test for an arithmetic distribution of q_u
(McGinn and O'Rourke 2003)

In this research, the goodness of fit for the normal, lognormal, uniform, and triangular distributions was evaluated for the strength data from each project included in Table 8-1. The distribution function and the cumulative distribution function are plotted together with the data for each case in Navin and Filz (2005). For example, Figure 8-3 shows data from the Glen Road Interchange Ramps H & E plotted with normal, lognormal, uniform, and triangular distribution functions. It can be seen that the lognormal distribution provides a good fit to the data.
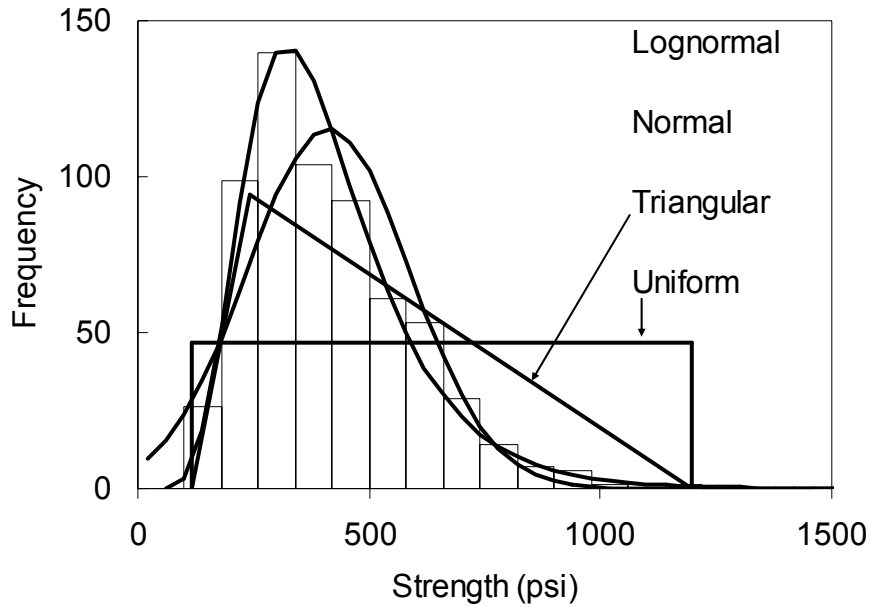
Figure 8-3. Four distribution types for strength data from Glen Road Interchange
Ramps H&E

The Chi-square test and the Kolmogorov-Smirnov (K-S) test were used to evaluate the goodness
of fit for each distribution to the data from each source.

The results of the Chi-square test are shown in Table 8-2. Low values of the test statistic
indicate a better fit of the data to the distribution than do high values. The Chi-squared test is
based on the distance from the measured number of samples to the predicted number of samples
from the distribution function. Outlying strength values greatly increase the Chi-square
goodness-of-fit parameter, particularly when the distribution function has low values, such as at
the extremes of the normal and lognormal distributions. Because the predicted value is in the
denominator of the Chi-square goodness-of-fit parameter, the result can be calculations of poor
fit for the normal and lognormal distributions due to a few outlying strength values.

The results of the K-S test are shown in Table 8-3. Low values of the test statistic for K-S also
indicate a better fit of the data to the distribution than do high values. As mentioned previously,
the K-S test is based on the distance from the measured number of samples to the predicted
number of samples from the cumulative distribution function. The results in Table 8-3 clearly

show that the lognormal distribution provides the best fit to the data. Figure 8-4 shows data from the Glen Road Interchange Ramps H & E plotted with the lognormal cumulative distribution function, and it can be seen that the fit is very good.

Table 8-2. Chi-squared goodness-of-fit parameter for deep-mixing strength data

Project	Distribution			
	Normal	Log-normal	Uniform	Triangular
Baker Library	14.3	16.8	6.10	265
Capitol Visitor Center	10.08	7.82	16.3	212
Knafel Center	42	24	140	12.8
Port of Oakland	2505	34.9	9.41	620
Oakland Airport	10.2	20.4	7.84	356
Glen Road Interchange Ramps G&F	17.3	38.2	14.4	750
Glen Road Interchange Ramps H&E	529810	136	33.5	908
Blue Circle / Kinder Morgan Cement Silos	7×10^{10}	152	26.1	44.8
Jackson Lake Dam - Core Samples	1213985	112	24.9	488
Jackson Lake Dam - CYC Samples	6557	441	119	226
Jackson Lake Dam - Wet Samples	2608	166	46.4	86.2
I-95 Interchange - Dry method	102	132	51.9	75.0
I-95 Interchange - Wet method	9122	334	86.0	137

Table 8-3. Kolmogorov-Smirnov goodness-of-fit parameter for deep-mixing strength data

Project	Distribution			
	Normal	Log-normal	Uniform	Triangular
Baker Library	0.125	0.044	0.334	0.159
Capitol Visitor Center	0.197	0.127	0.326	0.255
Knafel Center	0.140	0.043	0.332	0.209
Port of Oakland	0.092	0.053	0.488	0.348
Oakland Airport	0.0739	0.0465	0.339	0.169
Glen Road Interchange Ramps G&F	0.081	0.026	0.339	0.163
Glen Road Interchange Ramps H&E	0.064	0.025	0.774	0.135
Blue Circle / Kinder Morgan Cement Silos	0.097	0.039	0.622	0.334
Jackson Lake Dam - Core Samples	0.107	0.021	0.882	0.286
Jackson Lake Dam - CYC Samples	0.077	0.043	0.467	0.045
Jackson Lake Dam - Wet Samples	0.102	0.070	0.464	0.260
I-95 Interchange - Dry method	0.110	0.080	0.277	0.495
I-95 Interchange - Wet method	0.068	0.050	0.999	0.078
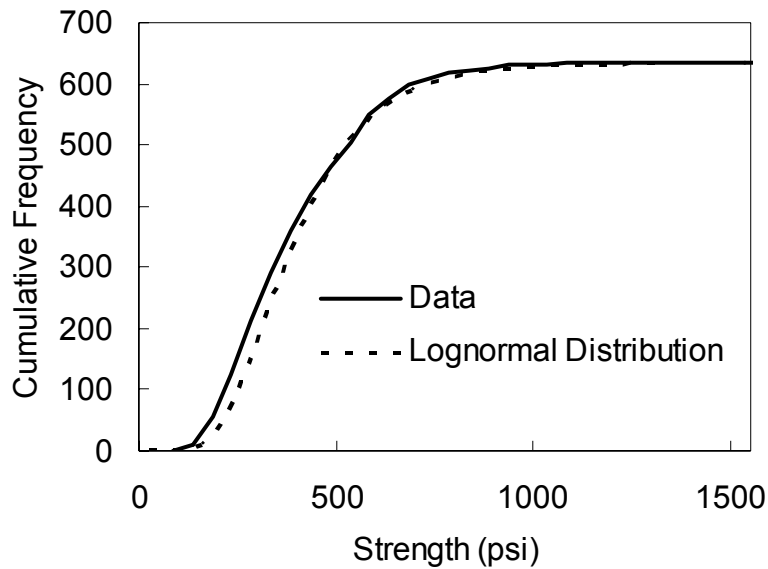
Figure 8-4. Cumulative distribution of strength data from Glen Road Interchange Ramps H&E

8.4. Regression analysis

The influence of five variables (cement content of the mixture, water-to-cement ratio of the slurry, age of cured specimens, water content of the mixture after curing, and specimen depth) on unconfined compression strength was investigated using multiple variable regression analyses. Every contact provided a different combination of these five variables along with unconfined compression strength. The number of data for each variable from every project is shown in Table 8-4.

Table 8-4. Number of recorded values for each variable

Source	Strength values	Cement content	Water-to-cement	Water content	Age	Depth
Weatherby (2004)	231		231		231	231
Yang (2004)	302			302	302	302
Dasenbrock (2004)	818	818	818	184	818	818
Burke (2004)	487	470			474	487
Farrar (2004)	3083 [1]	3089	3089	2078	3088	3097
Sheills (2004)	2672		124	2670	2672	2672
Total	7593	4377	4262	5235	7586	7608

[1] Farrar (2004) included 514 strength values from tests other than unconfined compressive strength.

Table 8-5 identifies every variable as either "controlled" or "uncontrolled" based on whether or not the variable can be accounted for in design or controlled during construction. For example, the effects of water-to-cement ratio of the slurry, age, and depth are known and/or controllable variables, so they can be accounted for in design. However, the water content of the cured mixture is an outcome of the process, and the values provided to us were measured after curing and testing, so this variable cannot be accounted for during the design process. In the case of cement content, when it is reported as a target value, this parameter can be accounted for in design and is considered controlled; when it is reported as measured on specimens after mixing and curing, it is an outcome of the mixing process and it represents variability that cannot be accounted for in design, and so it is considered uncontrolled in this case.

Sources in the literature suggest that the strength of cement-mixed soil is a function of the natural logarithm of age as well as the natural logarithm of water content (e.g., McGinn and O'Rourke 2003, Jacobson et al. 2003). Accordingly, the influence of the natural logarithm of those variables was investigated, along with a linear relationship with cement content, water-to-cement ratio of the slurry, and depth.

Table 8-5. Variables considered in regression analysis

Source	Cement content[1]	Water-to-cement	Water content	Age	Depth
Weatherby (2004)		controlled		controlled	controlled
Yang (2004)			uncontrolled	controlled	controlled
Dasenbrock (2004)	controlled[2]	controlled	uncontrolled	controlled	controlled
Burke (2004)	uncontrolled			controlled	controlled
Farrar (2004)	uncontrolled	controlled	uncontrolled	controlled	controlled
Sheills (2004)			uncontrolled	controlled	controlled

(1) Cement content is listed as controlled when it is a specified value, whereas cement content is listed as uncontrolled when it is a measured quantity from the sample.

(2) Ramps G&F are at a cement content of 180 lb/ft, and Ramps H&E are at a cement content of 200 lb/ft.

The regression analyses were performed for the following eight cases, where "*wc*" denotes water content of the cured mixtures, and "*w:c*" indicates the water-to-cement ratio of the slurry:

1) q_u = intercept + A * ln (age)
2) q_u = intercept + B * (depth)
3) q_u = intercept + A * ln (age) + B * (depth)
4) q_u = intercept + A * ln (age) + B * (depth) + C * ln (*wc*)
5) q_u = intercept + A * ln (age) + B * (depth) + D * (*w:c*)
6) q_u = intercept + A * ln (age) + B * (depth) + E * cement content
7) q_u = intercept + A * ln (age) + B * (depth) + D * (*w:c*) + E * cement content
8) q_u = intercept + A * ln (age) + B * (depth) + C * ln (*wc*) + D * (*w:c*)
   + E * cement content

Table 8-6 provides a summary of R^2 values for each of the cases listed above. The R^2 value can range from zero to one. An R^2 value of zero indicates no correlation with the trend, while an R^2 value of one indicates a perfect correlation with the trend.

Table 8-7 provides a summary of *P*-values for each variable for every project. The *P*-value provides a measure of the importance of each parameter in the trend, where lower *P*-values indicate the parameter has a more significant contribution to the trend. Based on the *R*-values in Table 8-6 and the *P*-values in Table 8-7, it is evident that age and water-to-cement ratio of the slurry are the two parameters that can be controlled and that may have a significant impact on measured strength.

Table 8-6. R^2 values for regression analyses

Project	Case Number							
	1	2	3	4	5	6	7	8
Baker Library	0.47	0.01	0.48		0.62			
Capitol Visitor Center	0.68	0.03	0.71		0.71			
Knafel Center	0.49	0.05	0.51		0.69			
Total	0.39	0.06	0.51		0.63			
Oakland Airport	0.00	0.01	0.05	0.07				
Port of Oakland	0.01	0.07	0.04	0.11				
Total	0.00	0.04	0.07	0.09				
Glen Road Interchange Ramps G&F	0.23	0.01	0.24	0.33				
Glen Road Interchange Ramps H&E	0.21	0.05	0.26		0.48			
Total	0.22	0.02	0.24					
Blue Circle / Kinder Morgan Cement Silos	0.22	0.00	0.22			0.27		
Jackson Lake Dam - Core Samples	0.03	0.05	0.03	0.58	0.07	0.07	0.07	0.60
Jackson Lake Dam - CYC Samples	0.27	0.01	0.61	0.29	0.61	0.61	0.62	0.29
Jackson Lake Dam - Wet Samples	0.52	0.02	0.55	0.55	0.55	0.55	0.55	0.57
Total	0.36	0.01	0.44	0.38	0.44	0.44	0.45	0.38
I-95 Interchange - RAS (dry method)	0.00	0.08	0.08	0.48				
I-95 Interchange - CDSM (wet method)	0.00	0.00	0.00	0.53				
Total	0.00	0.01	0.01	0.53				

Table 8-7. *P*-Values for regression analyses

	ln(age)	depth	ln(*wc*)	*w:c*	cement content
Project	*A*	*B*	*C*	*D*	*E*
Baker Library	1.2×10^{-14}	0.31		5.2×10^{-07}	
Capitol Visitor Center	4.12×10^{-12}	0.03		1.00	
Knafel Center	2.62×10^{-23}	2.3×10^{-5}		5.1×10^{-12}	
Total	8.02×10^{-43}	3.6×10^{-4}		1.6×10^{-15}	
Oakland Airport	0.94	0.24	0.01		
Port of Oakland	0.19	1.8×10^{-4}	9.6×10^{-3}		
Total	0.44	0.01	2.8×10^{-4}		
Glen Road Interchange Ramps G&F	1.8×10^{-14}	0.07	1.7×10^{-6}		
Glen Road Interchange Ramps H&E	4.1×10^{-43}	0.15		2.0×10^{-49}	
Total	1.5×10^{-46}	9.8×10^{-7}			
Blue Circle / Kinder Morgan Cement Silos	2.2×10^{-27}	0.10			3.6×10^{-9}
Jackson Lake Dam - Core	0.28	0.66	3.2×10^{-4}	0.25	0.35
Jackson Lake Dam - CYC	4.0×10^{-57}	4.8×10^{-3}	9.9×10^{-4}	0.57	0.02
Jackson Lake Dam - Wet	3.1×10^{-55}	6.0×10^{-6}	1.2×10^{-3}	0.07	0.07
Total	2.9×10^{-114}	4.1×10^{-6}	2.7×10^{-7}	0.26	0.08
I-95 Interchange - RAS (dry method)	0.04	7.2×10^{-9}	3.7×10^{-60}		
I-95 Interchange - CDSM (wet method)	0.30	2.4×10^{-7}	0		
Total	0.08	1.4×10^{-11}	0		

Based on the results in Tables 8-6 and 8-7, an additional set of regression analyses were performed using only age and water-to-cement ratio of the slurry as potentially significant variables that can be controlled. Case 9 below correlates a linear value of strength with the logarithm of age and a linear contribution from water-to-cement ratio of the slurry. As mentioned earlier, strength is a function of the natural logarithm of age and water content of the mixture (McGinn and O'Rourke 2003, Jacobson et al. 2003), so there may also be a logarithmic relationship between column strength and water-to-cement cement ratio of the slurry. Case 10 uses a linear value of strength with the logarithm of age and logarithm of water-to-cement ratio of the slurry. Case 11 uses the logarithm of strength with the logarithm of age and the logarithm of the water-to-cement ratio of the slurry. Tables 8-8 through 8-10 present results of analyses for Cases 9 through 11.

9) q_u = intercept + A * ln (age) + D * (w:c)

10) q_u = intercept + A * ln (age) + D * ln(w:c)

11) ln(q_u) = intercept + A * ln (age) + D * ln(w:c)

Table 8-8. Regression parameters and R^2 values for significant and controllable strength factors represented in Case 9

Project	Intercept	A	D	R^2
Baker Library	573	72	-324	0.62
Capitol Visitor Center	-89	71	32	0.68
Knafel Center	283	91	-166	0.64
Total	395	79	-227	0.61
Oakland Airport	562	-15		0.00
Port of Oakland	168	78		0.01
Total	485	-6		0.00
Glen Road Interchange Ramps G&F	173	111		0.23
Glen Road Interchange Ramps H&E	633	127	-5	0.48
Total	80	131		0.22
Blue Circle / Kinder Morgan Cement Silos	21	226		0.22
Jackson Lake Dam - Core Samples	-2458	-4	2500	0.04
Jackson Lake Dam - CYC Samples	-414	220	138	0.61
Jackson Lake Dam - Wet Samples	-163	168	53	0.52
Total	-590	194	344	0.43
I-95 Interchange - RAS (dry method)	427	-4		0.00
I-95 Interchange - CDSM (wet method)	562	-18		0.00
Total	551	-19		0.00

Figure 8-5 shows the relationship between the measured strength values and the strengths calculated using regression Case 1 with the coefficients in Table 8-8 for the data from the Baker Library/Capitol Visitor Center/Knafel Center projects, for which the value of R^2 is 0.61. Figure 8-6 shows the same type of relationship for the data from the Blue Circle/Kinder Morgan project, for which the value of R^2 is 0.22. It can be seen that the predictive value of the regression is greater for the data in Figure 8-5 than for the data in Figure 8-6. Regressions with high values of R^2 could be useful for optimizing construction operations.
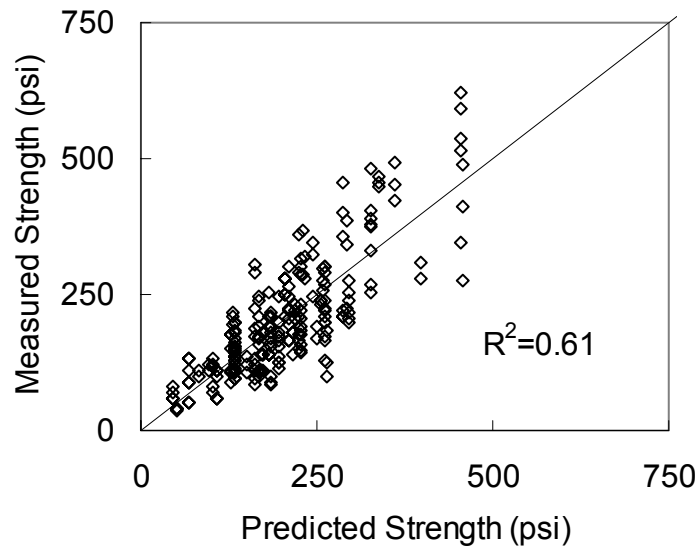
Figure 8-5. Measured vs. predicted strengths for deep-mixing data from the
Baker Library / Capitol Visitor Center / Knafel Center
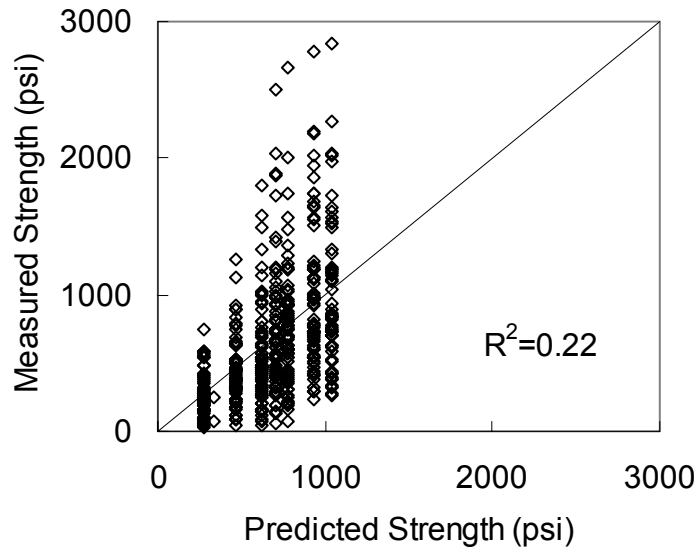
Figure 8-6. Measured vs. predicted strengths for deep-mixing data from the
Blue Circle / Kinder Mogan cement silos

Table 8-9. Regression parameters and R^2 values for significant and controllable strength factors represented in Case 10

Project	Intercept	A	D	R^2
Baker Library	304	72	-533	0.62
Capitol Visitor Center	-17	71	-25	0.68
Knafel Center	133	91	-246	0.64
Total	191	79	-344	0.61
Oakland Airport	562	-15		0.00
Port of Oakland	168	78		0.01
Total	485	-6		0.00
Glen Road Interchange Ramps G&F	173	111		0.23
Glen Road Interchange Ramps H&E	2763	127	-563	0.48
Total	80	131		0.22
Blue Circle / Kinder Morgan Cement Silos	21	226		0.22
Jackson Lake Dam - Core Samples	-56	-4	3242	0.04
Jackson Lake Dam - CYC Samples	-279	220	168	0.61
Jackson Lake Dam - Wet Samples	-112	168	72	0.52
Total	-253	194	418	0.43
I-95 Interchange - RAS (dry method)	427	-4		0.00
I-95 Interchange - CDSM (wet method)	562	-18		0.00
Total	551	-19		0.00

Table 8-10. Regression parameters and R^2 values for significant and controllable strength factors represented in Case 11

Project	Intercept	*A*	*D*	*R²*
Baker Library	5.63	-2.37	0.33	0.64
Capitol Visitor Center	2.05	2.58	0.52	0.75
Knafel Center	4.98	-1.22	0.37	0.56
Total	5.18	-1.72	0.37	0.58
Oakland Airport	6.4	-0.1		0.01
Port of Oakland	5.2	0.2		0.02
Total	6.1	0.0		0.00
Glen Road Interchange Ramps G&F	5.5	0.2		0.21
Glen Road Interchange Ramps H&E	11.47	-1.34	0.33	0.49
Total	5.1	0.3		0.23
Blue Circle / Kinder Morgan Cement Silos	5.1	0.4		0.29
Jackson Lake Dam - Core Samples	5.20	4.74	0.01	0.05
Jackson Lake Dam - CYC Samples	3.70	0.72	0.65	0.64
Jackson Lake Dam - Wet Samples	4.65	-0.45	0.45	0.49
Total	3.98	1.14	0.52	0.53
I-95 Interchange - RAS (dry method)	427	-4		0.00
I-95 Interchange - CDSM (wet method)	562	-18		0.00
Total	551	-19		0.00

The regression analysis results for Cases 9 through 11 in Table 8-8 through 8-10 show that strength is correlated with age and water-to-cement ratio of the slurry for some of the project data sets. None of the R^2 values are especially high, and several values are equal to or close to zero. The differences among the R^2 values for Cases 9 through 11 are small, indicating that these three methods are approximately equivalent.

The value of variance with the trend of controllable variables removed is more representative of variability due to in-situ conditions and construction procedures than is the total variability. By removing systematic influences of age and water-to-cement ratio of the slurry, the variation of strength data should be reduced. The results of such analyses are presented in Table 8-11, where it can be seen that the reduction in variance is significant in cases where the R^2 values in Tables 8-8 through 8-10 are significantly greater than zero. It can also be seen in Table 8-11 that there is not much difference in the reduction in variance among the three methods of correlating strength with age and water-to-cement ratio of the slurry represented by Cases 9 through 11.

Using Case 10 as an example, Table 8-11 shows that removing the systematic influences of age and water-to-cement ratio of the slurry reduces the values of coefficient of variation such that they range from 0.17 to 0.67, with an average value of about 0.40.

Table 8-11. Variation in strength with and without consideration of trends due to age and water-to-cement ratio of the slurry

Project	Variance	Variance with trend removed		
		Case 9	Case 10	Case 11
Baker Library	0.459	0.179	0.174	0.169
Capitol Visitor Center	0.494	0.168	0.168	0.130
Knafel Center	0.522	0.194	0.199	0.235
Total	0.520	0.205	0.209	0.221
Oakland Airport	0.521	0.524	0.524	0.521
Port of Oakland	0.445	0.443	0.443	0.440
Total	0.494	0.496	0.496	0.496
Glen Road Interchange Ramps G&F	0.343	0.265	0.265	0.272
Glen Road Interchange Ramps H&E	0.425	0.223	0.223	0.215
Total	0.421	0.330	0.330	0.325
Blue Circle / Kinder Morgan Cement Silos	0.742	0.589	0.589	0.530
Jackson Lake Dam - Core Samples	0.633	0.608	0.608	0.604
Jackson Lake Dam - CYC Samples	0.633	0.246	0.246	0.225
Jackson Lake Dam - Wet Samples	0.534	0.255	0.255	0.273
Total	0.672	0.386	0.386	0.313
I-95 Interchange - RAS (dry method)	0.669	0.670	0.670	0.670
I-95 Interchange - CDSM (wet method)	0.663	0.662	0.662	0.662
Total	0.669	0.668	0.668	0.668

8.5. Spatial correlation

8.5.1. Introduction

Spatial correlation is a measure of how closely values at one location match values at other locations. For variables that are spatially correlated, values measured at locations closer together are more representative of one another than are values measured farther apart. When measurements are taken at great distance from one another, there should be no spatial correlation

between values. Studies of spatial correlation are applicable to measurements of deep-mixed material strength from samples taken at various locations in the field.

The amount of spatial correlation can be estimated using plots of correlation versus distance. These plots, known as correlograms, were determined for unconfined compression strength measurements from installed deep-mixed columns using a four-step process: (1) column coordinates are used to find the distance from each column to every other column in a data set, (2) pairs of columns are then sorted according to separation distance and stored along with the strength measurements for the columns, (3) a "lag distance" is used to collect pairs of columns into discrete bins according to their separation distance, and (4) the correlation between strength values for pairs of columns is plotted as a function of separation distance. Variowin (Pannatier 1995) is a computer program that was used to perform all four of these steps in two dimensions.

El-Ramly et al. (2002) demonstrate the use of the autocorrelation distance, δ, to represent the spatial correlation in engineering analyses. In this approach, measurements from points closer than the autocorrelation distance are assumed to be perfectly correlated, while measurements from points farther than the autocorrelation distance are assumed to be completely independent. Baecher and Christian (2003) illustrate how to estimate the autocorrelation distance by matching Equation 8-2 to a plot of correlation versus separation distance for a particular data set:

$$\rho = e^{-\frac{s}{\delta}} \tag{8-2}$$

where s = the separation distance. According to Equation 8-2, ρ equals 1 when $s = 0$, and ρ asymptotically approaches zero as s increases.

The degree of spatial correlation of unconfined compression strength was studied for three projects: (1) the I-95/Rt. 1 interchange, (2) the Glen Road interchange, and (3) the Oakland airport. Table 8-12 shows the number of locations, as well as pairs of locations, with strength information at each project investigated. The sites where strength information is known at many locations show a trend between correlation and separation distance that does appear to follow the

132

shape of Equation 8-2. A plot of this equation is included in the figures presented below for the wet-mix samples taken at the I-95/Rt. 1 interchange, the samples taken at the Glen Road interchange ramps H & E, and the samples taken at the Oakland Airport. A plot of this equation is not included for figures presented below for dry-mix samples taken at the I-95/Rt. 1 interchange or the samples taken at the Glen Road interchange ramps G & F because there is no trend in the data at these locations.

The collection of 18 locations with strength information at the Port of Oakland project is insufficient for an investigation to be performed at that site. It should also be noted that if adjacent column locations are at separation distances much greater than the autocorrelation distance, they do not help determine spatial correlation.

Table 8-12. Number of locations and pairs for each site

Site	Number of locations	Number of pairs
I-95/Rt.1 dry-mix samples	36	630
I-95/Rt.1 wet-mix samples	170	14365
Glen Road ramps G & F	28	378
Glen Road ramps H & E	73	2628
Oakland airport	56	1540
Port of Oakland	18	NA

At each of these sites, a single column location may have multiple strength values because columns were sampled at several depths, and these samples were tested at different curing times. The Variowin software cannot perform a 2D analysis with multiple strength values at the same X-Y coordinates. Two approaches have been considered for addressing this, both of which are recommended in the Variowin manual: (1) average all values at each location and (2) use the minimum value at each location. For each site investigated, correlation versus separation distance is shown for minimum strength values and average strength values at each column location. Either approach yields the same autocorrelation distance when spatial correlation is evident. Neither approach indicates spatial correlation when spatial correlation is not evident.

The lag distance, which is used to collect pairs of strength values based on separation distance, has no effect on autocorrelation distance for the data sets investigated. The investigations presented below use a range of lag distances (10 ft, 20 ft, 30 ft, and 40 ft). Each lag distance shows the same autocorrelation distance, when spatial correlation is evident, and looking at results for the range of lag distances may help show the trend more clearly than looking at a single lag distance. This is particularly true for data sets that have only a moderate number of locations with strength information.

8.5.2. I-95/Rt. 1 Interchange

Figures 8-7 and 8-8 plot correlation versus separation distance for strengths measured from wet-mix samples at the I-95/Route 1 Interchange project. The figures also include plots of Equation 8-2 with the autocorrelation distance, δ, equal to 40 feet. This function approximates the spatial correlation of the strength data very well, for both the average strength in Figure 8-7 and the minimum strength in Figure 8-8. Figures 8-9 and 8-10 show very little spatial correlation for either the average strength or minimum strength from columns installed by the dry method. This may simply be due to the relatively small number of sample pairs available for the dry mix method in this data set, or it may reflect a real difference between the spatial correlations produced by the dry mixing method and the wet mixing method.
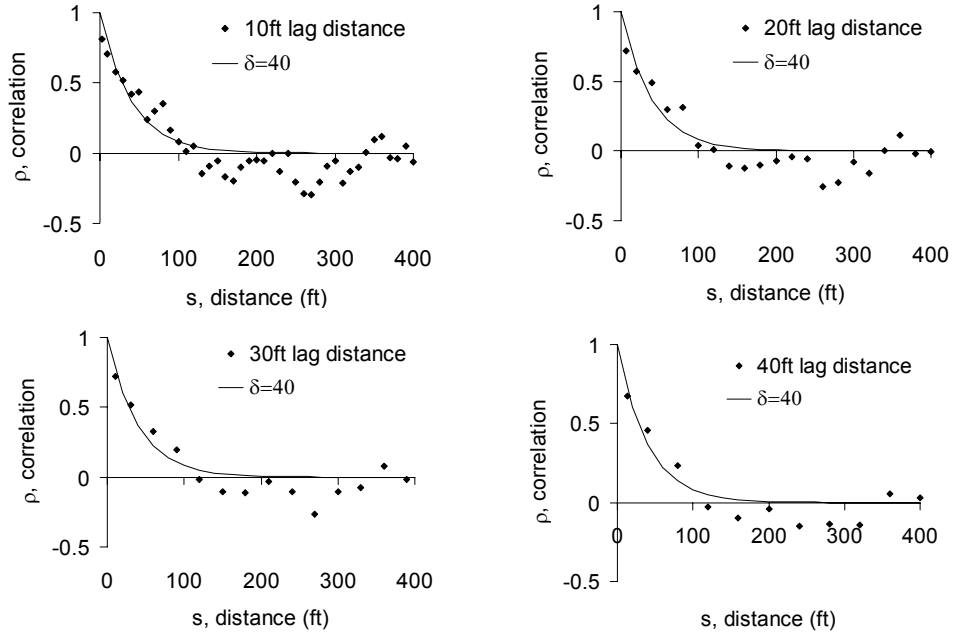
Figure 8-7. I-95/Rt. 1 average wet-mix strengths with four lag distances
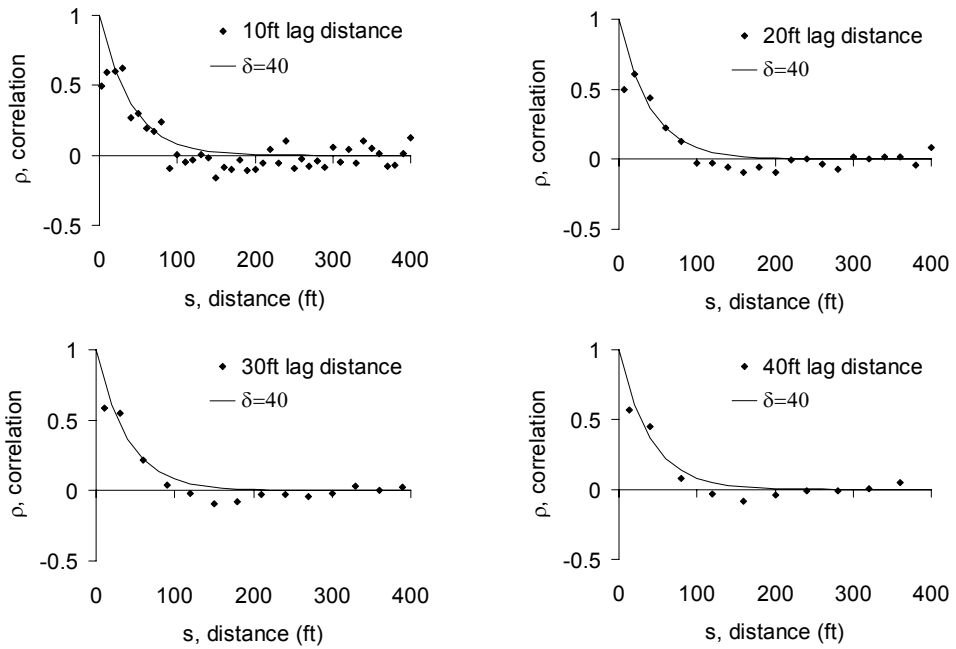
Figure 8-8. I-95/Rt. 1 minimum wet-mix strengths with four lag distances

135
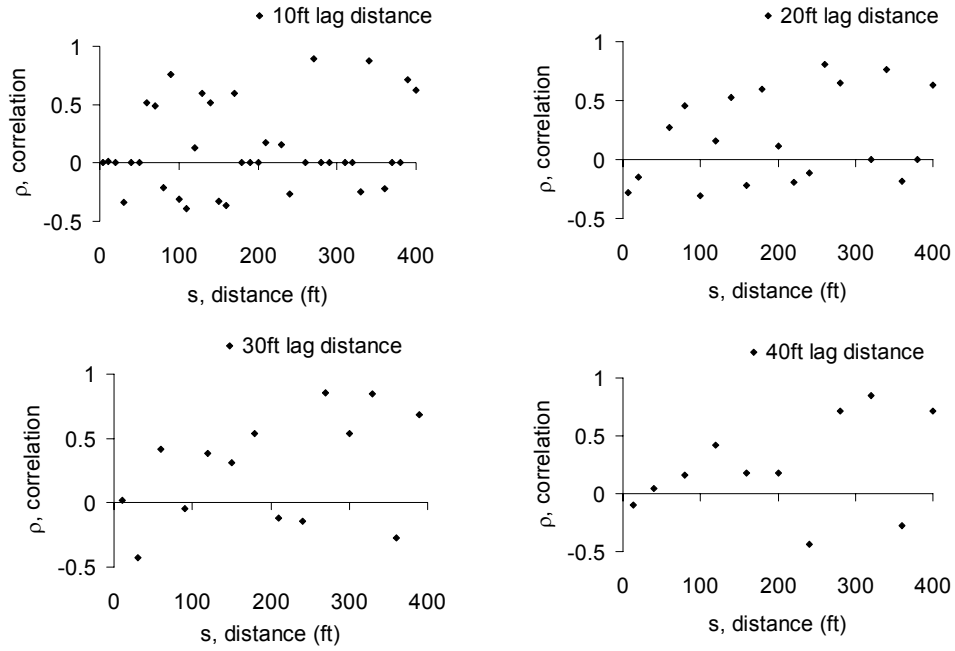
Figure 8-9. I-95/Rt. 1 average dry-mix strengths with four lag distances
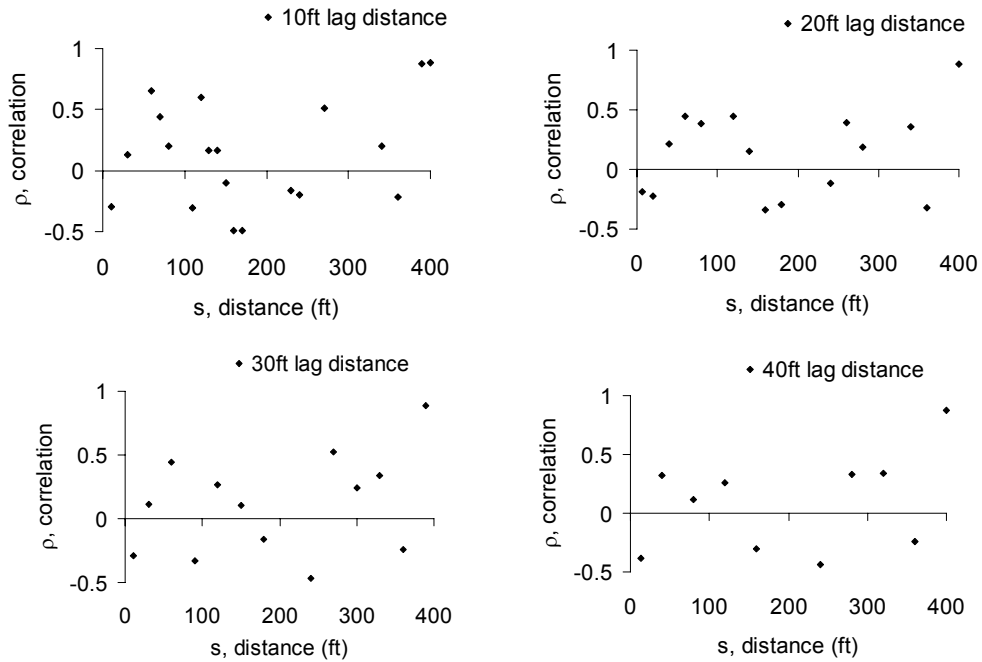
Figure 8-10. I-95/Rt. 1 minimum dry-mix strengths with four lag distances

136

8.5.3. Oakland Airport

Figures 8-11 and 8-12 plot correlation versus separation distance for strengths measured at the Oakland Airport project. These figures also include plots of Equation 8-2 with the autocorrelation distance, δ, equal to 60 feet. This function approximates the spatial correlation of the strength data well, for both the average strength in Figure 8-11 and the minimum strength in Figure 8-12.

Yang (2004) indicated that in-situ soils and the resulting quality of mix strength at the Oakland Airport site are much more spatially uniform than in-situ soils and the resulting quality of mix strength at the I-95/Rt. 1 interchange. This trend is reflected in the autocorrelation distance. For data at the I-95/Rt. 1 interchange, the tests collected at 170 locations clearly show an autocorrelation distance of 40 ft, as shown in Figures 8-7 and 8-8. What this number represents is that columns within 40 ft of one another are heavy correlated, and columns beyond that distance are not. Because only 56 locations were tested at the Oakland Airport, spatial correlation is not as clear as the I-95/Rt. 1 site; however, as shown in Figures 8-11 and 8-12, an autocorrelation distance of 60 ft appears to be reasonable.
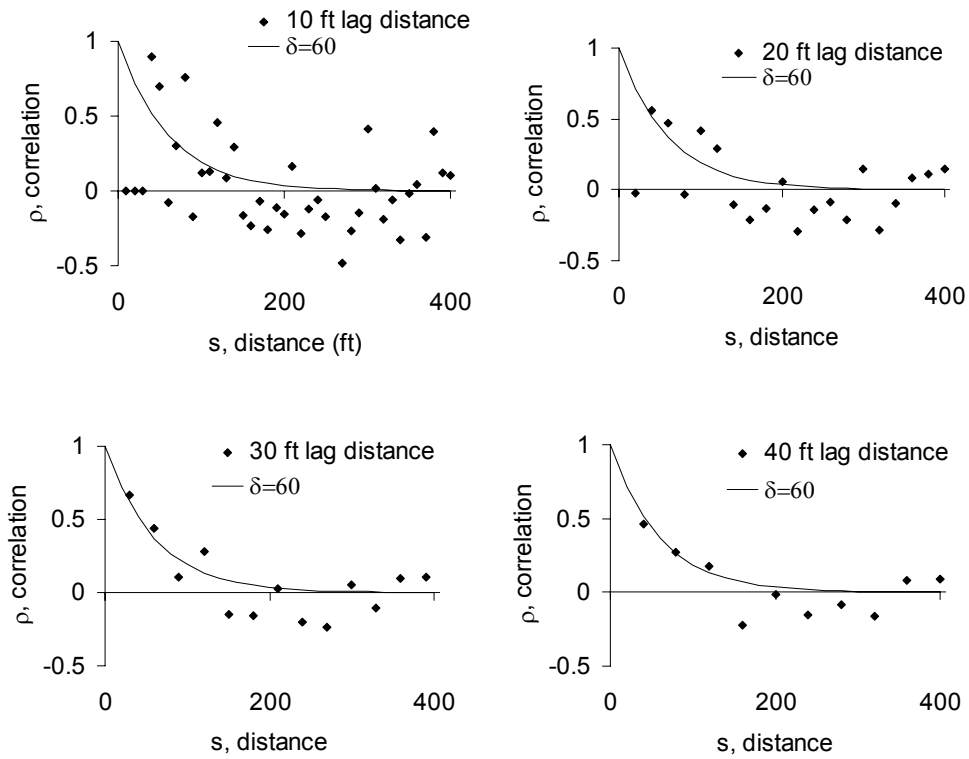
Figure 8-11. Oakland Airport average strengths with four lag distances
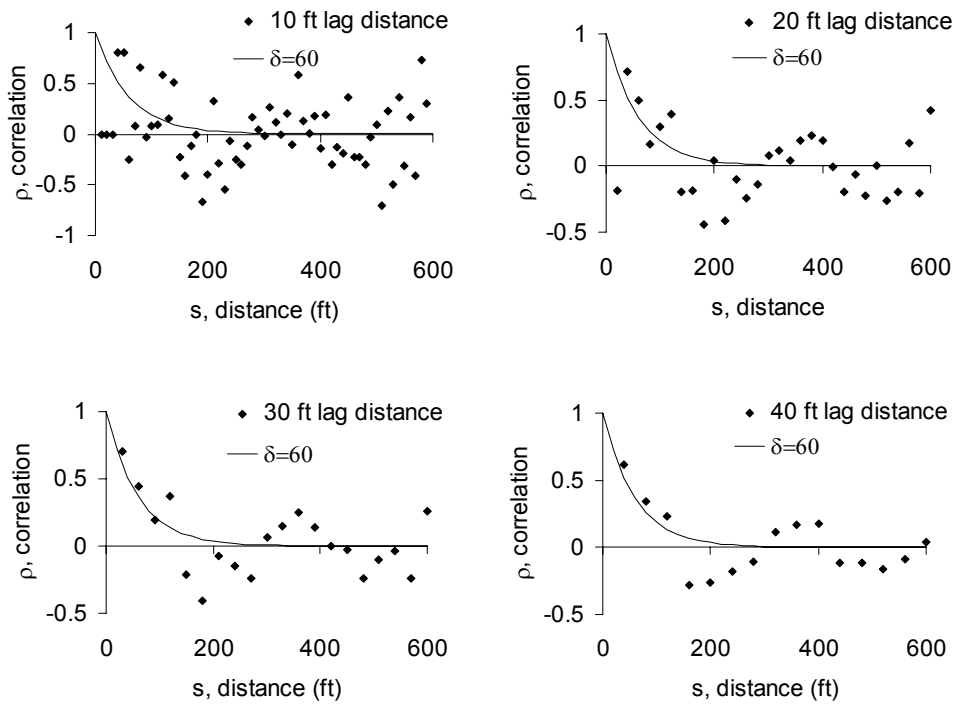
Figure 8-12. Oakland Airport minimum strengths with four lag distances

8.5.4. Glen Road interchange

Figures 8-13 and 8-14 plot correlation versus separation distance for strengths measured at the Glen Road Interchange project, Ramps H & E. These figures also include plots of Equation 8-2 with the autocorrelation distance, $\delta = 60$ feet. This function approximates the spatial correlation of the strength data reasonably well, for both the average strength in Figure 8-13 and the minimum strength in Figure 8-14 . Figures 8-15 and 8-16 show very little spatial correlation for either the average strength or minimum strength from columns installed at Glen Road Interchange project, Ramps G & F. This may simply be due to the relatively small number of sample pairs available at Ramps G & F, or it may reflect a real difference between the spatial correlations produced at the two sites.
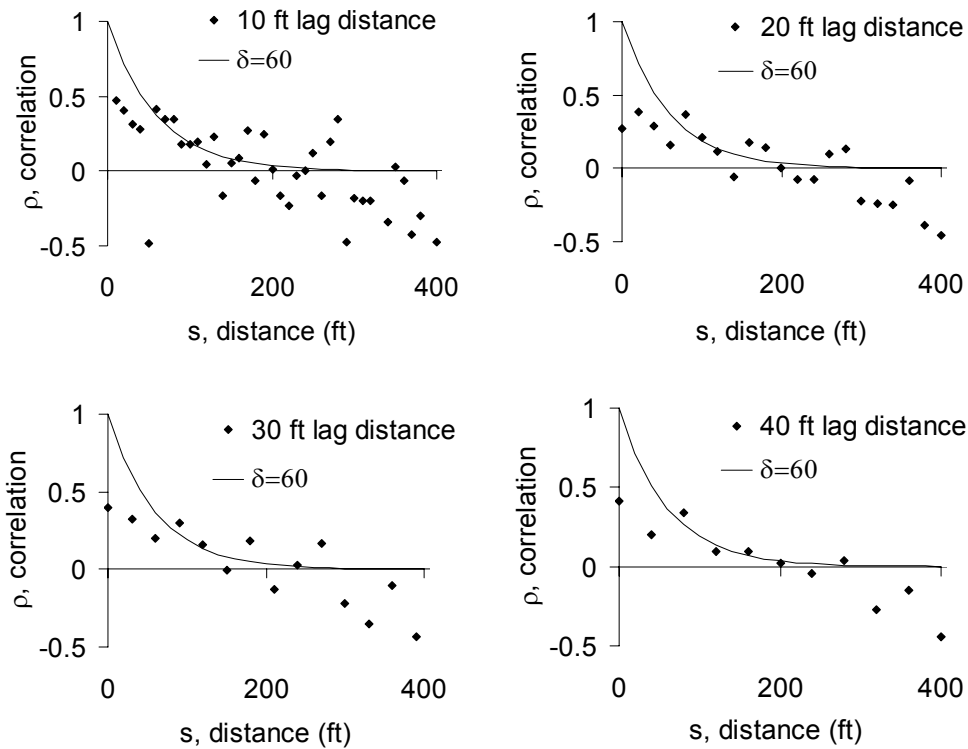
Figure 8-13. Glen Road Ramps H&E average strengths with four lag distances
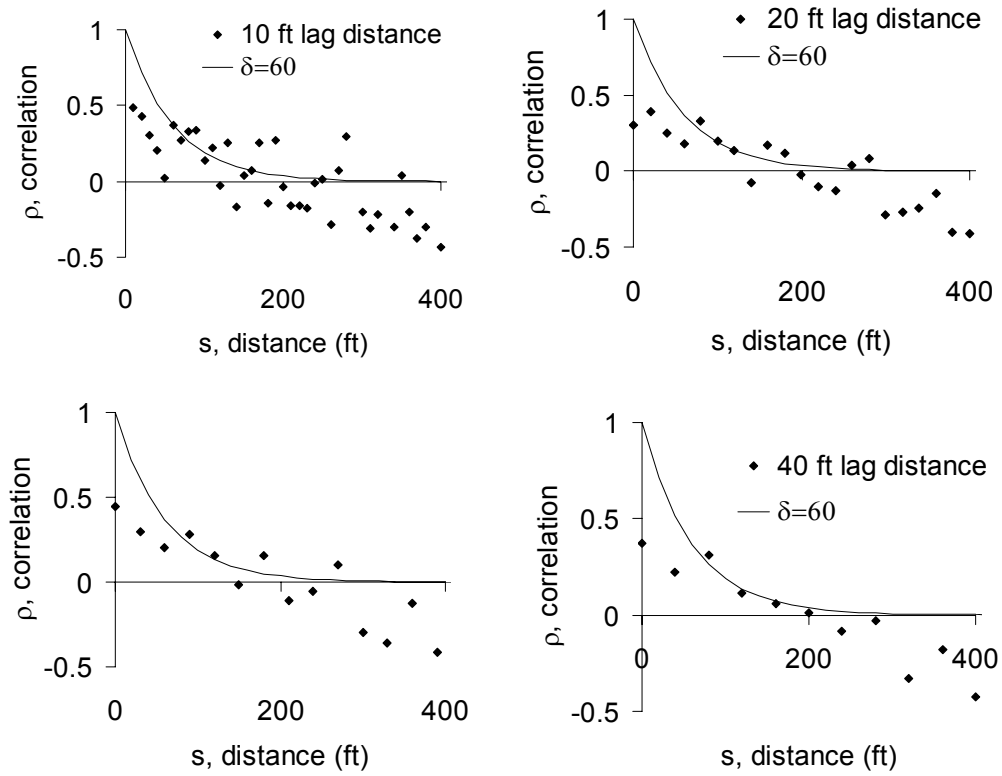
Figure 8-14. Glen Road Ramps H&E minimum strengths with four lag distances
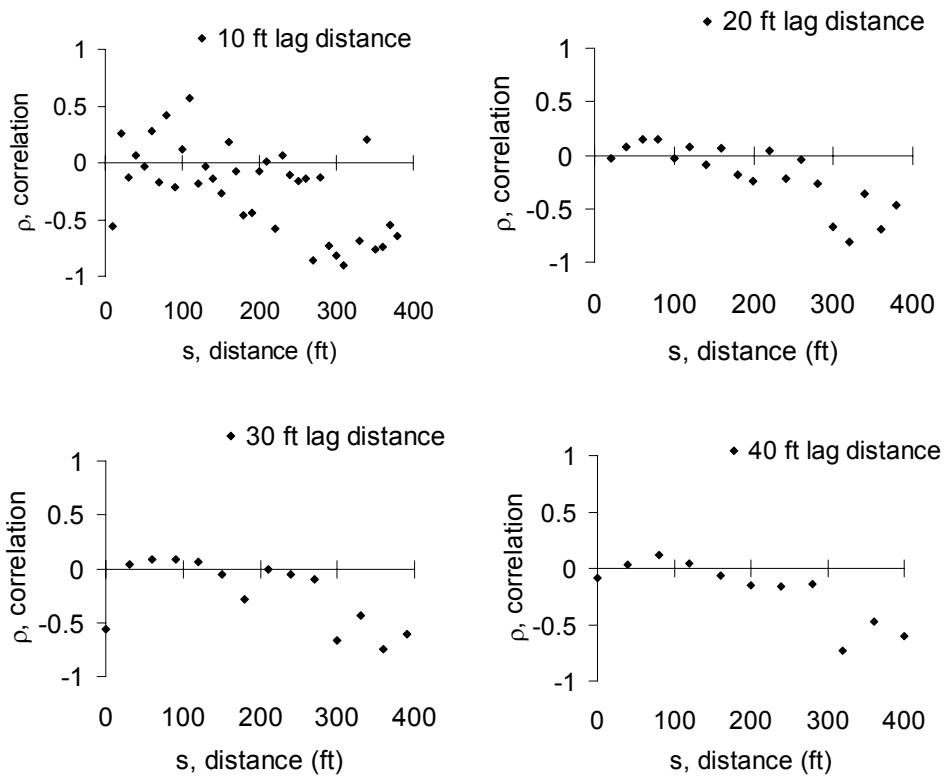
Figure 8-15. Glen Road Ramps G&F average strengths with four lag distances
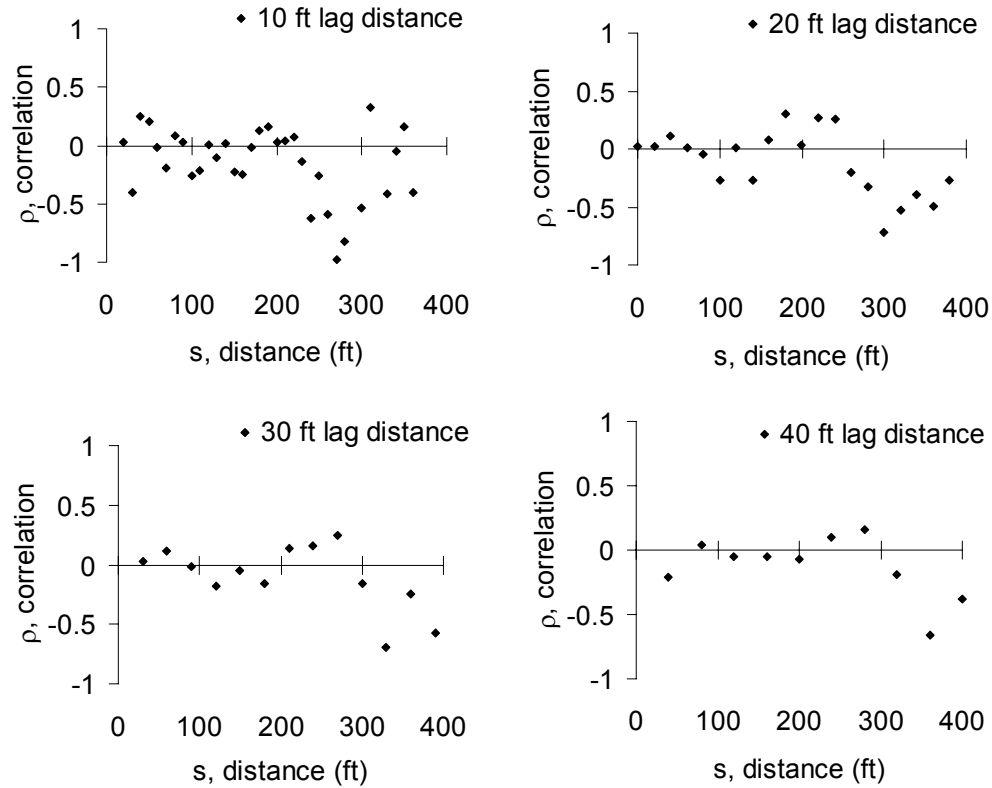
Figure 8-16. Glen Road Ramps G&F minimum strengths with four lag distances

8.6. Modulus values

Many sources summarized in Appendix D of this report present the relationship between Young's Modulus, E, and the unconfined compression strength, q_u. The ratio of E/q_u ranges from 75 to 1000 for wet-mix soils and ranges from 75 to 300 for dry-mix soils, according to these sources.

The secant modulus of elasticity, E_{50}, is defined as the slope of the line extending from the origin of the stress-strain plot to the point corresponding to half the maximum stress. The value of E_{50} is frequently used as the Young's Modulus for deep-mixed materials. In this research, E_{50} values were determined from 2672 unconfined compression tests performed on samples from the I-95/Route 1 interchange project. Judgment is sometimes required in choosing the secant modulus from the plot of stress versus strain in an unconfined compression test in order to account for seating effects at the specimen ends. To standardize determination of modulus values from all samples, the E_{50} values presented here are the slope of the line from the point corresponding to

one quarter of the maximum stress to the point corresponding to one half the maximum stress. Due to erratic stress-strain data in some of the tests, 144 values of E_{50} determined in this manner were judged to be unacceptable. The set of data presented as "All samples" in Table 8-13 are the 2528 samples that remained after values deemed unacceptable were removed. Using linear regression, the E_{50}/q_u value was determined to be 391 for this set of data. This data set is plotted in Figure 8-17 along with the trend line, and again at a different scale in Figure 8-18, which also shows three other lines that represent E_{50}/q_u ratios of 100, 300, and 500 for comparison purposes.

Table 8-13. E_{50}/q_u values for both wet method and dry method columns

Data Set	# Samples	%	E_{50}/q_u	R^2
All samples	2528		391	0.22
After removing q_u values between 950 psi and 1050 psi	2208	100	319	0.18
Less 1% extreme E_{50}/q_u values	2188	99	285	0.40
Less 2% extreme E_{50}/q_u values	2166	98	280	0.44
Less 5% extreme E_{50}/q_u values	2100	95	262	0.51

As can be seen in both Figure 8-17 and Figure 8-18, there is a large concentration of values with an unconfined compression strength around 1000 psi. Many of these values are listed in the data set as ">1000." These facts suggest that the laboratory procedure often involved terminating the unconfined compression test when the sample reached approximately 1000 psi. The E_{50} value is determined based on the lower part of the stress-strain curve, so the E_{50} values are probably accurate while the reported q_u values clustered around 1000 psi are probably low. Thus, including these results would result in artificially high values of the ratio E_{50}/q_u. Removing the cluster of samples with an unconfined compression strength between 950 and 1050 psi results in the case with 2208 samples listed in Table 8-13. Removing the samples in this range does lower the E_{50}/q_u ratio from 391 to 319.

Next, outliers in the data set of 2208 samples were removed by progressively removing 1%, 2%, and 5% of the extreme E_{50}/q_u values such that an equal number of extreme high and low values of E_{50}/q_u were removed for each percentage. This process tends to lower the E_{50}/q_u ratio, as can

be seen in Table 8-13. The R^2 values lose some significance in the process because the data removal eliminates the points that contribute most to low values of R^2. Nevertheless, this process is useful because it shows that the values of E_{50}/q_u are only moderately affected as extreme values are trimmed from the data set.
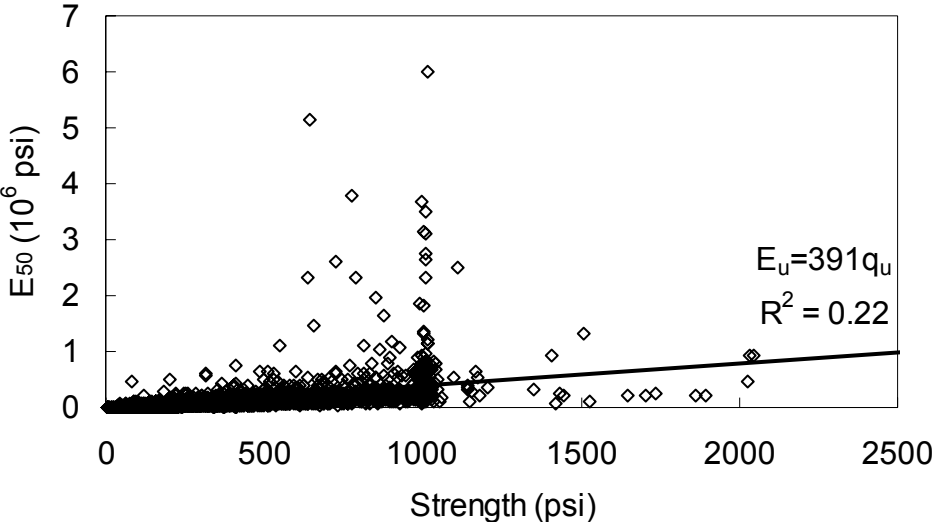
Figure 8-17. Plot of E_{50} vs. q_u for all samples
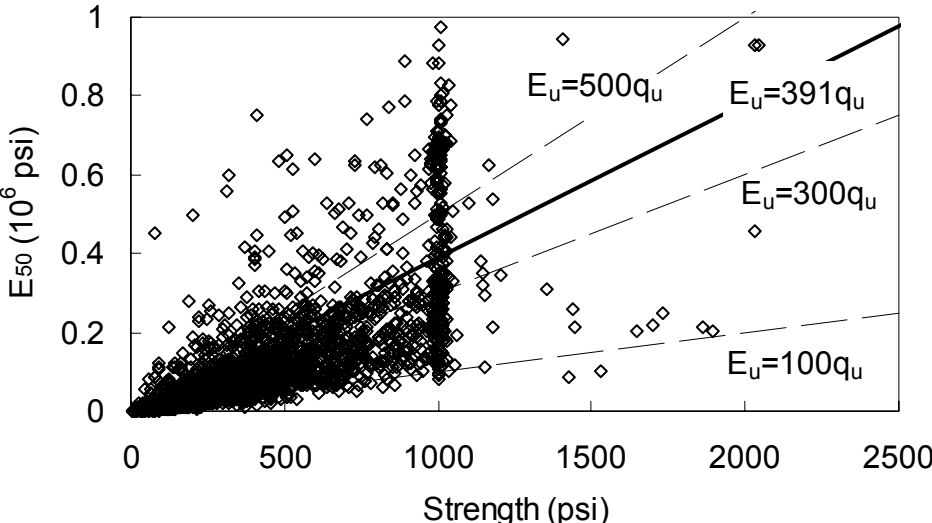
Figure 8-18. Plot of E_{50} vs. q_u for E_{50} values up to 1×10^6 psi

The same type of investigation was performed after separating columns installed by the wet method from columns installed by the dry method. Results for the wet method are shown in Table 8-14, and results for the dry method are shown in Table 8-15. Although the wet-mix column strengths are much higher than the dry-mix column strengths, the values of E_{50}/q_u are very comparable for the two methods of constructing columns. There is a lot of scatter in these trends, as indicated by the relatively low R^2 values, but it appears that a value of E_{50}/q_u around 300 is reasonable for both the wet method and the dry method of column construction, based on the data from the I-95/Route 1 project. It is important to note that the data for the dry mix method from this project are dominated by cement-soil mixtures without lime.

Table 8-14. E_{50}/q_u values for wet method columns

Data Set	# Samples	%	E_{50}/q_u	R^2
All Samples	2071		394	0.21
After removing q_u values between 950 psi and 1050 psi	1785	100	314	0.18
less 1%	1769	99	286	0.43
less 2%	1751	98	281	0.45
less5%	1697	95	267	0.50

Table 8-15. E_{50}/q_u values for dry method columns

Data Set	# Samples	%	E_{50}/q_u	R^2
All Samples	457		368	0.26
After removing q_u values between 950 psi and 1050 psi	423	100	344	0.19
less 1%	419	99	303	0.25
less 2%	415	98	268	0.33
less5%	403	95	249	0.45

An investigation was also made into the coefficient of variation in E_{50} values recorded at the I-95/Rt. 1 interchange. The variation of E_{50} values is higher than the variation of q_u values when the entire data set is included in the analysis. High modulus values have a larger impact on the

variation of E_{50} than high strength values have on the variation of q_u. This trend holds for both wet-mix and dry-mix samples. As shown in Figure 8-19, the variation of E_{50} is about 60% when high values are not included in the data set, but the variation is much higher when high value are included. Figure 8-19 also shows that the variation of q_u is not as sensitive to high values.
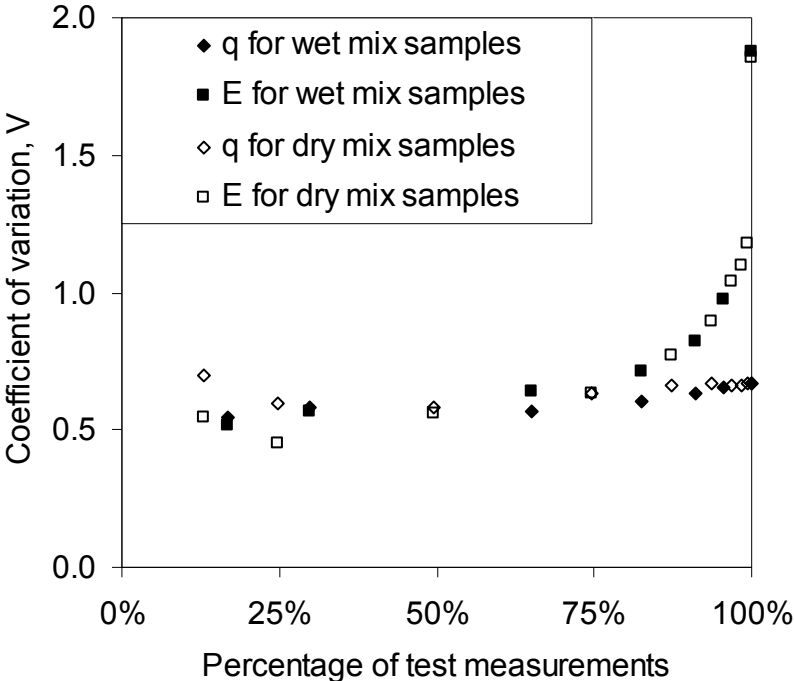
Figure 8-19. Coefficient of variation in E_{50} and q_u at the I-95/Rt. 1 Interchange

8.7. Summary and Conclusions

Data sets of unconfined compressive strength for deep-mixed materials were analyzed to determine basic statistical data, goodness of fit to standard distributions, and regressions against controllable parameters. Altogether, 13 data sets from 6 sources at 9 sites were analyzed. In addition, spatial correlations were evaluated for the data from three sites, and the ratio of modulus to unconfined compressive strength was evaluated for the data from one of the sources. Key findings include the following:

- Values of the coefficient of variation ranged from about 0.34 to 0.79, with an average value of about 0.55.

- Regression analyses indicated that the strongest correlations to unconfined compressive strength provided by controllable parameters were with age and water-to-cement ratio of the slurry. The values of R^2 for these correlations ranged from zero to 0.68 for the 13 data sets.

- When the trend from the regression analyses using age and water-to-cement ratio of the slurry were removed from the data, the coefficients of variation decreased such that the minimum value was 0.17, the maximum value was 0.67, and the average value was about 0.40. This result indicates that some of the scatter in deep-mixing strength data is associated with controllable factors. Values of variation with the controllable trends removed should be used for reliability analyses.

- Deep-mixing strength data tends to fit a lognormal distribution better than a normal distribution, a uniform distribution, or a triangular distribution.

- Analyses of spatial correlation for strength data disclose an autocorrelation distance when samples are tested from several column locations. An autocorrelation distance of 40 ft is evident in wet-mix columns tested from the I-95/Route 1 interchange. An autocorrelation distance of 60 ft is evident in wet-mix columns tested from Glen Road ramps H&E and from the Oakland Airport project.

- An insufficient number of sample locations were tested to determine an autocorrelation distance for strength measurements at Glen Road ramps G&F, at the Port of Oakland, or for the dry-mix columns at the I-95/Route 1 interchange,.

- Analysis of a large data set from the I-95/Route 1 project indicates that an E_{50}/q_u ratio of about 300 is appropriate for soil-cement columns constructed by either the wet method or the dry method of deep mixing without lime.

9. RELIABILITY ANALYSIS

9.1. Introduction

Reliability analyses make use of other quantitative analysis methods to determine the probability of exceeding a limit state. In geotechnical engineering, the limit state is typically either a specified deflection or a factor of safety equal to one. In this research, reliability analyses are used with stability analyses to determine the probability of failure, $p(f)$, which can also be referred to as the probability of unsatisfactory performance, $p(u)$. The probability of satisfactory performance, $p(s)$, or equivalently, the reliability, is numerically equal to one minus $p(u)$. There is a large degree of uncertainty inherent in geotechnical analyses resulting from natural materials that can be highly variable, limited availability of information on those materials, and analysis methods that many times have an empirical basis for justifying simplifying underlying assumptions. Just as factors of safety in geotechnical engineering are rarely precise and require engineering judgment, results from reliability analyses are subject to interpretation and should also be scrutinized with engineering judgment. That being said, reliability analysis is a useful tool to assist the geotechnical engineer in understanding the effects of uncertainty on the calculated values of factor of safety. This section presents the application of reliability analysis to stability of roadway embankments supported on deep-mixed columns.

First, the Taylor Series method is briefly described. Then an example embankment is described, and its stability is analyzed using limit equilibrium and numerical analyses. Reliability analyses are applied using values of coefficient of variation for the strength from Chapter 8 and Appendix D, and values of coefficient of variation for the strength of soils from typical values in the published literature. The influence of limited spatial correlation of columns strength on reliability is also analyzed, using an autocorrelation distance similar to the values found in the statistical analyses of case history data in Chapter 8.

9.2. Taylor Series Analysis

Taylor Series is a simple First Order, Second Moment (FOSM) analysis that requires only a few additional calculations of factor of safety to determine the reliability index, β. Application of the Taylor Series Method to reliability analyses in geotechnical engineering is discussed in Baecher

and Christian (2003), Duncan (2000), Harr (1987), and Ang and Tang (1975). β has been used effectively in design as a relative measure of reliability, as indicated in Table 9-1. However, β is more frequently used to estimate the probability of failure, as will be demonstrated in the following sections.

Table 9-1. Reliability Index, β (from USACE ETL 1110-2-547)

Expected Performance Level	Beta, β	Probability of Unsatisfactory Performance
High	5	0.0000003
Good	4	0.00003
Above Average	3	0.001
Below Average	2.5	0.006
Poor	2.0	0.023
Unsatisfactory	1.5	0.07
Hazardous	1.0	0.16

Whereas a deterministic factor of safety is obtained from one calculation, reliability analysis requires several calculations based on the number of random variables whose impact on reliability is being determined. The required number of calculations, N_c, to perform a Taylor Series analysis can be determined from the number of random variables, N_v, by Equation 9-1.

$$N_c = 1 + 2N_v \tag{9-1}$$

In the Taylor Series method, variance of the factor of safety is calculated by changing random input parameters by one standard deviation, repeating the process a number of times, and tabulating the results. The expected value and variance of factor of safety are then used to determine a value of the reliability index, β. As mentioned previously, this value of β is typically used to determine the probability of failure, $p(f)$. Baecher and Christian (2003) state that the method is easier to demonstrate than it is to describe. This report does not attempt to

further explain the Taylor Series method, but it does provide examples for geotechnical systems using deep-mixed columns to demonstrate its application. Examples for other applications are provided by Duncan (2000), who clearly presents a simplified version of the Taylor Series method. Baecher and Christian (2003) present a detailed Taylor Series analysis of an embankment for the James Bay Project, including some complex issues related to reliability analyses, such as separating the variation of a parameter into a spatial component and a systematic component.

Taylor Series is a simple method of reliability analysis that can provide the engineer with additional insight into behavior of embankments supported with deep-mixed columns. More rigorous methods of reliability analysis may provide refinement over the solution from the simple Taylor Series analysis, but that level of refinement may not be worthwhile for the performance modes investigated here. When analysis methods are developed that better reflect performance of embankments supported on deep-mixed columns, it may become worthwhile to use more sophisticated methods of reliability analysis. In addition to providing an estimate of reliability, the Taylor Series method demonstrates the sensitivity of performance to the variability of input parameters, as will be shown in the following sections.

9.3. Example embankment

When deep-mixed columns are used to improve soft clay foundations for embankment construction, settlement and slope stability are important design considerations. In the following sections, deterministic analyses are combined with reliability analysis to estimate the probability of failure for an example embankment. A report by Navin and Filz (2005) describes reliability analyses to estimate probability of excessive settlement for column-supported embankments.

The eighteen-foot high example embankment shown in Figure 9-1 is placed on a two-foot thick layer of sand fill that overlies a 28-foot-thick clay layer. The water table is at the bottom of the sand fill. The clay is underlain by ten feet of sand. Isolated columns are used beneath the side slope as well as the full height of the embankment. Column lengths extend from the top of the sand fill, through the clay layer, and two feet into the base sand layer. Columns are three feet in

diameter, arranged in a square spacing with a six-foot center-to-center spacing, as shown in plan in Figure 9-2. This results in a replacement ratio of 20%.

Mean values of the material properties are listed in Table 9-2. The clay is assumed to be lightly overconsolidated, with the preconsolidation pressure equal to 500 psf plus the initial effective vertical stress. The undrained shear strength of the clay, s_u, is assumed to vary with preconsolidation pressure according to the relation in Equation 9-2.

$$\frac{s_u}{p_p} = 0.23 \tag{9-2}$$

where:

s_u = the undrained shear strength, or cohesion

p_p = the maximum past vertical stress, or preconsolidation pressure

Thus, the value of s_u is 168 psf at the top of the clay and 384 psf at the bottom of the clay layer. The average shear strength of the clay is 276 psf. The Young's modulus of the clay is assumed to equal 200 times its undrained shear strength. For short-term loading, the column is characterized as having a cohesion intercept of 10,000 psf and a total stress friction angle of zero. A Poisson's ratio, ν, of 0.45 is used for both the clay and the columns in the numerical analysis. Initial lateral stresses in the clay layer were computed based on an effective stress value of the lateral earth pressure coefficient, K_0, equal to 0.5. The hydrostatic pore water pressures were added to the effective lateral stresses to obtain the total lateral stresses.
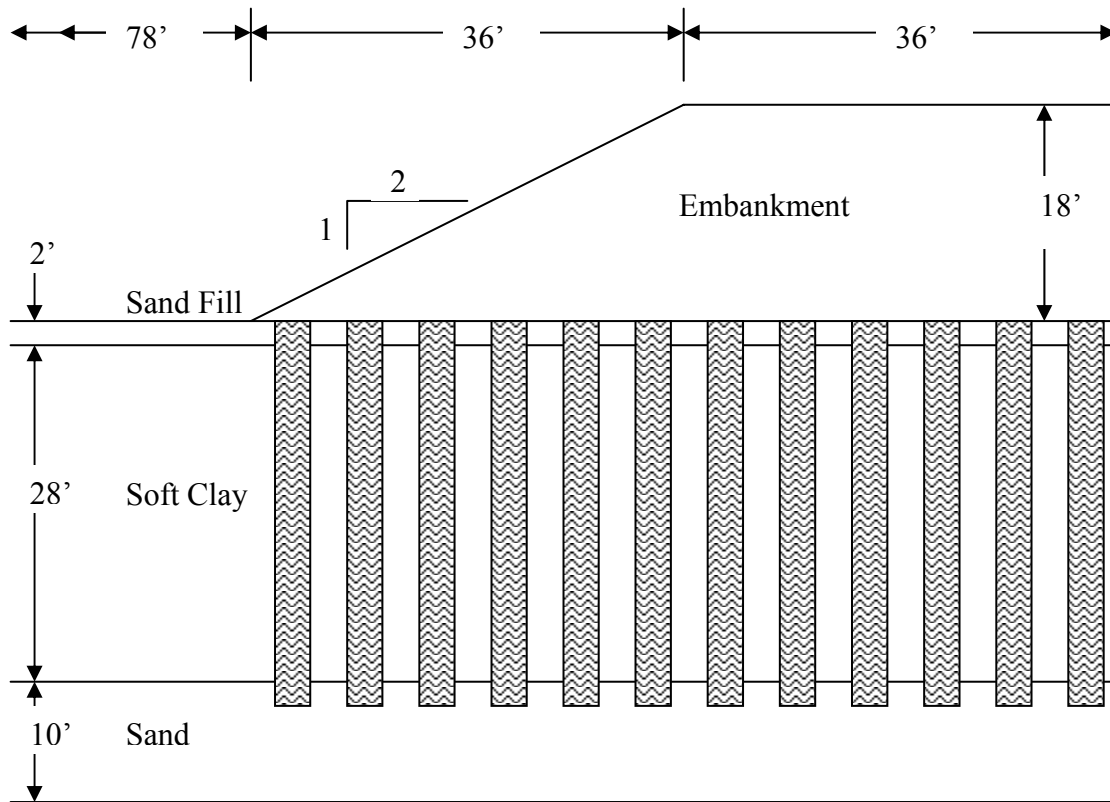
Figure 9-1. Profile of example deep-mixed, column-supported embankment
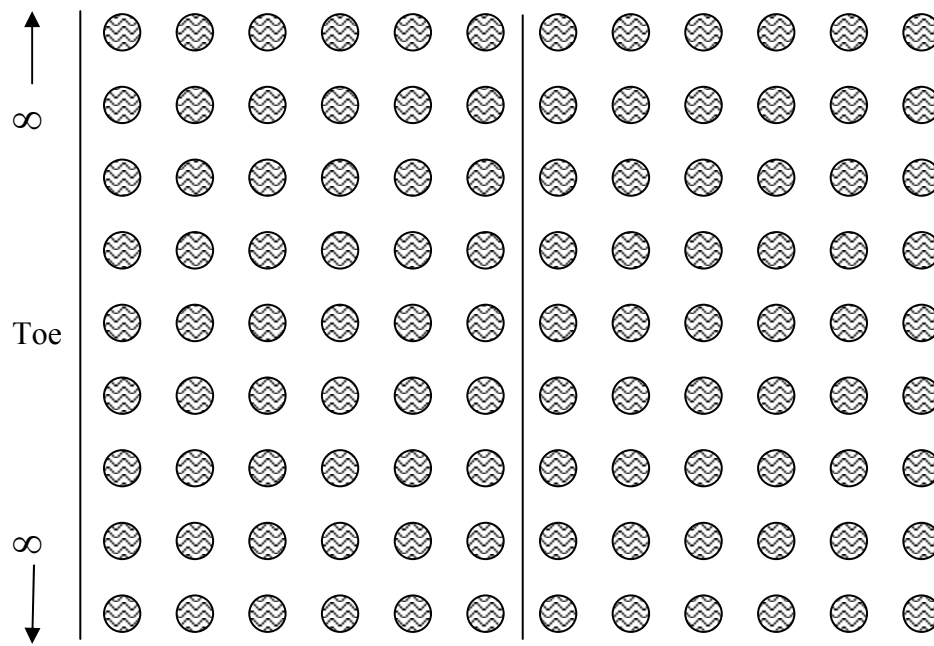
Figure 9-2. Plan of example deep-mixed, column-supported embankment

151

Table 9-2. Properties values for the example embankment

Material	Unit Weight (psf)	E (psf)	ν	c (psf)	ϕ
Embankment	125	625,000	0.3	-	35°
Sand Fill	115	250,000	0.33	-	30°
Clay	96	200s_u	0.45	*	0
Base Sand	140	1,000,000	0.26	-	40°
Columns	96	3,000,000	0.45	10,000	0

* The shear strength of the clay depends on depth, as described in the text.

9.3.1. Limit equilibrium analysis of slope stability

Geotechnical engineers commonly perform slope stability analyses to determine the factor of safety against shear failure near the edge of an embankment. Ordinarily, limit equilibrium methods are used to find the critical failure surface that shears through the embankment, the deep-mixed column, and the unimproved soil in the foundation. However, deep-mixed columns are significantly stronger and stiffer than the surrounding soil, and they have very low tensile strength. Consequently, isolated columns may fail by tilting or bending instead of shearing. It may also be possible for soft soils to extrude between widely spaced columns. Possible failure modes for isolated columns used to support embankments are shown in Figure 9-3.

Circular Failure Surface

Column Tilting

Column Bending

Soil Extrusion
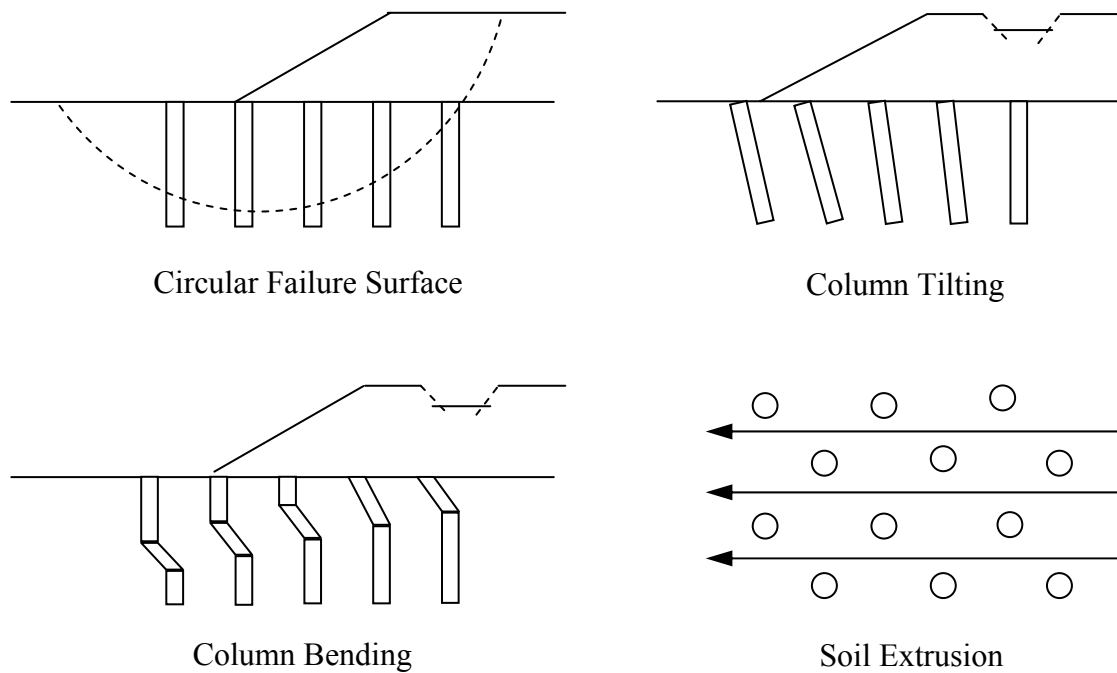
Figure 9-3. Multiple modes of failure for deep-mixed columns used to support embankments

Limit equilibrium slope stability analyses capture only composite shear failure. This is an important failure mode, and slope stability analyses using limit equilibrium methods are illustrated in this subsection. Numerical analyses addressing composite shearing, column tilting, and column bending are presented in Section 9.3.2. Reliability analyses are discussed in Sections 9.3.3 through 9.3.5.

Computer programs for limit equilibrium slope stability analyses are used to rapidly search many trial failure surfaces to determine where the factor of safety, *FS*, is lowest. For embankments supported on deep-mixed columns, an average cohesion value is used for the zone of the foundation that has been improved with columns. According to Equation 9-3, this value is simply a weighted average based on the replacement ratio.

$$c_{average} \; = \; c_{clay}(1\text{-}a_s) + c_{column}(a_s) \tag{9-3}$$

where:

a_s = the replacement ratio

$c_{average}$ = the average cohesion value

c_{clay} = the clay cohesion value

c_{column} = the column cohesion value

Geotechnical engineers generally use design values of strength that are lower than expected values. Although one aspect of reliability analysis is that conservatism should be avoided in selecting expected values, it should also be understood that clay strength and column strength cannot both achieve the maximum value at the same deflection due to strain incompatibility. For example, as described in Chapter 4, Kitazume et al. (2000) use a residual strength for columns which is 80% of peak strength. CDIT (2002) recommends the use of a reduced strength of clay as described in Appendix C.

The program UTexas (Wright, 1999) was used to analyze the example embankment. The critical failure surface is shown in Figure 9-4, and the value of FS is 3.2.
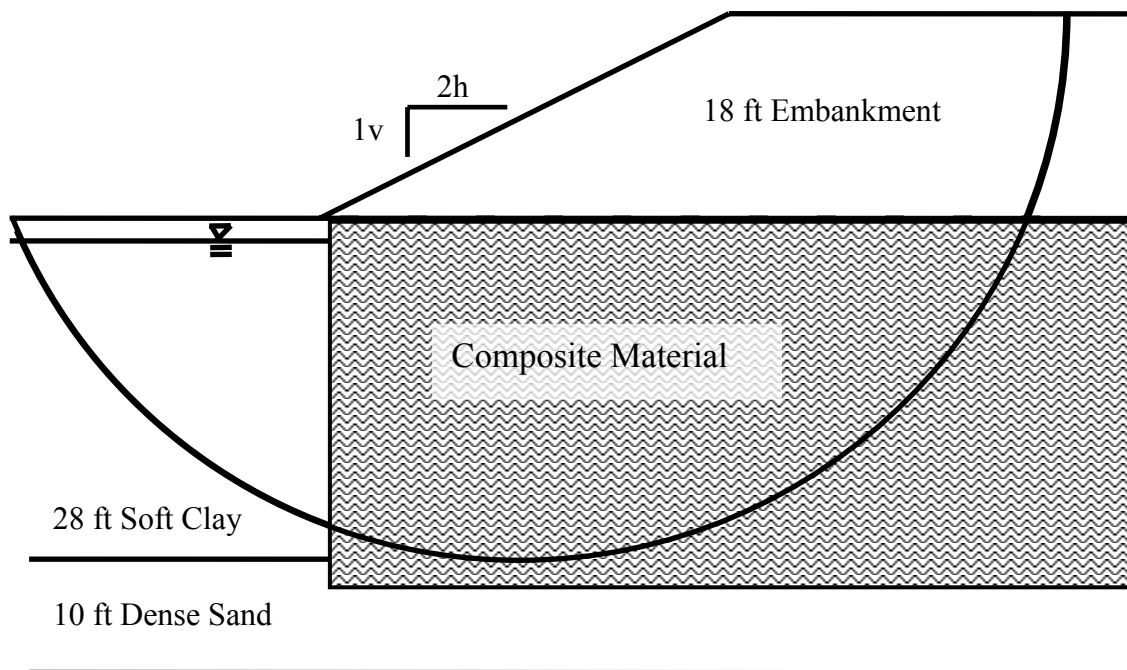
Figure 9-4. Shear failure through composite foundation

As an alternative to using a weighted average strength in the improved zone, the deep-mixed columns may be represented in profile view by vertical strips in the foundation. Strip widths are chosen to result in the same area replacement in plan view as circular columns, which for this example with a 20% replacement ratio and a center-to-center spacing of six feet results in a strip width of 1.2 ft. The column layout shown in Figures 9-1 and 9-2 is represented by the profile shown in Figure 9-5 when this adjustment is made to analyze the problem in two dimensions. A limit equilibrium slope stability analysis of the profile in Figure 9-5 results in the same value of $FS = 3.2$ as determined in the method using a composite material, as described previously.

3' Diameter DMM Columns
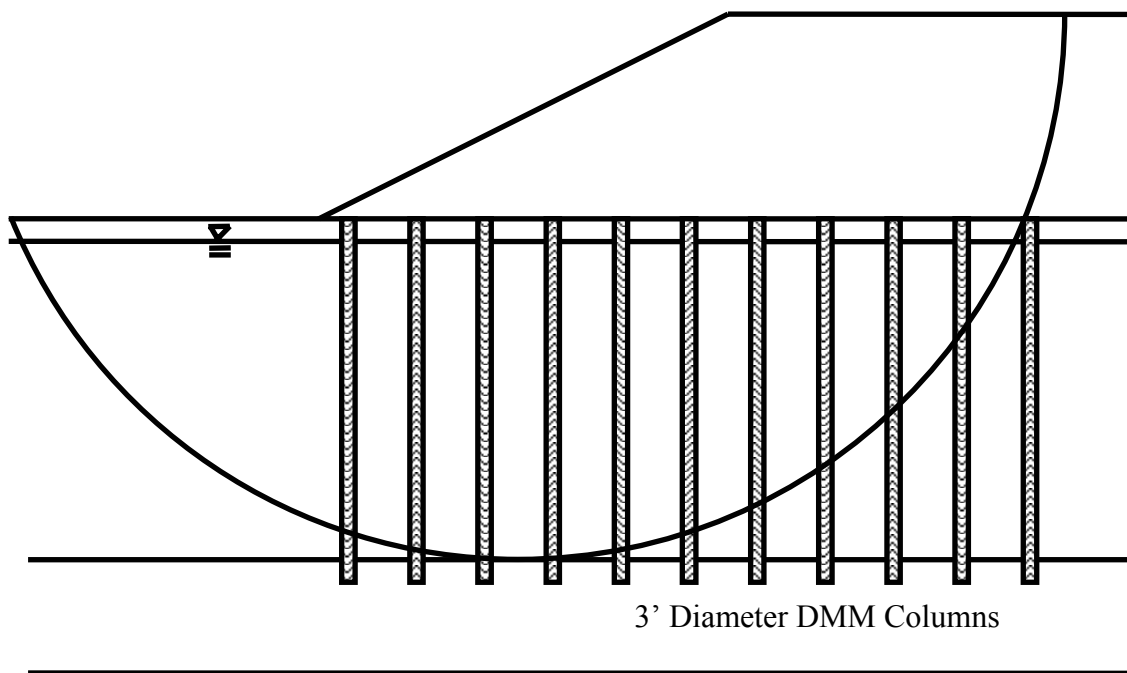
Figure 9-5. Shear failure through columns and soil in the foundation

9.3.2. Numerical Analysis of Slope Stability with Isolated Columns

Numerical analyses can be used to include tilting and bending failure in the analysis of slope stability for these systems. As one example, the computer program FLAC (Itasca 2002) can be used to perform numerical analyses of geotechnical systems. Generally, numerical analyses are used to determine stresses and deflections. FLAC has an automated procedure to evaluate the factor of safety by reducing strength values to determine the point of impending failure, at which the model is no longer in equilibrium. This factor of safety procedure, fos, in FLAC can only be used when all zones in the mesh are represented by the Mohr-Coulomb model.

For the FLAC analysis, the 18-foot-high embankment is applied in a series of 10 lifts, according to the schedule in Table 9-3. Each lift is allowed to reach equilibrium before placement of the next lift. The fos calculation in this example is made after the 10 lifts have been placed, and the geometry has reached equilibrium, as recommended in the FLAC manual.

Table 9-3. Lift thickness of the embankment

Lift	Embankment Height (ft)
1	1
2	2
3	3
4	4
5	6
6	8
7	10
8	12
9	15
10	18

The embankment shown in Figure 9-5 has a factor of safety equal to 3.2 when analyzed using limit equilibrium procedures, as demonstrated in Section 9.3.2. The same embankment was analyzed using FLAC and found to have a factor of safety equal to 1.4. The reason that the factor of safety is so much lower in the numerical analyses is that they allow other failure modes, such as bending and tilting, which are not considered in limit equilibrium slope stability analyses. Figure 9-6 shows shear, tilting, and bending failure that occurred in the numerical analysis of this column-supported embankment.
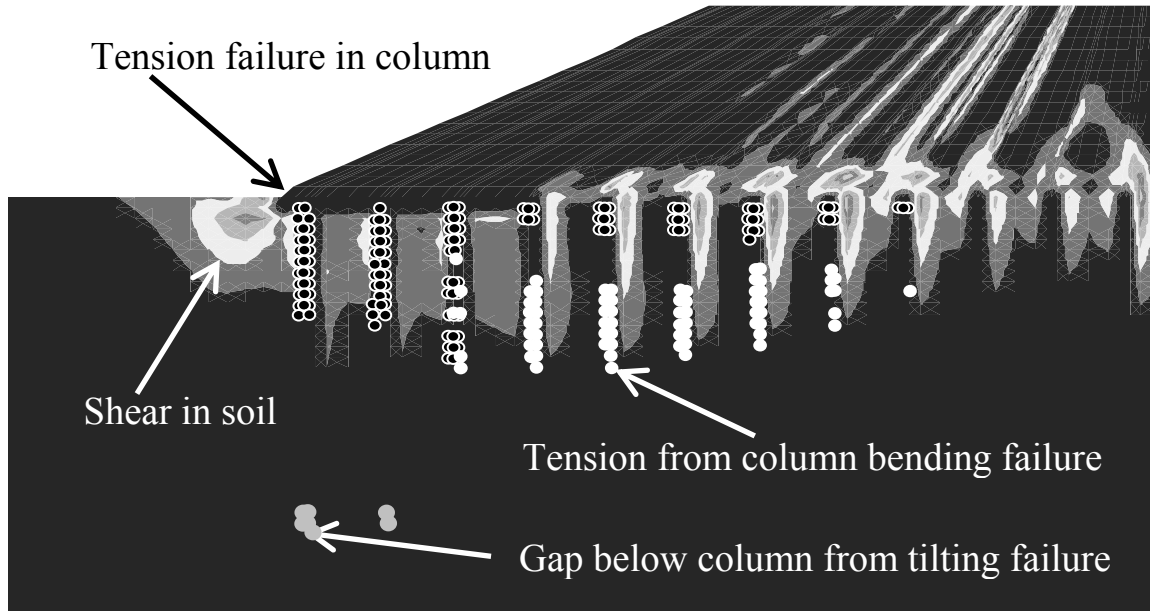
Figure 9-6. Numerical analysis of the foundation improved with isolated columns at failure

9.3.3. Reliability Analysis of Slope Stability with Isolated Columns

In this section, reliability analyses are combined with the limit equilibrium analysis described in Section 9.3.1 and the numerical analysis described in Section 9.3.2 to determine the probability of slope stability failure. This probability incorporates uncertainty in column strength, unimproved clay strength, and the embankment strength. The column cohesion in this example has a coefficient of variation of 60%, which is based on values found in the literature summarized in Appendix D, and the evaluation of data in Chapter 8. The clay cohesion has a coefficient of variation of 40%, and the embankment friction angle has a coefficient of variation of 10%, both based on values found in the literature (Harr 1986, Duncan and Wright 2004).

The calculation of factor of safety from the expected case and two calculations of factor of safety for each random variable are used to determine the variation in factor of safety. These calculations are collected to determine the change in factor of safety, ΔFS, due to each random variable, as shown in Table 9-4. In this table, the factor of safety values obtained using mean values for each of the three random variables were determined in Section 9.3.1 and Section 9.3.2. The two additional calculations for each random variable are performed by changing the random variable one standard deviation above and below the mean, while keeping the other random

variables constant. The standard deviation of factor of safety, σ_{FS}, is determined using Equation 9-4. The coefficient of variation of factor of safety, V_{FS}, is the standard deviation divided by the expected value of factor of safety, FS.

$$\sigma_{FS} = \sqrt{\left(\frac{\Delta FS_1}{2}\right)^2 + \left(\frac{\Delta FS_2}{2}\right)^2 + \ldots\ldots + \left(\frac{\Delta FS_{Nv}}{2}\right)^2} \text{ , for } N_v \text{ random variables} \qquad (9\text{-}4)$$

The reliability index for factor of safety, β_{FS}, is calculated using Equation 8-5.

$$\beta_{FS} = \frac{\ln\left[\dfrac{\mu}{\sqrt{1+V_{FS}^2}}\right]}{\sqrt{\ln\left(1+V_{FS}^2\right)}} \qquad (9\text{-}5)$$

The value of the reliability index obtained from Equation 9-5 can be converted to a probability. In Excel©, the expression to determine the probability of failure is $p(f) = 1\text{-NORMSDIST}(\beta_{FS})$.

Table 9-4. Computations for edge stability reliability analysis

Case	c_{col} (psf)	c_{clay} (psf)	ϕ_{emb} (degrees)	FLAC FS	FLAC ΔFS	UTexas FS	UTexas ΔFS
Mean Values	10,000	0.23*p	35	**1.42**		**3.20**	
Mean - 1σ c_{col}	4,000	0.23*p	35	1.21	0.250	1.76	2.79
Mean + 1σ c_{col}	16,000	0.23*p	35	1.46		4.55	
Mean - 1σ c_{clay}	10,000	0.138*p	35	1.17	0.450	2.92	0.540
Mean + 1σ c_{clay}	10,000	0.322*p	35	1.62		3.46	
Mean - 1σ ϕ_{emb}	10,000	0.23*p	31.5	1.35	0.160	3.18	0.0400
Mean + 1σ ϕ_{emb}	10,000	0.23*p	38.5	1.51		3.22	
				σ_{FS} = 0.270		σ_{FS} = 1.421	
				V_{FS} = 0.190		V_{FS} = 0.444	
				β_F = 1.77		β_F = 2.53	
				p(f) = **0.038**		p(f) = **0.0057**	

Results for this embankment are summarized in Table 9-5, where it can be seen that limit equilibrium slope stability analyses indicate that the embankment has a high factor of safety and

a low probability of failure. However, the numerical stress-strain analyses indicate that the factor of safety is much lower and the probability of failure is much higher than the values determined from limit equilibrium analyses. This occurs because numerical analyses capture several real failure modes that are not disclosed by limit equilibrium analyses. The probability of failure according to the numerical stress-strain analyses is about 4 percent, which is a much higher value than would normally be considered acceptable.

Table 9-5. Results from edge stability analysis with isolated columns

Analysis	FS	p(f)
Limit Equilibrium	3.20	0.6%
Numerical	1.42	3.8%

9.3.4. Numerical Analyses of Slope Stability with Continuous Panels

It is common practice to overlap deep-mixed columns to form continuous panels under the side slopes of embankments where slope stability is a concern. A two-dimensional numerical analysis was performed on the example embankment with panels used under the side slope rather than isolated columns. The profile used in the analysis is shown in Figure 9-7. The plan view for the embankment is included as Figure 9-8, although it is recognized that the three-dimensional panel geometry cannot be completely accounted for in a two-dimensional analysis. Two-dimensional numerical analyses use average strength and modulus values based on an area replacement ratio to represent both the panels and the soil between panels under the embankment side slopes. The panel widths are selected to retain an area replacement ratio of 20% so that comparisons between the two cases can be made directly.
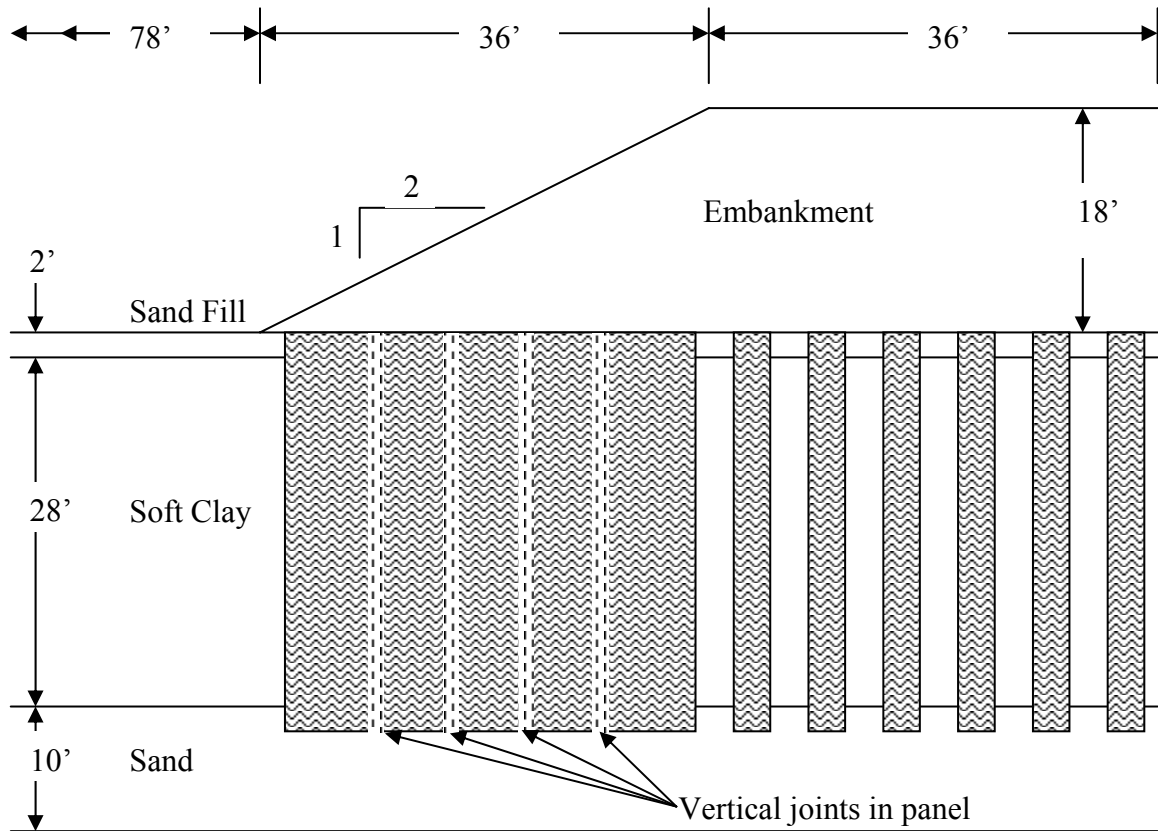
Figure 9-7. Profile view of model embankment with panels
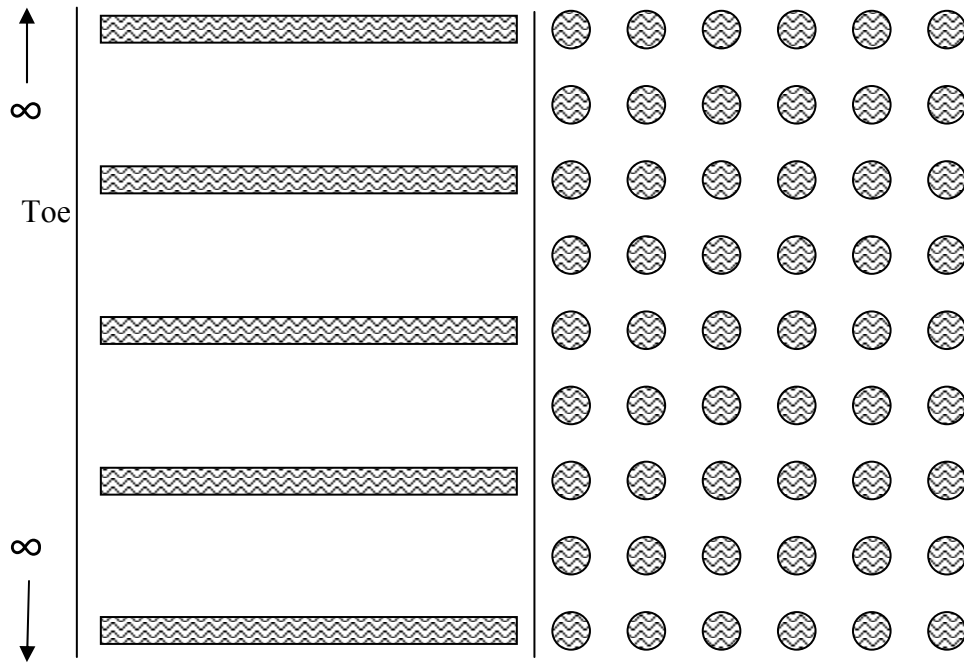
Figure 9-8. Plan view of panels under side slopes of embankment

The cohesion values used to represent panels and soil between panels in the numerical analyses are the same as the average cohesion values used for the limit equilibrium analyses, which are determined by Equation 9-3. In a similar manner, bulk and shear modulus values used to represent both panels and soil between panels are average values weighted by the area replacement ratio as shown in Equations 9-6 and 9-7.

$$K_{average} = K_{clay}(1\text{-}a_s) + K_{column}(a_s) \tag{9-6}$$

$$G_{average} = G_{clay}(1\text{-}a_s) + G_{column}(a_s) \tag{9-7}$$

where:

$K_{average}$ = the average bulk modulus value used for panels and soil between panels

K_{clay} = the clay bulk modulus value

K_{column} = the panel bulk modulus value

$G_{average}$ = the average shear modulus value used for panels and soil between panels

G_{clay} = the clay shear modulus value

G_{column} = the panel shear modulus value

In Japanese practice, where overlapping columns are used extensively, the CDIT (2002) recommends reducing column strength where columns overlap. Broms (2003) also recommends using reduced column strength in the areas where columns overlap. Vertical joints are included in the example embankment to represent areas where columns overlap as shown in Figure 9-6. These joints are assumed to have half the strength of the intact portions of the panel, which is in line with the recommendations in CDIT (2002) and Broms (2003).

Numerical reliability analyses of the cross-section shown in Figure 9-7 were performed using FLAC, and the results are shown in Table 9-6 and summarized in Table 9-7. The limit equilibrium analyses of slope stability with panels produce the same results as obtained previously with isolated columns reported in Table 9-4, and these results are repeated again in Tables 9-6 and 9-7 for convenience. The numerical analyses with continuous panels produce values for factor of safety that are much higher, and values for probability of failure that are much lower, than for isolated columns. Thus, the numerical analyses indicate that the

161

arrangement with panels beneath the side slopes of the embankment would be an acceptable design, whereas the arrangement with isolated columns beneath the side slopes would produce a probability of failure that is too high.

Table 9-6. Reliability calculations with panels

Case	c_{col} (psf)	c_{clay} (psf)	ϕ_{emb} (degrees)	FLAC		UTexas	
				FS	ΔFS	FS	ΔFS
Mean Values	10,000	0.23*p	35	**2.58**		**3.20**	
Mean - 1σ c_{col}	4,000	0.23*p	35	1.57	1.330	1.76	2.79
Mean + 1σ c_{col}	16,000	0.23*p	35	2.90		4.55	
Mean - 1σ c_{clay}	10,000	0.138*p	35	2.29	0.530	2.92	0.540
Mean + 1σ c_{clay}	10,000	0.322*p	35	2.82		3.46	
Mean - 1σ ϕ_{emb}	10,000	0.23*p	31.5	2.51	0.120	3.18	0.0400
Mean + 1σ ϕ_{emb}	10,000	0.23*p	38.5	2.63		3.22	
				σ_{FS} = 0.718		σ_{FS} = 1.421	
				V_{FS} = 0.278		V_{FS} = 0.444	
				β_F = 3.33		β_F = 2.53	
				p(f) = 0.00043		**p(f) = 0.0057**	

Table 9-7. Results from edge stability analysis with panels

Analysis	*FS*	*p(f)*
Limit Equilibrium	3.20	0.6%
Numerical	2.58	0.04%

9.3.5. Spatial variation incorporated into reliability analysis

Spatial variation is not included in the slope stability analyses presented in Sections 9.3.3 and 9.3.4. For the reliability analyses performed in those sections, it was assumed that deep-mixed strengths were completely correlated across the entire cross section of the embankment. The phrase "complete spatial correlation" is used here to refer to the analyses in Sections 9.3.3 and 9.3.4. The same types of reliability analyses performed in those sections were repeated, but with spatial variation included in the analyses, and the results are described in this section. The phrase "limited spatial correlation" is used here to refer to analyses that include spatial variation.

Spatial variation of column strengths can be incorporated into reliability analysis in the same manner that El-Ramly et al. (2002) incorporated spatial variation of clay strength in the James Bay Dike example. For this example, an autocorrelation distance of 36 feet is used, which is slightly smaller than the values of 40 to 60 feet for the case histories analyzed in Chapter 8. The strength of columns in the 36 feet under the side slope of the example embankment are treated as an independent variable from the strength of columns located within the 36 feet under the full height of the embankment. The reliability calculations for isolated columns with limited spatial correlation are shown in Table 9-8. The reliability calculations when panels are used beneath the side slopes with limited spatial correlation are shown in Table 9-9. The results from the eight cases investigated in Sections 9.3.1 through 9.3.5 are summarized in Table 9-10.

Table 9-8. Reliability calculations for isolated columns everywhere,
with limited spatial correlation

Case	Slope c_{col} (psf)	Center c_{col} (psf)	c_{clay} (psf)	ϕ_{emb} (degrees)	FLAC FS	FLAC ΔFS	UTexas FS	UTexas ΔFS
Mean Values	10,000	10,000	0.23·p	35	**1.42**		**3.20**	
Mean - 1σ c_{col}	4,000	10,000	0.23·p	35	1.24	0.210	1.97	2.01
Mean + 1σ c_{col}	16,000	10,000	0.23·p	35	1.45		3.98	
Mean - 1σ c_{col}	10,000	4,000	0.23·p	35	1.25	0.170	2.56	0.880
Mean + 1σ c_{col}	10,000	16,000	0.23·p	35	1.42		3.44	
Mean - 1σ c_{clay}	10,000	10,000	0.138·p	35	1.17	0.450	2.92	0.540
Mean + 1σ c_{clay}	10,000	10,000	0.322·p	35	1.62		3.46	
Mean - 1σ ϕ_{emb}	10,000	10,000	0.23*p	31.5	1.35	0.160	3.18	0.0400
Mean + 1σ ϕ_{emb}	10,000	10,000	0.23*p	38.5	1.51		3.22	

FLAC	UTexas
σ_{FS} = 0.274	σ_{FS} = 1.130
V_{FS} = 0.193	V_{FS} = 0.353
β_F = 1.74	β_F = 3.22
p(f) = 0.041	**p(f) = 0.00064**

Table 9-9. Reliability calculations for panels under the side slopes,
with limited spatial correlation

Case	Slope c_{col} (psf)	Center c_{col} (psf)	c_{clay} (psf)	ϕ_{emb} (degrees)	FLAC FS	FLAC ΔFS	UTexas FS	UTexas ΔFS
Mean Values	10,000	10,000	0.23·p	35	**2.58**		**3.20**	
Mean - 1σ c_{col}	4,000	10,000	0.23·p	35	1.72	1.130	1.97	2.01
Mean + 1σ c_{col}	16,000	10,000	0.23·p	35	2.85		3.98	
Mean - 1σ c_{col}	10,000	4,000	0.23·p	35	1.99	0.670	2.56	0.880
Mean + 1σ c_{col}	10,000	16,000	0.23·p	35	2.66		3.44	
Mean - 1σ c_{clay}	10,000	10,000	0.138·p	35	2.29	0.530	2.92	0.540
Mean + 1σ c_{clay}	10,000	10,000	0.322·p	35	2.82		3.46	
Mean - 1σ ϕ_{emb}	10,000	10,000	0.23*p	31.5	2.51	0.120	3.18	0.0400
Mean + 1σ ϕ_{emb}	10,000	10,000	0.23*p	38.5	2.63		3.22	

σ_{FS} = 0.711 σ_{FS} = 1.130

V_{FS} = 0.276 V_{FS} = 0.353

β_F = 3.37 β_F = 3.22

p(f) = 0.00038   **p(f) = 0.00064**

Table 9-10. Reliability analysis summary

Panels	Spatial Variation	FLAC FS	FLAC p(f)	Utexas FS	Utexas p(f)
no	no	1.42	3.8%	3.20	0.57%
no	yes	1.42	4.1%	3.20	0.064%
yes	no	2.58	0.043%	3.20	0.57%
yes	yes	2.58	0.038%	3.20	0.064%

The results in Table 9-10 show that including the effects of spatial variation in the analysis reduce the probability of failure when panels are used under the side slopes. Consequently, reliability analyses with panels can conservatively be performed by ignoring the effects of spatial variation. On the other hand, when isolated columns are used under the side slope of the embankment, the reliability analysis results based on numerical analyses show that including spatial variation increases the probability of failure for this example. This may be due to a progressive failure mechanism, or the relatively small increase in *p(f)* may be a result of the approximate nature of the Taylor Series method. Based on the results in Table 9-10, it may be slightly unconservative to ignore the effects of spatial variation in reliability analyses of an embankment supported on isolate columns under its full width.

9.4. Comparison between limit equilibrium method and numerical method of slope stability analysis for columns supported on deep-mixed columns

The columns used in the example problem in this chapter have an unconfined compressive strength of 139 psi, which is easily achievable using the wet method of deep mixing. With this strength, the factor-of-safety value computed using numerical analyses was much lower than with limit equilibrium analyses for the embankment supported everywhere on isolated columns. This indicates that numerical methods are needed, at least for strong columns, to perform meaningful stability analyses. For sufficiently low column strengths, it would be reasonable to presume that limit equilibrium analyses may give results similar to numerical analyses, because low strength columns would fail in shear before failing by tilting or bending.

To determine if such a threshold exists, the example embankment supported on isolated columns everywhere was re-analyzed with three changes: the first is that a clay layer thickness of 23 ft was used, the second is that the clay shear strength was set equal to 400 psf, and the third is that the column unconfined compressive strength was allowed to vary over the range from about 10 psi to 58 psi. The ratio of factor of safety from limit equilibrium analyses to factor of safety from numerical analyses, FS_{LE}/FS_{NM}, is plotted versus unconfined compressive strength, q_u, of the columns in Figure 9-9. It can be seen that the ratio of FS_{LE} to FS_{NM} diverges from unity at a q_u value of about 15 psi. This suggests that, for the conditions analyzed, limit equilibrium methods are suitable only for very low column strengths.

Han et al. (2005) performed FLAC plane-strain analyses for a 16.4 ft high embankment with a 2 horizontal to 1 vertical side slope. The embankment was founded on 32.8 ft of soft clay overlying 6.6 ft of firm soil. The soft clay was improved with 3.3 ft wide strips of deep-mixed columns at a replacement ratio of 40 percent. The deep-mixed column strips are located beneath the full width of the embankment and extend 8.2 ft beyond the toe. Strips extend from the ground surface down to 3.3 ft into the deeper firm soil. The soft clay and columns are assumed to be frictionless materials with cohesion values of 209 psf for the clay and with column strengths varied as shown in Figure 9-9. The embankment has a friction angle of 30 degrees with no cohesion. Figure 9-9 shows that the results of limit equilibrium analyses and numerical

analyses by Han et al. (2005) also show divergence at a column compressive strength of about 15 psi.
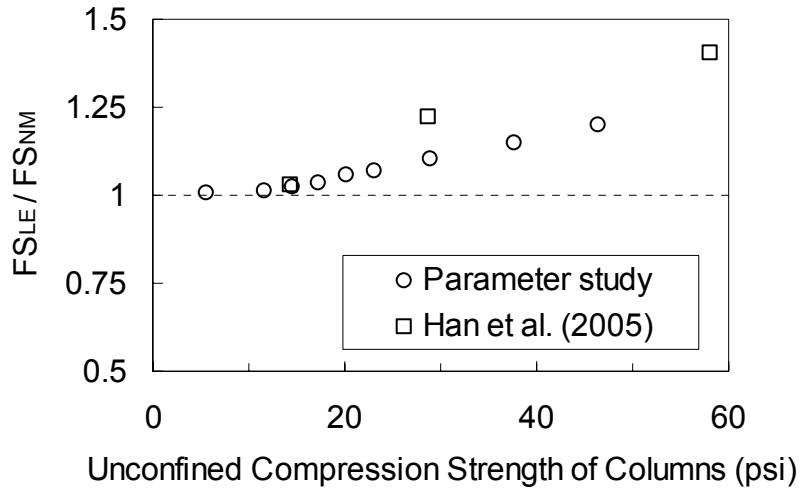
Figure 9-9. Comparison of limit equilibrium and numerical analyses of slope stability as a function of unconfined compressive strength of columns

9.5. Summary and Conclusions

The Taylor Series method for reliability analysis was described and then applied to an example embankment. Reliability analyses were performed for slope stability using limit equilibrium and numerical analyses. The probability of failure calculated by these analyses provides the designer with information that is not available by deterministic analyses. The calculated probability of failure can be used to help make design decisions regarding the area replacement ratio, mixture strength, and use of panels beneath side slopes.

Key findings include the following:

- The Taylor Series Analysis is a simple, straightforward method that can be used to evaluate the reliability of column-supported embankments.
- Limit equilibrium slope stability analyses do not capture some critical failure modes for embankments founded on soft soil improved with deep-mixed columns. Numerical analyses permit realistic failure modes, such as column bending and tilting, that the limit equilibrium analyses do not permit.

- For the embankment supported on isolated columns everywhere, the numerical analyses produce a much lower value of the factor of safety and a much higher value of probability of failure than produced by the limit equilibrium analyses.

- Spatial correlation can be incorporated into slope stability reliability analyses for column-supported embankments. Spatial variation of column strength reduced the probability of failure when the embankment side slopes are supported on panels, which suggests that spatial variation of column strength can be safely ignored in this case.

- Even though the factor of safety from the numerical analyses for the embankment supported everywhere on isolated columns is within the range normally considered acceptable for many roadway embankments, i.e., 1.4, the probability of failure is unacceptably high, i.e., 3.8%. This demonstrates that customary values of the factor of safety are not applicable to complex systems like column-supported embankments that incorporate materials with high inherent variability and the potential for brittle failure in tension.

- For the embankment supported on panels under the side slopes, the values of factor of safety are high and the probability of failure is low for both limit equilibrium analyses and numerical stress-strain analyses.

- The limit equilibrium analyses do not distinguish between isolated columns and continuous panels under the side slopes.

- The numerical analyses demonstrate the value of continuous panels under the side slopes. Compared to isolated columns, continuous panels at the same area replacement ratio produce higher values of factor of safety and greatly reduced values of probability of failure.

- Numerical analyses determine a lower factor of safety than limit equilibrium analyses for embankments that are supported on isolated columns with unconfined compressive strength greater than about 15 psi.

10. RECOMMENDATIONS FOR ANALYSIS AND DESIGN

10.1. Introduction

An important objective of this research was to develop recommendations that employ limit equilibrium methods to the greatest extent possible because they are easy to use and familiar to all geotechnical engineers. For embankments founded on piles and stone columns, limit equilibrium procedures are described in the published literature, and these are summarized in Appendices A and B. For embankments supported on columns installed by the deep mixing method, limit equilibrium procedures can be used for low strength columns, but numerical analyses of stability are necessary for high strength columns. This chapter provides recommendations for stability analysis and design of embankments supported on deep-mixing-method columns, including: selection of column property values for design, analysis methods, and strength specifications for construction contracts. An example is provided to illustrate the recommendations.

10.2. Property values of deep-mixed materials

The engineering properties of soils stabilized by the deep mixing method are influenced by many factors including the water, clay, and organic contents of the soil; the type, proportions, and amount of binder materials; installation mixing process; installation sequence and geometry; effective in-situ curing stress; curing temperature; curing time; and loading conditions. Given all the factors that affect the strength of treated soils, the Japanese Coastal Development Institute of Technology (CDIT 2002) states that it is not possible to predict within a reasonable level of accuracy the strength that will result from adding a particular amount of reagent to a given soil, based on the in-situ characteristics of the soil. Consequently, mix design studies must be performed using soils obtained from a project site. Laboratory preparation and testing of specimens is discussed by Jacobson et al. (2005) for the dry method and by Filz et al. (2005) for the wet method. Even relatively modest variations in binder materials may result in greatly different properties of the mixture. Furthermore, engineering properties of mixtures are time dependent, due to long-term pozzolanic processes that occur when mixing cement or lime with soil. Design is generally based on the 28-day strength of the mixture.

Laboratory mixing is often more complete than field mixing, and the strength of laboratory mixed specimens can be greater than the strength of field mixed materials at the same mixture proportions. According to EuroSoilStab (2002), the strength of field mixed materials may be 20 to 50 percent of the strength of laboratory mixed specimens, and according to CDIT (2002), the strength of field mixed materials may be 20 to 100 percent of the strength of laboratory mixed specimens. The percentage depends on the type and operation of the mixing equipment, as well as the soil type and curing conditions.

Most strength and stiffness information about deep mixed materials comes from unconfined compression tests. Numerous studies (e.g., Takenaka and Takenaka 1995, Dong et al. 1996, Bruce 2000, CDIT 2002, Matsuo 2002, Miura et al. 2002, EuroSoilStab 2002, Hayashi 2003, Shiells et al. 2003, Filz et al. 2005, Jacobson et al. 2005) show that the unconfined compressive strength of deep mixed materials increases with increasing stabilizer content, increasing mixing efficiency, increasing curing time, increasing curing temperature, decreasing water content of the mixture, and decreasing organic content of the base soil. One interesting interaction of these factors is that increasing the water content of the mixture can increase mixing efficiency, so that in the case of low-water-content clays, adding water to the mixture can increase the mixture strength (McGinn and O'Rourke 2003). Nevertheless, it remains true that, for thoroughly mixed materials, a decrease in the water-to-cement ratio of the mixture produces an increase in the unconfined compressive strength.

For soils treated by the dry method of deep mixing, values of unconfined compressive strength may range from about 2 to 400 psi, and for soils treated by the wet method of deep mixing, values of the unconfined compressive strength may range from about 20 to 4,000 psi (Japanese Geotechnical Society 2000, Baker 2000, Jacobson et al. 2003). The specified unconfined compression strengths for three recent deep mixing projects in the U.S. are as follows: at the Oakland Airport project, the minimum and average 28-day strengths were specified to be 100 and 150 psi, respectively (Yang et al. 2001); at the I-95/Route 1 interchange project, the minimum and average 28-day strengths were specified to be 100 and 160 psi, respectively (Lambrechts et al. 2003, Shiells et al. 2003); at the Boston Central Artery project, the minimum

and maximum 56-day strengths were specified to be 300 and 1000 psi, respectively (Lambrechts et al. 1998, McGinn and O'Rourke 2003).

During the design phase, designers should speak with deep-mixing contractors to get an idea of (1) the range of amendment dose rates that can be achieved with available construction equipment at a reasonable cost and (2) the relationship between the strength of laboratory mixed specimens and field mixed materials for soil conditions similar to those at the project site. Based on this information, the results of a laboratory mixing study, and the ranges mentioned above from EuroSoilStab (2002) and CDIT (2002), a range of realistic field strengths can be established.

Stabilized soils tested in triaxial conditions experience a decrease in strength once the strain at peak strength is exceeded (Kivelo 1998). Although soil-cement mixtures are typically brittle in unconfined compression tests, the residual strength of soil-cement under even low confining pressures is 65% to 90% of the unconfined compressive strength (Tatsuoka and Kobayashi 1983, CDIT 2002). Kitazume et al. (2000) used a residual compressive strength value equal to 80% of the unconfined compressive strength in limit equilibrium analyses of their centrifuge test results. The residual strength of deep-mixed materials can be used in slope stability analyses to provide safety against progressive failure effects.

There are differences of opinion regarding the most appropriate strength envelope for deep-mixed materials for use in stability analyses of column-supported embankments. Terashi (2005) indicated that the state of practice in Japan is to use a total stress, $\phi = 0$ and $c = \frac{1}{2} q_u$ envelope for deep-mixed material. Broms (2003) mentions use of total stress friction angles in the range of 25 to 30 degrees for deep-mixed materials. EuroSoilStab (2002), and Calsten and Ekstrom (1997) utilize a drained, effective stress friction angle of 30 degrees with a range of values for the cohesion intercept depending on the location of the failure surface. EuroSoilStab (2002) states that, for the dry methods of deep mixing, columns should not be used to resist tensile stresses. Terashi et al. (1980), Brandl (1981), Tanaka et al. (1986), and Takenaka and Takenaka (1995) report that the tensile strength of soil improved by the wet method is 10% to 20% of the unconfined compressive strength. Kitazume et al. (1996) reports that a value of 15% is used in

170

Japan with wet mix methods. Because there is not yet widespread agreement on strength characterization of these materials, a reasonable but conservative strength envelope should be used for design. The author's recommendations for a suitable strength envelope for deep-mixed materials for stability analysis are that (1) the total stress friction angle should be set equal to zero, (2) the total stress cohesion should be set equal to 40 percent of the unconfined compression strength to account for the reduction from peak strength to residual strength, and (3) no tensile strength should be included.

Secant values of Young's modulus of elasticity at 50% of the unconfined compressive strength, E_{50}, have been related to the unconfined compressive strength, q_u. For the dry method of deep mixing, values of the ratio of E_{50} to q_u have been reported in the range from 50 to 250 (Baker 2000, Broms 2003, Jacobson et al. 2005). For the wet method of deep mixing, values of the ratio of E_{50} to q_u have been reported in the range from 75 to 1000 (Ou et al. 1996).

Reported values of Poisson's ratio for deep-mixed material range from 0.25 to 0.50 (CDIT 2002, McGinn and O'Rourke 2003, Terashi 2003, Porbaha et al. 2005).

The unit weight of soils treated by deep mixing is not greatly affected by the treatment process. For the dry method of deep mixing, Broms (2003) reports that the unit weight of stabilized organic soil with high initial water content can be greater than the unit weight of untreated soil and that the unit weights of inorganic soils are often reduced by dry mix stabilization. The Japanese CDIT (2002) reports that the total unit weight of the dry-mixed soil increases by about 3% to 15% above the unit weight of the untreated soil. CDM (1985) indicates that, for soils treated by the wet method of deep mixing, the change in unit weight is negligible. However, at the Boston Central Artery/Tunnel Project, McGinn and O'Rourke (2003) report that a significant decrease in unit weight occurred because the initial unit weight of the clay was relatively high and water was added to pre-condition the clay before mixing.

10.3. Analysis methods

The inherent variability in deep-mixed material requires that reliability analyses be performed to rationally develop cost-effective and reliable designs. Chapter 9 illustrates the use of reliability

analysis for embankments founded on deep-mixed columns. Values of the coefficient of variation, V, found in the literature for deep-mixed materials are included in Appendix D. The results from the nine sites studied in Chapter 8 showed that the value of V, after removing the systematic influences of age and water-to-cement ratio, ranged from 0.17 to 0.67 with an average of about 0.4. Based on the information in Appendix D and Chapter 8, it is recommended that values of V in the range from 0.4 to 0.7 for deep mixed materials can be used for reliability analysis. Typical values of V for strength parameters of other geotechnical materials can be found in the literature (Harr 1987, Duncan 2000).

For embankments supported on deep-mixing-method columns, if the column unconfined compression strength is less than 15 psi, which is rare in the U.S., the results in Chapter 9 indicate that reliability analyses can be based on limit equilibrium rather than numerical analysis. If the unconfined compression strength is more than 15 psi, the factor of safety computed with limit equilibrium is higher than the factor of safety computed with numerical analysis due to failure modes other than shear that can occur for these systems. For embankments founded on deep-mixed columns with typical column strengths used in the United States, the physical mechanics of the problem require that numerical analyses be performed using the procedures described in Chapter 7.

Table 9-1 provides the designer with typical values of the probability of failure, $p(f)$, used in practice. Acceptable values of $p(f)$ used in design of a particular project will depend on the consequences that could occur from failure, prevailing practice in the area, and the policies and objectives of the project owner. The designer must realize that, as demonstrated in Chapter 9, achieving suitably low values of $p(f)$ for these systems will require higher values of factor safety, when using mean parameter values, than are customarily used for design of embankments.

10.4. Specified strength requirements

The amount of improvement and the strength required from deep-mixed columns is determined in the design process. In the construction process, specifications and quality assurance (QA) procedures are written to ensure that deep-mixed columns installed in the field will fulfill the

design intent. Understanding the variability of deep-mixed materials provides a basis for developing appropriate contract specifications.

If design of an embankment supported on deep-mixing-method columns is based on reliability analyses, then the coefficient of variation used in the analyses can also be used to rationally establish the acceptance criteria for strength in the contract documents. Three strength values can be specified: the median value, the 90% value, and the minimum strength value.

The median value is the deep-mixing strength that should be exceeded by 50% of the samples tested in the construction process. Because the strength of deep-mixed materials is distributed lognormally, the median value is more appropriate for contract specifications than is the mean (average) value. The mean value may be higher than the median value due to a few very strong samples taken from columns in the field that are not representative of most columns at a site. Thus, it is recommended that the required median strength value in the specifications be based on the mean value used in reliability-based design.

The 90% value is the deep-mixing strength that should be exceeded by 90% of the samples tested. The 99% value is the deep-mixing strength that can be used as the minimum strength value for every sample tested. Figure 10-1 gives the 90% and 99% values as a percentage of the mean value, based on a lognormal distribution of strength.
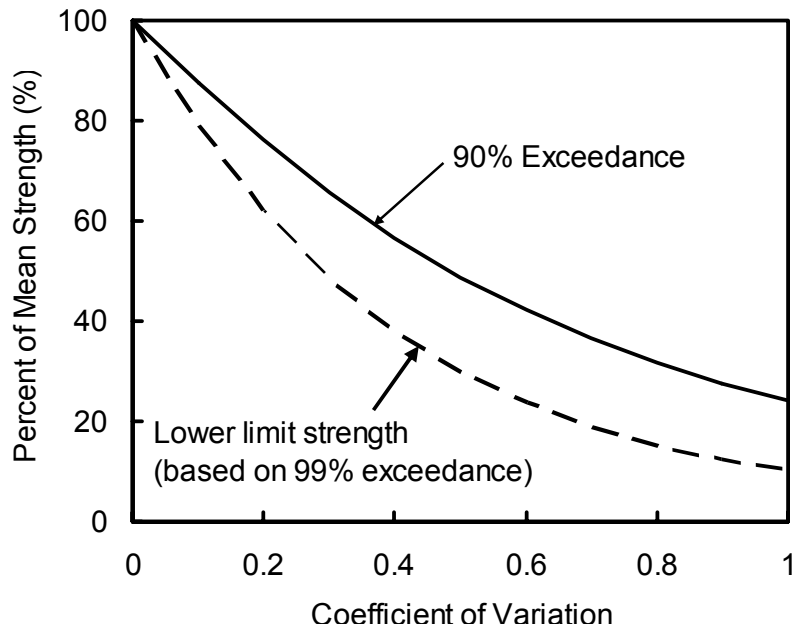
Figure 10-1. 90% strengths and lower limit strengths for use in reliability-based specifications

10.5. Example

The following example illustrates these recommendations. Based on a laboratory mixing program, combined with conversations with deep mixing contractors, and considering the ranges mentioned above from EuroSoilStab (2002) and CDIT (2002), it is determined that a median value of the unconfined compressive strength equal to 200 psi can be economically achieved for field mixed materials at a proposed construction site. Using this value, a total stress, residual strength envelope defined by a cohesion intercept of 80 psi and a friction angle of zero, with no tensile strength is established for use in design. A trial column layout is analyzed using the numerical analysis procedures described in Chapter 7 and the reliability analysis procedures described in Chapter 9 with a variation, V, of 0.6 for the deep-mixed material, and it is found that the probability of failure is at a satisfactorily low level.

The construction specifications are written to require that the median value of the unconfined compression strength tests equal or exceed 200 psi. According to Figure 10-1 for $V = 0.6$, the 90% strength value is equal to 42% of the mean value, and the lower limit strength value is equal to 24% of the mean value. Thus, the specifications would be written to require that at least 50% of the QA strength test results must meet or exceed 200 psi, at least 90% of the strength test

174

results must meet or exceed 84 psi, and all samples tested must exceed 48 psi. In the event that these criteria are not satisfied during construction, the specifications would require that additional suitable columns must be installed or other remedial measures approved by the engineer would be employed.

Specifications written in this fashion achieve the design intent without imposing excessively restrictive requirements on the minimum strength of the deep-mixed material.

11. SUMMARY AND CONCLUSIONS

This research shows that failure mechanisms like column tilting and bending can cause failure of column-supported embankments at lower load levels than would induce composite shearing through the columns and soft ground. Limit equilibrium methods, as currently employed in engineering practice, do not capture tilting and bending failure modes of strong columns. Consequently, such methods are not safe for analysis of embankments supported on strong columns when actual column strengths are used. Numerical analyses of slope stability are needed to capture the realistic failure modes that can control embankment performance and for which there is no practical alternative at present.

A related benefit of numerical analyses is that, if properly performed, they also capture the potential for block sliding and bearing capacity failure. Current practice is to perform separate analyses for these failure modes using approximate analytical models (e.g., CDIT 2002), as described in Appendix C. With properly conducted numerical analyses, a single analysis method can address all these aspects of system performance.

This research also shows that reliability analyses are a necessary component of design for embankments supported on columns installed by the deep mixing method. The strength of deep-mixed materials is quite variable, and reliability analyses permit this variability to be rationally incorporated in the design process. Furthermore, these systems are complex, and typical variations in clay strength, if not accounted for, could induce abrupt bending failure in isolated columns. Consequently, the ordinary values of factor of safety that geotechnical engineers use to develop reliable designs for other embankment systems are not applicable to embankments supported on columns installed by the deep mixing method. For instance, an example embankment supported on isolated columns was analyzed and found to have a factor of safety equal to 1.4. This value would be considered acceptable in many other situations, but reliability analyses showed that the embankment has a 4% probability of failure, which is excessively high for public transportation applications. This result demonstrates that typical values of the factor of safety are not adequate for judging acceptability of these systems, and reliability analyses are needed.

Another benefit of reliability analyses is that the value of the coefficient of variation of column strength that is used to analyze and design the embankments can also be used to write a statistically based specification. Such specifications have great potential to reduce construction disputes because they avoid specification of unrealistic minimum strengths while still fully meeting the design intent. Statistically based specifications should require that at least 50% of the quality assurance tests meet or exceed the mean strength used in reliability-based design. The specifications should also require that 90% of the quality assurance tests meet or exceed the strength value indicated in Figure 10-1. This 90% value depends on the mean strength value and the value of the coefficient of variation of strength used in reliability-based design of the embankment.

The numerical and reliability analysis procedures discussed in this report were applied to deep-mixing-method columns, but the procedures should also be relevant and applicable to vibro-concrete columns, which, like deep-mixing-method columns, have the characteristics of being much stronger than the surrounding soil and having low tensile capacity.

The following additional conclusions can be drawn from this research:
- The coefficient of variation of unconfined compressive strength for 13 data sets from nine deep-mixing projects in the U.S. range from 0.17 to 0.67 and average 0.40, after removing the variation due to controllable trends of age and water-to-cement ratio of the slurry.
- The autocorrelation distance ranged from 40 to 60 ft for three wet-mixing-method projects.
- The value of E_{50}/q_u is about 300 for soil-cement mixtures created by either the wet method or the dry method of deep mixing without lime.
- The Taylor Series Method is a simple method that can be used to evaluate the reliability of column-supported embankments.
- The numerical analysis procedures recommended in Chapter 7 have been successfully verified against the I-95/Route 1 case history and the two sets of centrifuge model tests.

177

- For embankments supported on deep-mixing-method columns, two-dimensional analyses produce about the same lateral deflections as three-dimensional analyses at the same area replacement ratio.

- Numerical analyses demonstrate the beneficial effects of continuous panels beneath the side slopes of embankments on stability.

It is recommended that engineers use the numerical stress-strain and reliability analysis procedures described in this report to evaluate the stability of embankments supported on columns installed by the deep mixing method. The procedures described in this research provide a rational basis for designing and specifying deep-mixed support of embankments. Many of the results would also be applicable to deep-mixed support of structures.

Although the results of this research represent a significant advancement that should be implemented in design practice immediately, much remains to be done to further advance deep-mixing technology. Specific items worthy of mention include the following:

- Characterize deep-mixed material behavior properly, including such important issues as (1) effective stress versus total stress characterization, (2) tensile strength, (3) ductility as a function of confining pressure, and (4) nonlinear stress-strain response.

- Establish relationships among (1) specimens mixed, cured, and tested in the laboratory; (2) specimens mixed and cured in the field, but tested in the laboratory; and (3) in-situ measures of column property values.

- Investigate the influence of geosynthetic reinforcement on stability of column-supported embankments.

- Evaluate the interaction of geosynthetic reinforcement used for stability with geosynthetic reinforcement used for vertical load transfer and differential settlement control.

12. ACKNOWLEDGEMENTS

13. REFERENCES

Aboshi, H., Ichimoto, E., Enoki, M., and Harada, K. (1979). "The "Compozer" - a method to improve characteristics of soft clays by inclusion of large diameter sand columns." Proceedings of International Conference on Soil Reinforcement, 211-216.

Ahnberg, H. (1996). "Stress dependent parameters of cement stabilised soil." Grouting and Deep Mixing, Proceedings of IS-Tokyo 96, 2nd International Conference on Ground Improvement Geosystems, 387-392.

Alamgir, M., Miura, N., Poorooshasb, H. B., and Madhav, M. R. (1996). "Deformation analysis of soft ground reinforced by columnar inclusions." Computer and Geotechnics , 18(4), 267-290.

Almeida, M. S. S., Davies, M. C. R., and Parry, R. H. G. (1985). "Centrifuge tests of embankments on strengthened and unstrengthened clay foundations." Géotechnique, 35 (4), 425-441.

Ang, A. and Tang, W. (1975). Probablility concepts in engineering planning and design: Volume I - basic principles, John Wiley and Sons, Inc., New York.

Asaoka, A., Kodaka, T., and Nozu, M. (1994). "Undrained shear strength of clay improved with compaction piles." Soils and Foundations, 34(4), 23-32.

Aubeny, C. P., Li, Y., and Briaud, J. L. (2002). "Geosynthetic reinforced pile supported embankments: numerical simulation and design needs." Proceedings, Geosynthetics - 7th ICG, Swets & Zeitlinger, Lisse, 365-368.

Bachus, R. C. and Barksdale, R. D. (1989). "Design methodology for foundations on stone columns." Foundation Engineering: Current Principles and Practices, ASCE GSP No. 22, 244-257.

Baecher, G. and Christian, J. (2003). Reliability and statistics in geotechnical engineering, Wiley, West Sussex.

Bai, X., Kim, Y. U., and Wang, M. C. (2001). "Load transfer behavior of soil-cement columns in soft ground." Foundations and Ground Improvement, Proceedings of Specialty Conference, 61-73.

Baker, S. (2000). "Deformation behaviour of lime/cement column stabilized clay." Chalmers University of Technology.

Baker, S. (1999). "Three dimensional consolidation settlement of stabilized soil using lime/cement columns." International Conference on Dry Mix Methods: Dry Mix Methods for Deep Soil Stabilization, 207-213.

Baker, R.F. and Yonder, E.J. (1972). "Stability analysis and density control works in landslides and engineering practice." E.B. Eckel, Ed., Highway Research Board Special Report 29, 189-216.

Balaam, N. P. and Booker, J. R. (1985). "Effect of stone columns yield on settlement of rigid foundations in stabilized clay." International Journal for Numerical and Analytical Methods in Geomechanics, 9(4), 331-351.

Barksdale, R. D. and Bachus, R. C. (1983). "Design and construction of stone columns, Volume 1." Federal Highway Administration, RD-83/026.

Barksdale, R. D. and Takefumi, T. (1991). "Design, construction and testing of sand compaction piles." Deep Foundation Improvements: Design, Construction, and Testing ASTM STP 1089, 4-18.

Brinch Hansen, J. (1961), "The ultimate resistance of rigid piles against transversal forces." Copenhagen, The Danish Geotechnical Institute, Bulletin No. 12.

British Standards Institution (1995). BS8006 Code of Practice for Strengthened/Reinforced Soils and Other Fills, BSI, London, U.K.

Broms, B. B. (2003). Royal Institute of Technology, Stockholm, Sweden.

Broms, B. B. (1999). "Keynote Lecture: Design of lime, lime/cement and cement columns." International Conference on Dry Mix Methods: Dry Mix Methods for Deep Soil Stabilization, 125-153.

Broms, B. B. (1999). "Progressive failure of lime, lime/cement and cement columns." International Conference on Dry Mix Methods: Dry Mix Methods for Deep Soil Stabilization, 177-184.

Broms, B. B. (1972). "Stabilization of slopes with piles." 1st International Symposium on Landslide Control, 115-123.

Broms, B. B. (1987). "Stabilization of soft clay in southeast Asia." Proceedings of the 5th International Geotechnical Seminar on Case Histories in Soft Clay, 163-198.

Broms, B.B. (1964) "Lateral resistance of piles in cohesive soils." Journal of Soil Mechanics and Foundation Division, ASCE, Vol. 90, 27-63

Broms, B. B. and Boman, P. (1979). "Stabilization of soil with lime columns." Ground Engineering, 12(4), 23-32.

Bruce, D. A. (2001). "An introduction to the deep mixing methods as used in geotechnical applications. Volume 3: The verification and properties of treated ground." Federal Highways Administration, FHWA-RD-99-167.

Burke, G. (2004). Personal communication.

CDIT (Coastal Development Institute of Technology) (2002). The Deep Mixing Method: Principle, Design and Construction, A.A. Balkema: The Netherlands.

CDM (Cement Deep Mixing) (1985). Design and Construction Manual for CDM Institute, Partial English Translation

D'Appolonia, D.J., D'Appolonia, E., and Brisette, R.F. (1970). "Settlement of Spread Footings on Sand", (closure), Proc. Journal of the Soil Mechanics and Foundations Division, 96(SM2), 754-761.

Dasenbrock, D. (2004). Personal communication.

DeBeer, E.E. and Wallays, M. (1970). "Stabilization of a slope in Schist by means of bored piles reinforced with steel beams." Proceedings of the 2nd International Congress on Rock Mechanics, Belgrade, Vol. 3, 361-369.

Dong, J., Hiroi, K., and Nakamura, K. (1996). "Experimental study on behavior of composite ground improved by deep mixing method under lateral load." Grouting and Deep Mixing, Proceedings of IS-Tokyo 96, 2nd International Conference on Ground Improvement Geosystems, Tokyo, 585-590.

Duncan, J. M. (2000). "Factors of safety and reliability in geotechnical engineering." Journal of Geotechnical and Geoenvironmental Engineering, 126(4), 307-316.

Duncan, J. M. and Wong, K. S. (1999). Center for Geotechnical Practice and Research, Blacksburg, VA.

Duncan, J. M. and Wright, S. G. (2005). Soil strength and slope stability., John Wiley & Sons, Inc., New Jersey.

Duncan, J. M. and Buchignani, A. L. (1976). "An Engineering Manual for Settlement Studies." Department of Civil Engineering, University of California.

Ekström, J. C., Berntsson, J. A., and Salfors, G. B. (1994). "Test fills of clays stabilized with cement columns." Proceedings, 13th International Conference on Soil Mechanics and Foundation Engineering, 1183-1186.

Enoki, M., Yagi, N., Yatabe, R., and Ichimoto, E. (1991). "Shearing characteristics of composite ground and its application to stability analysis." Deep Foundation Improvements: Design, Construction, and Testing, ASTM STP 1089, 19-31.

EuroSoilStab (2002). "Development of design and construction methods to stabilise soft organic soils." Design Guide Soft Soil Stabilization, CT97-0351, Project No.: BE 96-3177.

Fang, Y. S., Chung, Y. T., Yu, F. J., and Chen, T. J. (2001). "Properties of soil-cement stabilised with deep mixing method." Ground Improvement, 5(2), 69-74.

Farrar, J. (2004). Personal communication.

Filz, G. M., Hodges, D. E., Weatherby, D. E., and Marr, W. A. (2005). "Standardized Definitions and Laboratory Procedures for Soil-Cement Specimens Applicable to the Wet Method of Deep Mixing." *Innovations in Grouting and Soil Improvement*, Reston, Virginia , 13.

Filz, G. M. and Stewart, M. E. (2005) "Design of Bridging Layers in Geosynthetic-Reinforced, Column-Supported Embankments." Virginia Transportation Research Council, Charlottesville, VA

Forte, E. (2002). "Underpinning and Foundation Constructors, Inc." personal conversation.

Fukouka, M. (1977). "The effect of horizontal loads on piles due to landslides." Proceedings of Special Session 10, 9th International Conference of Soil Mechanics and Foundation Engineering, Tokyo.

Greenwood, D. A. (1991). "Load tests on stone columns." Deep Foundation Improvements: Design, Construction, and Testing, ASTM STP 1089, Esrig and Bachus, eds. (ASTM Philadelphia), 148-171.

Haley & Aldrich (2000). I-95/Route 1 Interchange, VDOT Project No. 0095-96A-106, PE-101.

Han, J. and Gabr, M. A. (2002). "Numerical analysis of geosynthetic-reinforced and pile-supported earth platforms over soft soil ." Journal of Geotechnical and Geoenvironmental Engineering, 128(1), 44-53.

Han, J., Huang, J., and Porbaha, A. (2005). "2D numerical modeling of a constructed geosynthetic-reinforced embankment over deep mixed columns." Geo-Frontiers 2005.

Hansbo, S. and Massarsch, K. R. (2005). "Standardisation of Deep Mixing Methods ." Deep Mixing '05: International conference on deep mixing best practice and recent advances.

Harr, M. (1987). Reliability-based design in civil engineering, McGraw-Hill, New York.

Hassiotis, S. and Chameau, J. L. (1984). "Stabilization of slopes using piles - final report." Rep. No. JHRP-84-8, Joint Highway Research Program.

Hayashi, H., Nishikawa, J., Ohishi, K., and Terashi, M. (2003). "Field observation of long-term strength of cement treated soil." Grouting and Ground Treatment, Proceedings of the 3rd International Conference, New Orleans, 598-609.

Hebib, S. and Farrell, E. R. (2000). "Laboratory determination of deformation and stiffness parameters of stabilized peat." Proceedings of the ASCE Geo-Institute Soft Ground Technology Conference, 182-193.

Holm, G. (2002). "Nordic Dry Deep Mixing Method Execution Procedure." Tokyo Workshop 2002 on Deep Mixing, Port and Airport Research Institute (CDIT), 102-109.

Honjo, Y. (1982). "A probabilistic approach to evaluate shear strength of heterogeneous stabilized ground by the deep mixing method." Soils and Foundations, 22(1), 23-38.

Hutchinson, J.H. (1977). "Assessment of the effectiveness of corrective measures in relation to geological conditions and types of soil movement." Bulletin of the International Association of Engineering Geology, No. 16, 131-155.

Ilander, A., Forsman, J., and Lahtinen, P. (1999). "Combined mass- and column stabilization in Kivikko test embankment - Designing by traditional and FE methods." International Conference on Dry Mix Methods: Dry Mix Methods for Deep Soil Stabilization, 185-191.

Inagaki, M., Abe, T., Yamamoto, M., Nozu, M., Yanagawa, Y., and Li, L. (2002). "Behavior of cement deep mixing columns under road embankment." Physical Modelling in Geotechnics: ICPMG '02, 967-972.

ITASCA (2002a). "Fast Lagrangian Analysis of Continua, FLAC^{2D}." Itasca Consulting Group, Ltd.

ITASCA (2002b). "Fast Lagrangian Analysis of Continua, FLAC^{3D}." Itasca Consulting Group, Ltd.

Ito, T. and Matsui, T. Methods to estimate lateral force acting on stabilizing piles. Japanese Society of Soil Mechanics and Foundation Engineering. Soils and Foundations 15[4], 43-59. 1975.

Jacobson, J. R., Filz, G. M., and Mitchell, J. K. (2003). Report prepared for the Virginia Transportation Research Council, Virginia Polytechnic Institute and State University.

Jacobson, J. R., Filz, G. M., and Mitchell, J. K. (2005). "Factors Affecting Strength of Lime-Cement Columns Based on a Laboratory Study of Three Organic Soils." Deep Mixing '05: International conference on deep mixing best practice and recent advances.

Jagannatha, R. P., Kumar, S., Yadav, O. P., and Singh, J. P. (1991). " Improvement of bearing capacity of soft marine clay using stone columns." Proceedings International Conference on Geotechnical for Coastal Development (GEO-COAST '91), 323-327.

Japanese Geotechnical Society (2000). "Standard practice for making and curing stabilized soil specimens without compaction (JGS 0821-2000)." Rep. No. Chapter 7 (in Japanese).

Jones, C. J. F. P., Lawson, C. R., and Ayres, D. J. (1990). "Geotextile reinforced piled embankments." Proceedings, 5th International Conference on Geotextiles, Geomembranes, and Related Products, 155-160.

Kaiqiu, L. (2000). "Behaviour of DCM Columns under Highway Embankment at Bridge Approaches.".

Karastanev, D., Kitazume, M., Miyajima, S., and Ikeda, T. (1997). "Bearing capacity of shallow foundation on column type DMM improved ground." Proceedings, 14th International Conference on Soil Mechanics and Foundation Engineering , 1621-1624.

Kawasaki, T., Niina, A., Saitoh, S., Suzuki, Y., and Honjyo, Y. (1981). "Deep mixing method using cement hardening agent." Proceedings of the 10th International Conference on Soil Mechanics and Foundation Engineering, Stockholm, 721-724.

Kempfert, H.-G., Stadel, M., and Zaeske, D. (1997). "Design of geosynthetic-reinforced bearing layers over piles." Bautechnik 74, Heft 12, 818-825.

Kempton, G., Russell, D., Pierpoint, N. D., and Jones, C. J. F. P. (1998). "Two- and three-dimensional numerical analysis of the performance of piled embankments." Proceedings, 6th International Conference on Geosynthetics, 767-772.

Kimura, T., Nakase, A., Saitoh, K., and Takemura, J. (1983). "Centrifuge test on sand compaction piles." Proceedings, 7th Asian Conference on Soil Mechanics and Foundation Engineering, 255-260.

Kitazume, M. and Karastanev, D. (1996). "Bearing capacity of improved ground with column type DMM." Grouting and Deep Mixing, Proceedings of IS-Tokyo 96, 2nd International Conference on Ground Improvement Geosystems.

Kitazume, M., Okano, K., and Miyajima, S. (2000). "Centrifuge model tests on failure envelope of column type deep mixing method improved ground." Soils and Foundations, 40(4), 43-55.

Kivelo, M. (1998). "Stabilization of embankments on soft soil with lime/cement columns ." Doctoral Thesis, Royal Institute of Technology.

Kivelo, M. and Broms, B. B. (1999). "Mechanical behaviour and shear resistance of lime/cement columns." International Conference on Dry Mix Methods: Dry Mix Methods for Deep Soil Stabilization, 193-200.

Lambrechts, J. R., Ganse, M. A., and Layhee, C. A. (2003). "Soil mixing to stabilize organic clay for I-95 widening, Alexandria, VA." Grouting and Ground Treatment, Proceedings of the 3rd International Conference, New Orleans, 575-585.

Lambrechts, J. R. and Layhee, C. A. (2003). "Stability analyses of deep soil mix buttresses in organic clay for I-95 widening, Alexandria, VA." Proceedings 12th Panamerican Conference on Soil Mechanics and Geotechnical Engineering, Essen, Germany, 2097-2104.

Lambrechts, J. R., Roy, P. A., and Wishart, E. (1998). "Design conditions and analysis methods for soil-cement in Fort Point Channel." Design and Construction of Earth Retaining Structures, Proceedings of Sessions of Geo-Congress '98, Reston, Virginia, 153-174.

Larsson, S. (2005). "On the use of CPT for quality assessment of lime-cement columns." Deep Mixing '05: International conference on deep mixing best practice and recent advances.

Long, P. D. and Bredenberg, H. (1999). "Deep excavations with soil stabilized by lime-cement columns: A parameter study using finite element analysis." International Conference on Dry Mix Methods: Dry Mix Methods for Deep Soil Stabilization, 201-206.

Matsuo, O. (2002). "Determination of design parameters for deep mixing." Tokyo Workshop 2002 on Deep Mixing, Coastal Development Institute of Technology, 75-79.

McGinn, A. J. and O'Rourke, T. D. (2003). "Performance of deep mixing methods at Fort Point Channel." Cornell University.

Mitchell, J.K., and Gardner, W.S. (1975). "In-situ measurement of volume change characteristics." State-of-the-art report. Proceedings of the Conference on In-situ Measurement of Soil Properties, Specialty conference of the Geotechnical Division, North Carolina State University, Raleigh, Vol II, 279-345.

Miura, N., Horpibulsuk, S., and Nagaraj, T. (2002). "Engineering behavior of cement stabilized clay at high water content." Soils and Foundations, 41(5), 33-45.
Notes: Jesse's Referenece

Miyake, M., Wada, M., and Satoh, T. (1991). "Deformation and strength of ground improved by cement treated soil columns." Proceedings International Conference on Geotechnical for Coastal Development (GEO-COAST '91), 369-380.

Nakanishi, M. (2002). "Execution and equipment of cement deep mixing (CDM) method." Tokyo Workshop 2002 on Deep Mixing, Port and Airport Research Institute (CDIT), 80-90.

Navin, M. P. and Filz, G. M. (2005a) "Stability of embankments founded on ground improved with deep mixed columns." Center for Geotechnical Practice and Research, Blacksburg, VA.

Navin, M. P. and Filz, G. M. (2005b) "Statistical Analysis of Strength Data from Ground Improved with DMM Columns." Deep Mixing '05: International conference on deep mixing best practice and recent advances

Okumura, T. (1996). "Deep mixing method of Japan." Grouting and Deep Mixing, Proceedings of IS-Tokyo 96, 2nd International Conference on Ground Improvement Geosystems, 879-887.

Ou, C. Y., Wu, T. S., and Hsieh, H. S. (1996). "Analysis of deep excavation with column type of ground improvement in soft clay." Journal of Geotechnical Engineering, 122(9), 709-716.

Pannatier, Y. (1996). Variowin: Software for Spatial Data Analysis in 2D, Springer-Verlag, New York.

Porbaha, A. (2001). "State of the art in construction aspects of deep mixing technology." Ground Improvement, 5(3), 123-138.

Porbaha, A. (1998). "State of the art in deep mixing technology; Part I. Basic concepts and overview." Ground Improvement, 2, 81-92.

Porbaha, A. (1998). "State of the art in deep mixing technology; Part II. Applications ." Ground Improvement, 2, 125-139.

Porbaha, A. (2000). "State of the art in deep mixing technology, Part IV. Design considerations." Ground Improvement, 3, 111-125.

Porbaha, A., Ghaheri, F., and Puppala, A. J. (2005). "Soil Cement Properties from Borehole Geophysics Correlated with Laboratory Tests." Deep Mixing '05: International conference on deep mixing best practice and recent advances.

Poulos, H. G. (2002). "Simplified design procedures for piled raft foundations." Deep Foundations 2002, 441-458.

Reese, L.C., Wang, S-T., and Fouse, J.L. (1992). "Use of drilled shafts in stabilizing a slope." Stability and Performance of Slopes and Embankments II, 1318-1332.

Roark, R.J., and Young, W.C. (1975) "Formulas for stress and strain." 5th edition, McGraw-Hill Book Company, New York, 624 pp.

Rogbeck, Y., Gustavsson, S., Sodergren, I., and Lindquist, D. (1998). "Reinforced piled embankments in Sweden - design aspects." Proceedings, Sixth International Conference on Geosynthetics, 755-762.

Russell, D. and Pierpoint, N. (1997). "An assessment of design methods for piled embankments." Ground Engineering, 30(11), 39-44.

Saye, S. R., Esrig, M. I., Williams, J. L., Pilz, J., and Bartlett, S. F. (2001). "Lime cement columns for the reconstruction of Interstate 15 in Salt Lake City, Utah." Foundations and Ground Improvement, Proceedings of Specialty Conference, 827-841.

Shiells, D. (2004). Personal communication.

Stocker, M. and Seidel, A. (2005). "Twenty-seven Years of Soil Mixing in Germany: The Bauer Mixed-in-Place-Technique." Deep Mixing '05: International conference on deep mixing best practice and recent advances.

Takemura, J., Tean, L. B., Suemasa, N., Hirooka, A., and Kimura, T. (1991). "Stability of soft clay improved with sand compaction piles under fill." Proceedings International Conference on Geotechnical Engineering for Coastal Development (GEO-COAST '91), Yokohama, 399-404.

Takemura, J., Watabe, Y., Suemasa, N., Hirooka, A., and Kimura, T. (1991). "Stability of soft clay improved with sand compaction piles." Proceeedings 9th Asian Regional Conference on Soil Mechanics and Foundation Engineering, 543-546.

Takenaka, D. and Takenaka, K. (1995). "Deep chemical mixing method - using cement as hardening agent." Takenaka Corporation, Tokyo.

Tatsuoka, F. and Kobayashi, A. (1983). "Triaxial strength characteristics of cement-treated soft clay." Proceedings of the 8th European Conference of SMFE, 421-426.

Terashi, M. (2003). "The state of practice in deep mixing methods." Grouting and Ground Treatment, Proceedings of the 3rd International Conference, New Orleans, 25-49.

Terashi, M. and Tanaka, H. (1983). "Settlement analysis for deep mixing method." Proceedings, 8th European Conference on Soil Mechanics and Foundation Engineering, 955-960. Reprint: <12 Reprint Status>

Terashi, M. (2002). "Development of deep mixing machine in Japan." Tokyo Workshop 2002 on Deep Mixing, Port and Airport Research Institute (CDIT), 317-325.

Ting, W. H., Chan, S. F., and Ooi, T. A. Design methodology and experiences with pile supported embankments. Development in Geotechnical Engineeering Balkema, Rotterdam, 419-432. 1994.

Unami, K. and Shima, M. (1996). "Deep mixing method at Ukishima site of the Trans-Tokyo Bay Highway." Grouting and Deep Mixing, Proceedings of IS-Tokyo 96, 2nd International Conference on Ground Improvement Geosystems, 777-782.

Viggiani, C. (1981). "Ultimate lateral load on piles used to stabilize landslides." Proceedings 10th international conference on Soil Mechanics and Foundation Engineering, 555-560.

Watabe, Y., Takemura, J., and Kimura, T. (1996). "Failure mechanism of clay deposits improved by SCP and pile foundations." Second International Conference on Soft Soil Engineering, Nanjing, 449-454.

Watn, A., Christensen, S., Emdal, A., and Nordal, S. (1999). "Lime cement stabilization of slopes - experiences and design approach." Dry Mix Method for Deep Soil Stabilization, Bredenberg, Holm & Broms (eds), 169-176.

Weatherby, D. (2004). Personal communication.

Wright, S. G. (1999). UTEXAS4: A Computer Program for Slope Stability Calculations, Shinoak Software, Austin.

Yang, D. S., Scheibel, L. L., Lobedan, F., and Nagata, C. (2001). "Oakland Airport Roadway Project." Soil Mixing Specialty Seminar, 26th DFI Annual Conference.

Yang, D. (2004). Personal communication.

Yasui, S., Yokozawa, K., Yasuoka, N., and Kondo, H. (2005). "Recent technical trends in Dry Mixing (DJM) in Japan." Deep Mixing '05: International conference on deep mixing best practice and recent advances.

APPENDIX A. STABILITY ANALYSIS OF EMBANKMENTS SUPPORTED ON DRIVEN PILES

According to Ting et al. (1994), piles in embankment support applications are designed to carry the full embankment load, and vertical piles are not designed to carry any lateral forces. The lateral resistance of piles beneath embankments is often low, especially in soft soils (Broms 1987). Current practice is to account for possible lateral spreading of the embankment and foundation with either battered piles near the edge of embankments as shown in Figure A-1, or a geosynthetic layer as shown in Figure A-2 (Jones et al. 1990).
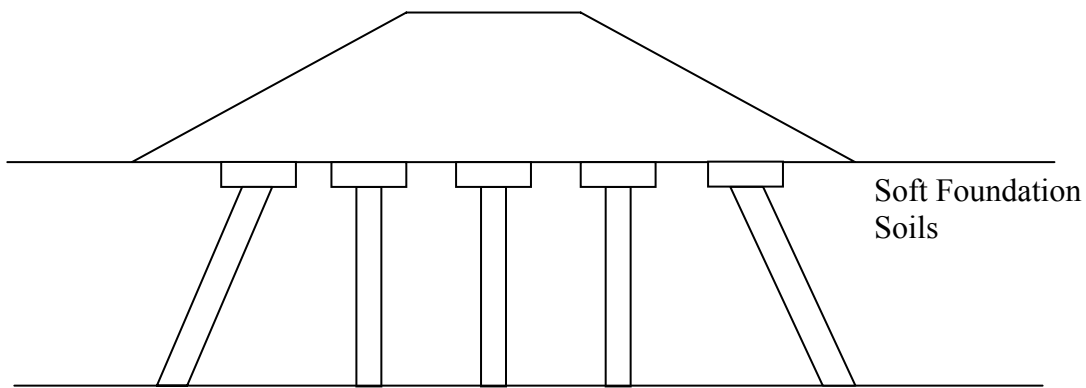

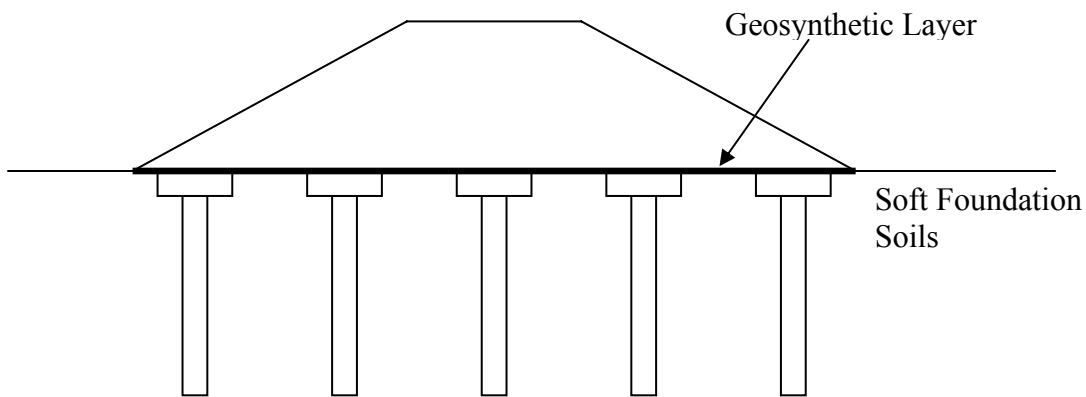Figure A-1. Pile-supported embankment with batter piles (after Jones et al. 1990)

Figure A-2. Pile-supported embankment with geosynthetic reinforcement (after Jones et al. 1990)

A bridging layer consisting of compacted granular soil is often used to distribute the vertical embankment load to piles. Geosynthetic reinforcement may be employed in the bridging layer to

enhance load transfer to the piles. Analysis and design of geosynthetic reinforcement for vertical load transfer in bridging layers is described in Filz and Stewart (2005). Geosynthetic reinforcement can also be used in the bridging layer to provide tensile capacity to stabilize the embankment side slopes. This tensile capacity can counteract the lateral spreading force that could otherwise cause slope stability problems, potentially eliminating the need for battered piles.

Stability analysis of pile-supported embankments with geosynthetic reinforcement can be performed according to the method in BS 8006 (1995). This method assumes a circular failure surface, and the analysis is performed as shown in Figure A-3.
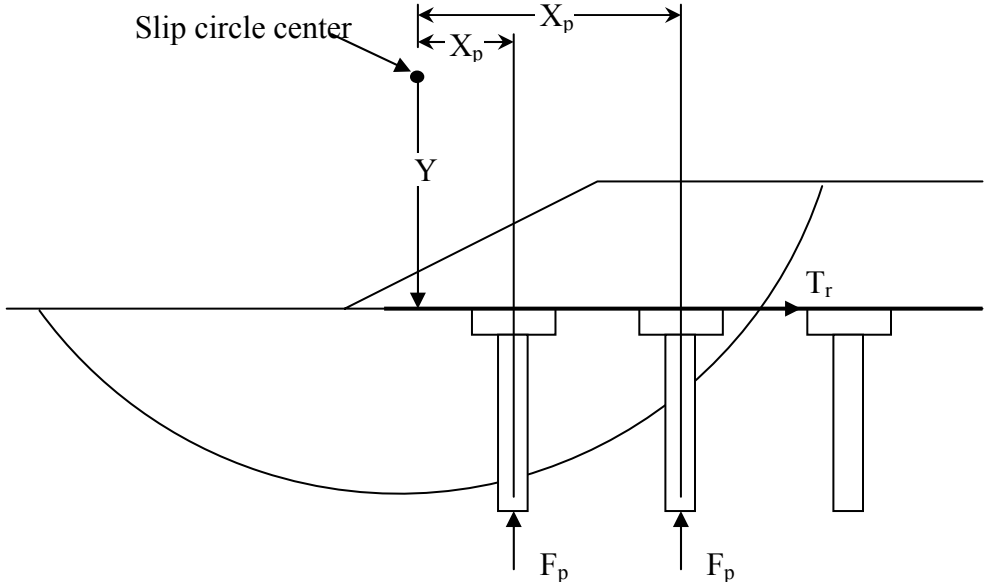
Figure A-3. Stability analysis of pile-supported embankments (after BS8006 1995)

The vertical forces in the piles, F_{P1}, F_{P2}, etc., are assumed to be equal to the embankment load over the tributary area associated with each pile. The restoring moment due to the pile forces, M_{RP}, is calculated from Equation A-1 based on the pile forces and the horizontal distance from the center of the slip circle to the piles, X_{P1}, X_{P2}, etc.

$$M_{RP} = F_{P1}X_{P1} + F_{P2}X_{P2}$$

(A-1)

The tension in the geosynthetic reinforcement due to lateral spreading of the embankment, T_r, is determined according to Equation A-2.

$$T_r = \frac{1}{2} K_a \gamma H^2 + q K_a H \tag{A-2}$$

where:

K_a = active earth pressure coefficient

γ = unit weight of the embankment material

H = full height of the embankment

q = surcharge pressure on the embankment surface

The geosynthetic reinforcement should be selected to safely carry the tension force, T_r, needed to provide slope stability. If geosynthetic reinforcement is also used to enhance vertical load transfer to the piles, then the required tensile capacity for vertical load transfer, T_v, should be added to T_r to obtain the total required tensile capacity, T, of the geosynthetic reinforcement. The geosynthetic reinforcement should be selected to provide an allowable tension capacity equal to or greater than T in the transverse direction and a tension capacity equal to or greater than T_v in the longitudinal direction of the embankment.

The restoring moment due to the tension in the geosynthetic reinforcement, M_{RR}, is calculated from Equation A-3.

$$M_{RR} = T_r Y \tag{A-3}$$

where:

Y = vertical distance from the center of the slip circle to the geosynthetic reinforcement.

The driving moment, M_D, and resisting moment, M_R, are calculated for the case without piles. The additional resisting moments due to piles, M_{RP}, and geosynthetic reinforcement, M_{RR}, are then added to M_D and M_R. The factor of safety, FS, of the improved ground is then calculated from Equation A-4.

$$FS = \frac{M_R + M_{RP} + M_{RR}}{M_D} \qquad (A\text{-}4)$$

If no geosynthetic reinforcement is used in the embankment, a horizontal force equal to the tension force computed in Equation A-2 should be provided by the axial component of battered piles, as shown in Figure A-1. Piles in soft ground under embankments should not be relied upon to carry lateral loads. In order to maintain stability during construction and prevent overstressing piles, Broms (1987) recommends that construction of embankments supported on inclined piles should start at the center of the embankment and proceed simultaneously towards both sides.

Ting (1994) states the Swedish State Road Department (1974) allows the safe structural load of piles in embankment support applications to be 1.5 times that commonly used for buildings.

APPENDIX B. STABILITY ANALYSIS OF EMBANKMENTS FOUNDED ON STONE COLUMNS

In stability analyses of embankments supported on stone columns, the failure mechanism that is typically assumed is a sliding failure surface that mobilizes the shear strength of the soil and the columns. Two of the three analysis methods described below seek to define an average shear strength that can be applied to the composite ground. The third method represents the soil and the stone columns by alternating vertical strips of material, but the shear surface passes through the columns and the soil, so that composite action is incorporated in this method also. Although composite shearing is the primary failure mode that is considered in slope stability analyses of embankments supported on stone columns, it is worthwhile recognizing that other failure modes can occur. For example, Bachus and Barksdale (1989) indicates that using composite strengths is inappropriate for area replacement ratios less than 20% because weak soils can flow around widely spaced columns.

The composite shear strength depends on the shear strength of the soil, the shear strength of the columns, and the area replacement ratio. The shear strength of the columns depends on the stress concentration ratio in the columns. According to Barksdale and Takefumi (1991), the stress concentration ratio equals one immediately after rapid loading and increases as consolidation occurs and load is shifted to the more rigid columns. The stress concentration that develops in the columns as the embankment settles increases the frictional shear resistance of the columns. Use of a bridging layer may increase the stress concentration both immediately following construction and after consolidation.

The methods presented herein consider the short-term, undrained condition for the soft clay between columns. This is considered to be the critical condition since the edge stability of the embankment should improve over time as consolidation occurs. All of the methods assume a long embankment that is reinforced with stone columns having constant diameter and spacing.

B.2. Circular Sliding Surface Method

The Circular Sliding Surface Method, or the Japanese Method, was developed for sand compaction piles, but it has also been applied to stone columns. The Circular Sliding Surface Method evaluates stability using circular failure surfaces and a composite shear strength. The assumed failure surface is illustrated in Figure B-1.
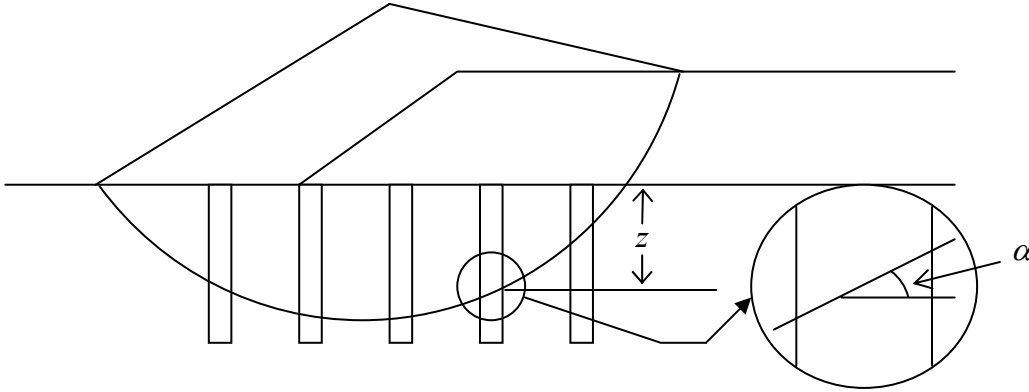

Figure B-1. Circular Sliding Surface Method for Granular Piles (after Aboshi et al. 1979)

The composite shear strength is determined based on a proportionate average of soil strength and stone column strength for a given area replacement ratio and stress concentration ratio (Aboshi et al. 1979). The composite shear strength at any point along the failure surface is obtained from Equation B-1. This equation uses undrained strengths for the soil and drained strengths for the column.

$$\tau = (1 - a_s)\left[c_u + (\gamma_{soil} z + \sigma \mu_{soil})\tan \phi_{soil} \cos^2 \alpha\right] + a_s (\gamma'_{col} z + \sigma \mu_{col})\tan \phi'_{col} \cos^2 \alpha \qquad \text{(B-1)}$$

where:

τ = composite shear strength along the sliding surface

a_s = area replacement ratio

c_u = undrained cohesion intercept of the soil

γ_{soil} = unit weight of the soil

z = distance from ground surface to failure surface

σ = average applied vertical stress from the embankment

194

μ_{soil} = ratio of stress change in the soil from the embankment load to the average applied vertical stress from the embankment

ϕ_{soil} = undrained friction angle of the soil = 0 for saturated clay in undrained loading

μ_{col} = ratio of stress change in the stone column from the embankment to the average applied vertical stress from the embankment

ϕ'_{col} = drained friction angle of the column

γ'_{col} = effective unit weight of the column

α = inclination of the failure surface, as shown in Figure B-1.

The composite shear strength determined from Equation B-1 is typically used in conjunction with the Fellenius method, which is also known as the Ordinary Method of Slices, to determine the stability of the stabilized ground (Enoki 1991).

B.3. Average Strength Parameter Method

Similar to the Circular Sliding Surface Method, the Average Strength Parameter Method determines composite shear strength parameters to evaluate stability (Goughnour 1991). The composite cohesion, or average cohesion, is determined based on the cohesion intercept of the soil and the area replacement ratio according to Equation B-2.

$$c_{av} = c_u \left(1 - a_s \right) \tag{B-2}$$

where c_{av} = average cohesion, c_u = cohesion intercept of the soil, and a_s = area replacement ratio.

The composite, or average, friction angle is determined as a weighted average between the friction angle of the soil and the friction angle of the stone columns, and it is influenced by the orientation of the assumed failure surface. The composite friction angle is determined by Equation B-3.

$$\tan \phi_{av} = \frac{\left(1 - a_s \right) \tan \phi_{soil} + S_r a_s \tan \phi_{col}}{1 + a_s \left(S_r - 1 \right)} \tag{B-3}$$

where ϕ_{av} = average friction angle, ϕ_{soil} = friction angle for the soil, ϕ_{col} = friction angle for the column, and S_r = stress ratio appropriate to the orientation of the failure surface at that location, which is determined by Equation B-4.

$$S_r = 1 + (n\text{-}1) \cdot \cos\alpha \qquad (\text{B-4})$$

where n = stress concentration ratio = the ratio of the vertical stress in the column to the vertical stress in the soil, and α = inclination of the assumed failure surface.

The composite, or average, unit weight is determined by Equation B-5.

$$\gamma_{av} = (1 - a_s)\gamma_{soil} + a_s\gamma_{col} \qquad (\text{B-5})$$

where γ_{av} = average unit weight, γ_{soil} = unit weight of the soil, and γ_{col} = unit weight of the column.

The average parameter values as determined by Equations B-2, B-3, and B-5 are then used to evaluate stability by means of existing slope stability analysis methods, such as Bishop's or Spencer's methods.

B.4. Profile Method

The Profile Method is recommended by Barksdale and Bachus (1983) for evaluating the stability of stabilized ground using computer programs for slope stability analysis. In the Profile Method, the stone columns are replaced by equivalent "strips" in profile and the composite foundation is simplified as a series of alternating strips of columns and native soil. For example, for the equilateral triangle arrangement of columns shown in Figure B-2, the column strips have a centerline-to-centerline distance of 0.866·s, where s = the center-to-center spacing of the columns. The width, w, of the strips in a two-dimensional representation may be calculated from Equation B-6.

$$w = 0.866 a_s s \qquad (\text{B-6})$$

where w = width of strips, a_s = replacement ratio, and s = column spacing.

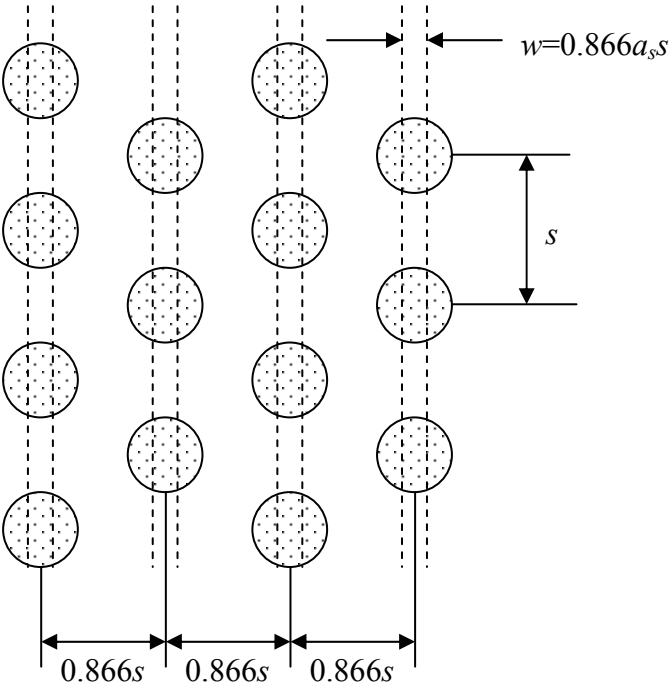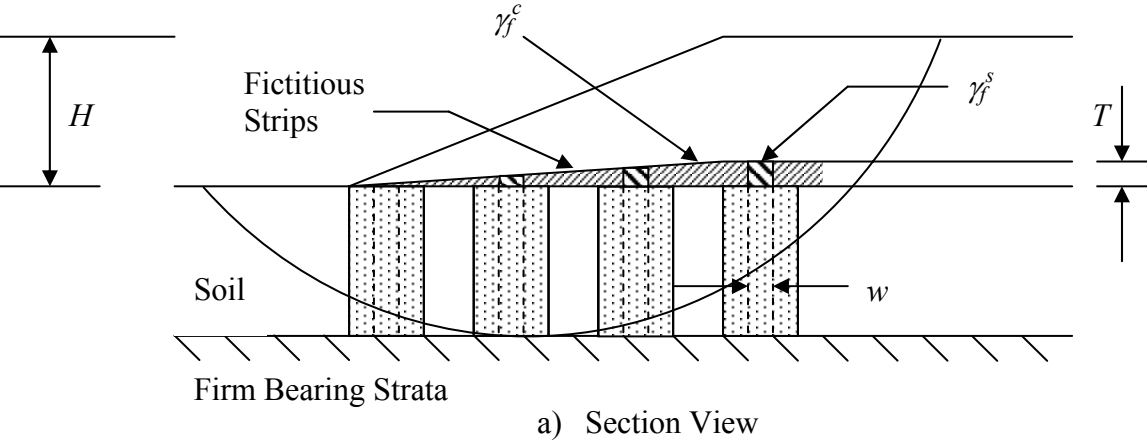a) Section View

b) Plan View

Figure B-2. Stone Column Strip Idealization (after Barksdale and Bachus 1983)

Within the computer model, a fictitious layer is placed at the interface between the embankment and the foundation to generate stress concentrations in the stone columns. The fictitious layer is

assigned no strength, and its thickness, *T*, should be as small as practical. Barksdale and Bachus (1983) recommend a constant thickness of 0.25 to 0.5 ft beneath the full height of embankment, with the thickness tapering to zero at the toe, as illustrated in Figure B-2. The layer should have a high unit weight in the areas above the stone column strips, and a negative unit weight over the soil strips. The unit weights in the fictitious layer are calculated based on the layer thickness, the stress ratios, and the embankment loading to give the correct load in the columns and the surrounding soil. Equations B-7 and B-8 are used to determine the unit weights for the fictitious layer (Barksdale and Bachus 1983):

$$\gamma_f^{col} = \frac{(\mu_{col} - 1)\gamma_1 H}{T} \tag{B-7}$$

$$\gamma_f^{soil} = \frac{(\mu_{soil} - 1)\gamma_1 H}{T} \tag{B-8}$$

where:

γ_f^{col} = unit weight of the fictitious layer above the stone column

γ_f^{soil} = unit weight of the fictitious layer above the soil

γ_1 = unit weight of the embankment

H = height of the embankment at that location

B.5. Comparison of Stability Analysis Methods

The Profile Method is an adaptation of the Circular Sliding Surface Method for use with a computer program for slope stability analysis. For any value of stress concentration ratio, the Circular Sliding Surface Method and the Profile Method give the same result when using the Ordinary Method of Slices (OMS). The Circular Sliding Surface Method of analysis is commonly used in conjunction with OMS to model the composite soil in Japan (Enoki 1991).

The Average Parameter Method is difficult to use with a computer program for slope stability analysis because the average friction angle changes with inclination of the failure surface.

A computational difference between the Circular Sliding Surface Method and the Average Parameter Method relates to the effect of the stress concentration ratio, n. For the Circular Sliding Surface Method, stress concentration in the columns only pertains to the embankment loading. For the Average Parameter Method, stress concentration in the columns pertains to both the embankment loading and the weight of the foundation soils above the sliding surface.

According to Barksdale and Takefumi (1990), the stress concentration ratio equals one immediately after rapid loading, and it increases as consolidation occurs. For a stress concentration ratio of one, the Average Parameter Method gives approximately the same result as the other two methods when OMS is used. The only difference, in this situation, is that shear strength of the soil and the stone columns is calculated based on an average unit weight of the foundation for the Average Parameter Method, and the shear strengths are based on the separate unit weights of the soil and the stone columns for the Circular Sliding Surface Method and the Profile Method.

The authors of this report recommend that the Profile Method be used with a computer program for slope stability analysis of embankments supported on stone columns. This permits easy searching for the critical failure surface. For stone columns installed in soft ground, it is most conservative to use a value of the stress concentration ratio, n, equal to one, which corresponds to $\mu_{soil} = \mu_{col} =$ unity. However, even with rapidly applied embankment loads, the stress concentration ratio is very likely greater than one because the drainage path length for consolidation of the near surface soils is short, which means that some consolidation and stress concentration onto the columns will occur during embankment construction. For values of n greater than one, the corresponding values of μ_{soil} and μ_{col} can be determined from Equations B-9 and B-10.

$$\mu_{soil} = \frac{1}{1+(n-1)a_s} \tag{B-9}$$

$$\mu_{col} = \frac{n}{1+(n-1)a_s} \tag{B-10}$$

APPENDIX C. STABILITY ANALYSIS OF EMBANKMENTS FOUNDED ON DEEP-MIXING-METHOD COLUMNS: SCANDINAVIAN AND JAPANESE PROCEDURES

C.1. Introduction

This appendix presents the procedures used in Scandinavia and Japan for analysis and design of embankments supported on deep-mixed columns. This appendix is included to provide useful background information, but it is recommended that the numerical and reliability analysis procedures described in the main body of this dissertation be used in practice because they more accurately represent the behavior of these complex systems.

Section C.2 covers aspects of analysis and design of embankments founded on deep-mixed columns that are common to both Scandinavia and Japan. Section C.3 presents the methodology used in Scandinavia, where most experience is with the dry method of deep mixing. Section C.4 presents the methodology used in Japan, where the wet method of deep mixing is used extensively.

C.2. Analysis and design approach common to both Scandinavia and Japan

A circular shear surface is analyzed as shown in Figure C-1, with Equation C-1 used to determine the total undrained shear resistance along the assumed failure plane. The undrained shear strength, τ_u, is then used in conjunction with common slope stability analyses to determine the stability of the embankment on improved soil.

$$\tau_u = \tau_{u,col} a_s + \tau_{u,soil}(1 - a_s) \qquad \text{(C-1a)}$$

$$\tau_{u,col} = c_{u,col} + \sigma_n \tan \varphi_{u,col} \qquad \text{(C-1b)}$$

$$\tau_{u,soil} = c_{u,soil} + \sigma_n \tan \varphi_{u,soil} \qquad \text{(C-1c)}$$

where:

τ_u = composite undrained shear strength along the sliding surface

$\tau_{u,col}$ = undrained shear strength of the column

a_s = area replacement ratio

$\tau_{u,soil}$ = undrained shear strength of the soil

σ_n = total normal stress on the failure plane

$c_{u,col}$ = undrained total stress cohesion intercept for column

$\phi_{u,col}$ = undrained total stress friction angle for column

$c_{u,soil}$ = undrained total stress cohesion intercept for soil

$\phi_{u,soil}$ = undrained total stress friction angle for soil
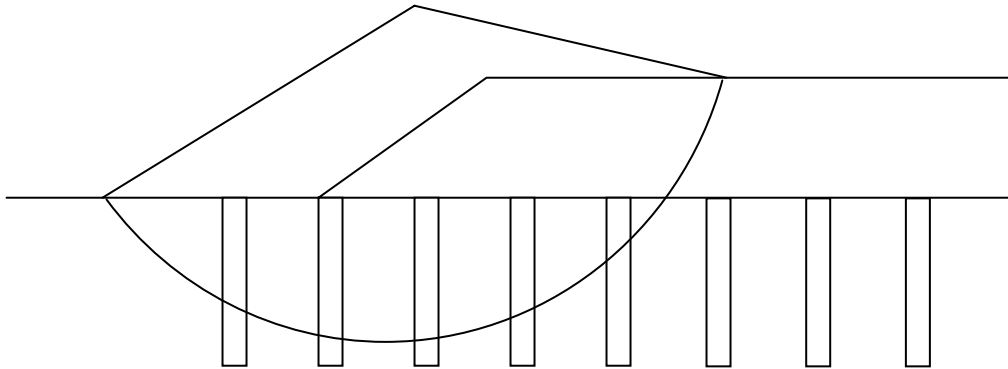

Figure C-1. Circular sliding surface (after Broms and Boman 1979)

If $\phi_{u,soil} = \phi_{u,column} = 0$, as commonly used by many practitioners and researchers for deep-mixing-method columns in starated soft clays, then $\tau_{u,soil}$ is equal to $c_{u,soil}$, and $\tau_{u,col}$ is equal to $c_{u,col}$. When these simplifications are made, the equation for undrained shear strength of ground improved with columns takes the form of Equation C-1d (Wei et al. 1990).

$$\tau_u = c_{u,col}a_s + c_{u,soil}\left(1 - a_s\right)$$ (C-1d)

Typically an undrained shear strength, $\tau_{u,col}$, equal to one half of the unconfined compression strength, $q_{u,col}$ has been used with deep-mixing-method columns. The designer should be aware of column strengths that have been used in practice. Unconfined compression strength values that have been used for projects in the United States are listed in Table D-2. When selecting column strengths, the strength used in design should be lower than the strength determined in the lab from mixed samples. The quality of mixing is generally lower in the field than can be obtained in the lab, and CDIT (2002) states that a correction factor ranging from 0.5 to 1 has been used in the past.

In stability analyses, it may be necessary to use a residual strength, particularly when including the full strength of the soil, which reaches peak strength at strains considerably greater than does soil-cement. Stabilized soils tested in triaxial conditions experience some definite decrease in strength once the peak strength is exceeded (Kivelo 1998). The peak column strength is typically reached at strains of 1% to 2%. Strains for some organic soil and plastic and sensitive clays may exceed 10% to 20% before reaching their peak strength (Ahnberg 1996). However, as strain continues, all column strength is not lost, but goes to a lower residual value. Soil-cement is very brittle in unconfined compression tests, but under even low confining pressures, the residual strength of soil-cement is 65% to 90% of the unconfined compressive strength (Tatsuoka and Kobayashi 1983, CDIT 2002). Kitazume et al. (2000) use a residual column strength value of 80% in analyses of their centrifuge test results.

Several constraints are placed on limit equilibrium, slope stability analyses of embankments founded on deep-mixed columns. These constraints are summarized in Table 2-1 in the main text of this dissertation, and discussed in the following two sections.

C.3. Analysis and design procedures used in Japan

In the method used in Japan, a factor, η, is applied to account for the difference in strain at failure between the comparatively stiff columns and the soft surrounding soil (Kaiqui, 2000). The basis for evaluating η is shown in Figure C-2.
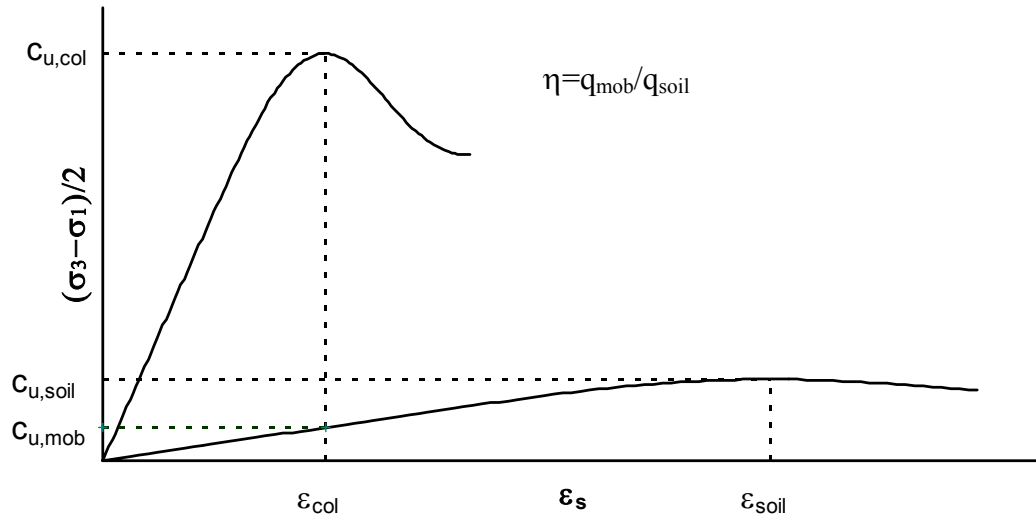
Figure C-2. Mobilized shear strength of stabilized soil (CDIT 2002)

When the reduced soil strength is taken into account, the composite undrained shear strength of ground improved with soil-cement columns takes the form of Equation C-1e (Kaiqiu 2000).

$$\tau_u = c_{u,col} a_s + \eta c_{u,soil} \left(1 - a_s\right)$$
(C-1e)

Tatsuoka et al. (1983) conducted a series of triaxial compression tests and proposed that the residual strength of columns should be used in the slip circle analysis instead of the peak strength. Tatsuoka et al. (1983) suggest residual column strengths are 80% of peak strength values.

The Coastal Development Institute of Technology in Japan (CDIT 2002) developed a flowchart for the design of isolated deep-mixing-method columns. The portion of the flowchart related to embankment stability is shown in Figure C-3. This flowchart uses an iterative procedure to design isolated columns with respect to slope stability. Concurrent with the slope stability analysis is a study of lateral displacement, which includes a finite element analysis and an investigation of sliding stability.
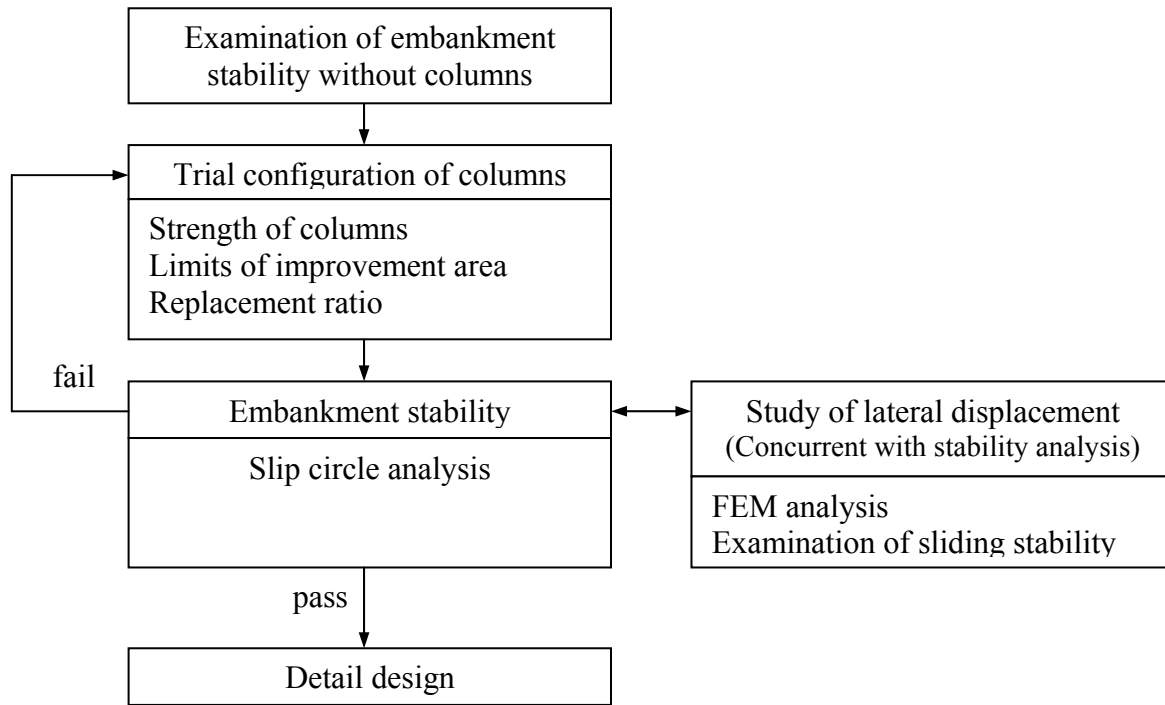
Figure C-3. Flowchart for design of isolated "group" columns

(adapted from CDIT 2002)

CDIT (2002) provides a simple method for sliding stability analysis using Equation C-2 and Figure C-4.

$$FS_S = \frac{Pp_S + F_R}{Pa_E + Pa_S} = \frac{Pp_S + (W_E + W_I)\tan\varphi'}{Pa_E + Pa_S} \qquad (C-2)$$

where:

F_R = shear strength acting on the bottom of the improved ground

FS_S = safety factor against sliding failure

Pa_E = active earth pressure of embankment

Pa_S = active earth pressure of soft ground

Pp_S = passive earth pressure of soft ground

W_E = weight of embankment

W_I = weight of improved ground

ϕ' = internal friction angle of stiff ground underlying columns
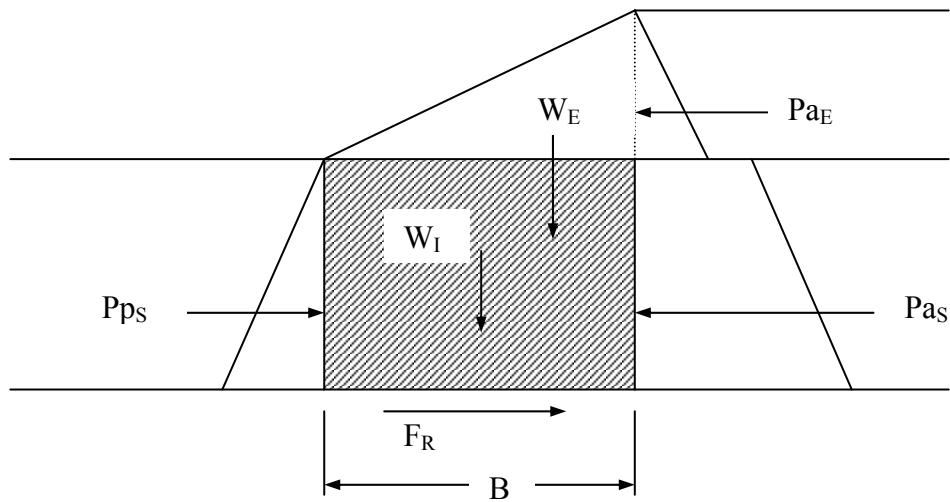
204

Figure C-4. Sliding failure analysis (CDIT 2002)

In a conversation with Terashi (2002), he noted that, while the CDIT (1999) does not prohibit the use of isolated deep-mixing-method columns for slope stabilization, the design engineer is responsible for ensuring that failure modes other than shear failure do not occur. CDIT (2002) notes that block, wall, or grid type improvements are frequently used for permanent structures because systems of isolated soil-cement columns may fail progressively by bending as a result of the low tensile and bending strength of the columns.

A design flowchart for walls, grids or blocks of deep-mixing-method columns is also given by CDIT (2002), as shown in Figure C-5. Walls, grids, and blocks are analyzed for overturning and bearing capacity analogous to gravity structures, in addition to performing the analyses described previously for isolated columns.

Examination of embankment stability without columns

Trial configuration of columns

Trial replacement ratio

External stability analysis
Calculation of weight and external forces acting on improved soil mass
1. sliding
2. over-turning
3. bearing capacity

Internal stability analysis
1. toe pressures
2. shear stress analysis
3. extrusion of untreated soil
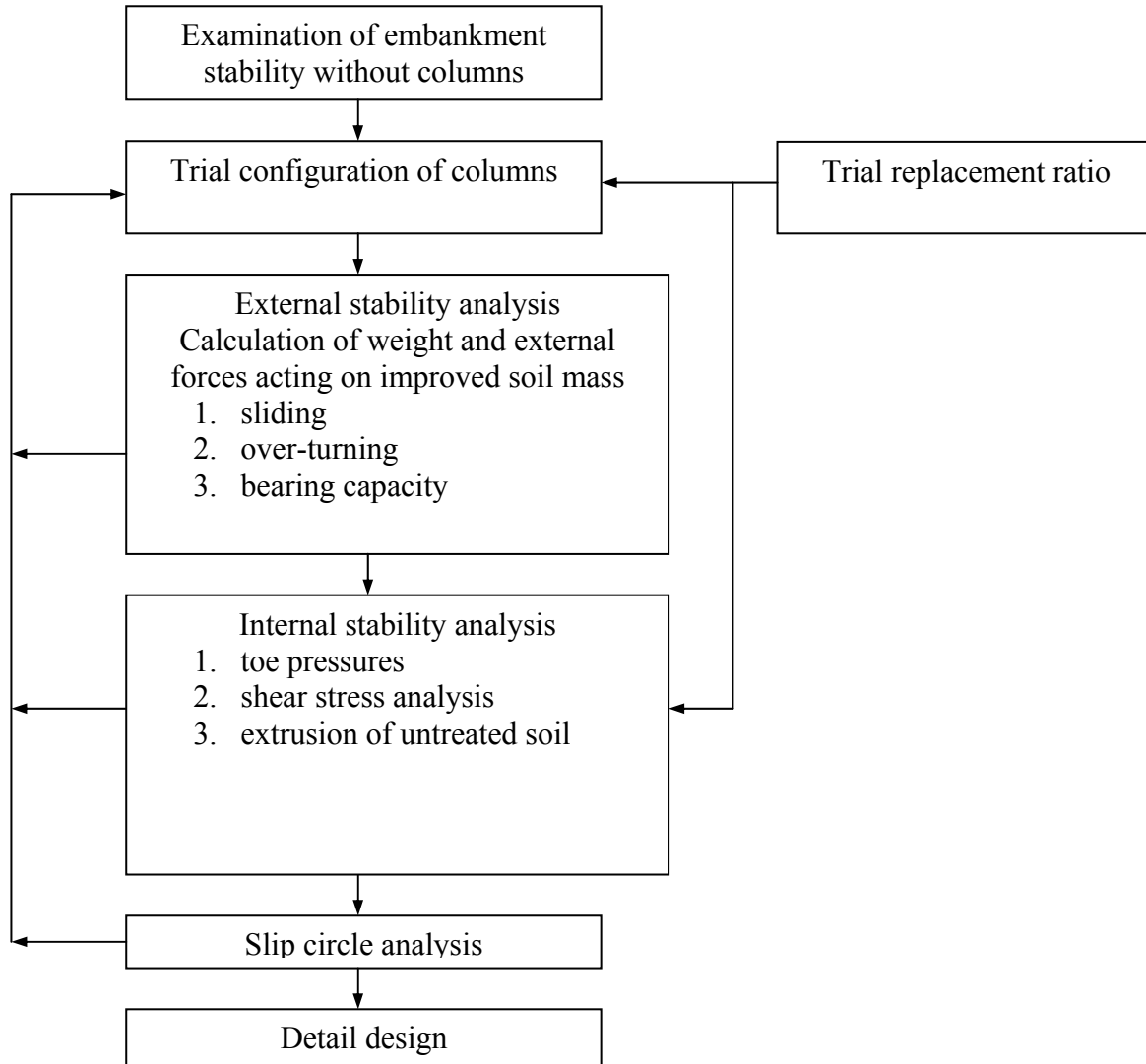
Slip circle analysis

Detail design

Figure C-5. Flowchart for design of wall, grid and blocks of columns

(adapted from CDIT 2002)

According to CDIT (2002), walls of deep-mixed material should be checked for extrusion of the untreated soil between the walls according to Equation C-3 and Figure C-6. This method was formulated by CDIT (2002) based on the results of centrifuge tests.

$$FS = \frac{2(L_s + D_i)Bc_u + P_p'}{P_a' + k_h \gamma BD_i L_s + h_w \gamma_w D_i L_s}$$

(C-3)

where:

D_i = height of prism (m)

c_u = mean undrained shear strength of the untreated soil
γ = unit weight of treated soil
k_h = design seismic coefficient
h_w = residual water level
γ_w = unit weight of water
P_a' = total of active earth pressure
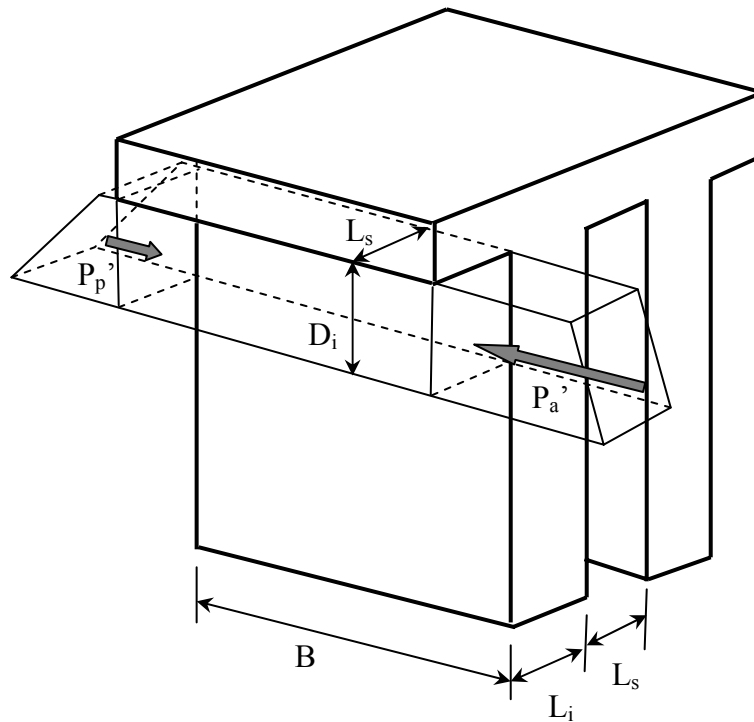P_p' = total of passive earth pressure

Figure C-6. Extrusion of soft clay between panels (after CDIT 2002)

C.4. Analysis and design procedures used in Scandinavia

In Scandinavia, regardless of test results, limits have been placed on lime and lime-cement column strength used in slope stability analysis to ensure acceptable performance of these composite foundations. The undrained shear strength of the columns is typically limited to 100 kPa, but column undrained shear strengths up to 150 kPa can be used when "favorable conditions exist, i.e., at greater depths and a factor of safety for the unimproved foundation greater than 1.2" (Carlsten 1997). According to Watn (1999), strengths greater than 200 kPa have been used when deep-mixed columns are overlapped in the form of panels.   According to Broms (2003), when deep-mixed columns are designed to carry the full load of the embankment, similar to driven piles, column undrained shear strengths up to 500 kPa can be used.

Typically, an undrained shear strength, $\tau_{u,col}$, equal to one half of the unconfined compression strength, $q_{u,col}$ has been used with deep-mixing-method columns. Kivelo (1998) pointed out that this could be unconservative for low confining pressures based on a Mohr-Coulomb representation of column strength with $\phi > 0$.

According to Broms (1999), the shear strength of the composite soil should be evaluated for both drained and undrained conditions, and the lowest calculated shear resistance, either drained or undrained, should be used in design.

The drained strength of the composite soil, τ_d, is determined by Equation C-4.

$$\tau_d = \tau_{d,col} a_s + \tau_{d,soil}\left(1 - a_s\right) \tag{C-4a}$$

$$\tau_{d,col} = c'_{col} + \sigma'_n \tan \varphi'_{col} \tag{C-4b}$$

$$\tau_{d,soil} = c'_{soil} + \sigma'_n \tan \varphi'_{soil} \tag{C-4c}$$

where:

$\quad \tau_d$ = drained shear strength along the sliding surface

$\quad \tau_{d,col}$ = drained shear strength of the column

$\quad a_s$ = area replacement ratio

$\quad \tau_{d,soil}$ = drained shear strength of the unimproved soil

$\quad \sigma'_n$ = effective normal stress on the failure plane

$\quad c'_{soil}$ = drained effective stress cohesion intercept for soil

$\quad \phi'_{soil}$ = drained effective stress friction angle for soil

If it is assumed that $\phi'_{soil} = \phi'_{col} = \phi'$, then Equation C-4d can be used to determine the drained shear strength of the composite soil.

$$\tau_d = c' + \sigma'_n \tan \varphi' \tag{C-4d}$$

where:

$$c' = c'_{col} a_s + c'_{soil}\left(1 - a_s\right) \tag{C-4e}$$

Most existing methods for in-situ and laboratory testing of lime-cement and soil-cement generate undrained strength parameter values based on total normal stresses (Watn et al. 1999). When no testing data is available, drained shear strength parameters of lime-cement columns can be estimated from column undrained shear strengths by Equation C-5.

$$c'_{col} = \beta c_{u,col}$$ (C-5a)

$$\varphi_{col} = 30°$$ (C-5b)

where:

$\beta = 0$ in the passive zone

$\beta = 0.1$ in the shear zone

$\beta = 0.3$ in the active zone

The strength parameters used in Equation C-5 are determined based on location along the failure surface for active, shear, and passive zones. The active, shear, and passive zones are delineated as shown in Figure C-7.
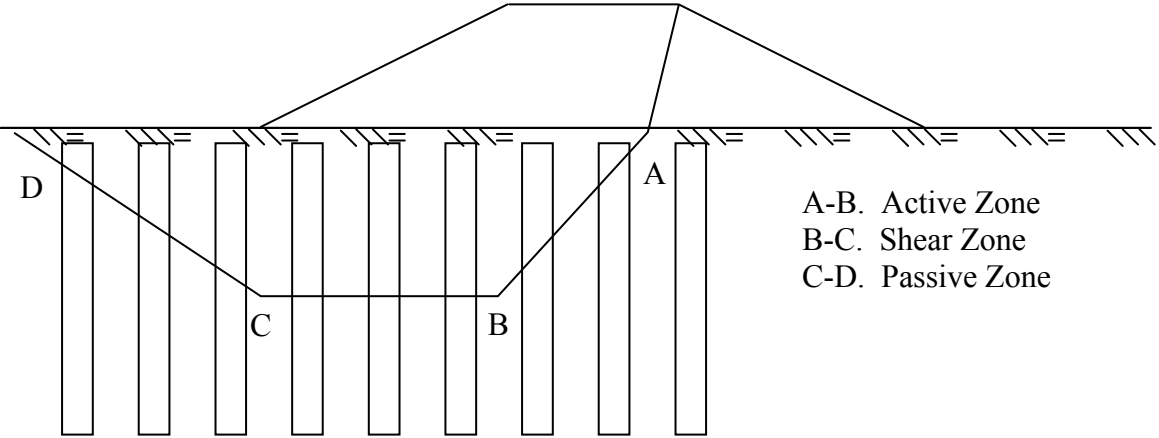

Figure C-7. Zones of shear surface (Kivelo, 1998)

Kivelo (1998) does not define the limits of the active, shear, and passive zones for a circular failure surface. From conversation with Magnus Ruin (2002), the distinctions between these zones are made based on practical considerations for roadway embankments and are shown in Figure C-8. The active zone is designed for settlement and employs a uniform distribution of

columns beneath the roadway to ensure even settlement of the roadway surface. Frequently, the shear zone is designed for slope stabilization and extends from the toe to the crest. No improvement is constructed in the passive zone. The boundary between the passive zone and the shear zone can be shifted beneath the slope to the point where settlement with an unimproved foundation is not a problem.
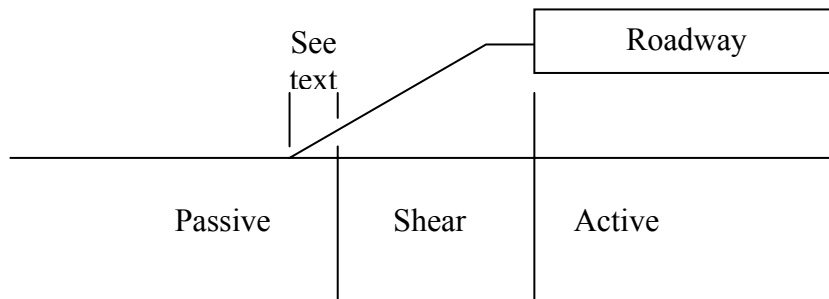

Figure C-8. Limits of passive, shear and active zones

Carlsten and Ekstrom (1997) recommend a combined analysis when column reinforcement exists in the passive or shear zones. The lowest value of undrained shear strength, τ_u, (from Equation C-1a or C-1d) or drained shear strength, τ_d, (from Equation C-4a or C-4d) is then used for each location along the shear surface. This combined analysis would be subject to the same issues regarding limits of the active, shear, and passive zones previously mentioned with regard to implementing a circular search routine for the drained analysis.

According to conversations with Magnus Ruin (2002), contractors in the Netherlands routinely perform undrained slope stability analyses by taking the minimum of the undrained column shear strength and the drained column shear strength. The drained columns strengths provided by Carlsten et al. (1997) are similar to the residual strength recommendation given by Broms (1999). The logic behind this approach is that the column shear strength may be reduced to its residual shear strength when the peak soil shear strength is eventually reached.

Carlsten and Ekstrom (1997) established design guidelines for the use of lime and lime-cement columns for embankment foundations in Sweden. Carlsten and Ekstrom's recommendations for

slope stability analysis were incorporated into EuroSoilStab (2002), which seems to be intended primarily for dry-mix methods of column installation. Carlsten et al. (1997) and EuroSoilStab (2002) recommend that isolated deep-mixing-method columns should not be used in the shear zone when the factor of safety for the unimproved foundation is less than 1.0; instead, rows of overlapping columns are recommended. When the slope of the original ground surface is steeper than one vertical to seven horizontal and the factor of safety for the unimproved foundation is less than 1.2, rows of overlapping columns are recommended beneath the entire embankment. These reports also state that "reinforcement in the passive zone of slip surfaces should be avoided unless it is designed in the form of slabs or blocks." The recommendations given by Carlsten (1997) and EuroSoilStab (2002) for the design of deep-mixing-method columns are summarized in the procedural flow chart shown in Figure C-9.
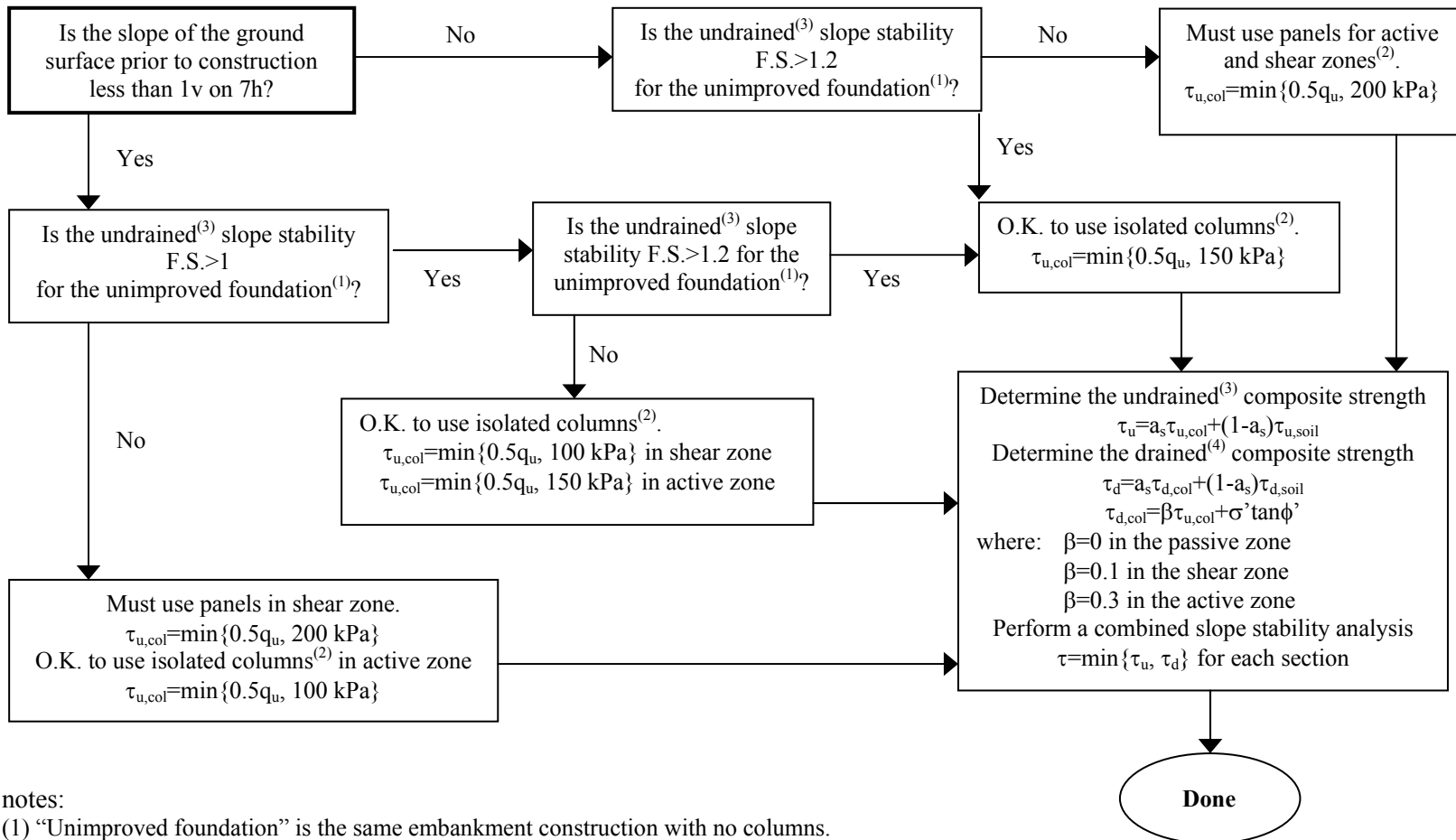
Watn et al. (1999) states that isolated lime-cement columns in the passive and shear zones should be avoided in all cases because the columns are sensitive to lateral displacements when they are not subjected to large axial loads.

Strain incompatibility between stiff piles and soft surrounding soil, a key aspect of the analysis and design method used in Japan, as described in Section C.3, is also addressed in literature based on Scandinavian methods of analysis and design. These references recommend either assuming a low failure strain and reducing the strength of unimproved soil or assuming a high failure strain and using a residual strength for the columns.

In Finland, strain incompatibility is considered by neglecting soil strength between columns when column shear strength exceeds 100 kPa and the factor of safety of the embankment on improved ground is less than 1.2 (Kivelo 1998). Otherwise, the full soil strength is included.

Broms (1999) recommends performing an undrained slope stability analysis using residual column strength to account for strain incompatibility between columns and surrounding soil. Residual column strengths are commonly assumed to have no cohesion intercept, with the residual friction angle equal to the peak friction angle (Broms 1999).

Start Here

Is the slope of the ground surface prior to construction less than 1v on 7h?

No →

Is the undrained[3] slope stability F.S.>1.2 for the unimproved foundation[1]?

No →

Must use panels for active and shear zones[2].
$\tau_{u,col}=\min\{0.5q_u, 200 \text{ kPa}\}$

Yes ↓

Yes ↓

Is the undrained[3] slope stability F.S.>1 for the unimproved foundation[1]?

Yes →

Is the undrained[3] slope stability F.S.>1.2 for the unimproved foundation[1]?

Yes →

O.K. to use isolated columns[2].
$\tau_{u,col}=\min\{0.5q_u, 150 \text{ kPa}\}$

No ↓

No ↓

O.K. to use isolated columns[2].
$\tau_{u,col}=\min\{0.5q_u, 100 \text{ kPa}\}$ in shear zone
$\tau_{u,col}=\min\{0.5q_u, 150 \text{ kPa}\}$ in active zone

Must use panels in shear zone.
$\tau_{u,col}=\min\{0.5q_u, 200 \text{ kPa}\}$
O.K. to use isolated columns[2] in active zone
$\tau_{u,col}=\min\{0.5q_u, 100 \text{ kPa}\}$

Determine the undrained[3] composite strength
$\tau_u=a_s\tau_{u,col}+(1-a_s)\tau_{u,soil}$
Determine the drained[4] composite strength
$\tau_d=a_s\tau_{d,col}+(1-a_s)\tau_{d,soil}$
$\tau_{d,col}=\beta\tau_{u,col}+\sigma'\tan\phi'$
where: $\beta=0$ in the passive zone
$\beta=0.1$ in the shear zone
$\beta=0.3$ in the active zone
Perform a combined slope stability analysis
$\tau=\min\{\tau_u, \tau_d\}$ for each section

Done

notes:
(1) "Unimproved foundation" is the same embankment construction with no columns.
(2) Use of columns should be avoided in the passive zone unless they are arranged in rows or blocks.
(3) As used here, the term "undrained" indicates that the shear strengths of clay and columns are characterized in terms of total stresses, but the shear strengths of sand layers are characterized in terms of effective stresses.
(4) As used here, the term "drained" indicates that the shear strengths of all soils and columns are characterized in terms of effective normal stresses.

Figure C-9. Flowchart for stability analysis of embankments on ground improved with lime-cement columns according to EuroSoilStab (2002), Carlsten and Ekstrom (1997), and Watn (1999)

APPENDIX D. ENGINEERING PROPERTIES OF DEEP-MIXED COLUMNS

D.1. Introduction

This appendix addresses the engineering properties, especially strength and stiffness, of deep-mixed materials created by the wet and dry methods. In the wet method, water-cement slurry is mixed with the soil, and in the dry method, dry lime and/or cement is mixed with the soil. Deep mixing methods are described by Porbaha (1998), Bruce (2000), CDIT (2002), EuroSoilStab (2002), Broms (2003), and others.

The engineering properties of soils stabilized by the deep mixing method are influenced by many factors including the water, clay, and organic contents of the soil; the type, proportions, and amount of binder materials; installation mixing process; installation sequence and geometry; effective in-situ curing stress; curing temperature; curing time; and loading conditions. Given all the factors that affect the strength of treated soils, the Japanese Coastal Development Institute of Technology (CDIT 2002) states that it is not possible to predict within a reasonable level of accuracy the strength that will result from adding a particular amount of reagent to a given soil, based on the in-situ characteristics of the soil. Consequently, mix design studies must be performed using soils obtained from a project site. Laboratory preparation and testing of specimens is discussed by Filz et al (2005) for the wet method and by Jacobson et al. (2005) for the dry method. Even relatively modest variations in binder materials may result in greatly different properties of the mixture. Field mixed and cured materials will differ from laboratory mixed and cured material. Furthermore, engineering properties of mixtures are time dependent, due to long-term pozzolanic processes that occur when mixing cement or lime with soil.

Most strength and stiffness information about deep-mixed materials comes from laboratory tests performed on (1) samples made in the laboratory by mixing cement grout or dry cement-lime reagent with soil from a project site, (2) wet grab samples taken during construction, and (3) core samples obtained from installed deep-mix elements. In-situ tests have also been performed. The primary focus of this literature review is on test results from wet grab samples and core samples obtained from deep-mixed elements installed in the field, not on tests performed on laboratory-prepared specimens. Engineering property values are obtained from unconfined compression

tests, triaxial compression tests, direct shear tests, oedometer tests, and hydraulic conductivity tests. Of these tests, the unconfined compression test is by far the most common.

In this literature review, one particular source was found to be especially valuable. A report by McGinn and O'Rourke (2003) describes the results of a large deep-mixed-testing program from the Boston Central Artery/Third Harbor Tunnel (CA/T) Project. This report provides abundant data concerning many engineering properties of the improved soil, and it presents statistical analyses to illustrate the variability in this form of ground improvement for an important project. Consequently, the work of McGinn and O'Rourke (2003) is cited often in this literature review, and it is recommended as an important resource.

This appendix begins by discussing some of the factors that affect the unconfined compressive strength of deep-mixed materials. Next, the ranges and variability of the unconfined compressive strength of deep-mixed materials are reviewed. Finally, other engineering properties of deep-mixed materials are discussed, and correlations with unconfined compressive strength are provided where available.

D.2. Factors that Affect the Unconfined Compressive Strength

In this section, the effects of water-to-cement ratio, reagent factor, field construction processes, and curing time on unconfined compressive strength are discussed.

D.2.1. Water-to-Cement Ratio

The general trend is that the strength of deep-mixed materials decreases as the amount of water in the mixture increases. For Hong Kong clay, Miura et al. (2002) showed that the unconfined compressive strength of materials created by the wet method of deep mixing decreases as the total-water-to-cement ratio increases. The total-water-to-cement ratio includes both the soil water and the water in the slurry. The data generated by Filz et al. (2005) support this finding.

Jacobson et al. (2003, 2005) applied the same concept to the dry method of deep mixing, and they also found that mixture strengths decrease as the water-to-cement ratio increases. For the dry method, the water-to-cement ratio of the mixture is numerically equal to the ratio of the soil

water content to the cement content of the mixture, because both the water content of the soil and the cement content of the mixture are determined relative to the dry weight of soil solids. Figure D-1 shows the data from Jacobson et al. (2003) along with the trend line from Miura et al. (2002).
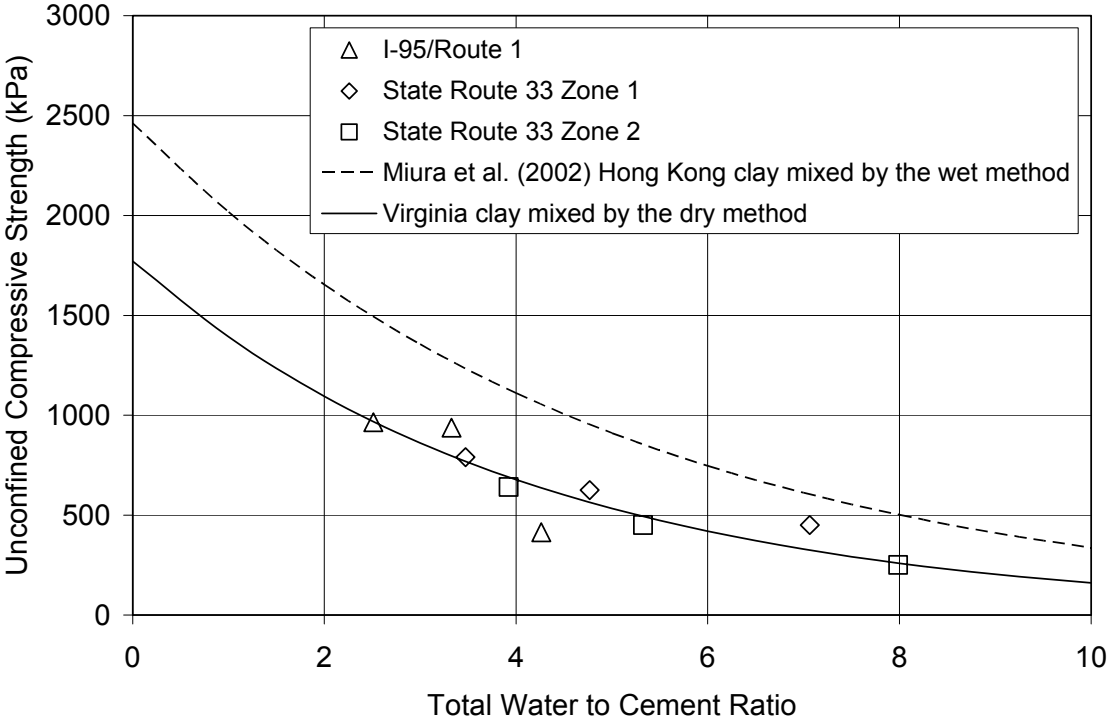

Figure D-1. Unconfined Compressive Strength versus Total Water to Cement Ratio
(Jacobson et al. 2003)

An interesting exception to this trend occurred for the marine clay that was treated by the wet method of deep mixing for the Boston CA/T project. Although there is much scatter in the data, a threefold increase in unconfined compressive strength resulted from increasing the grout water/cement ratio from 0.7 to 0.9 for a fixed cement dosage rate (McGinn and O'Rourke 2003). This occurred because the clay soil at this site is relatively stiff, with a natural water content of 35% to 40%, which is low compared to the natural water content of many other clay soils treated by the deep mixing method. The increased water provided by the higher water-to-cement ratio in the slurry permitted more thorough mixing of this relatively stiff clay. Improved mixing

increases strength, as discussed below. The influence of water-to-cement ratio of the slurry on mixture strength for the CA/T project is shown in Figure D-2.
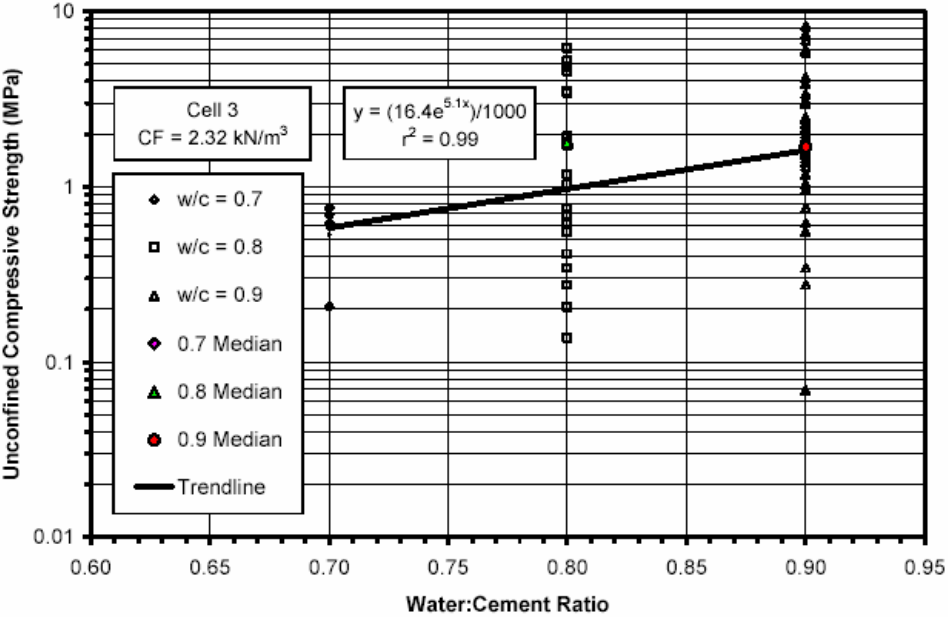
Figure D-2. Unconfined compressive strength as a function of water-to-cement ratio of the slurry (McGinn and O'Rourke 2003)

D.2.2. Reagent Factor

Other factors being equal, an increase in the reagent factor produces an increase in mixture strength. As one example, Figure D-3 shows the increase in unconfined compression strength due to an increase in cement factor for the CA/T project (McGinn and O'Rourke 2003). This is also demonstrated by the trend for increasing strength with decreasing total-water-to-cement ratio of the slurry presented by Miura et al. (2002), Filz et al. (2005), and others.
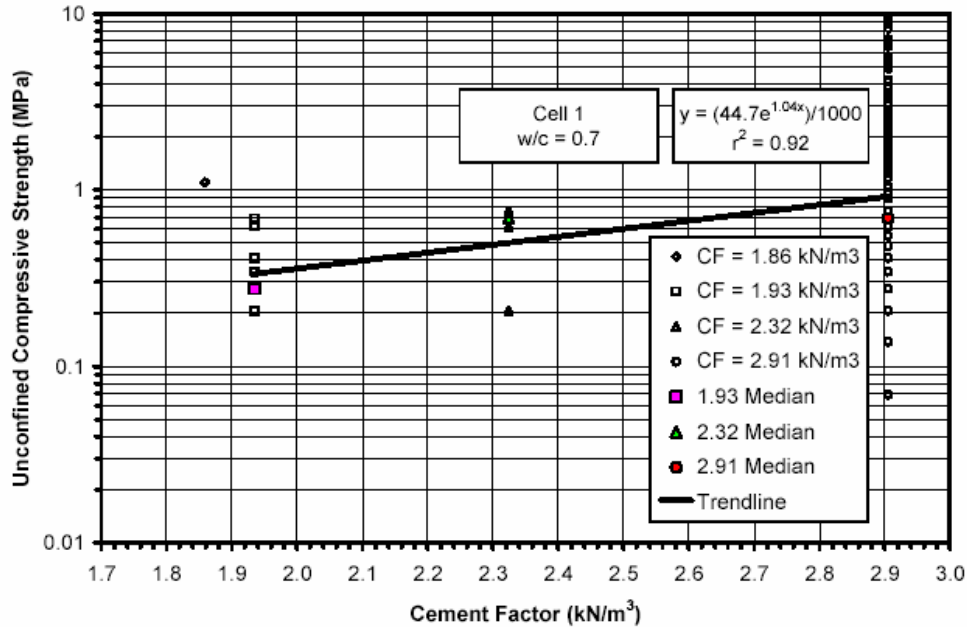
Figure D-3. Unconfined compressive strength as a function of cement factor
(McGinn and O'Rourke 2003)

D.2.3. Field Construction Processes and Conditions

Increasing mixing energy and efficiency produces more homogenous mixtures with higher
strengths and less variation of strength (CDIT 2002, Shiells et al. 2003). Increased mixing
energy and efficiency can be achieved by using increased rotation rate, decreased penetration
rate, multiple-mixing strokes, and multiple-mixing shafts. Multiple-mixing shafts allow for
opposite rotation of mixing paddles. The shape and arrangement of moving and fixed-mixing
paddles also affect mixing efficiency.

Dong et al. (1996) used the four different types of mixing blades shown in Figure D-4 to perform
a series of tests, listed in Table D-1, to study the effect of installation methods on measured
strengths in the field. Higher strengths are achieved from faster rotation rates, and reduced
penetration rates. A thin mixing blade contributed to greater in-situ strengths than a thick blade.
The test results are shown in Figures D-5 and D-6.

(a) TypeA-1(thick blade)   (b) TypeA-2(thin blade)   (c) TypeB-1(thick blade)   (d) TypeB-2(thin blade)
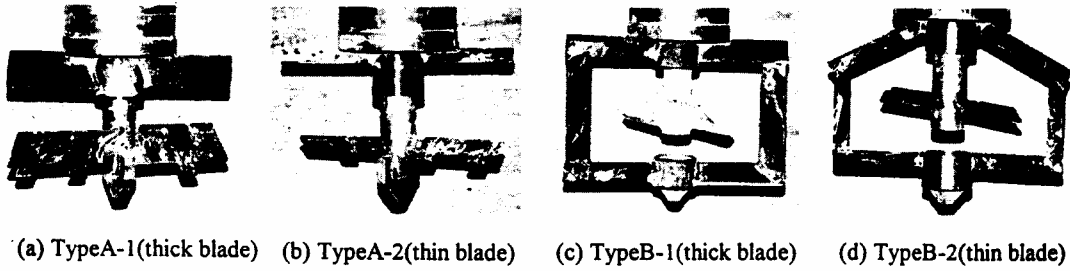
Figure D-4. Photo of mixing blades used in study by Dong et al. (1996)

Table D-1. Series of tests performed by Dong et al. (1996)

Test No.	Shape of Mixing blade	Rotary speed (rpm)	Lifting speed (m/min)	Total number of blade revolution (cycles/min)	Injecting velocity of slurry (l/min)	Injecting volume of slurry (l/one column)
1	TypeA-1	3 0	1. 0	6 0	2 8	2 8
2	TypeA-2	3 0	1. 0	6 0	2 8	2 8
3	TypeA-2	1 5	0. 5	6 0	1 4	2 8
4	TypeA-2	3 0	0. 5	1 2 0	1 4	2 8
5	TypeA-2	4 5	0. 5	1 8 0	1 4	2 8
6	TypeA-2	6 0	0. 5	2 4 0	1 4	2 8
7	TypeB-1	3 0	1. 0	9 0	2 8	2 8
8	TypeB-1	3 0	0. 5	1 8 0	1 4	2 8
9	TypeB-1	6 0	1. 0	1 8 0	1 4	2 8
1 0	TypeB-2	1 5	0. 5	9 0	1 4	2 8
1 1	TypeB-2	3 0	0. 5	1 8 0	1 4	2 8
1 2	TypeB-2	4 5	0. 5	2 7 0	1 4	2 8
1 3	TypeB-2	6 0	0. 5	3 6 0	1 4	2 8

218
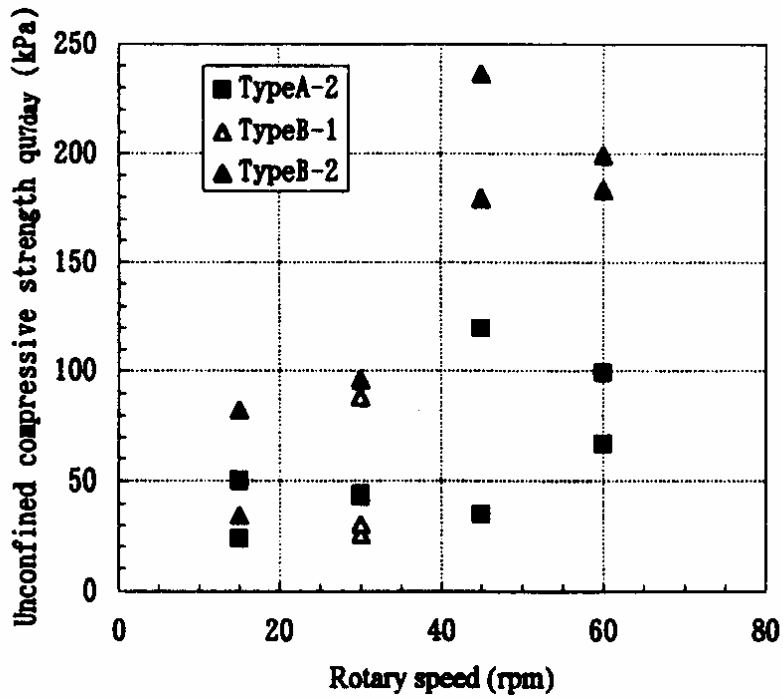
Figure D-5. Relationship between q_u and rotary speed (Dong et al. 1996)
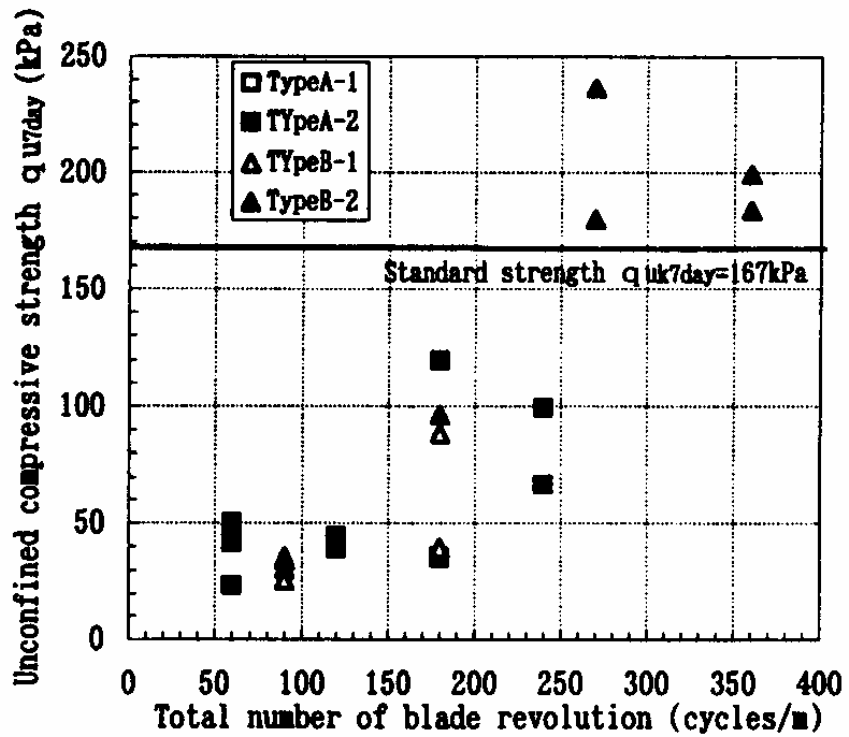
Figure D-6. Relationship between q_u and blade revolutions (Dong et al. 1996)

Other Japanese researchers have shown that unconfined compressive strength decreases with decreasing mixing time, and that strength variability increases with decreasing mixing time (CDIT 2002).

When stabilized columns are overlapped, the boundary surfaces between adjacent columns may become weak points in the stabilized structure. During the overlapping procedure, a partially hardened column is remixed by the overlapping column, and the strength in the overlapped area may be lower than the strength of other parts of the column, according to CDIT (2002).

For the dry methods of deep mixing, experience has shown that, by injecting one-half of the lime/cement mixture during down-driving of the mixing tool and one-half the mixture during the withdrawal, the column uniformity and the ability to adjust to different soil conditions are improved (Saye et al. 2001, Forte 2002).

McGinn and O'Rourke (2003) evaluated the unconfined compressive strength of core samples from two different installation rigs used on the CA/T project. Figures D-7 and D-8 show histograms of the natural logarithm of unconfined compressive strength, q_u, for core samples taken from elements installed with the M250 and 608 rigs, respectively. They found the mean strength of core samples installed with the 608 rig was 130% higher than the mean for the M250 rig, and the results for the 608 rig do not fit a lognormal distribution. These data indicate that different drill rigs can produce different results at the same site.
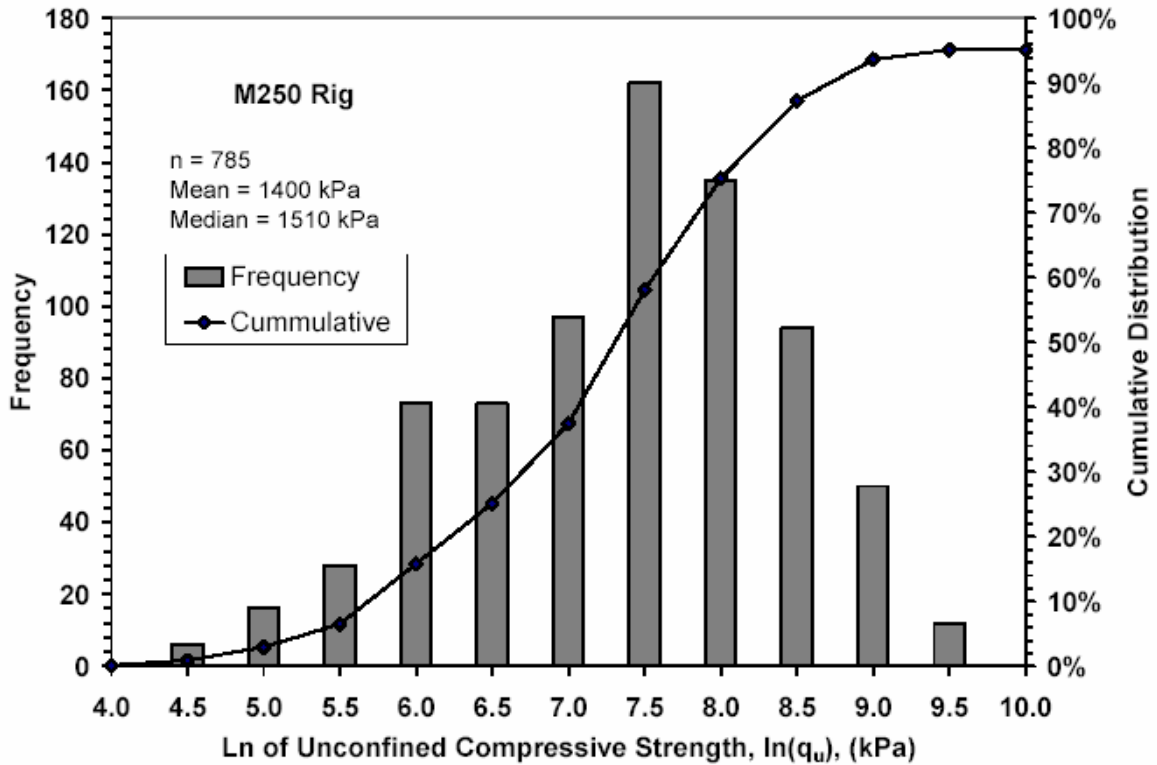
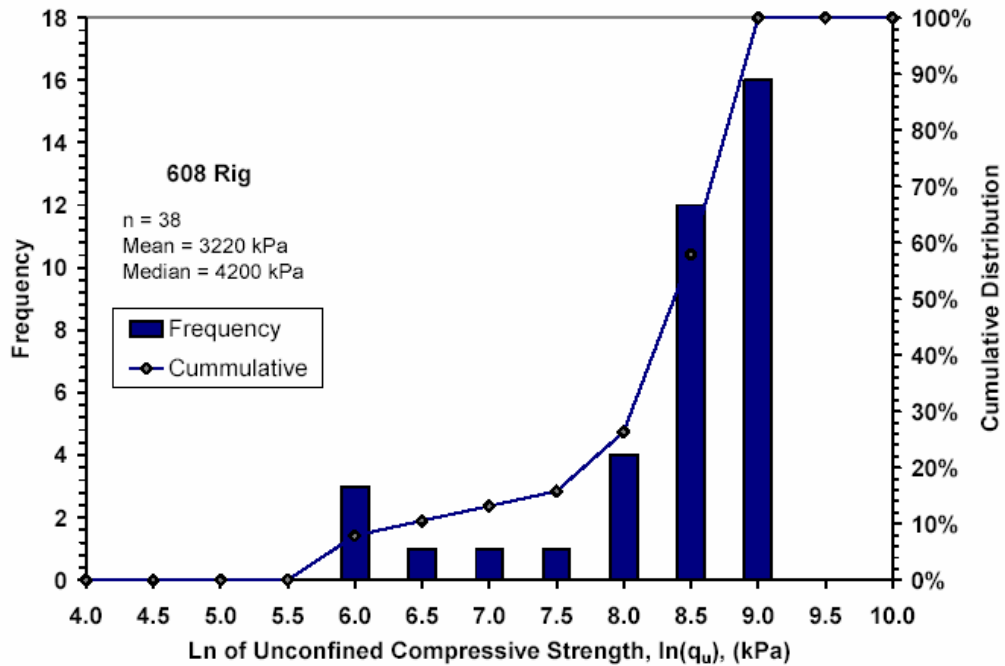Figure D-7. Distribution of $\ln(q_u)$ for the M250 rig (McGinn and O'Rourke 2003)

Figure D-8. Distribution of $\ln(q_u)$ for the 608 rig (McGinn and O'Rourke 2003)

The impacts of construction procedures on mixture strength highlight one of the difficulties that may be encountered when attempting to predict field strengths based on laboratory prepared specimens. Mixing in the laboratory is often more complete than mixing in the field, and the strengths of laboratory prepared specimens may be higher than the strength of field mixed specimens, as shown in Figure D-4 and also reported by EuroSoilStab (2002). CDIT (2002) states that the unconfined compressive strength of deep-mixed columns in the field can be as low as one-fifth of the unconfined compressive strength of laboratory mixed specimens. According to EuroSoilStab (2002), field strengths are on the order of 0.2 to 0.5 times the strengths of laboratory mixed specimens. Matsuo (2002) presents data in Figure A-10 that shows the strength of field mixed material can equal or exceed the strength of laboratory mixed specimens. His data also illustrate the significant variability that occurs in the ratio of the strength of field mixed materials to laboratory mixed materials.
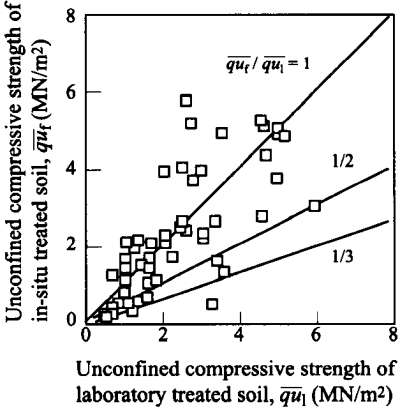
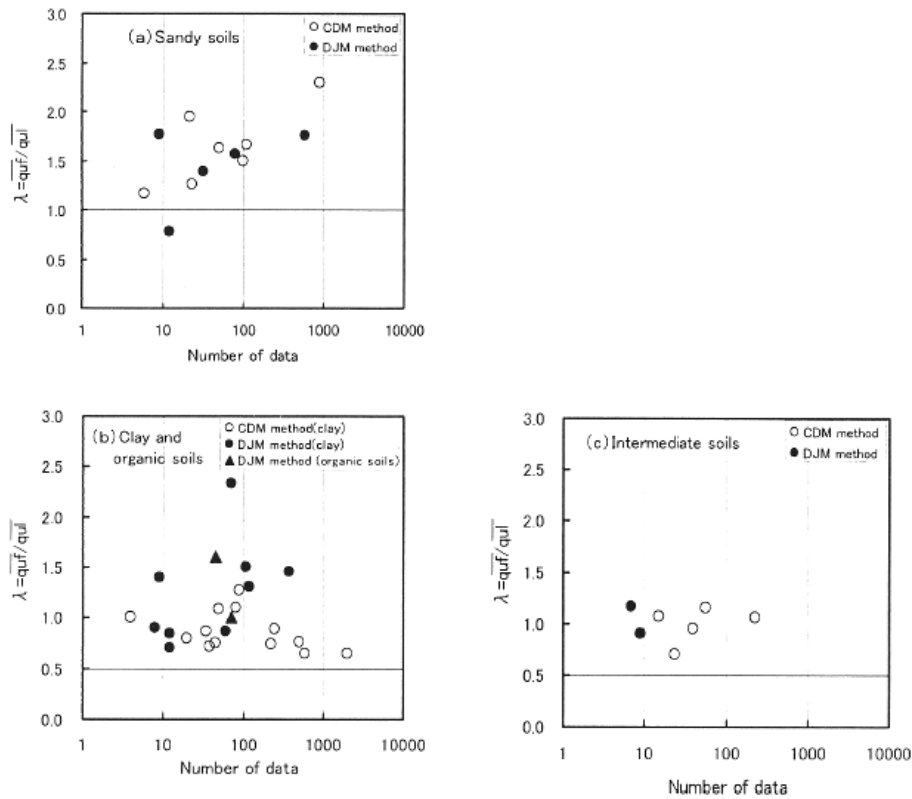Figure D-9. Relationship between field and lab strength (CDIT 2002)

Figure D-10. Distribution of λ, ratio of field to laboratory strength (Matsuo 2002)

In addition to differences between field and laboratory mixing, confining pressures during curing can influence strength values. Stengths determined from laboratory cured specimens may be less than the strengths from field cured samples because the confining pressure in-situ is generally not replicated in laboratory curing (Kivelo 1998). According to Bruce (2000), measured strengths of core samples are generally higher than those of wet grab samples by up to 50%.

D.2.4. Changes with Time

Depending on the type of binder and soil, some of the chemical reactions will take place relatively quickly, but some may develop more slowly. When finely ground cement is used, the shear strength increases rapidly during the first month after construction, with a slower rate of strength gain thereafter (Broms 2003). When using binders such as lime, gypsum, furnace slag and/or ash, the strength will continue to increase significantly after the first month. The increase in shear strength with time is typically faster in the field than in the laboratory, mainly due to higher temperature and higher confining pressure (Bruce 2000). Designers may be able to

223

optimize the time schedule for construction based upon the rate of strength gain in the columns (EuroSoilStab 2002).

Design of deep-mixed columns is typically based on the estimated strength 28 days after the installation of the columns. For soils stabilized by the wet method of deep-mixing, the 28-day unconfined compressive strengths are generally about 1 to 2 times the 7-day values, and at least 1.6 times the 3- or 4-day values. The 60-day strengths can be 1.2 to 2.5 times the 28-day values of strength (Bruce 2000, Takenaka and Takenaka 1995). Similarly, for soils stabilized by the dry method, the 28-day unconfined compressive strengths are about 1.5 to 2.4 times the 7-day values (Bruce 2000). For the CA/T project, McGinn and O'Rourke (2003) show the strength gain with time for wet grab samples with water-to-cement ratio of the slurry equal to 0.7 and 0.9 in Figures D-11 and D-12, respectively.
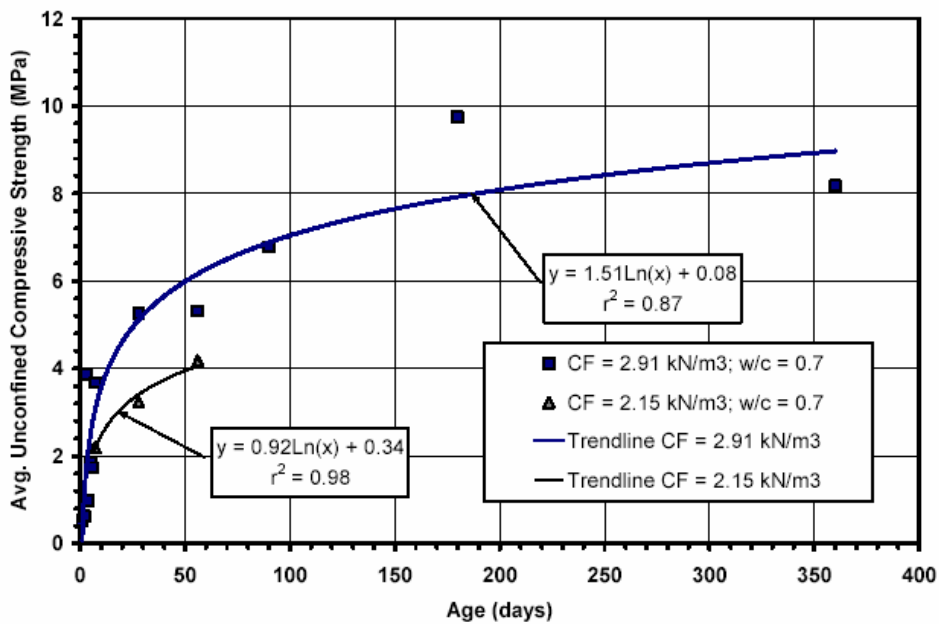
Figure D-11. Strength gain with time for wet grab samples with water-to-cement ratio equal to 0.7 (McGinn and O'Rourke 2003)
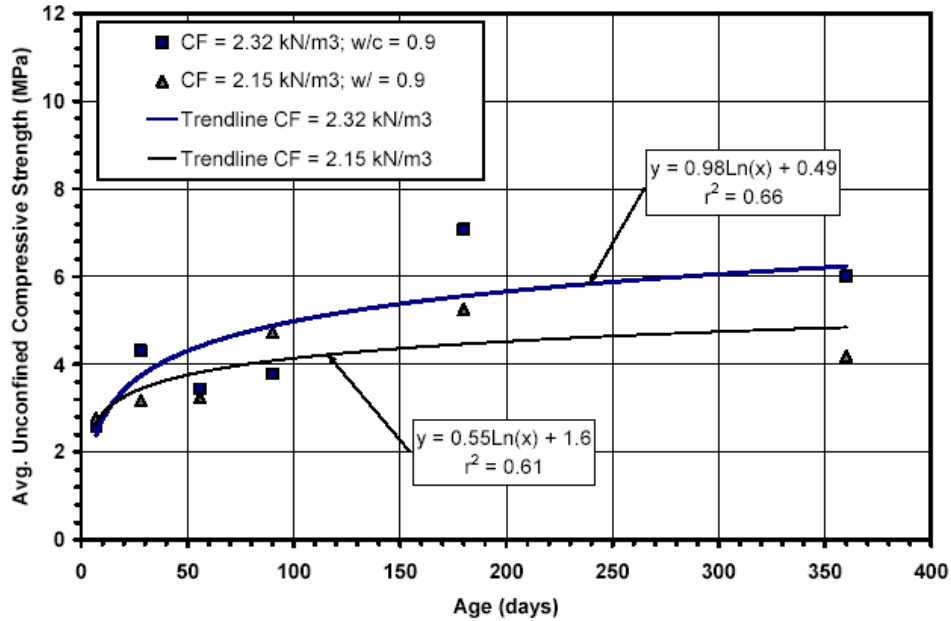
Figure D-12. Strength gain with time for wet grab samples with water-to-cement ratio equal to 0.9 (McGinn and O'Rourke 2003)

Generally speaking, the strength of treated soils increases almost linearly with the logarithm of time (CDIT 2002). Hayashi (2003) took continuous core samples on 17-year-old columns constructed by the wet method of deep-mixing. No substantial change in properties such as water content and dry density were measured; however, the strength of the columns as measured by unconfined compression testing had increased to three to seven times the 28-day strength over the span of 17 years.

Information about long-term degradation of deep-mixed materials is very limited. The addition of lime, bentonite, and higher cement factors can improve durability (Bruce 2000). Deterioration caused by sulfides has been documented in subgrades stabilized with lime. For soils treated with lime/cement or cement, an increase in the volume of the mixture, which can reduce the bonding and shear strength, can occur with time when flowing groundwater contains sulfides.   Concern has also been expressed about the possible reduction of shear strength of lime/cement and cement columns caused by cyclic and dynamic loading (Broms 2003).

D.3. Variability of Unconfined Compressive Strength

D.3.1. Introduction

This section describes the range and variability of unconfined compressive strength, q_u, produced by deep mixing methods. While several different types of laboratory tests can be used to evaluate the strength and stiffness of deep-mixed materials, the most frequently used test is the unconfined compression test, mainly because of the simplicity of the test. Although the unconfined compressive strength is often considered an index rather than a true measure of the mixture strength, it is frequently the only measure of mixture strength available on a project. For these reasons, considerable attention is devoted to unconfined compressive strength and its variation.

D.3.2. Range of Unconfined Compressive Strength

For a wide variety of soil types and binder mixes, the 28-day unconfined compressive strengths for soils treated by the wet method may range from 20 to 4,000 psi (Japanese Geotechnical Society 2000). The 28-day unconfined compressive strengths for soils treated by the dry method may range from 2 to 400 psi (Haley & Aldrich 2000, Jacobson et al. 2003, Baker 2000). A summary of contract specified values of unconfined compressive strength, q_u, for three recent projects in the U.S are presented in Table D-2.

Table D-2. Specified values of q_u on deep-mixing projects in the U.S

Project	Soil Type / Binder Amount	Specified q_u	Reference(s)
I-95 Route 1, Alexandria, VA	Wet mix method: Soft organic clay; 300 kg/m^3 cement (1:1 w:c slurry)	**Average** q_u at 28 days must be greater than 1,100 kPa (160 psi), with all values capped at 1,517 kPa (220 psi) for the purpose of computing the average. **Minimum** q_u at 28 days must be greater than 690 kPa (100 psi). Values of q_u measured on cored specimens.	Shiells et al. (2003); Lambrechts et al. (2003); Lambrechts and Layhee (2003)
Central Artery Project, Boston, MA	Wet mix method: Fill, organics and Boston Blue Clay; 220 - 300 kg/m^3 cement (0.9:1 w:c slurry)	**Minimum** q_u at 56 days $\geq$ 2,100 kPa (305 psi); **Maximum** q_u at 56 days $\leq$ 6,900 kPa (1,000 psi)	McGinn and O'Rourke (2003); Maswoswe (2001); Lambrechts et al. (1998)
Oakland Airport Roadway, California	Wet mix method: Loose sandy fills and soft clay; 160 – 240 kg/m^3 cement	**Average** q_u at 28 days must be greater than 1,035 kPa (150 psi). **Minimum** q_u at 28 days must be greater than 690 kPa (100 psi). Values of q_u measured on cored specimens.	Yang et al. (2001)

D.3.3. Variation of Unconfined Compression Strength

Statistical information in the literature indicates there is a large variation of strength for improved soil created by deep mixing methods. Common statistical measures that are frequently used to characterize deep-mixed strength are mean, μ, standard deviation, σ, and coefficient of variation, V. The mean is given by Equation D-1, where n is the number of measurements and x_i are the measurement values.

$$\mu = \frac{\sum\limits_{i=1}^{n} x_i}{n} \qquad\qquad (D\text{-}1)$$

The standard deviation is given by Equation D-2, and the coefficient of variation is given by Equation D-3. The coefficient of variation is simply the standard deviation divided by the mean, and it is often more useful than the standard deviation.

$$\sigma = \sqrt{\frac{\sum\limits_{i=1}^{n} (x_i - \mu)^2}{n}} \qquad\qquad (D\text{-}2)$$

$$V = \frac{\sigma}{\mu} \qquad\qquad (D\text{-}3)$$

Figure D-13 relates standard deviation to mean, and graphically illustrates the usefulness of coefficient of variation for accumulated field unconfined compression strength data from a case study in Japan.
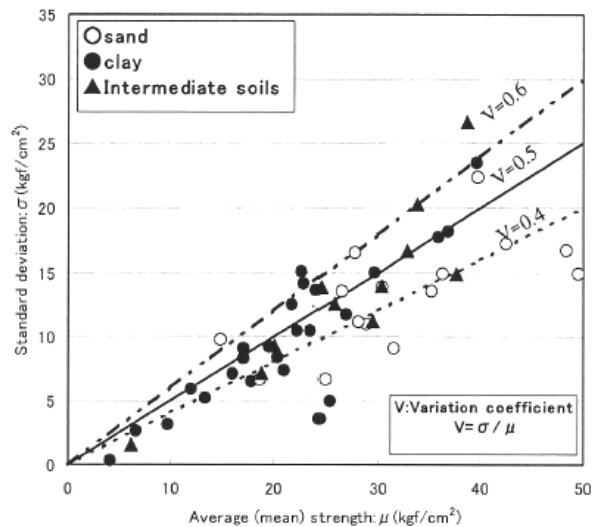
Figure D-13. Relationship between standard deviation and mean for treated soils (Matsou 2002)

As a reference point, Harr (1987) suggests that the coefficient of variation, V, for the undrained shear strength of clay is about 0.4. This provides a useful value for comparison with values of V reported in the literature for the strength of soils improved by the deep mixing method. Kawasaki et al. (1981) reported values of V from 0.25 to 0.35 for deep-mixed soils; however, more recent findings suggest a wider range of values of the coefficient of variation for deep-mixed soils. Honjo (1982) and later Takenaka and Takenaka (1995) collected data from several deep-mixing projects in Japan, and some of their results are summarized in Table D-3. The values of variation range from 0.21 to 0.59. Honjo (1982) and Takenaka and Takenaka (1995) also supply additional information including mixing tool penetration velocity, rotation speed of blades during penetration, withdrawal velocity, rotation velocity during withdrawal, cement content, and curing time. The Design Manual for Cement Deep Mixing (1996) is in Japanese, but it presents a summary table for a few other deep-mixing projects using the same categories as Honjo (1982) and Takenaka and Takenaka (1995). The projects listed in the Design Manual for Cement Deep Mixing (1996) show a range in the coefficient of variation from 0.15 to 0.50.

A collection of unconfined compression strength results summarized by Unami and Shima (1996) are presented in Table D-4. Matsuo (2002) collected unconfined compression strength results for cores taken from deep-mixed columns and presented these results in the form of a frequency distribution shown in Figure D-14. The data sets from Unami and Shima (1996) and Matsuo (2002) indicate relatively high values of the coefficient of variation from 0.41 to 0.57.

A presentation by O'Rourke and Druss (2002) contained the distribution of unconfined compression strength results for core samples from the Boston Central Artery project, as shown in Figure D-15. This figure highlights one of the problems with statistical interpretation of q_u data from deep mixing. Outlying samples of very high strength in this example likely led to the high standard deviation reported in this figure, which would result in $V = 1.35$. The cumulative distribution indicated by the solid line shows these results only include 95 percent of the data collected, with 5 percent of strengths being higher than 1470 psi. For this reason, the distribution is described as truncated. McGinn and O'Rourke (2003) show data in Figure D-16 for core samples and data in Figure A-17 for wet grab samples. For these data, $V = 1.36$ for core samples and $V = 0.84$ for wet grab samples. These coefficients of variation are much higher than the

values reported in the Japanese literature. For QA/QC on the Woodrow Wilson Bridge Project, Shiells et al. (2003) describe how very high strength test results obtained from deep-mixed columns were not included in statistical interpretation of field results for contract specification purposes.

Table D-3. Test results for deep-mixing projects in Japan (after Honjo 1982)

| Construction Site | | Improvement Elevation (m) | Unimproved c_u (kPa) | Improved q_u | | | |
Prefecture	Classification			q_u (kPa)	σ (kPa)	V	n
Hiroshima		-9.0 to -22.0	$3.5 + 1.5z$ ($z = 0$ at -9)	3844	1360	0.35	236
Yoshima	No. 1	-14.0 to -22.0	2.9z ($z = 0$ at -11)	4780	1720	0.36	346
	No. 1	-22.0 to -25.0		4760	1860	0.39	138
	No. 1	-25.0 to -28.0		8500	3390	0.40	110
	No. 4	-14.0 to -20.5		4630	1380	0.30	209
	No. 4	-20.5 to -26.0		5210	1660	0.32	129
Tokyo		-9 to -27	$3 + 1.4z$ ($z = 0$ at -9)	993	395	0.40	44
		-9 to -27		583	346	0.59	46
		-9 to -39		2090	802	0.38	114
		-9 to -39		1800	567	0.32	51
		-9 to -39		1860	638	0.34	38
		-9 to -39		2120	949	0.45	106
		-9 to -39		3310	1090	0.33	78
		-9 to -37		2070	1170	0.57	87
Koto-ku Ariake		-2 to -8	5 to 30	2090	595	0.28	47
		-2 to -8.5		2970	1050	0.35	47
Chiba	T.C.	-11 to -23	25 to 35	4545	1160	0.30	73
		-9 to -22	10 to 35	4328	898	0.21	95

Notes: T.C. indicates test construction, q_u indicates unconfined compression strength test results, elevation refers to a local datum in each prefecture, and n indicates the number of values in the data set.

Table D-4. q_u test results from four layers (Unami and Shima 1996)

	Whole layers				Deposit fill layer				Ac1 layer				Ac2 layer			
	n Number	qu Average	On Standard deviation	X Variation coefficient	n Number	qu Average	On Standard deviation	X Variation coefficient	n Number	qu Average	On Standard deviation	X Variation coefficient	n Number	qu Average	On Standard deviation	X Variation coefficient
Total	151	14.1	7.7	0.54	22	15.1	8.6	0.57	668	11.5	5.3	0.46	261	20.7	8.6	0.41

n: Number of samples   qu: Average unconfined compressive strength (kgf/cm²)
On : Standard deviation (kgf/cm²)
X: Variation coefficient (=n/qu)
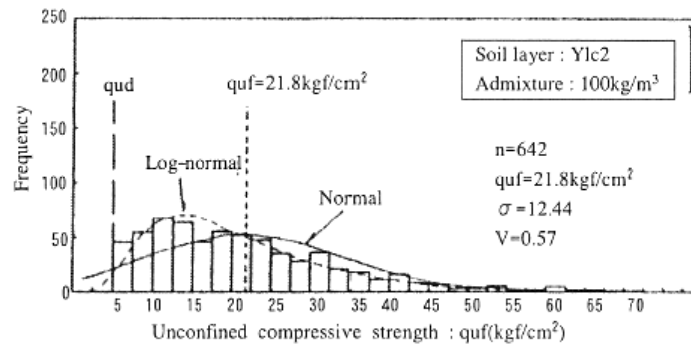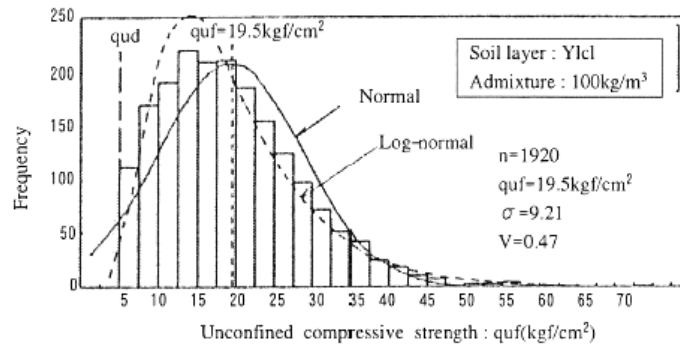
Figure D-14. Frequency distribution of measured field strengths (Matsuo 2002)
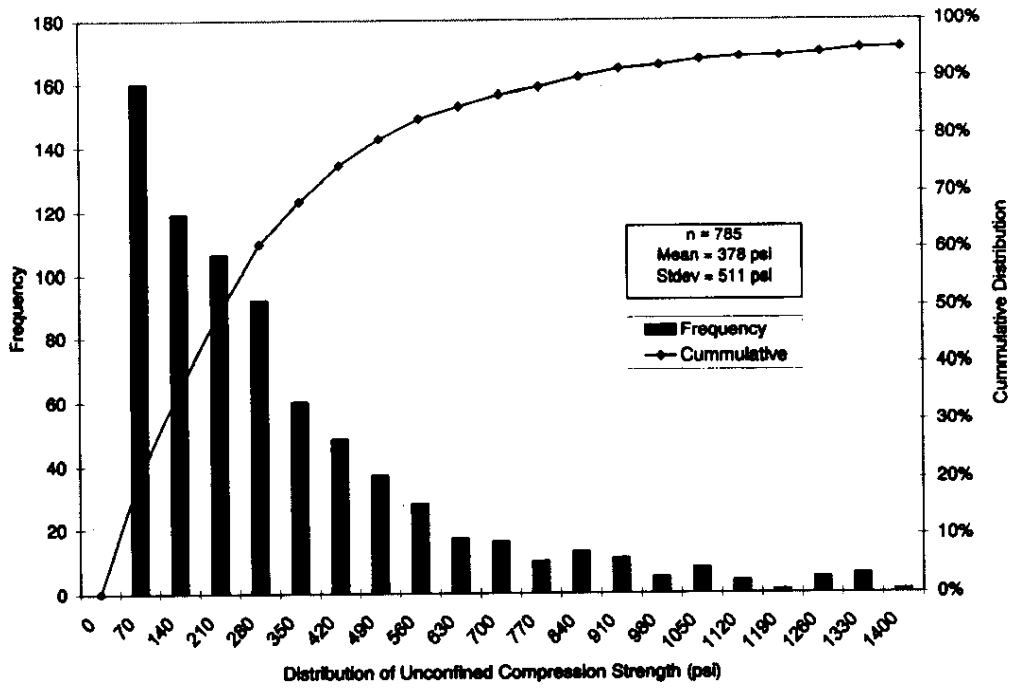
Figure D-15. Truncated distribution of q_u for core samples (O'Rourke and Druss 2002)
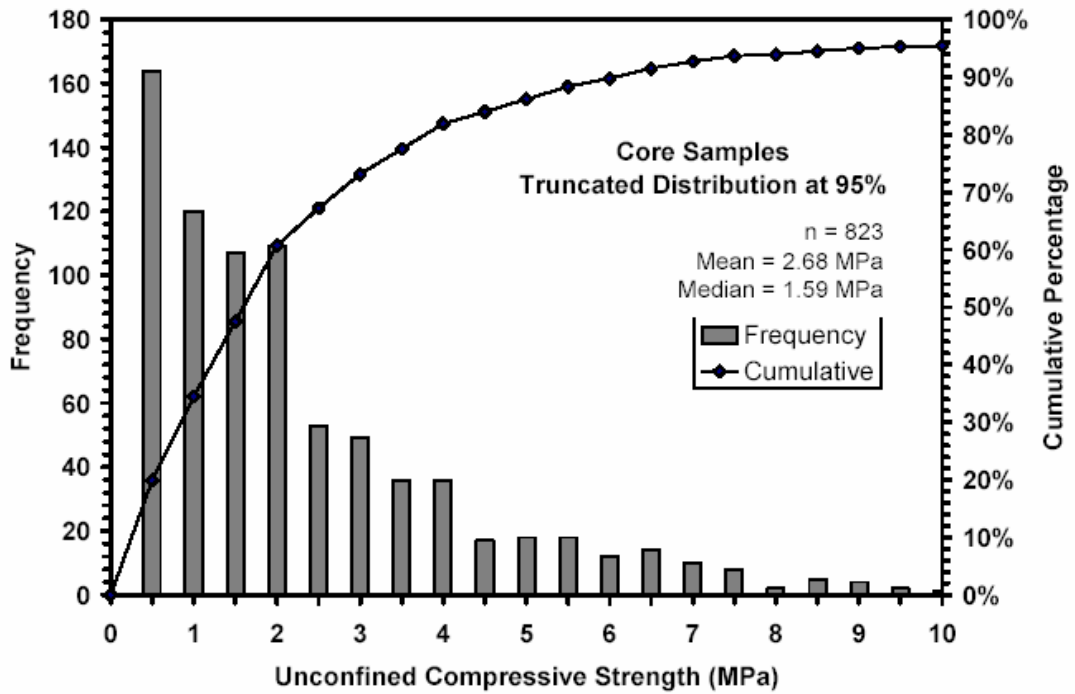
Figure D-16. Truncated distribution of q_u for core samples (McGinn and O'Rourke 2003)
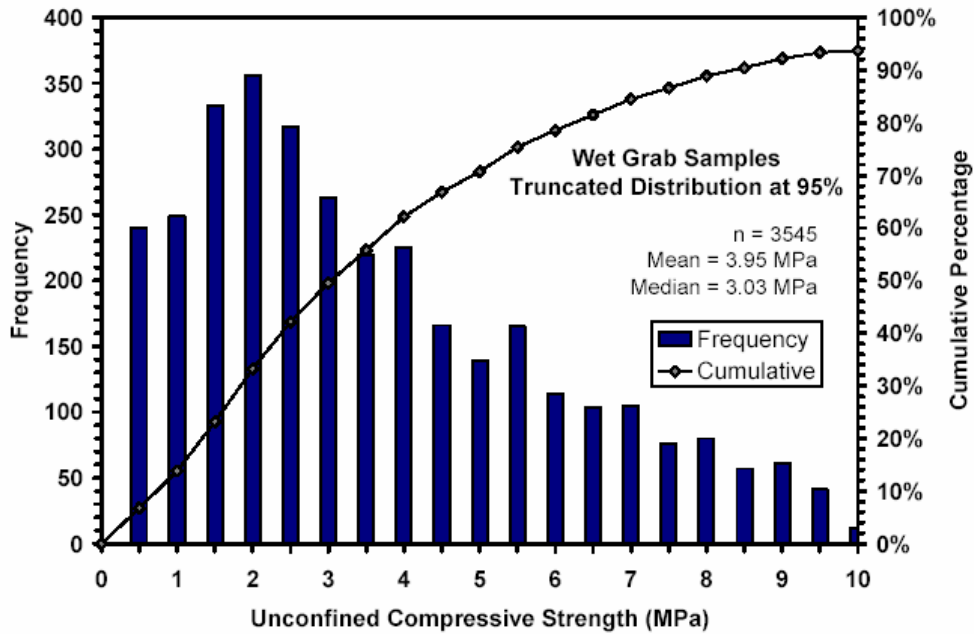
Figure D-17. Truncated distribution of q_u for wet grab samples (McGinn and O'Rourke 2003)

Because these q_u results tend to fit a lognormal distribution, McGinn and O'Rourke (2003) also present the natural logarithm of the data from Figures D-16 and D-17, as shown in Figures D-18 and D-19.
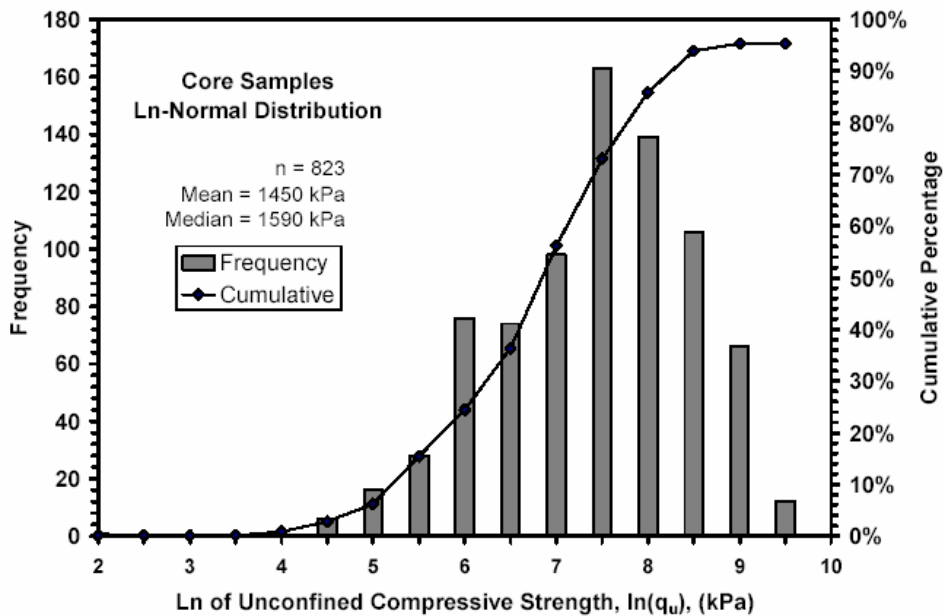

Figure D-18. Truncated distribution of $\ln(q_u)$ for core samples (McGinn and O'Rourke 2003)
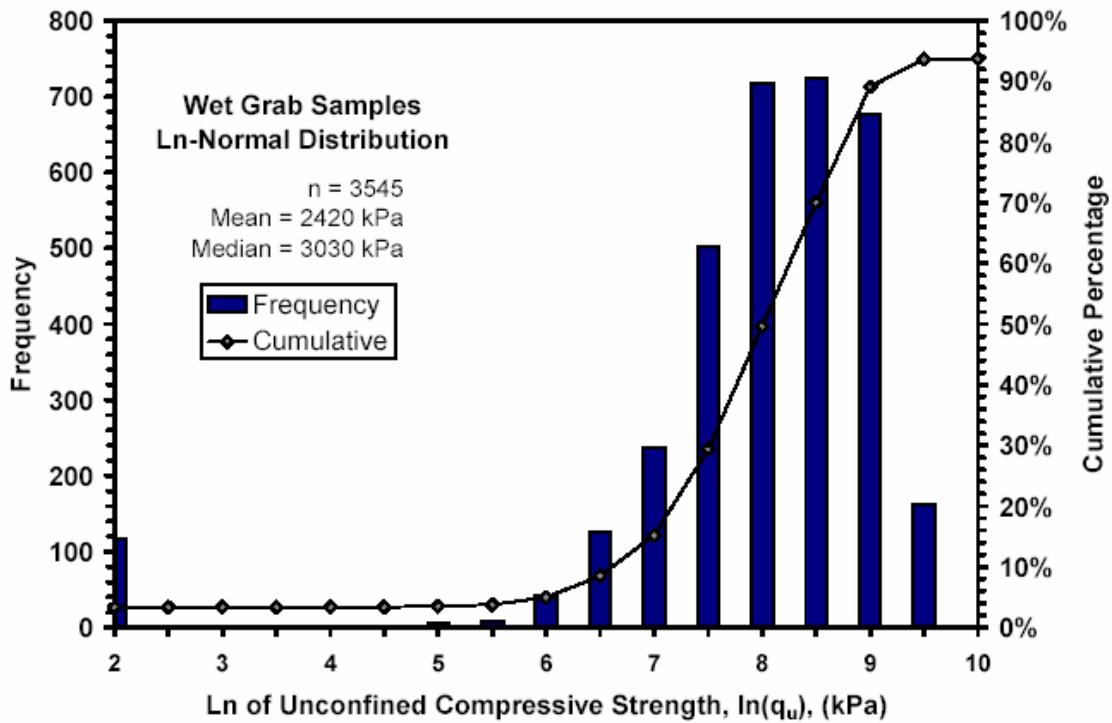
Figure D-19. Truncated distribution of $\ln(q_u)$ for wet grab samples
(McGinn and O'Rourke 2003)

D.3.4. Variation of Unconfined Compression Strength with Depth

Baecher and Christian (2003) discuss how statistical data that is collected and presented as a group, as was done in the previous section can mask some trends in the data. Unami and Shima (1996), Matsuo (2002), McGinn and O'Rourke (2003), Fang et al. (2001), and Herlach (2001) provide plots of unconfined compression strength results versus depth or elevations as shown in Figures D-20, D-21, D-22, D-23, and D-24, respectively. Several of these plots show that the mean value and variation of strength are higher at greater depths.
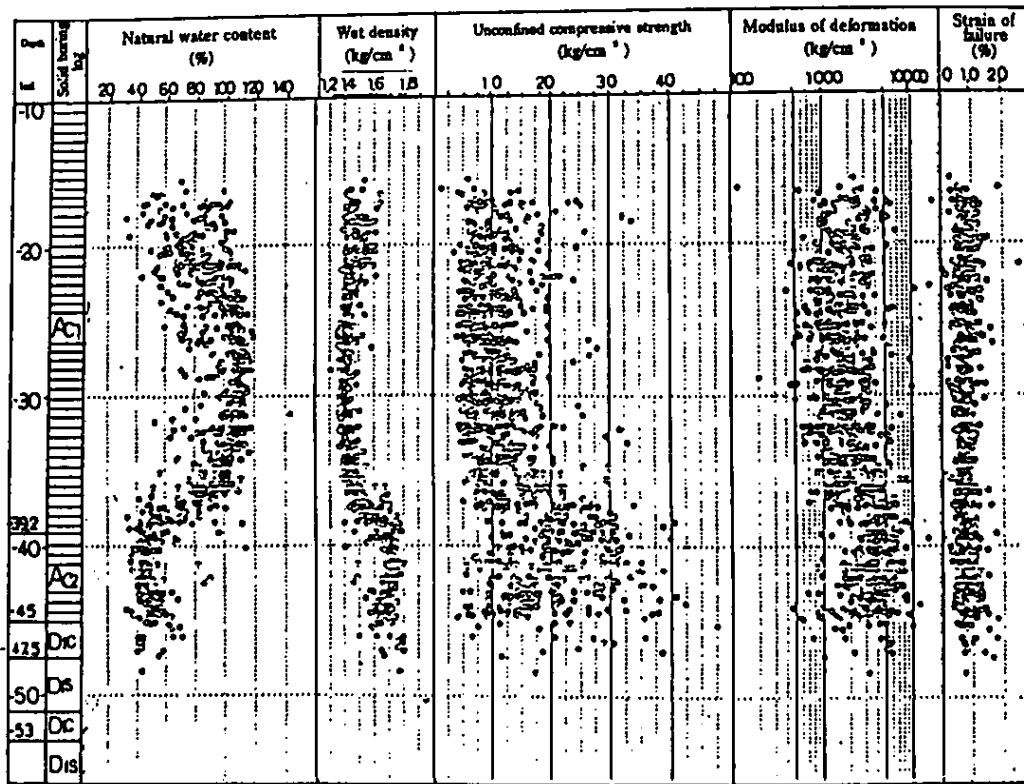
Figure D-20. Results of post execution laboratory tests for deep-mixed soil
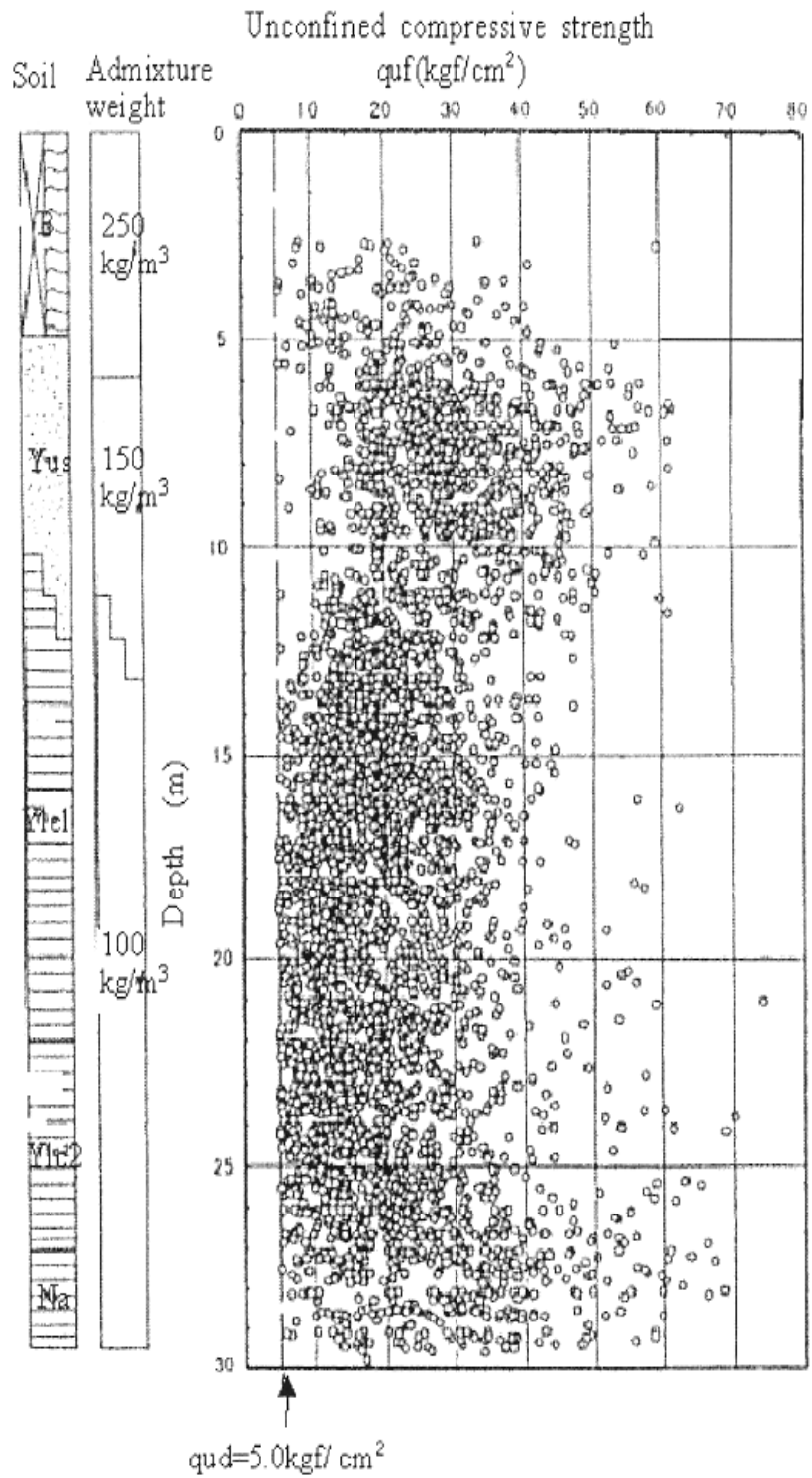(Unami and Shima 1996)

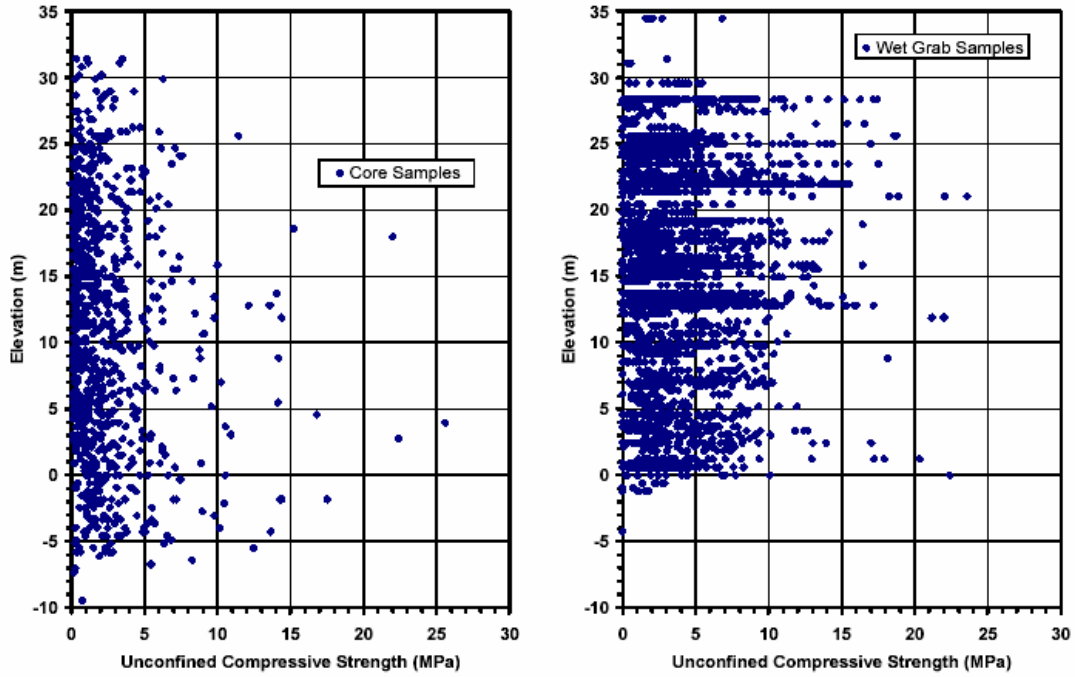Figure D-21. Distribution of q_u results measured in the field (Matsuo 2002)

Figure D-22. Field strengths obtained from cores and wet grab samples
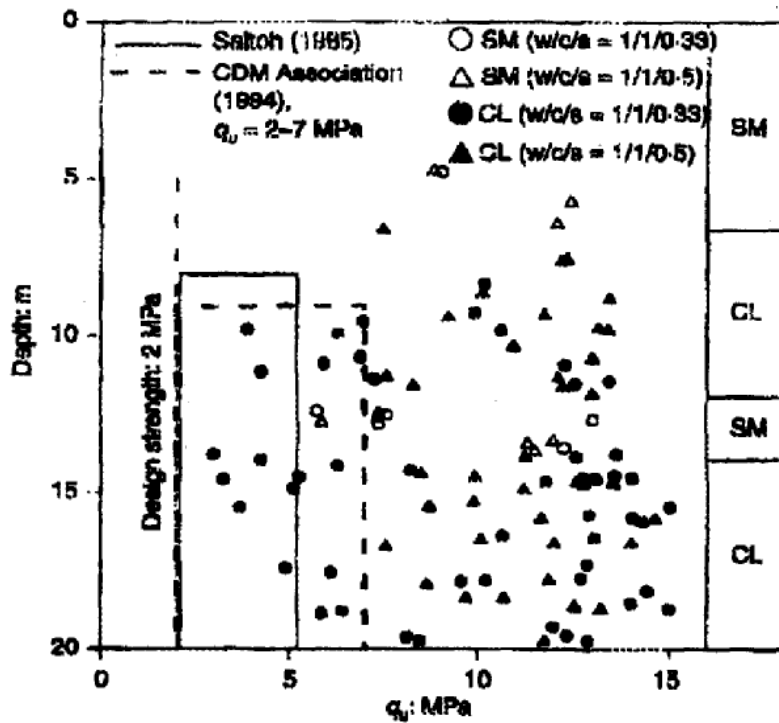(McGinn and O'Rourke 2003)

Figure D-23. Results of uniaxial compression test results for deep-mixed soils (Fang 2001)
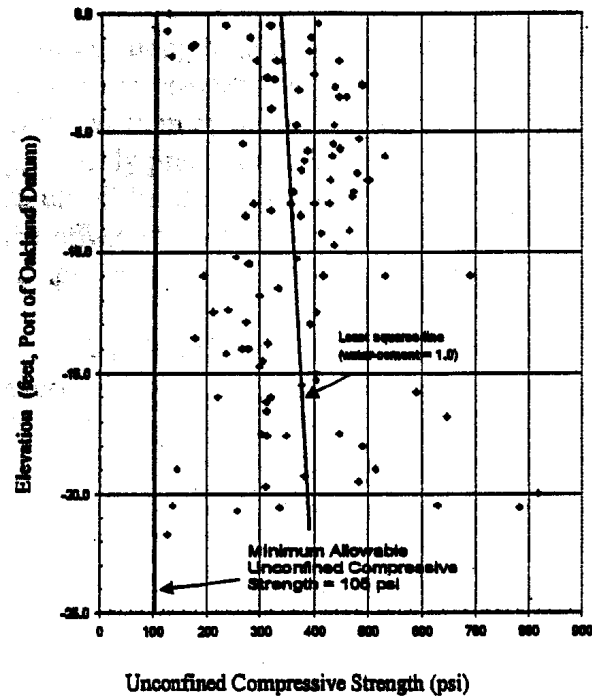
Figure D-24. Distribution of q_u results measured in the field (Herlach 2001)

D.4. Other engineering properties of deep-mixed soils

D.4.1. Introduction

Besides the unconfined compressive strength, q_u, other engineering properties that may be important on deep-mixing projects include modulus of elasticity, Poisson's ratio, constrained modulus, tensile strength, bending strength, unit weight, and hydraulic conductivity. This section discusses these properties, and provides correlations with unconfined compressive strength where available.

D.4.2. Modulus of Elasticity

The secant modulus of elasticity, E_{50}, is determined as the slope of the line extending from the origin of the stress-strain plot to the point corresponding to half the maximum stress, and it is typically determined from unconfined compression or triaxial compression tests. E_{50} is typically used as the design value of the modulus of elasticity of the column, E_{col}. However, consideration should be given to the operable value of modulus at small strains (McGinn and O'Rourke 2003). According to Ekström et al. (1994), the modulus of elasticity as determined by unconfined

238

compressive tests on samples prepared in the laboratory is typically higher than the modulus determined on cores samples obtained in-situ from actual columns.

For columns installed by the dry method, the ratio of E_{50} to unconfined compressive strength ranges from 50 to 180 for lime/cement columns and from 65 to 250 for cement columns (Baker 2000, Broms 2003). Based on laboratory tests performed on three different soil types treated with dry lime/cement, Jacobson et al. (2003) found that the ratio of E_{50} to unconfined compressive strength was approximately 75. However, for peats stabilized with dry cement, the relationship between the modulus of elasticity and the undrained shear strength is not linear, as typically assumed for other soil types (Hebib and Farrel 2000).

For cement treated soils using the wet method and prepared in the laboratory, the modulus of elasticity, E_{50}, has been reported in research done more than 20 years ago to be 350 to 1,000 times the unconfined compressive strength for a wide variety of silts and clays (Kawasaki et al. 1981). More recently, however, in a series of unconfined compressive tests performed on soils treated by cement slurry with a water/cement ratio of 1.0, Fang (2001) reported that the modulus of elasticity, E_{50}, was 30 to 300 times the unconfined compressive strength. On the Boston Central Artery/Tunnel Project, wet mixing in the laboratory produced E_{50} values that were about 150 times the unconfined compressive strength, as shown by O'Rourke and Druss (1998). Ou et al. (1996) compiled published relationships between E_{50} and q_u in Table D-5 for wet mix methods in Japan. Table D-6 lists other published relationships between E_{50} and q_u.

Table D-5. Relationships between E_{50} and q_u for the wet method of deep mixing (Ou et al. 1996)

E_{50}/q_u	Soil type	Reference
200	Taipei silty clay	Woo (1993)
105-390	Taipei silty clay	Chen (1985)
160-340	Taipei silty clay	Lin (1992)
200-500	Taipei silty clay, silty sand	Fang et al. (1992)
350-1000	Tokyo, Chiba, Kanagawa, Aichi, Osaka, Mie, and Fukuoka clays	Kawasaki et al. (1981)
75-200	Honmoku marine clay	Gangtin and Sunben (1984)
200-1000	Kawasaki clay	Gangtin and Sunben (1984)
100-300	---	JSG (1986)

Table D-6. Additional published relationships between E_{50} and q_u

Binder type	E_{50}	Reference
Dry lime/cement	$50 - 180q_u$	Baker (2000); Broms (2003)
	$75q_u$	Jacobson et al. (2003)
Dry cement	$65 - 250q_u$	Baker (2000); Broms (2003)
Wet cement	$30 - 300q_u$	Fang (2001)
	$150q_u$	O'Rourke and Druss (1998)

The wide range in ratios of E_{50} to q_u from these various sources indicates that there is considerable uncertainty in estimating E_{50} by means of correlation with q_u. There is also a large amount of scatter in the test results used to determine these relationships, as can be seen in Figures D-25, D-26, and D-27.
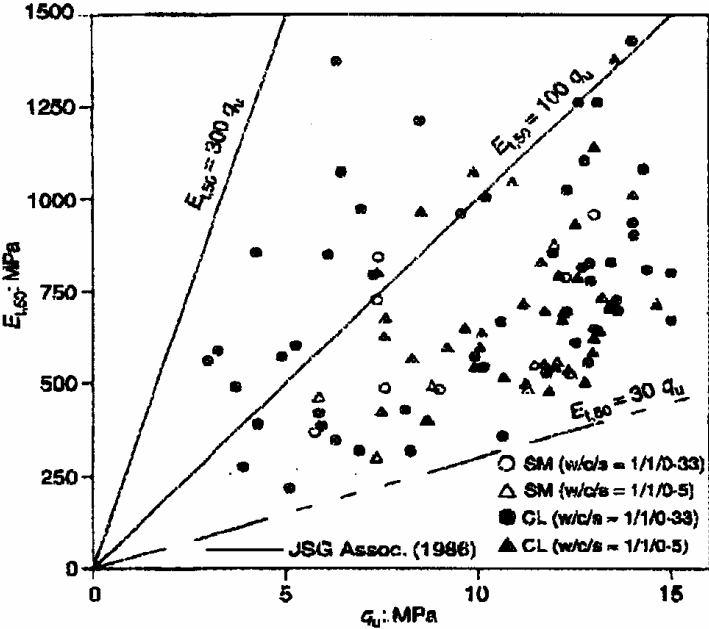

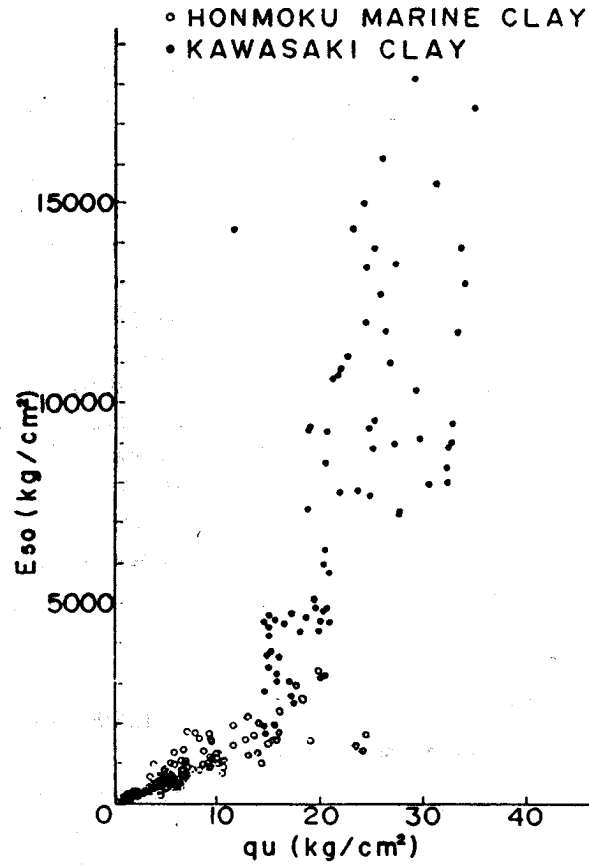Figure D-25. Relationship between E_{50} and q_u (Fang 2001)

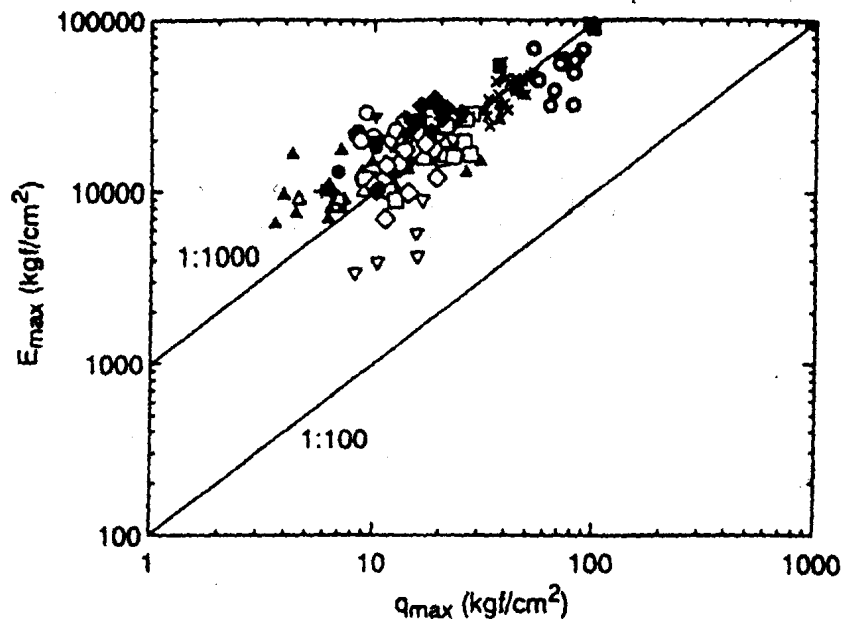Figure D-26. Relationship between E_{50} and q_u (Okumura 1997)

Figure D-27. Summary of E_{max} to q_{max} relations for cement-treated soils

(Tatsuoka and Kobayashi 1997)

242

D.4.3. Poisson's Ratio

In general, the Poisson's ratio, v_{col}, of deep-mixed-treated soil ranges from 0.25 to 0.50, irrespective of the unconfined compressive strength (CDIT 2002, Terashi 2003). However, for peats stabilized with dry cement, Hebib and Farrell (2000) measured Poisson's ratio values on the order of 0.1 for strains less than 1%. McGinn and O'Rourke (2003) used a Poisson's ratio of 0.25 in their numerical analysis. Porbaha et al. (2005) used seismic methods to determine a Poisson' ratio value of 0.25 to 0.45 for small strain behavior of deep-mixed material created using the wet method.

D.4.4. Constrained Modulus

The value of constrained compression modulus of the column, M_{col}, can be measured in laboratory oedometer tests. However, according to Broms (2003), laboratory values are typically lower than in-situ values of constrained modulus, so the constrained modulus from oedometer tests can be considered as a lower limit.

When determined from oedometer tests, the constrained modulus is equal to the inverse of the compressibility parameter, m_v, as in Equation D-4:

$$M_{col} = \frac{1}{m_v} \qquad\qquad (\text{D-4})$$

The constrained modulus of the column, M_{col}, can also be related to the modulus of elasticity, E_{col}, and Poisson's ratio, v_{col}, by Equation D-5:

$$M_{col} = \frac{(1-v_{col}) \cdot E_{col}}{(1+v_{col}) \cdot (1-2 \cdot v_{col})} \qquad\qquad (\text{D-5})$$

D.4.5. Tensile Strength and Bending Strength

EuroSoilStab (2002) states that, for the dry methods of deep mixing, columns should not be used to resist tensile stresses.

Terashi et al. (1980), Brandl (1981), Tanaka et al. (1986), and Takenaka and Takenaka (1995) all report that the tensile strength of soil improved by the wet method is 10% to 20% of the unconfined compressive strength. Kitazume et al. (1996) reports that a value of 15% is used in Japan with wet mix methods. Dong et al. (1996) provide a relationship between unconfined compressive strength and tensile strength in Figure D-28, based on the series of tests described previously and listed in Table D-1. It can be seen in Figure D-28 that the tensile strengths are about 30% of the unconfined compressive strengths, which is a higher percentage than the values cited above.

Dong et al. (1996) also provide a relationship between unconfined compressive strength and bending strength shown in Figure D-29 based on the series of tests in Table D-1. Dong et al. (1996) do not describe how the bending strength was determined, but it is assumed specimens of improved ground were subjected to a bending moment and the bending strength was taken to be equal to the maximum tensile stress from bending. According to Figure D-29, the values of bending strength are about 60% of the unconfined compressive strength. This percentage is higher than the percentages cited above for tensile strength, and it is higher than the value reported by Kitazume et al. (2000), who found that the bending strength is equal to 40% of q_u.
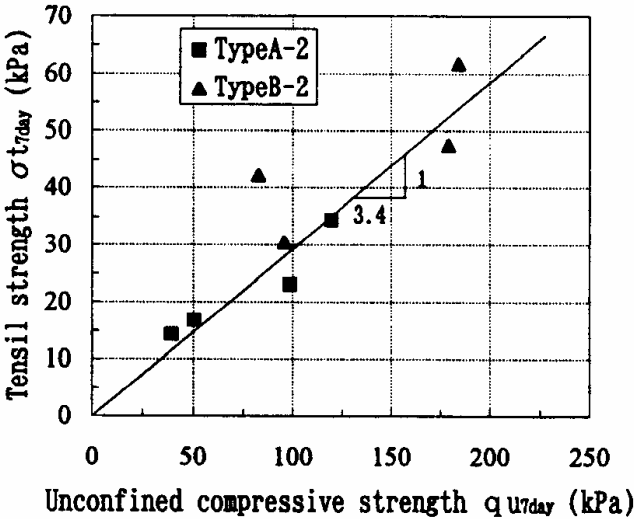

Figure D-28. Relationship between q_u and tensile strength (Dong et al. 1996)
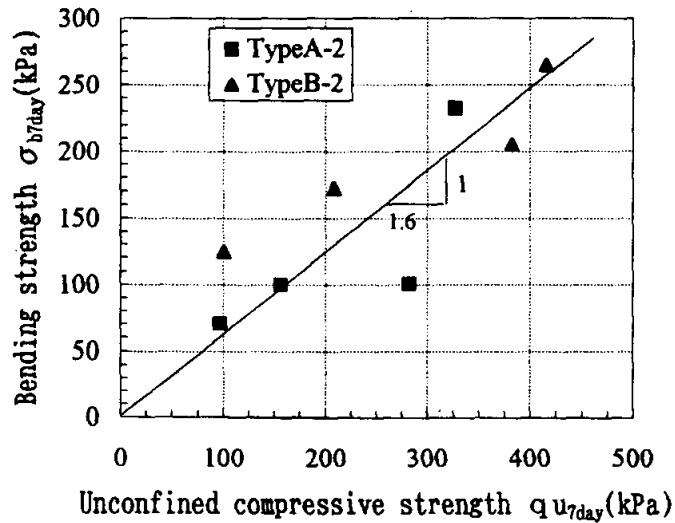
Figure D-29. Relationship between q_u and bending strength (Dong et al. 1996)

D.4.6. Unit Weight

For the dry method of deep mixing, Broms (2003) reports that the unit weight of stabilized organic soil with high initial water content increases to be above the unit weight of untreated soil, and it becomes greater with increasing cement and lime content. However, he also notes that the unit weights of inorganic soils are often reduced by dry-mix stabilization. The Japanese CDIT (2002) reports that, for soils treated by the dry method of deep mixing, the total unit weight of the treated soil increases by about 3% to 15% above that of the untreated soil.

For the wet method of deep mixing, Takenaka and Takenaka (1995) report that, as the cement content increases, the unit weight of the improved soil also increases. For clayey soils, the unit weight may increase by 0.5 to 1.0 kN/m^3 (3 to 6 lb/ft^3), but in the case of sandy soil, there is little change in the unit weight. CDM (1985) generalizes by saying that, for soils treated by the wet method of deep mixing, the density change is negligible. However, at the Boston Central Artery/Tunnel Project, a substantial decrease in unit weight occurred, as reported by McGinn and O'Rourke (2003). The decrease was primarily a result of the initial unit weight of the clay having a relatively high value of 20 to 21 kN/m^3 (120 to 125 lb/ft^3), and there being need to add water to pre-condition the clay before wet mixing with cement grout. McGinn and O'Rourke (2003) provide the distribution of total unit weight for both core samples and wet grab samples, and their data are included here as Figures D-30 and D-31, respectively.
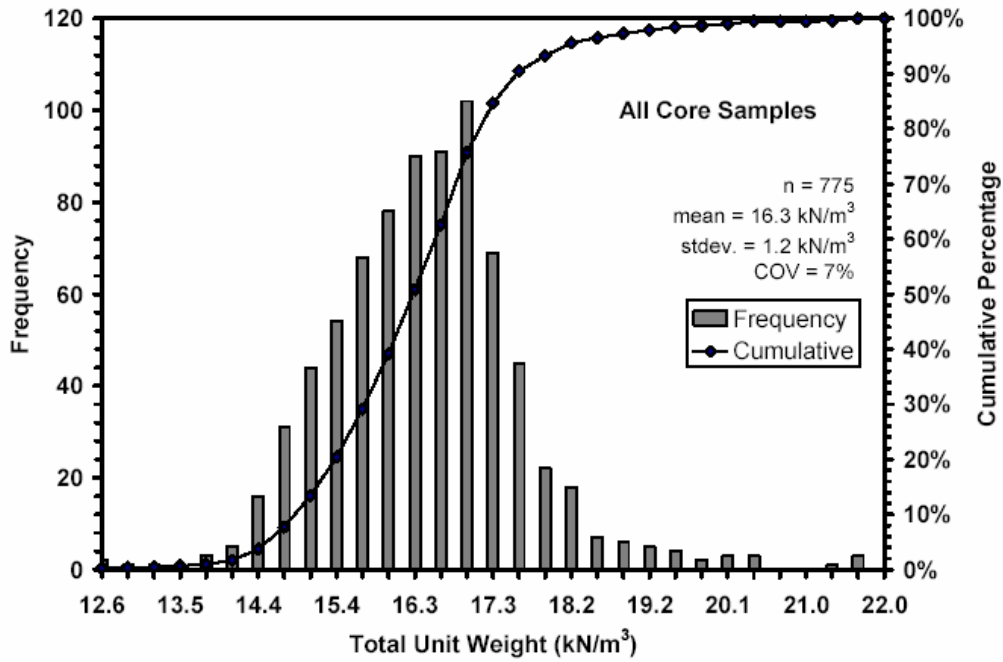
245

Figure D-30. Distribution of unit weight for core samples (McGinn and O'Rourke 2003)
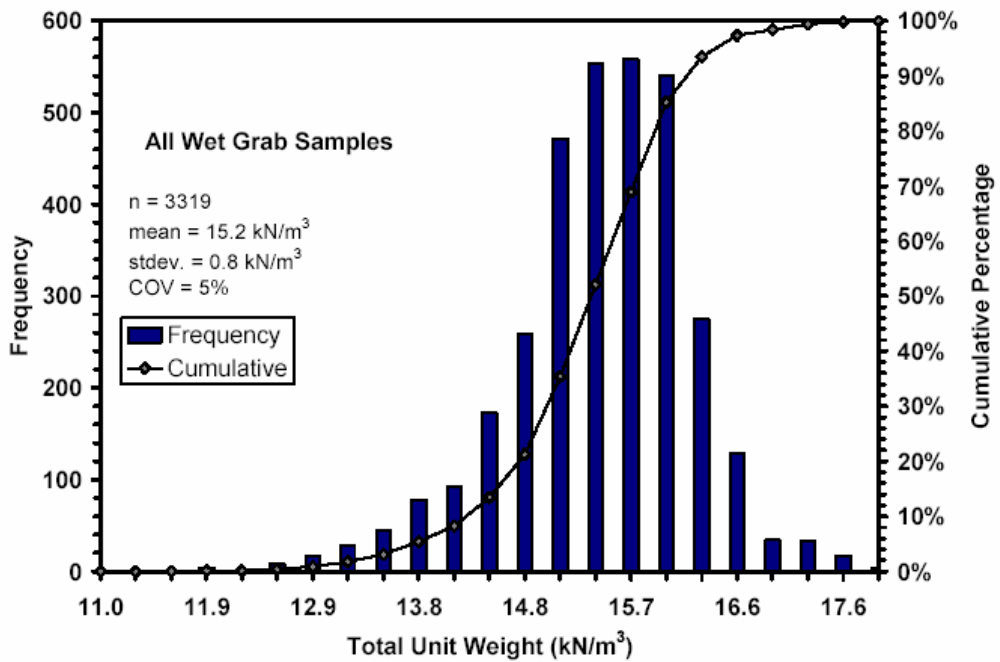

Figure D-31. Distribution of unit weight for wet grab samples (McGinn and O'Rourke 2003)

D.4.7. Hydraulic Conductivity

The addition of lime typically increases the hydraulic conductivity of soft clay; however, the addition of lime and cement may only increase the hydraulic conductivity slightly, or it may even decrease the hydraulic conductivity (Baker 2000).

For the dry methods of deep mixing, EuroSoilStab (2002) states that the permeability of soil treated with dry lime and cement can be assumed to be 200 to 600 times as high as that of unstabilized soil. Field tests performed by Baker (2000) indicated that the hydraulic conductivity varied between 10 and 100 times that of the original soil.

For the wet methods of deep mixing, hydraulic conductivity in the range of 10^{-7} to 10^{-8} m/s (3.3×10^{-7} to 3.3×10^{-8} ft/s) are routinely achievable (CDM 1994). Increasing the cement factor and adding bentonite content will serve to decrease the hydraulic conductivity for mixtures created by the wet method. Soil-cement elements installed by the wet method are not considered to function as vertical drains (Broms 1999).